CHARACTERISATION OF METAL CONTACT SURFACES AND STRUCTURAL-DYNAMICS DESIGN AND ANALYSIS OF A MICRO-STAMPING MACHINE

Mei Zhou

March 2011

This thesis is submitted to the Department of Design, Manufacture and Engineering Management, University of Strathclyde, for the degree of Doctor of Philosophy

Dedication

The author wishes to dedicate the thesis to her mother, her father, her husband and her daughter, without whose support and sacrifice, the thesis would not have been completed

Acknowledgements

The work reported herein was carried out at the Department of Design, Manufacture and Engineering Management, University of Strathclyde, through part-time study. Permission to register for a PhD degree provided by the University of Strathclyde is gratefully acknowledged.

The author wishes to express her gratitude to Professor Yi Qin for his phenomenal supervision of the research and constant support.

The author would like to thank the colleagues of the Manufacturing Research Group for their support and kindly co-operation.

The author is grateful to Mr. Robert Hay and Mr. Jim McEwan for their assistance in the laboratory, and Mr. Alasdair Downes and Mr. Russell Black for their assistance in the computer management.

Abstract

The aim of this study was to investigate methods to improve the design of a micro-stamping machine system with high precision and mass-manufacture capability. The investigation has been carried out through finite element simulations and experimental methods. The content of the study included macro problems and micro problems. For micro problems, the research was focused on the deformation of the surfaces in contact and the influence of the roughness of the contacting surfaces on the thermal conductance and the lubricant retained on the surfaces. For the macro problems, the research was carried out on the dynamics analysis of a micro-stamping machine and a micro-stamping tool.

ABAQUS was employed to carry out the finite element analysis. Two dimensional and three dimensional finite element models were constructed for the investigations of the characteristics of contacting surfaces and of a micro-stamping machine and a micro-stamping tool.

Based on the conceptual design and analysis of the micro-stamping machine, a test micro-stamping machine and a micro-stamping tool were designed by working in a group and manufactured by Pascoe Engineering Ltd for experimental study. The results of investigations from the finite element analysis and experimental measurement were analysed. The comparison of the results between the finite element analysis and experimental measurement gave a satisfactory agreement.

The experimental study for the contacting surfaces analysis included the measurement of the change of the characteristics of the surfaces before and after contacting under different conditions and the measurement of the thermal conductance of dry metal surfaces and lubricated metal surfaces in contact.

The experimental study for the micro-stamping machine/tool included the forming force, the responses of the top plate and the punch guide plate of the micro-stamping tool at different working frequencies and different amplitudes of the ram movement, as well as when using dry and lubricated rollers.

The main findings gained from the finite element analysis and experiments included the influence of surface roughness on the precision of the micro-formed products and the thermal conductance of the metal surfaces in contact, the major cause of the vibration of the micro-stamping machine system, and factors that influence the punch behaviour during the micro-stamping process. These findings formed the base for further improving the design of the micro-stamping manufacturing system. Based on the analysis of the findings, recommendations for the integrated design of a micro-stamping machine system were made for further study.

CONTENTS

Chapter 1 Introduction

1.1   Background of the Research

There are increasing demands on miniaturized/micro products, which are popularly used in vehicles, aircraft, IT facilities, and so on. Around the issues on how these products could be manufactured, Micro-manufacturing engineering is a field which deals with how micro-products are designed, manufactured, delivered and managed. Micro-manufacturing engineering is a general term which concerns a series of relevant activities within the chain of manufacturing micro-products/features, including design, analysis, materials, processes, tools, machinery, operational management methods and systems, etc. among these, manufacturing machinery being key to the chain of manufacturing. Design of bench-top machines for micro-manufacturing, especially for high-speed micro-manufacturing, is still a challenging task due to lack of sufficient standards, design/manufacturing rules and understanding of the manufacturing processes, plus, dynamics characteristics of the machine will have to be considered. There is also a lack of effective models and software to support the design activities (Qin, 2006). Further, achieving higher machine-precision is, currently, a major target for most of the micro-forming machine developers for which both macro- and micro-scale problems need to be addressed in design and analysis. In order to do so, some questions will have to be answered, e.g. how local micro-scale contacts influence the accuracy of the machine model which involves, usually, many contact structure-parts, how dynamics behaviours of a machine system predicted by the numerical simulation is influenced by simplification of the model of the tool (subsystem) which also involves many structural parts, etc.

The issues focused in this study as a problem-solving project associated with the development of a bench-top micro-stamping machine are summarised as follows:

(i).   What are the influences of metal surfaces (contact pair) characteristics on the contacts at the micro-scale, and hence, influences on FE analysis results ?

(ii).   What are the factors that could cause vibration of a bench-top micro-stamping machine?

(iii).   How does the stamping tool-system perform when subjected to a high-speed impact during high-speed stamping?

(iv).   For machine-system analysis as a whole, how the interactions among various machine-parts/elements could be considered in an integrated model?

(v).   How the dynamics analysis could be better linked to the machine design?

These were lacked in previous research and technological development concerning bench-top stamping-machines and systems.

1.2   Objectives

The objectives of the PhD research were defined as follows:

(i).   Investigation of micro-deformations of metal surfaces in contact to determine the factors influencing the contact-behaviours.

(ii).   Experimental study of thermal-contact conductance under the conditions of dry surfaces and lubricated surfaces in contact.

(iii).   Dynamics analysis of a bench-top micro-stamping machine to determine the factors influencing the micro-stamping process, hence, the precision of the parts produced.

(iv).   Development of considerations for the machine-frame design, based on the machine dynamics analysis.

(v).   Dynamics analysis of a micro-stamping tool-system to determine the factors influencing the stamping process, hence, the precision of the parts produced.

(vi).   Experimental validation of the models and analysis procedures developed.

1.3   Methodology

In order to achieve the objectives defined, FE analysis and experimental investigations were employed in this study. The FE analysis included investigation of micro-deformations of metal surfaces in contact and heat transfer and temperature distribution at interfaces of contact. These provided information for creating more accurate FE models for the machine and tool analysis which involved multi-bodies contact problems. This fundamental study was followed by analysing several machine-frame concepts. The best concept was selected with reference to the dynamics performance of the machine-frame analysed. Further to this, detail machine-frame design was developed and analysed again for its dynamics behaviours. The analysis was further conducted by incorporating the tool-system into the machine model, hence, a complete FE machine-model could be created for more accurate analysis, in order to predict the precision of the machine system in a condition which is closer to a real stamping-condition. These were accompanied with experimental conditioning of the FE models and validation of the FE results.

1.4   Programme

The following work was planned as a PhD research project:

(i).   Literature review on the characterisation of metal contact-surfaces and design of micro-stamping machines and micro-stamping tools.

(ii).   Experimental investigation of metal-surface contact characteristics.

(iii).   FE simulations of micro-deformations of metal surfaces in contact and temperature distributions at the interfaces.

(iv).   Analysis of machine concepts of a micro-stamping machine on their dynamics performance.

(v).   FE analysis of dynamic behaviours of the micro-stamping machine (detail design) and a micro-stamping tool-system.

(vi).   Experimental investigation of the dynamic response of the micro-stamping tool-system and comparison to the FE results.

(vii).   Drawing conclusions on the study and making recommendations on the future research.

1.5   Scope of the Thesis

The thesis consists of 9 chapters. Chapter one is introduction. Chapter two provides a general literature review on the micro-forming systems, problems and methodologies relating to the improvement of the design of a micro-forming manufacturing system. Chapter three presents experimental investigation of the characteristics of surface roughness and thermal conductance of the metal-surfaces in contact. Chapter four deals with FE analysis of micro-deformations and temperature distributions at the interfaces of metal surfaces in contact. Chapter five presents conceptual designs of a bench-top micro-stamping machine. Chapter six concerns dynamics analysis of the micro-stamping machine and Chapter seven dynamics analysis of the micro-stamping tool-system. Chapter eight presents experimental measurement of the stamping force and dynamic response of the micro-stamping tool-system. The final chapter, Chapter nine, summarises findings from the study and discusses considerations for future work.

Chapter 2 Literature Review

2.1   Contact analysis of solid contact surfaces

Contact analysis of solid contact surfaces mainly contains geometrical analysis, mechanical analysis, and thermal-conductance analysis. Two kinds of problems exist in each analysis. One is the macro problem and the other is the micro problem. The latter has become increasingly more important for high-precision design. Different finite element models have been used to analyse the deformation of rough contact surfaces. Several models that were based on elastic deformation were subsequently extended to the plastic range of the material (Sridhar, 1994). Elastic-plastic surface-deformation models have been proposed (Francis, 1977; Ishigaki, 1979). The "equivalent asperity" model greatly simplified the procedure of the analysis of real surface contact (Chen, 2004).

2.1.1   Geometrical analysis

The geometrical problems of contact surfaces concern two aspects. The first is surface roughness, which is a micro problem, whilst the second is out-of-flatness of the surfaces, which is a macro problem.

2.1.1.1 Micro geometrical analysis

Solid surfaces are not completely smooth, but are microscopically rough. This roughness can be thought of as the surface deviation from the nominal topography. The "Gaussian surface" can be used to describe such a surface, where its asperities are isotropic and randomly distributed over the surface.

A common methodology to model surface roughness is the representation of surface asperities by simple geometrical shapes with a probability distribution with the different asperity parameters involved (Bahrami, et al., 2003). Greenwood and Williamson (1966) assumed that each asperity summit had a spherical shape, of which the height above a reference plane had a Gaussian distribution.

2.1.1.2 Macro geometrical analysis

Real engineering surfaces are not perfectly flat. Considering the waviness of contacting surfaces is a very complicated problem. Some simplifications must be introduced to describe the macroscopic topography of surfaces. Macro-contacts can be divided into the following three cases:

- Rough flat surface and flat surface contact
- Rough spherical surface and flat surface contact
- Rough spherical surface and spherical surface contact

In the case of a rough flat surface and flat surface contact, the macro waviness of the contact surfaces is assumed to be negligible. In the case of a rough spherical surface and flat surface contact, the waviness of the contact surfaces is simplified to a flat surface and a spherical surface. In the case of a rough spherical surface and spherical surface contact, the waviness of two contact surfaces is simulated by two spherical surfaces.

The second case and the third case are simplified to contact between a rigid smooth sphere and a rough plane. Combining the waviness of the two original spherical surfaces forms the waviness of the plane. This is called the equivalent sphere-flat contact. The effective radio of curvature is:

$$\frac{1}{\rho} = \frac{1}{\rho_1} + \frac{1}{\rho_2}$$

where ρ_1 and ρ_2 are the radii of the two original contact spherical surfaces. The summary of the geometrical contact model is shown in Fig. 2.1 (Bahrami, et al., 2003).
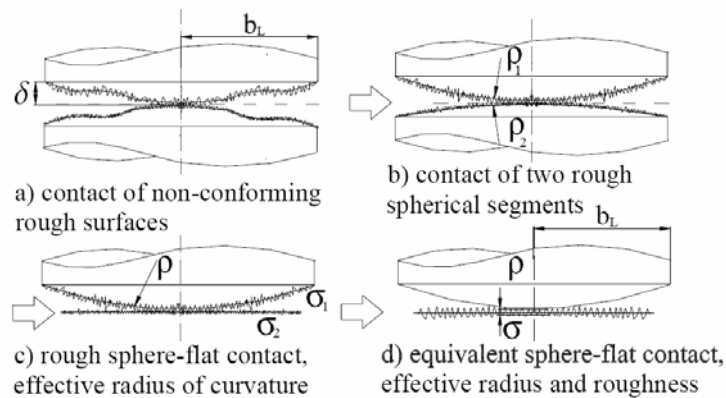
Fig. 2.1 Geometrical contact model

2.1.2 Mechanical analysis

Depending on material properties, structural geometry as well as external loading (including temperature, boundary conditions, etc), there are 3 kinds of deformation, viz, elastic deformation, plastic deformation and elastic-plastic deformation. Therefore, in mechanical analysis, the materials are described by three different models. These are:

- Elastic model
- Plastic model
- Elastic-plastic model

2.1.2.1 Elastic model

Hertz's elastic contact theory. This theory states that each body can be regarded as an elastic half-space loaded over a small contact region of its surface. Elastic contact theory assumes that surfaces are continuous and non-conforming, strains are within the elastic limit, and the surfaces are frictionless (Bahrami, et al., 2003).

Archard's model. In this model, each asperity is covered with micro asperities, and each micro asperity is covered with micro-micro asperities.

When two nominally mating surfaces are brought together, they touch at the tips of the higher asperities and the total area of real contact is determined by the deformation of the materials in contact, which is, in general, a small part of the nominal area. The number, size and distance of separation of these asperities will affect the contact resistance and local temperature caused by frictional heating during sliding (Archard, 1953).

The Greenwood and Williamson's model. Greenwood and Williamson (1966) proposed an elastic model for rough flat surfaces based on the deformation of the average size of the summits. They assumed that all summits have the same radius of curvature at their top and possess a Gaussian distribution about the mean reference plane and that the distribution of summit heights is the same as the standard deviation of height.

This model required three input parameters:

- Surface density of the asperities
- Standard deviation of the height of summit distribution
- The radius of curvature of the summits (assumed to be constant)

The extended model can also be used for complex geometric surface (Greenwood, 1967).

Whitehouse and Onions's model. This is a statistic model which represents the profile of rough surfaces with a random structure by using two parameters: standard deviation and the exponent of an exponential correlation function. This theory is compared with surfaces presented in digital form (Whitehouse, 1970; Onions, 1973).

2.1.2.2 Elastic-plastic models

For a material subjected to indentation, when the yield point is first exceeded the plastic zone is small and fully contained by material that remains elastic so that the plastic strains are the same order of magnitude as the surrounding elastic strains. The plastic zone expands as the load is increased. Eventually the plastic zone breaks out to the free surface and the displaced material is free to escape by plastic flow to the

sides of the indenter. Chang, et al. (1987) presented a model based on the volume conservation of an asperity control volume during plastic deformation. Zhao, et al. (2000), using the Chang's model, developed an elastic-plastic micro-contact model for a nominally-flat rough surfaces.

2.1.2.3 Plastic model

When the plastic strains are large compared with the elastic strains, the elastic deformation can be neglected. Thus the material may be treated as a rigid-plastic material. The loaded body of rigid-plastic material contains two regions. One region has no deformation due to the assumption of rigidity and the other is the region in which plastic deformation takes place (Bahrami, et al., 2003).

Abott and Firestone developed the most widely used model for fully plastic contact (1933). The model assumes that the asperities are flattened or equivalently penetrated into a smooth surface without any change in the shape of the parts of the surface not yet in contact. The pressures at the top of the peaks are very large because the real contact area is much smaller than the nominal contact area. The normal load is supported by plastic flow of the asperities (Bowden, 1951; Holm, 1958).

Pullen and Williamson (1972) investigated plastic flow under large loads through an experimental method. They made the suggestion that material displaced from the contacting region will move to some non-contacting part of the surface and make the surface rise.

2.1.3 Surface profile analysis

Surface roughness is a basic physical characteristic of an engineering solid surface. A statistic method is efficient in giving a description of surface behaviour due to a random asperity distribution. The real contact area is a part of the nominal surface and it will change with the contact pressure. When lubricant is used on the contact solid surfaces, the real contact area and the condition of the lubricant remaining have a special significance for the thermal conductance between the contact surfaces under load. The bearing area curve is an important parameter for describing the statistical properties of the contact surface. Finite element simulation of the surface contact can

be used to simulate the real contact of a rough metal surface. Kucharski, et al. (1994) presented a finite element model of surface contact deformation, in which a spherical asperity was considered.

The roughness profile of a surface is usually described by standardized parameters. There are several kinds of standards for surface-texture description, such as OLDMIX, JIS1982, JIS1994, ISO1997 and ANSI1995. Different standards contain different parameters. The ISO1997 standard is used in this study. The relative parameters are listed in Table 2.1.

Table 2.1 Roughness profile parameters in ISO1997

Parameter	Parameter Name
Ra	Average roughness
Rq	Root mean square roughness
Rsk	Skewness
Rku	Kurtosis
Rp	Peak roughness
Rv	Valley roughness.
Rz	Ten point average roughness
Rt	Total roughness
Rc	Mean peak-to-valley height of the profile
Rk	Core roughness depth
Rpk	Reduced peak height
Rvk	Reduced valley height
Mr1	Material portion 1
Mr2	Material portion 2
A1	Peak area
A2	Valley area
ADF	The amplitude distribution function
BAC	Bearing area curve

The average roughness R_a, also known as the arithmetical mean deviation of the profile or the central line average, is the area between the roughness profile and its

mean line divided by the evaluation length. It can be described by the integral of absolute value of the roughness profile height over the evaluation length L (Fig. 2.2).

$$R_a = \frac{1}{L}\int_0^L |z(x)|dx$$

When evaluated from digital data, the integral can normally be approximated into the following equation.

$$R_a = \frac{1}{N}\sum_{n=1}^N |z_n|$$

N is the sum of the number of peaks and the number of valleys over the evaluation length L.
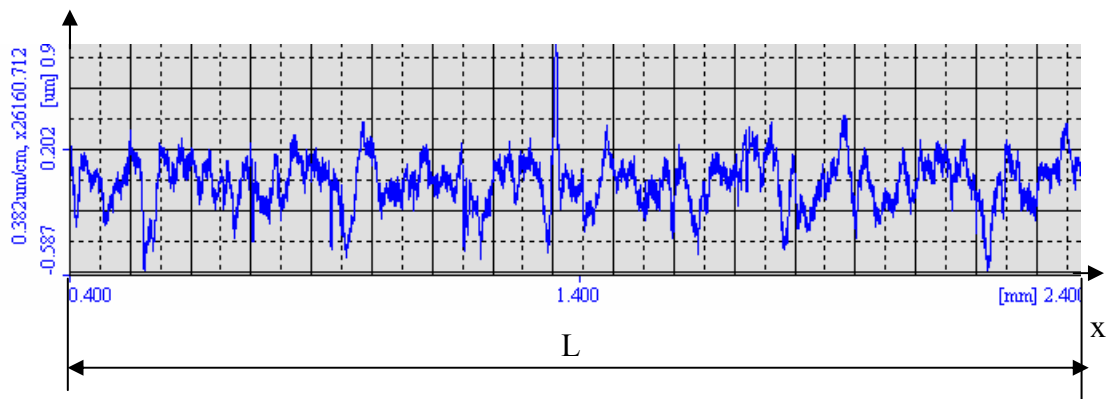
Fig. 2.2   Roughness of a surface

The three surfaces shown in Fig. 2.3 all have the same value of R_a, but it is easy to recognize that they are quite different surfaces. The first has sharp peaks, the second has deep valleys, and the third has neither. In some applications they will perform very differently also. In the case of surfaces in contact, it is not difficult to understand that the real contact area will be different for these three surfaces under the same interfacial pressure. The situations of lubricant remaining on the surfaces are different after the surface has been compressed.
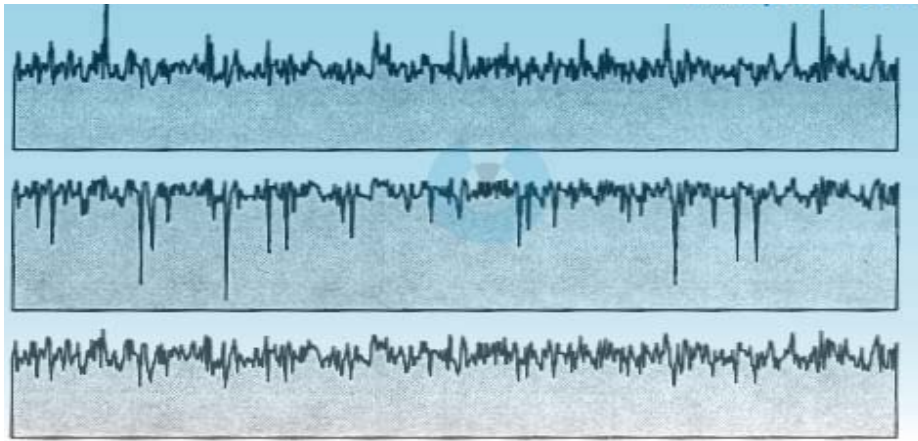
Fig. 2.3   Different surfaces with the same average roughness

To distinguish between surfaces that differ in shape or spacing, other parameters for a surface, that measure peaks, valleys, profile shape, and spacing, need to be calculated. The more complicated the shape of the surface that is wanted, the more sophisticated the method that is needed in measuring the parameters.

There are a few kinds of methods for surface-profile metrology. For instance, Byoung-Chang Kim and Seung-Woo Kim (2003) devised an interferometer system for surface-profile metrology with multiple two-point diffraction sources that are made of a pair of single-mode optical fibres. This system is capable of profiling rough surfaces with high precision without increasing the wavelength of the light that is used.

2.1.4   Friction between contact metal surfaces

Friction between contacting metal surfaces is an important factor for surface deformation analysis and contact analysis between micro-forming machine components. Extreme care is needed in choosing the friction coefficient (www.enigineeshandbook.com). The friction coefficient is relevant in respect of the roughness of the surfaces and the situation of the lubricants, as well as the velocity of sliding between the contacting surfaces. (www.roymesh.co.uk).

An effective lubrication system results in low friction levels, which reduces the loads imposed on the tooling and the workpieces. Lower force levels also reduce tooling deflection and can improve the dimensional accuracy of the product (Wilson, 1978)

A study focused on the investigation of the effect of the surface roughness on the frictional properties for different materials and conditions was conducted by S. Mumin (2007), the friction coefficient being obtained by means of a ring compression test.

Jan Lundberg (1995) carried out an experiment to investigate how surface roughness affects the characteristics of the lubricant film under the conditions of combined normal and sliding motion. The experimental arrangement consisted of a roller which impacted a stationary ball in the presence of a lubricant. Under the same conditions as for a normal surface approach, increasing the surface roughness significantly decreased the level of the roller sliding that could occur without breakdown of the lubricating film. Surface roughness had a greater effect on oil film breakdown than did either viscosity or load.

Li (2004) proposed an experimental method to investigate the effect of surface lay on the lubricated rolling/sliding of ground roller surfaces. By using the rough friction test rig, different surface lay contacts can be simulated and the friction can be measured. At around 60° of contact angle, the friction-coefficient value appeared to reach a minimum for lubricated rolling/sliding contact. At the same time, the contact pressure has little effect on the frictional behaviour.

2.1.5 Thermal-properties analysis of contact surfaces

The rate of heat transfer across a joint depends on a number of parameters: the thermal properties of solids and interstitial gas between the contact surfaces, gas pressure, surface-roughness characteristics, the properties of lubricant on the surfaces, the applied load, and the contact micro-hardness. Most of the thermal contact-resistance models depend on the following common assumptions (Bahrami, et al., 2003).

Common assumptions:

- The contacting solids are isotropic, and the thermal conductivity and physical parameters are constant.
- The contacting solids are thick relative to the roughness or waviness.
- The surfaces are clean and static.
- Radiation heat-transfer is negligible.
- The micro contacts are circular.
- There is steady-state heat transfer at the micro contacts.
- Micro contacts are isothermal (Cooper, 1969).
- The micro contacts are flat, with the surface asperities usually having a very small slope (Mikic, 1966).

Based on these assumptions, the contact resistance under vacuum conditions can be calculated by the superposition of microscopic and macroscopic constriction resistances (Yovanovich, 1969; Nishino, 1995; Lambert, 1997).

The thermal resistance of a gaseous gap for a conforming rough-contact model and the thermal resistance of a gaseous gap for a non-conforming rough-contact model were derived by Bahrami, et al. (2004). These models cover four regions of a heat-conduction model of a gas, i.e. continuum, temperature-jump, transition and free molecular. The models account for the mechanical and thermal properties of a gas and a solid, e.g., gas pressure, temperature, surface roughness and the applied load. The main input parameters are:

- Thermal accommodation coefficient
- Radius of the specimens
- Radius of curvature
- Gas pressure
- Surface roughness
- Mean absolute surface slope
- External force
- The thermal conductivity of the gas

- Gas temperature

- Vickers micro-hardness coefficient.

Using these models, Bahrami, et al. (2004) investigated the effects of external load, surface roughness, gas pressure, and surface radius of curvature on the joint thermal resistance.

If the asperities of a surface are isotropic and randomly distributed over the surface, it may be modelled by a Gaussian distribution. It has been shown experimentally that many of the techniques used to produce engineering surfaces give a Gaussian distribution of surface heights (Williamson, 1969). The contact between two Gaussian rough surfaces can be simplified to the contact between a single Gaussian surface with a perfectly smooth surface (Greenwood and Williamson, 1966). Bahrami, et al. (2003), by assuming plastically-deformed asperities and using scaling analysis techniques, developed an analytical model to predict the thermal contact resistance of conforming rough contacts in a vacuum.

2.2   Development of micro-forming machine systems

Today, forming, particularly precision forming, is still one of most widely-used technologies in industry. Micro-forming machine systems have been developed very quickly over recent years. Miniature/micro-equipment developed to date for micro-factories has been largely for micro-machining and/or micro-assembly. Research efforts in miniature/micro-forming, to date, have been with reference to the fact that traditional knowledge may not be able to be directly scaled down to enable conversion of miniature/micro-materials into miniature/micro-components. In most cases, research undertaken has referred to the theoretical analyses of prevailing issues with a view to gaining sufficient insight into micro-forming processes and materials, the results not being sufficiently complete to enable the mass-manufacture of miniature/micro-products in an industrial environment. More particular considerations will have to be given to machine design to meet the requirements of engineering application, e.g. greater precision, handling of micro-parts/materials with higher rates and positional precision. Micro-machines that were only of "laboratory-prototype" nature, or ignored handling issues, etc., were not ready for application in a

mass-manufacturing environment. Further, the absence of attributes for interfacing to the related manufacturing facility reduced their significance in the mass-manufacturing environment. The development of micro-forming technology will rely largely on the development of micro-machining or even nano-machining technologies. To match the mass-production characteristics of micro-forming, new design considerations will have to be developed for micro-machining facilities, such as the scale of the equipment, the flexibility of the set-up, the incorporation of the cutting of new materials, and integration with the micro-forming facilities, etc.

Micro-factory technologies have been developed in Japan. The downsizing production system, which has proposed to be called the "micro-factory", can help to save energy, space and resources in addition to improving flexibility for model change and controllability of the atmosphere. Eventually, the micro-factory will be able to realize a miniaturized production system. The key to the micro-factory is to downsize the machine tools and elements without reducing the accuracy. Moreover, design theory to assemble them properly is necessary (Mechanical Engineering Laboratory, 2006). Several demonstration miniature-/micro-manufacturing systems have been developed. The Japanese MCL model of the micro-factory has been widely cited in most of the literature concerning the micro-factory (Mishima, 2002 and 2003; Okazaki, 2002).

MASMICRO was an EU FP6 Integrated Project for the mass-manufacture of miniature/micro-products, with micro-forming as one of the core technologies. The overall objective of the project was to develop an integrated solution for the European miniature/micro-manufacturing industry — an integrated manufacturing facility for the mass-manufacture of miniature/micro-products and a technology transfer/training package for transferring knowledge to, and developing skills in, industry. The developments included:

- A series of methods for the design and analysis of miniature/micro-forming processes, materials, tools and machinery.
- Flexible, intelligent tools for miniature/micro-forming and machining.

- Flexible, intelligent machine systems for miniature/micro-forming and machining.
- Intelligent handling devices, assembly and an inspection system for micro-forming/machining, assembly, and inspection.
- An integrated manufacturing facility for the customised mass-manufacture of miniature/micro-products, which integrates design, analysis, testing, tool-fabrication, forming, machining, assembly, and inspection.

Evaluation criteria included:

- Precision
- Stiffness
- Force capability
- Stroke control
- Size
- Speed and productivity
- Cycling adaptability
- Space for handing and feeding
- Maintenance
- Easy design
- Easy manufacture
- Easy assembly
- Easy control
- Cost

Research was conducted to resolve individual and technological issues concerning the mass-manufacture of miniature/micro-products, with a view to achieving several breakthroughs. The mass-manufacturing facilities developed were validated through trials and demonstrated on products selected from industry; the knowledge and technologies generated were transferred directly to the targeted groups.

2.3   Dynamics design and analysis of forming machines

The demand for micro products is growing in the markets, especially for electronics applications and high precision machines. Micro technology and manufacturing process are being used widely and improved quickly. Many investigations into improving and optimising the manufacture of micro products, in particular for the micro-forming machine system, have been carried out. In order to achieve the efficient and economical production of micro parts with high demands on precision and accuracy, the integrated design of a modern machine system is developing and improving. New methods in the micro-forming machine system are being investigated through numerical analysis and experiment methods (Proche and Schnecier, 2004)

A micro-forming machine concept is available for all three micro forming processes, i.e., bulk forming, sheet forming and tubular forming. A large number of investigations have been conducted for the numerical analysis of micro-forming machine systems in recent years. Further increases in performance require not only the design and dimensioning of the components, but also reductions in the weight of the components to lowest possible level. However, reduction in material usage results in loss of stiffness in the region of the machine frame and components. The integral design of a machine frame structure and a whole machine system will therefore become more important in the development of future machine generations.

To start with, the term micro-forming, in the context of metal forming, is understood to be the production of parts or structures with at least two dimensions in the sub-millimetre range (Geiger, 2001). Parts of such a size are commonly used and are becoming increasingly more required in extremely high numbers, in particular for electronic components in micro-system technologies and micro-electro-mechanical systems, as they presently characterize many products pushing forward their miniaturization. Typical examples include pins for IC-carriers, fasteners, micro-screws, lead frames, sockets, and any kind of connecting element (Engel and Eckstein, 2002).

Micro-forming may also be effected by miniature/micro-machines. These machines are of much a smaller size compared to that of conventional, large-scale presses. Various new concepts are being experimented upon to design and fabricate prototypes of the micro-machines (Qin, 2006).

2.3.1 Micro-forming machine systems

The forming of small metal parts has been undertaken in industry for many years. However, challenges do arise when the size/features reduce to tens of microns or precision requirements for miniature/macro-parts reduce to less than a few microns. Metal-forming offers some attractive characteristics, superior to those of other processes, for example, machining and chemical-etching. It includes such features as a greater production rate, better material integrity, less waste, lower manufacturing costs, etc. Therefore, micro-forming could be a better option in the mass-manufacture of miniature/micro-parts at a reduced cost if current technology is advanced further and a proper manufacturing facility is developed (Qin, 2006).

A micro-forming system may consist of five key elements. These are material, process, tool, machine, and other equipment. For the best use of the technologies and manufacturing facilities in achieving high efficiency, the manufacturing system that is developed has to be integrated.

Rigidly-coupled multi-body simulation can be used to simulate the kinematic behaviour of the machine tool while considering the control loops of the drives (Prischow, 2002). Multi-body simulation is also used to optimise the accuracy of machine tools under acceleration loads for the demands of high-speed machining (Rehsteiner et al, 1998). Numerical simulations for the hydraulic system are used to investigate the interaction of the machine and the hydraulic drive system (Neugebauer et al, 2003).

2.3.1.1 Micro-forming machines of large size

Some significant research has been carried out in the micro-forming field during recent years. One kind of machine is of large size but is incorporated into micro-

forming. LFT Erlangen and WAFIOS worked jointly on this type of machine design and developed a prototype. The machine has a modular structure in which every forming station has its individual drive unit and can be controlled independently. A transfer system with a vacuum gripper was developed for the handling of parts between the forming stations. Another machine was developed jointly by SCHULER, PtU Darmstadt, ILT, IPA and other partners. The machine has a modular arrangement and a high-rigidity design. Linear motors are used for driving the ram. Linear driving has the advantage of high reproducible accuracy. Lubrication is not needed to a great extent, thus maintenance can be reduced, hence it is an attractive option for clean-room manufacturing. Other advantages include low noise-emission and high reliability and endurance (Qin, 2006). Another development is the SCHMIDT Servo Press 4000 machine (SCHMIDT technology, 2007). The modular power-head is an attractive feature of this design that enables easy change of the power-level whilst not altering other settings of the machine. Another feature is that the dual-channel light-curtain control system, with a complete guarding of the work area, offers optimum protection of the operator against injury (SCHMIDT technology, 2007).

2.3.1.2 Micro-forming machines of small size

Another kind of machine is miniature/micro-machines. These machines are of much smaller size compared to that of conventional machines. The development of this kind of micro-forming machine has attracted substantial interest from researchers during the last 10 years (Qin, 2006). A typical model machine has been developed in Japan for super-plastic backward extrusion (Saotome and Iwazaki, 2002, 2001). This machine is hand-size and a piezoelectric actuator is used to drive the punch. Another micro-machine prototype using the working principle of incremental micro-forming has also been developed. Small indentations in sheet metal could be generated by hitting the metal with a small punch installed at the end of a swinging arm. By repeated hammering, incremental deformations could be achieved over small areas of thin sheets. This system is schematised in Fig.2.4. (Saotome and Okamoto, 2001).
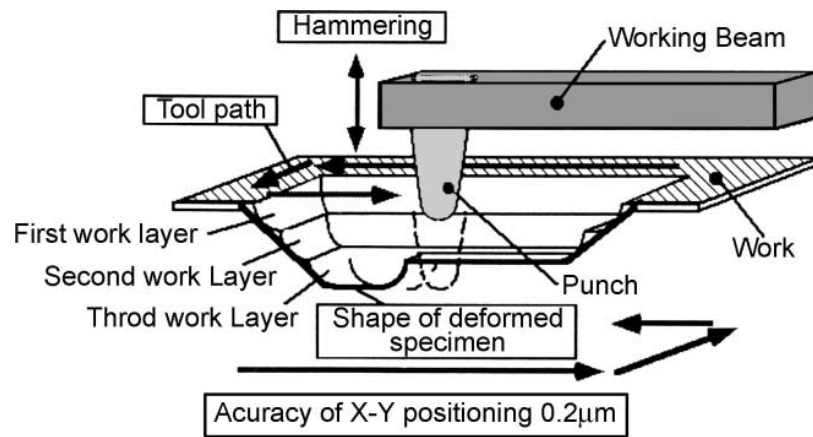
Fig.2.4 The Principle of CNC incremental sheet metal forming by hammering

Other developments include the use of combinations of piezo-actuation with hydraulic devices to amplify the punch stroke (Park, et al., 2002; Hess, 2000), e.g. the piezo-electric-driven press developed by Zentrum Fertigungstechnik Stuttgart (ZFS), Germany (Hess, 2000). A piezo driven prestressing of die-system for micro forming of metal components was developed by Paldan, et al. (Paldan, et al., 2008). A typical mechanical micro-press was that developed in the Mechanical Engineering Laboratory, Ministry of Trade and Industry, Japan (Mechanical Engineering Laboratory, 2006). The machine has a size of 111mm×66mm×170mm, powered with an AC servo motor with a 100-W rated power which can generate a force of up to 3kN. The transmission is effected with a ball screw/nut structure, plus timing pulleys and belts. The micro progressive die enables four blanking and two bending strokes to be used. The stroke and speed of the machine can be controlled and 60 strokes per minute can be achieved (Qin, 2006).

The achievements in the development of micro-forming machine systems, to date, can be described as follows:

- Conventional micro-forming machines with improved mechanical structure can function at high speed, with high precision and as highly-automatic punching presses. However, some problems still exist: these problems, such as huge conventional geometry, high maintenance cost, and low flexibility, are unavoidable (Geiger, 2001).

- Micro-forming machines with a clean-room structure developed by SCHULER & PtU Darmstadt can provide a maximum forming force from 20kN to 40kN and a maximum rate of 1200SPM. They made the machine maintenance-free due to the use of the linear motor. However, the non-modular structure and geometry of the machines seem to be too big for micro-parts production (Groche and Schneider, 2004).
- A modular-structure micro-forming machine developed by WAFIOS and LFT Erlangen was well equipped with a transfer system and a vacuum griper for handling parts between the different forming stations, but it is only suitable for bulk forming, and there is no evidence, so far, of its industrial application (Geiger, 2001).
- A modern micro-forming system is being developed to provide high-speed, mass-manufacture, as well as a fully-incorporated parts-handling system for industrial application.

2.3.2 Design of a micro-forming machine

Machines, forming-tools and handling devices are critical in the industrial applications of micro-forming technology. Examining the practices in the forming of miniature/micro-products in industry and in research groups led to the recognition of the strategies to be used in machine development/application for micro-forming (Qin, 2006).

In recent years, advanced software and hardware systems have enabled design engineers to evaluate and optimise product characteristics with virtual prototypes, which reduces the cost and time of hardware testing and iterative improvement of the physical prototype, before the first physical prototype is built. Engineers are able to realistically simulate the kinematic-, static- and dynamic-behaviour of the whole machine-tool system. Thus, it is possible to quickly analyse multiple design variations until achieving an optimised prototype which satisfies the requirements. A wide range of software tools is available for the different design stages. Computer-aided design involving kinematics studies, finite element analysis and coupled

flexible multi-body-simulation has become increasingly more important in the design of modern micro-forming machine systems.

Three machine-related factors could significantly influence the accuracy of the formed components. These are the stiffness of the machine, the guide clearance, and the movement of the ram (Nakano, 1997). Improving the accuracy of the components requires greater frame-stability, better ram-guidance and reduced ram-tilt (Schmoeckel, 1992)

2.3.2.1 Machine frame design

For a micro-components manufacturing machine frame, high stiffness and static characteristics are a basic demand in being able to achieve high precision and retain low deflection. The dynamic characteristics of the frame structure are more important for retaining high machine stability. The flexibility/mobility of the frame structure can provide high efficiency for mass production. Its light weight and large workspace make the machine more economical and convenient. The frame structure also should be easy to connect with the power source, the machine tool, the material feeder and the workpiece-handling device (Qin, 2006).

2.3.2.2 Micro-stamping tool design

The machine tool is an important part of a micro-forming manufacturing system. The design of metal-stamping dies is a complex process. It is also an inexact process, so that considerable trial-and-error adjustments during tryout are often required (Nine, 1978). Within mm size steel dies have been investigated through experimental method for production of microcomponents (Wert, et al., 2009). The precision of the tool system is crucial owing to the low tolerances on the dimensions of the micro-components (P-Withen, 2005).

In machine tool design, optimisation offers the possibility of improving different properties of the design by using numerical optimization (Weule, et al., 2002; Weule, et al., 2003). Topology optimization is used to define the best material distribution within the given design space. This method is used mainly in the early design stages,

to support the engineer in finding a design concept with regard to given demands (Spath and Neithardt, 2002). Different approaches are used to simulate the interaction between the components during the early design stage of the machine tool (Zaeh and Baudisch, 2003). The high-level requirement of a machine tool should include consideration of the following aspects (Brecher and Witt, 2004):

- High static and dynamic stiffness
- High accuracy
- Low path deflection
- High speed and mass production
- Flexible mobile structure
- Easy connecting with feeder and handling devices

During the concept design stage, simplified simulation models can be used to estimate the influence of general design parameters on the machine performance.

All aspects about forming-tool design and intelligent tool-structures/systems for the precision-forming of engineering components include:

- Reducing forming-pressure
- Strengthening structure
- Improving product quality
- Extending forming-limits
- Enabling flexibility of production
- Improving tool life
- Improving system performance by control

Forming conditions are largely influenced by tool kinematics, a change in tool-kinematics may results in a beneficial effect on the forming process (Qin, 2006). The Finite element analysis is an efficient method for improving tool design.

2.3.2.3 Material feeder

Conventional press feeders have to meet three main criteria to be successful. Firstly, the feeder must be flexible in terms of set up. Secondly, delivery of material must be with sufficient precision as required for forming. The feeders must also do the feeding at the correct time. All of these are particularly difficult to meet when forming thin sheet metals (Razali et al, 2009)

For full realisation of the feasible drive performance of a machine system, the dynamic behaviour of the entire machine system must be analysed and optimised integrally during the design of the machine.

The feeding device plays an important role in achieving the overall objective of the machine system. The feeding device should be able to meet all the requirements of the maximum feeding rate and stroke length. A feeding device might be controlled by a piezoelectric device, a linear motor, or a combination of both. The dynamic behaviour of the feeder, as well as the interactions between the feeder and the machine tool and the feeder and the machine frame should be analysed.

2.3.2.4 Workpiece handling devices

A handling device is another important consideration. The dynamic behaviour should secure the overall achievement of other parts of the machine system .

2.3.2.5 Integrated design of modern micro-forming machine systems

A sheet-metal-forming operation must be analysed as an interactive system and the analysis of sheet-metal forming must incorporate the properties of the real material (Keeler, 1978). There are correlations among the deformation state, the deformation defects and the die geometry (Ishigaki, 1978). Important phenomena include strain localization, failure of the draw-piece, galling on the tool-material interface, wrinkling of the sheet metal and fracture of the tools. In many sheet-metal-forming processes the membrane theory is justifiable and therefore this idealization was introduced in building a finite element simulation model (Kobayashi, 1978).

Finite element analysis is used to calculate the static stiffness or dynamic characteristics of the machine and tool, e.g. natural frequencies and mode shapes (Altintas, Brecher and Witt, 2005). Simplified simulation or rigid multi-body models can be used in the first stage of the design (Weule, et al., 2002; Weule, et al., 2003). Coupled flexible multi-body simulation is used for the integrated design of a modern micro-forming-machine system: it is used to deal with the interaction between the parts of the machine system. Interaction between structural dynamics and control loops should be considered during the entire process of designing the micro-forming machine. To realise a good correlation between the results of measurement and multi-body simulation, the damping and stiffness parameters of the guiding system must be calibrated. The right geometrical dimensions should be determined after the optimisation of the kinematic- and dynamic-behaviour.

The multi-body simulation contains forces that usually include:

- Flexible connectors, such as a spring-dampers and pushers, which provide pre-defined compliant-force relationships
- Special force elements that provide a pre-defined force.
- Applied forces.
- Contact forces that specify how bodies react if they come into contact with each other while the model is in motion.
- Forming force.

The type of multi-body simulation required includes assembly analysis, static analysis, kinematic analysis and dynamics analysis.

2.3.3   Methods for dynamics analysis

Rigorously speaking, all physical structures behave dynamically when subjected to external actions such as loads and displacements. It is only when the loads or displacements are applied very slowly, that the dynamic effects can be neglected and the structural analysis can be treated as static: such an analysis is often referred to as quasi-static analysis. Whilst the dynamic effect can only be judged after a dynamic response analysis, the problem can basically be treated as a static problem if the

forces shake a structure at less than roughly one-third of its lowest natural frequency of vibration (Cook, 1981). More rapid shaking makes the inertia of the structure important and the problem must be considered as dynamic. In structural dynamics, the effect of damping can be significant and needs to be tackled properly.

Force equilibrium is fundamental in the dynamics analysis of structures. The equation of equilibrium as a function of time can be expressed by:

$$\mathbf{F}_I(t) + \mathbf{F}_D(t) + \mathbf{F}_S(t) = \mathbf{F}(t)$$

(2.1)

where the force vectors are all evaluated at time t and:

$F_I(t)$ is the vector of inertial forces,

$F_D(t)$ the vector of damping forces, or energy-dissipation forces,

$F_S(t)$ the vector of forces due to structural stiffness, and

$F(t)$ the vector of externally-applied loads.

Equation (2.1) is based on physical laws and is valid for both linear and non-linear systems if the equilibrium is established as per the deformed configuration of the structure.

A real structure has an infinite number of degrees-of-freedom. Therefore, the most critical step of structural analysis is to transform the problem into one with a finite number of degrees-of-freedom. For many structural problems, the approximation of linear structural behaviour is made to convert Eqn. (2.1) to a set of second-order, linear, differential equations (Cook, 1981; Wilson, 2002):

$$[M]\{\ddot{u}(t)\} + [C]\{\dot{u}(t)\} + [K]\{u(t)\} = \{F(t)\}$$

(2.2)

In the above equation, a dot over a letter denotes a derivative with respect to time, so $\{u(t)\}$, $\{\dot{u}(t)\}$ and $\{\ddot{u}(t)\}$ are the vectors of time-dependent nodal displacements, velocities and accelerations, respectively, and $[M]$, $[C]$ and $[K]$ are the mass matrix, damping matrix and stiffness matrix, respectively, of the structure. They are time-independent matrices in a linear regime. In a non-linear regime, they are constant in

one or a few time-steps, serving as linear approximations, and need to be updated if either material non-linearity or geometrical non-linearity develops.

Structural-dynamics problems fall into two broad classes: natural vibration (frequencies and the associated mode shapes) and dynamic response to rapid loading, impact, ground acceleration, etc. Furthermore, dynamic-response problems can be solved by either mode superposition or direct integration, and the direct integration can be fulfilled by the use of either an implicit method or an explicit method. Because of the complex nature of dynamic problems, it is usually difficult to say that a method is the best for all problems. Rather, a method can be superior to others in solving a certain class of problems. Some of the methodologies for dynamic structural analysis are reviewed briefly in the ensuing sub-sections. Chapter 7 presents a relatively-detailed description of the methods and algorithms frequently used in solving engineering problems.

2.3.3.1 Undamped free vibration

If there is no external loads acting on the structure, i.e. $\{F(t)\} = \{0\}$, and structural damping can be neglected, i.e. $[C] = [0]$, then the structural-dynamics problem reduces to undamped free vibration, which is governed by the differential equation:

$$[M]\{\ddot{u}(t)\} + [K]\{u(t)\} = \{0\} \tag{2.3}$$

Equation (2.3) can be transformed further to a linear eigenvalue equation:

$$([K] - \omega^2[M])\{\bar{u}\} = \{0\} \tag{2.4}$$

where ω^2 and $\{\bar{u}\}$ are respectively the eigenvalue and eigenvector.

This equation can be solved relatively easily by many numerical methods for eigenvalue problems. In the case of large structural problems, the sub-space iteration and the Lanczos method are often employed to solve the problem more economically.

It is also possible to find only the eigenvalues within a specified range or near to a specified value in order to cater for a particular problem and this has been implemented in most of the general-purpose programs.

2.3.3.2 Undamped harmonic response

Suppose the structure in question has zero damping, i.e. $[C]=[0]$, and is subjected only to steady-state harmonic loads:

$$\{F(t)\} = \{\overline{F}\}\sin(\overline{\omega}t)$$

(2.5)

where the vector $\{\overline{F}\}$ represents the amplitudes of the loads and is not a function of time, and $\overline{\omega}$ is the frequency of the input loads.

In this case the structural response is also harmonic and has a circular frequency $\overline{\omega}$. The solution of this problem can be transformed into one that is similar to the solution of a static problem. Therefore, many techniques to solve large-scale problems efficiently can be utilised.

2.3.3.3 General dynamic-response problem

The dynamic-response analysis of a structure with damping and subjected to external dynamic action requires the solution of Eqn. (2.2). There are two major types of method for such dynamics analysis, i.e. the modal method and direct integration. Furthermore, direct integration can be performed by the use of either explicit algorithms or implicit algorithms.

(1) The modal method

The modal method is also known as the mode-superposition method. The method can transform Eqn. (2.2) so that the displacement vector $\{u\}$ and its derivatives with respect to time are replaced by $\{z\}$ and its derivatives with respect to time, where $\{z\}$ is a vector of modal amplitudes. The transformed equations are uncoupled in the case where the damping matrix is orthogonal. The solutions of these modal equations are superimposed to yield the solution of the original problem (Clough and Penzien, 1975; Bathe and Wilson, 1976; Zienkiewicz, 1978).

The modal method is efficient if the response of the structure may be expressed in terms of a relatively small number of eigenmodes of the system. The orthogonality of the eigenmodes uncouples this system. Furthermore, only eigenmodes that are close to the frequency of interest are usually involved in the solution. For example, only

the lowest few frequencies are usually required to obtain an accurate estimate of a structure's linear dynamic response to relatively slow loading.

(2) Direct integration method

Direct integration is often referred to as step-by-step integration. Unlike the modal method, which decouples the dynamic equilibrium equation, the direct integration method directly copes with the equation of equilibrium. The direct integration may be either explicit or implicit. The explicit methods find $\{u\}_{t+\Delta t}$ from an equation written at time step t, while the implicit methods find $\{u\}_{t+\Delta t}$ from an equation written at time step $t + \Delta t$. Usually, the explicit methods require a small Δt, while the implicit methods allow a large Δt. However, solving the equations of implicit methods at each time step is more time consuming. Most explicit methods are conditionally stable. Most unconditionally stable methods are implicit, e.g. the Wilson-θ method. The critical time-step in the explicit methods is dictated by the smallest element (or the stiffest term in the element stiffness), so proper meshing can improve the efficiency. Most software packages of explicit methods provide an option of mass scaling to increase the critical time-step within an acceptable increase in mass.

(3) Remarks on dynamic-analysis methods

Generally, the mode-superposition method and the implicit direct method are more economical in inertial problems, whilst the explicit direct method is more economical in shock loading and wave-propagation problems (Cook, 1981). In linear problems, the modal method is favoured if only a few modes are needed to describe the response. For example, a vibrating machine may only excite the nearby frequencies of its support structure. In wave propagation and impact problems, many modes are excited and the response may be required for only a short time. In such a case, the explicit direct method would be favoured.

In non-linear problem, the modal method may still be favourable if the non-linearities are small and confined to a few regions in the structure. However, the modal method may require many modes if plastic action is to be followed properly. On the other hand, the explicit approach is often the best for non-linear problems, in particular, when extensive contacts are involved.

The form of matrices influences the choice of algorithm also. The damping matrix [C] must be orthogonal for the modal method. It must be diagonal (or null) for the explicit algorithm, but needs to have no special form for an efficient implicit algorithm. A non-diagonal damping matrix would drastically penalise the efficiency of an explicit method.

In addition to mode superposition and direct integration discussed above, it is also relevant to mention the frequency-domain approach for analysing structures under harmonic loading. The use of Fourier expansions eliminates the time variable, and hence Fast Fourier-Transformation can yield computational efficiency.

2.3.4 FE simulation of the micro-forming machine system

The finite element method (FEM) is the most powerful method that can be applied to a vast spectrum of physical problems if they are described as initial- or boundary-value problems. With the rapid development of software and hardware, the FEM is now successfully applied in the industrial world. However, from the users' point of view, three problems have to be pointed out (Mechanical Engineering Laboratory, 2006). (1) Mesh generation, an inevitable pre-requisite process for FE analysis, requires considerable time and effort, especially for three-dimensional cases. Although versatile pre-processors are available, user intervention is still required in FE modelling to enable the yielding of accurate results at an acceptable cost. (2) The quality of the solution not only depends on the quality of the mesh, but also on a suitable selection of element types and algorithm. (3) Distortion of the mesh, which can occur in highly non-linear FE analysis, sometimes causes failure to converge. Moreover, hour-glassing of elements using reduced integration may also be a matter of concern.

2.3.4.1 The types of FE simulation

The types of analysis of finite element simulations can be described as follows:

- Linear static analysis. Linear material properties and small deflections/rotations (geometric linearity) are considered in the analysis of the deformation and stress of a structure.

- Non-linear static analysis. Non-linear material properties, contact connection between components, or geometric non-linearity are considered in the analysis.

- Dynamics analysis. Dynamics analysis allows the examination of a structure with respect to time-varying effects. Dynamics analysis can be linear or non-linear. For a micro-forming machine system, the most important aspect is the analysis of normal mode dynamics to determine the vibration characteristics of a structure or structural components, as well as the analysis of the time-domain response of the machine and tool. Generally, these simulations are carried out separately for the process and the machine tool. Interactions between the machine tool, the workpiece and the process cause variations of the tolerances and characteristics of the workpiece, which are not taken into account by common simulation-approaches. An analysis and optimisation of the production process is only possible if all interactions between the machine tool, the workpiece and the process can be simulated accurately. Due to its time-dependent behaviour, the simulation of the machine tool and the process has to be carried out in the time domain (Altintas, et al., 2005). In the design of a micro-forming manufacturing system, the dynamic responses of the punches are normally taken as the critical parameter in the design of the system.

- Thermal analysis. The stress and temperature field in the cutting-tool edge and the finished workpiece surface are used in designing the cutting-edge shape as well as in optimising the feed, speed and depth of cut to avoid residual stresses in the finished surface (Altintas, et al., 2005). For a higher-speed machine, heat is generated during the forming process. When the temperature increases, the components expand. The analysis for the expansion of components, such as the punch tip or the die, is important for improving machining precision and preventing damage to the tool.

To realise the industrial application of the FE simulation of workpiece properties, both the simulation of the machine process interaction and the simulation of the workpiece properties will have to be improved in the future (Altintas, et al. ,2005).

2.3.4.2 Objectives of the dynamics analysis of the forming presses

For a micro-forming machine, the most important results required of the FE analysis are described as follows:

- The deflection of the central point of the tool under the forming process, the deflection of guiding ways, and the force in the guidance system.
- The natural frequency and mode shapes of the components, the machine tool, the feeder, the handling device, and the entire machine system.
- The stress distribution
- The temperature distribution and the thermal expansion of the components.

Based on the results of the above-mentioned analysis, the design of the micro-forming machine system can be improved and optimised.

2.4   Summary of findings

Micro-forming renders attractive characteristics to the mass-manufacture of miniature/micro-products. In addition to fundamental studies, more effort should be made to develop industrial equipment that matches the needs of the production of small-size products. The development of the micro-factory shows the trend of miniaturising the manufacturing machines and systems, the experience gained from which is useful in the development of micro-forming equipment. Finite element simulation is an efficient and economical approach to minimising structure mass, improving product precision and optimising micro-manufacturing machine system design.

2.5 References

Abott, E. J. and Firestone, F. A. (1933), 'Specifying Surface Quality,' *Mechanical Engineering,* 55, pp 569.

Altintas, Y., Brecher, C., Weck, M. and Witt, S. (2005), 'Virtual Machine Tool', *Annals of the report CIRPP*, Vol. 54/2, pp 651-772.

Archard, J. F. (1953), 'Contact and Rubbing Flat Surfaces,' *Journal of Applied Physics,* Vol. 24, pp 981-988.

Bahrami, M., Culham, J. R., Yovanovich, M. M. and Schneider, G. E. (2003), 'Review of Thermal Joint Resistance Models for Non-conforming Rough Surfaces in a Vacuum', *Proceedings of HTC'03, ASME Summer Heat Transfer Conference,* pp 1-21.

Bahrami, M., Culham, J. R., and Yovanovich, M. M. (2003), 'A Scale Analysis Approach to Thermal Contact Resistance,' *Paper No. IMEC2003-44283 ASME International Mechanical Engineering Congress and RDD Expo, November, pp 16-21.*

Bahrami, M., Culham, J. R., Yovanovich, M. M. and Schneider, G. E. (2003), 'Thermal Contact Resistance of Non-conforming Rough Surfaces, Part 1: Contact Mechanics Model,' *36th AIAA Thermophysics conference meeting and exhibit.*

Bahrami, M., Culham, J. R., Yovanovich, M. M. and Schneider, G. E. (2004), 'Thermal Resistance of Gaseous Gap for Conforming Rough Contacts,' *42th AIAA Thermophysics conference meeting and exhibit.*

Brecher, C. and Witt, S. (2004), 'Static, dynamic and Thermal Behaviour of Machine Tools with Regard to HPC,' *Proceedings of International CIRP Conference of High Performance Cutting (HPC),* pp 227-240.

Bowden, F. P. and Tabor, D. (1951), *Friction and Lubrication of Solid*, Oxford University Press, UK..

Chang, W. R., Etsion, I. and Bogy, D. B. (1987) 'An Elastic-plastic Model for The Contact of Rough Surfaces,' *J. Tribology,* Vol. 109, pp 257-263.

Chen X., Qin, Y. and Balendra, R. (2004), 'development of a statistical parameter-based surface model for the simulation of variation roughness with contact pressure,' *Journal of Mater. Process. Technol.* 145 pp 247-255.

Computers & Structure (2006) Available at:

  http://www.csiberkeley.com/support_technical_papers.html. [10 Dec 2006]

Cook, R. D. (1981), *Concepts and Applications of the Finite Element Analysis*, 2nd
Ed., John Wiley & Sons, New York

Cook, R. D. (1988) *Concept and Applications of Finite Element Analysis*, (Third ed.), *John Wiley, Madison*.

Cooper, M.G., Mikic, B. B. and Yovanovich, M. M. (1996), 'Thermal Contact Conductance,' *Int. J. Heat Mass Transfer,* Vol. 12, pp279-300.

Engel, R. and Eckstein, R. (2002), 'Microforming From Basic Research to Its Realisation,' *J. Mater. Process. Technol.* 125–126, pp. 35–44.

Francis, H. A. (1997), 'Application of spherical indentation mechanics to reversible and irreversible contact between rough surfaces,' *Wear*, 45, pp 221-269.

Gellert, M. and Haifa (1979) 'A direct Integration Method for Analysis of a Certain Class of Non-linear Dynamic Problems,' *ingenieur-Archiv*, 48 pp. 403-415.

Geiger, M. (2001) 'Micro-forming,' *Annals of the report CIRP*, Vol.50, pp 445-462.

Greenwood, J. A. and Williamson, B. P.,(1966), 'Contact of nominally flat surfaces,' *Proc., Roy. Soc., London,* pp 300-319.

Greenwood, J. A. (1967), 'The Area of Contact Between Rough surfaces and Flats,' *Journal of Lubrication Tech.,* pp 81-91.

Greenwood, J. A. and Tripp, J. H. (1967), 'The Elastic Contact of Rough Spheres,' *Journal of Applied Mechanics,* Vol.89, pp 153-159.

Groche, P. Schneider,R. (2004) 'Method for the Optimization of Forming Press for the manufacturing of micro parts,' *Annals of the report CIRP*, Vol. 53/1, pp.281-284.

Hess, A. (2000) 'Piezoelectric Driven Press for Production of Metallic Microparts by Forming,' *Proceedings of ACTUATOR 2000, 7th International Conference on New Actuators* Bremen, 19th–21st, pp. 427–430.

Holm, R.(1958), 'Electrical Contacts,' 3rd Ed. Springer Verlag, Berlin.

Ishigaki, H. (1978), 'Deformation Analysis of Large Sized Panels in the Press Shop,' *Mechanics of Sheet Metal Forming,* Plenum Press, pp 315-339.

Ishigaki, H. and Kawaguchi, I., (1979), 'A simple estimation of the elastic-plastic deformation of contacting asperities,' *Wear*, 177, pp 1-13.

Jung-Ho Park, K., Yoshida, Y., S. Nakasu, S. and Yokota (2002) 'A Resonantly-Driven Piezoelectric Micropump for Microfactory,' *Proceedings of ICMT 2002* Kitakyushu, pp. 417–422.

Keeler, S. P. (1978), 'Sheet Metal Stamping Technology-Need for Fundamental Understanding,' *Mechanics of Sheet Metal Forming,* Plenum Press, pp 3-17.

Kim B.C. and Kim S.W (2003), 'Absolute Interferometer for Three-dimensional Profile Measurement of Rough Surfaces,' *Optics Letters,* Vol.28, No.7, pp 528-530

Kobayashi, S. (1978), 'Deformation Analysis of Axisymmetric Sheet Metal Forming Processes by the Rigid-Plastic Finite Element Method,' *Mechanics of Sheet Metal Forming,* Plenum Press, pp 341-365.

Kucharski, S., Klimczak, T., Polijaniuk, A., and Kaczmarek, j. (1994), 'Finite-element model for the contact of rough surfaces,' *Wear* 1777, pp 1-13.

Lambert, M, A. and Fletcher, L. S. (1997), 'Thermal Contact Conductance of Spherical Rough Metals,' *Transactions of ASME,* Vol. 119, pp 684-690

Li X., Rosen, B. G. and Amini N. (2004), 'Surface Lay Effect on Rough Friction in Roller Contact,' *Wear,* Vol. 257, Issue 12, pp 1301-1307.

Lundberg, J. (1995),'Influence of surface roughness on normal-sliding lubrication,' *Tribol. Int.* 28 (5), pp. 317–322.

Marciniak, Z. (1978), 'Sheet Metal Forming Limits,' *Mechanics of Sheet Metal Forming,* Plenum Press, pp 215-234.

Mechanical Engineering Laboratory (2006), Available at http://www.mel.go.jp.

Mikic, B. B. and Rohsenow, W. M. (1966), 'Thermal contact conductance,' *Technical Report N4542-42, Dept. of Mech. Eng. MIT, Camridge, Massachustts, NASA* Contract No. NGR 22-009-06, September.

Mishima, N., Ashida, K., Tanikawa, T. and Maekawa, H. (2002), 'Design of a Micro-factory,' *Proceedings of the ASME Design Engineering Technical Conference-7th Design for Manufacturing Conference,* Vol. 3, pp 103-110.

Mishima, N. (2002), 'Design of a Miniature Manufacturing System for Micro-fabrication,' *Proceedings of the 10th ISPE International Conference on Concurrent Engineering,* pp 1129-1135.

Mumin S. (2007), 'Effect of Surface Roughness on Friction Coefficients During Upsetting Processes for Different Materials,' *Material and Design,* Vol. 28, Issue 2, pp 633-640.

Nakano, K. (1997), 'Process of Cold Forging,' *JSTP Int. Seminar on Precision Forging*, pp 141-14-7.

Neugebauer, R., Noack, S. and Klug, D. (2003), 'Simulation of Energy Flow in Hydraulic Drives of Forming Machines,' *1st International Conference on computational Method in Fluid Power Technology,* pp 333-348.

Nine, H. D. (1978), 'Drawbead Forces in Sheet Metal Forming,' *Mechanics of Sheet Metal Forming,* Plenum Press, pp 179-213.

Nishino, K., Yamashita, S. and Torii, K. (1995), 'Thermal Contact Conductance Under Low Applied Load in a Vacuum Environment,' *Experimental Thermal and Fluid Science,* Elsevier, New York*, 10*, pp 258-271.

Okazaki, Y., Mishima, N. and Ashda, K. (2002), 'Micro-factory and Micro Machine Tools,' *Proceedings of the 1ˢᵗ Korea-Japan Conference on Positioning Technology.* KIMM, Daejeon, Korea, pp 1-6.

Onions, R. A. and Archard, J. F. (1973), 'The contact of Surfaces Having a Random Structure,' *Journal of Physics D.,* 6, pp 289-304.

Paldan, N.A., Arentoft, M., Eriksen, R. S. and Mangeot, C. (2008), 'Piezo Driven Prestressing of Die-system for Microforming of Metal Components,' *Int J Mater Form,* Suppl 1, pp 467-470.

Park, J. H. (2002) 'Resontly-Driven Piezoelectric Micro Pump for Microfactory,' *Proc. Of ICMT*, Kitakyushu, pp.417-422.

Pritschow, G. and Cronn, N. (2002), 'Simulation Environment for Machine Tools,' *Production Engineering,* 9/2, pp 63-66.

Proche, P. and Schnecier, R. (2004), 'Method for The Optimization of Forming Presses for the Manufacturing of Micro Parts,' *Annals of the report CIRP*, Vol. 53/1, pp.281-284.

Pollen, J. and Williamson, J. B. P. (1972), 'On the Plastic Contact of Rough Surfaces,' *Roy. Soc. London,* A327, pp159-173.

P-Withen, C., Marstrand, J.R. and Arentoft, M. (2005), 'Flexible Tool System for Cold Forming of Micro-components,' *First International Conference on Multi-Material Micro Manufacture,* Germany, pp 143-146.

Qin, Y. (2006), 'Micro-forming and Miniature Manufacture system-development Needs and Perspectives,' *J. Mater. Process. Technol.* 177, pp 8-18.

Qin, Y. (2006), 'Forming-Tool Design Innovation and Intelligent Tool-Structure/system Concept,' *International Journal of Machine Tool and Manufacture,* Vol. 46, No.11, pp 1253-1260.

Qin, Y. (2010), Micro-Manufacturing Engineering and Technology, *ELSEVIER.*

Razali, R., Qin, Y., Harrison C. and Brockett, A. (2009), 'Investigation of Feeding Devices and Development of Design Considerations for a new Feeder for Micro-

sheet-forming,' *International Journal of Nanomanufacturing,* Vol.3, No 1/2, pp 45-54.

Rehsteiner, F., Weikert, S. and Rak, Z. (1998), 'Accuracy Optimization of machine Tools under Acceleration Loads for the Demands of High-Speed Machining,' *Proceedings of the ASPE 1998 Annual Meeting.*

Saotome,Y. and Iwazaki, H. (2002), 'Super-plastic Backward Micro-extrusion of Micro-parts for Micro-electro-mechanical Systems,' *J. Mater. Process. Technol.* 119 (1–3), pp. 307–311.

Saotome, Y. and Iwazaki, H. (2001) 'Super-plastic Extrusion of Microgear Shaft of 10 μm in Module,' *Microsyst. Technol.* 7, pp. 126–129.

Saotome, Y. and Okamoto, T. (2001), 'An in-situ incremental Microforming System for Three-dimensional Shell Structures of Foil Materials,' *J. Mater. Process. Technol.* 113, pp. 636–640.

SCHMIDT technology (2007), Available at: http://www.schmidtpresses.com/servo.html. (29 May 2007)

Schmoeckel, D. (1992), 'Cold and Hot forming Machine,' J. of Mater. Process *Technol.* Vol.35, No. 3-4, pp 399-413.

Spath, D. and Neithardt, W. (2002), 'Optimized design with topology and shape optimisation,' *Journal of Engineering Manufacture,* 219 Part B, pp 1187-1191.

Sridhar M. R. and Yovannovich, M. M. (1994), Review of elastic and plastic contact conductance models: comparson with experiment,' J. Thermophys. Heat Transfer 8 (4) pp 633-641.

Thomas J. R. Hughes (1987), 'The Finite Element Method-Linear Static and Dynamic Finite Element Analysis,' *Prentice Hall.*

Wert J. A., Thomsen, C., Jensen, R. D., and Arentoft, M., (2009), 'Forming of Bulk Metallic Glass Microcomponents,' *Journal of Materials Processing Technology,* 209 (2009) pp 1570-1579.

Weule, H., Albers, A., Haberkern, A., Neithardt, W. and Emmrich, D. (2002), 'Computer Aided Optimisation of the Static and Dynamic Properties of Parallel

Kinematics,' *Proceedings of the 3rd Chemnitz Parallel Cinematic Seminar,* pp527-546.

Weule, H., Fleischer, J., Neithardt, W., Emmrich, D. and Just, D. (2003), 'Structure Optimization of Machine Tools including the static and dynamic workspace behavior,' *Proceedings of the 36th CIRP International Seminar on Manufacturing System*, pp269-272.

Whitehouse, D. J. and Achard, J. F. (1970), 'The Properties of Radom Surfaces of Significance in Their Contact,' *Proc. Roy. Soc. London,* A316, pp 97-121.

Williamson, J.B., Pullen, J., Hunt, R. T., and Leonard, D., 'the shape of solid surfaces,' *Surface Mechniacs, ASME, New York,* pp 24-35.

Wilson, E.L., Farhoomand, I. and Bathe, K.J. (1973) 'Nonlinear Dynamic analysis of Complex Structures,' *Earthquake Engineering and Structure Dynamics.* 1, pp.241-252.

Wilson, E. L. (2002), *Three-Dimensional Static and Dynamic analysis of Structures*, 3rd Ed., Computers and Structures, Inc., Berkley, California, USA

Wilson, W. R. D. (1978), 'Friction and Lubrication in Sheet Metal Forming,' *Mechanics of Sheet Metal Forming,* Plenum Press, pp 157-177..

Yovanovich, M. M. (1969), 'Overall Constriction Resistance Between Contacting Rough, Wavy Surfaces,' *Int. J. Heat Mass Transfer 12,* pp 1519-1520.

Zaeh, M. F. and Baudisch, T. (2003), 'Simulation environment for designing the dynamic motion behaviour of the mechatronic system machine tool,' *Proceedings of the Institution of Mechanical Engineers Part B: Journal of Engineering Manufacture,* Vol. 217, pp 1031-1035.

Zhao, Y., Majetta, D. M. and Chang, L. (2000), 'An Asperity Microcontact Model Incorporating The Transition From Elastic Deformation to Fully Plastic Flow,' *Trans. of ASME,* Vol.122pp 86-93.

http://www.csiberkeley.com/support_technical_papers.html

http://www.engineeshandbook.com:80/Tables/frictioncoefficients.htm

http://www.schmidtpresses.com/servo.html

http://www.rogmesh.co.uk

Chapter 3 Experimental Investigation of Surface-Contact Characteristics

3.1   Introduction

Surface roughness is a basic physical characteristic of engineering surfaces. The need for knowledge of surface profiles arises in a variety of contexts ranging from purely theoretical problems to practical applications (Varnier, et al., 1984). A statistical method is efficient in giving a description of surface behaviour due to the random asperity-distribution. The ISO1997 standard is used in this study. The parameters are described in Appendix B. Surface-characteristic changes have been investigated through experimental measurements. Parameters such as interfacial pressure, interfacial temperature, roughness of the contacting metal surface and lubricant are taken into account during the experiments. The thermal conductance of the metal contact-surfaces has been measured for different contact situations.

The following are the problems to be investigated in this chapter:

- What are the changes of the characteristics of the surfaces in contact after being compressed at different interface pressures?
- What is the influence of the lubricant on the thermal conductance of the metal surfaces in contact?
- What is the relation between the thermal conductance and the contacting pressure?
- What is the influence of the surfaces in contact on the situation of the lubricant retained on the surfaces after being compressed?

3.2   Equipment

The equipment used in the experiments includes surface-measuring equipment and thermal-conductance measuring equipment: details of the equipment are given in the following sections.

3.2.1 Surface-measuring equipment

A Surface-Roughness Measurement Machine SV-2000 is used to measure the surface roughness of the specimens before and after interfacial pressure is applied, and the measurement data is analysed using the SURFPAK software. The Surface-Roughness Measurement Machine SV-2000 is shown in Fig. A3.1.

3.2.2 Thermal-contact-conductance measuring equipment

This system includes a heating system, a cooling system, an insulating system, eight thermocouples, an upper tool and a lower tool, a specimen, and a pressure-applying system: the latter includes a load cell and a hydraulic driver. The load cell and thermocouples are connected to a data-acquisition system. The heating system, cooling system and insulating system work together to make a steady one-dimensional temperature field along the axis of the tools and provide a test temperature in the range of 30-280 °C at the contact interfaces. A 500kN load cell is installed and the experiment can be carried out under an interface pressure of up to 800MPa. The tools and specimen can be changed enabling this equipment to be used to investigate the influence of interfacial pressure, interfacial temperature, surface texture, material, lubricant, and thickness of specimen, on the thermal-contact-conductance.

Both the upper tool and the lower tool are the parts of thermal-contact-conductance measuring equipment: they are cylinders of 18mm diameter, made of N1019 steel. The thermal conductivity of N1019 steel was measured at the National Physical Laboratory (NPL), and was defined by the following empirical equation:

$$k = 19.2561 + 1.43 \times 10^{-2} T + 3.4699 \times 10^{-6} \times T^2$$

This equation can be used for temperature up to 300°C. The tools were heat-treated to a hardness of HRC (High Rupturing Capacity) 58-62 prior to use. The surfaces of the tools were ground to a surface roughness of between 0.2~0.3 μm. A drawing of this equipment is shown in Fig. A3.2: the equipment was used previously to measure

the thermal conductance of dry metal surfaces in contact (Chen, 2002 and Rosochowska, et al., 2004).

3.2.3 Heater

The 1/16 DIN Temperature Controller Series 96 has one universal input, a second auxiliary input, and four outputs. The Series 96 can be programmed to perform temperature measurement, input event-switching, remote-set-point input, hearting, boost heating, cooling, and digital communication.

3.2.4 Cooler

The coolers are digital- and programmable-controllers. The digital circulating-bath and programmable circulating-bath are designed to provide precise fluid-temperature control: the temperature range is from 5 to 200ºC and temperature stability is ± 0.1ºC, which values can be affected by viscosity, specific heat and external heat-loss.

3.2.5 Data-acquisition system

The data-acquisition system consists of the following parts:

1) DAQ Card-1200
2) SCXI-1000 4-slot chassis
3) SCXI-1120 and SCXI-1121 modules
4) SCXI-1321 and SCXI-1328 terminal blocks
5) A computer system

3.2.6 Equipment for calibrating the thermocouples

The equipment for calibrating the thermocouples consists of the following parts, as shown in Fig. A3.3.

1) INFT 1000 –KF/E temperature indicator
2) TC08-300SKSUP-G-SLE-200-TT-K-24-1000WIRE calibrated thermocouple

3) A tank filled with oil that can be used over a temperature range of from −20 to 288ºC

4) Data-acquisition system

3.2.7 Analytical balance

The analytical balance is a high-precision item of equipment. Its vernier division is 0.1mg. It is used to weigh the specimens before and after dry powder lubricants are applied.

Dry powder lubricant, sprayed onto the surface of the specimens, can absorb water from the atmosphere and show a weight gain. Conversely, an open vessel containing a liquid such as water is prone to evaporation. Thus, in practice, the temperature and humidity of the laboratory should be kept stable. The specimen and lubricant should be allowed to acquire the laboratory temperature before being used.

The analytical balance is very sensitive to the environment: even a very gentle wind, a different temperature or slight vibration can influence the result. Thus the balance should be used carefully and the environment retained as unchanging as possible. It is important to ensure that the balance reading is zero before use.

3.2.8 Specimen

Specimens with different surface-roughness and different thickness, which are used for surface-characteristics analysis and thermal-conductance measurement, are shown in Fig. A3.4. They are cylinders of 18mm diameter and of different thicknesses. The surfaces of the specimens should be isotropic and uniform. Macro-irregularities of the surfaces should be as small as possible.

The specimens are made of 080M15(En32C) steel. The grade of surface roughness is defined as follows:

Table 3.1 Grade of surface roughness

Grade of surface roughness	A	B	C	D
Surface roughness Ra (μm)	0.37-0.48	0.74-0.94	1.74-2.21	2.49-2.86

The specimen code is designated R-T-P-L, where R stands for the surface roughness, T for the thickness of the specimen, P for the interfacial pressure, and L for the lubricant.

3.3 Contact-surface-characteristics measurement

Surface profiles of the dry contact surface and the contact surface with lubricant have been measured under different interfacial pressure. The details of the measurements are presented in Sub-sections 3.3.1 and 3.3.3 respectively, whilst the measured results are presented in Sub-sections 3.3.2 and 3.3.4 respectively.

3.3.1 Measurement of dry contact surfaces

Experiments have been conducted under an interfacial temperature of 100ºC and an interfacial pressure ranging from 100MPa to 600MPa. For dry contact surfaces, the experimental process can be described as follows:

Step 1 Cleaning the surface of the specimen

Step 2 Measuring the surface profile of the specimen

Step 3 Putting the specimen into the equipment

Step 4 Setting control system

Step 5 Applying pressure up to the design value

Step 6 Unloading

Step 7 Taking the specimen out of the equipment

Step 8 Measuring the surface profile of the specimen again

3.3.2 Results for dry contact surfaces

The measured results for surface-profile parameters for specimen B-3.5-300-Dry at an interfacial temperature of 100ºC are shown in Table 3.2 to Table 3.6. Figs. A3.5

and A3.6 show the surface-roughness change after contact pressures of 300MPa and 600MPa are applied respectively. Fig. A3.7 provides a comparison between the two cases. Figs. A3.8 to A3.11 show the change of parameters A1, A2, R_{pk} and Mr1 respectively. The definitions of these parameters are presented in Appendix B. In the figures above the range of the original surface-roughness is from grade A to grade D.

Fig. A3.12 presents a comparison of the bearing area curve (BAC) before and after the surface is compressed for specimens with original-roughness grade B. The applied interfacial pressures are 100, 200, 300, 400 and 600MPa. Fig. A3.13 shows the bearing area curves before and after a contact pressure of 600MPa is applied to specimens of original roughness grade C and under dry contact. Figs. A3.14 to A3.17 show the measured results for the amplitude-distribution function curve for specimens of surface roughness grade B under different contact pressures.

Table 3.2   Symbol used in Table 3.3 to Table 3.6

d1	Direction 1 on the surface of a specimen
d2	Direction 2 on the surface of a specimen. d1 and d2 are perpendicular to each other
s1	The first surface of a specimen
s2	The second surface of a specimen
Av1	The average value of a parameter in direction d1 and in direction d2 on the first surface of a specimen
Av2	The average value of a parameter in direction d1 and in direction d2 on the second surface of a specimen
R1	Measured result for the original surface
R2	Measured result for the surface after being compressed
Av1-Av1	Av1(R1)-Av1(R2)
Av2-Av2	Av2(R1)-Av2(R2)

Table 3.3   Surface-measurement results for specimen A-3.5-300-Dry
Contact pressure p=300MPa

Parameters	R1						R2						Av1-Av1	Av2-Av2
	s1-d1	s1-d2	s2-d1	s2-d2	Av1	Av2	s1-d1	s1-d2	s2-d1	s2-d2	Av1	Av2		
Ra	0.364	0.373	0.389	0.393	0.3685	0.391	0.351	0.371	0.354	0.344	0.361	0.349	0.0075	0.042
Rq	0.487	0.551	0.522	0.54	0.519	0.531	0.502	0.506	0.47	0.44	0.504	0.455	0.015	0.076
Rsk	-0.824	-1.438	-1.193	-1.112	-1.131	-1.1525	-1.839	-1.664	-1.18	-0.656	-1.7515	-0.918	0.6205	-0.2345
Rku	7.19	9.901	7.843	7.139	8.5455	7.491	12.519	9.74	6.508	3.584	11.1295	5.046	-2.584	2.445
Rp	1.413	1.408	1.253	1.158	1.4105	1.2055	0.936	1.021	0.942	1.012	0.9785	0.977	0.432	0.2285
Rv	2.249	2.896	2.631	2.646	2.5725	2.6385	2.997	2.843	2.331	1.599	2.92	1.965	-0.3475	0.6735
Rz	3.661	4.305	3.883	3.804	3.983	3.8435	3.933	3.864	3.273	2.61	3.8985	2.9415	0.0845	0.902
Rt	6.585	8.877	6.764	7.015	7.731	6.8895	7.312	6.317	4.808	3.447	6.8145	4.1275	0.9165	2.762
Rc	1.679	2.416	1.635	1.827	2.0475	1.731	1.995	1.639	1.522	1.346	1.817	1.434	0.2305	0.297
RSm	0.056	0.097	0.059	0.054	0.0765	0.0565	0.083	0.064	0.045	0.04	0.0735	0.0425	0.003	0.014
Rdq	0.139	0.14	0.141	0.142	0.1395	0.1415	0.14	0.14	0.135	0.129	0.14	0.132	-0.0005	0.0095
Rk	1.08	0.962	1.161	1.091	1.021	1.126	0.956	1.055	1.042	1.035	1.0055	1.0385	0.0155	0.0875
Rpk	0.454	0.484	0.327	0.337	0.469	0.332	0.262	0.23	0.237	0.263	0.246	0.25	0.223	0.082
Rvk	0.731	0.908	0.788	0.897	0.8195	0.8425	0.864	0.86	0.775	0.625	0.862	0.7	-0.0425	0.1425
Mr1	7.75	10.015	8.019	8.913	8.8825	8.466	8.206	4.738	6.321	7.451	6.472	6.886	2.4105	1.58
Mr2	87.152	84.671	87.029	85.591	85.9115	86.31	85.294	84.792	86.328	85.488	85.043	85.908	0.8685	0.402
A1	1.759	2.424	1.311	1.504	2.0915	1.4075	1.074	0.544	0.749	0.981	0.809	0.865	1.2825	0.5425
A2	4.698	6.961	5.112	6.461	5.8295	5.7865	6.351	6.541	5.295	4.533	6.446	4.914	-0.6165	0.8725

Table 3.4 Surface-measurement results for specimen B-3.5-300-Dry
Contact pressure p=300MPa

Parameters	R1						R2						Av1-Av1	Av2-Av2
	s1-d1	s1-d2	s2-d1	s2-d2	Av1	Av2	s1-d1	s1-d2	s2-d1	s2-d2	Av1	Av2		
Ra	0.833	0.828	0.75	0.768	0.8305	0.759	0.851	0.749	0.703	0.716	0.8	0.7095	0.0305	0.0495
Rq	1.072	1.074	0.955	0.985	1.073	0.97	1.064	0.929	0.894	0.895	0.9965	0.8945	0.0765	0.0755
Rsk	-0.904	-0.911	-0.552	-0.841	-0.9075	-0.6965	-1.006	-0.816	-1.054	-0.848	-0.911	-0.951	0.0035	0.2545
Rku	4.28	3.983	3.472	4.132	4.1315	3.802	3.97	3.391	4.534	3.6	3.6805	4.067	0.451	-0.265
Rp	2.074	2.056	1.99	1.923	2.065	1.9565	1.733	1.679	1.481	1.547	1.706	1.514	0.359	0.4425
Rv	4.139	3.858	3.235	3.792	3.9985	3.5135	3.982	3.393	3.589	3.206	3.6875	3.3975	0.311	0.116
Rz	6.213	5.913	5.225	5.714	6.063	5.4695	5.714	5.072	5.07	4.752	5.393	4.911	0.67	0.5585
Rt	8.398	7.165	6.762	6.853	7.7815	6.8075	7.649	6.334	6.432	5.828	6.9915	6.13	0.79	0.6775
Rc	3.333	3.233	2.877	2.951	3.283	2.914	3.167	2.89	2.555	2.666	3.0285	2.6105	0.2545	0.3035
RSm	0.076	0.066	0.066	0.064	0.071	0.065	0.071	0.077	0.063	0.06	0.074	0.0615	-0.003	0.0035
Rdq	0.184	0.192	0.174	0.181	0.188	0.1775	0.187	0.171	0.172	0.174	0.179	0.173	0.009	0.0045
Rk	2.38	2.314	2.286	2.316	2.347	2.301	2.08	2.285	2.151	2.006	2.1825	2.0785	0.1645	0.2225
Rpk	0.503	0.597	0.593	0.449	0.55	0.521	0.37	0.448	0.264	0.321	0.409	0.2925	0.141	0.2285
Rvk	1.674	1.781	1.345	1.625	1.7275	1.485	1.718	1.316	1.344	1.386	1.517	1.365	0.2105	0.12
Mr1	6.18	7.241	8.918	6.753	6.7105	7.8355	4.365	3.35	2.45	4.025	3.8575	3.2375	2.853	4.598
Mr2	83.812	83.94	87.146	87.197	83.876	87.1715	78.241	84.94	85.456	83.272	81.5905	84.364	2.2855	2.8075
A1	1.553	2.162	2.644	1.517	1.8575	2.0805	0.808	0.75	0.323	0.645	0.779	0.484	1.0785	1.5965
A2	13.553	14.298	8.644	10.403	13.9255	9.5235	18.695	9.907	9.776	11.596	14.301	10.686	-0.3755	-1.1625

Table3.5　　Surface-measurement results for specimen C-3.5-300-Dry

Contact pressure p=300MPa

Parameters	R1						R2						Av1-Av1	Av2-Av2
	s1-d1	s1-d2	s2-d1	s2-d2	Av1	Av2	s1-d1	s1-d2	s2-d1	s2-d2	Av1	Av2		
Ra	2.001	1.991	2.061	1.848	1.996	1.9545	1.857	2.02	1.934	1.867	1.9385	1.9005	0.0575	0.054
Rq	2.526	2.5	2.603	2.366	2.513	2.4845	2.286	2.529	2.35	2.316	2.4075	2.333	0.1055	0.1515
Rsk	-0.152	-0.042	0.421	-0.004	-0.097	0.2085	-0.302	-0.488	-0.19	-0.711	-0.395	-0.4505	0.298	0.659
Rku	3.214	3.016	3.07	2.998	3.115	3.034	2.814	3.317	2.406	3.384	3.0655	2.895	0.0495	0.139
Rp	5.89	6.408	7.187	6.237	6.149	6.712	4.513	4.709	4.301	3.67	4.611	3.9855	1.538	2.7265
Rv	7.541	6.736	5.54	6.135	7.1385	5.8375	6.878	7.491	6.027	7.819	7.1845	6.923	-0.046	-1.0855
Rz	13.431	13.144	12.727	12.372	13.2875	12.5495	11.392	12.201	10.329	11.489	11.7965	10.909	1.491	1.6405
Rt	16.651	16.723	15.287	13.828	16.687	14.5575	17.46	17.704	14.414	14.773	17.582	14.5935	-0.895	-0.036
Rc	7.945	7.241	8.072	8.03	7.593	8.051	6.976	8.027	6.683	6.387	7.5015	6.535	0.0915	1.516
RSm	0.101	0.098	0.119	0.097	0.0995	0.108	0.098	0.123	0.098	0.109	0.1105	0.1035	-0.011	0.0045
Rdq	0.308	0.299	0.302	0.301	0.3035	0.3015	0.266	0.27	0.241	0.247	0.268	0.244	0.0355	0.0575
Rk	6.094	6.304	6.119	5.146	6.199	5.6325	6.328	6.811	6.324	6.029	6.5695	6.1765	-0.3705	-0.544
Rpk	2.176	2.378	3.175	2.616	2.277	2.8955	1.427	1.109	1.257	0.591	1.268	0.924	1.009	1.9715
Rvk	3.024	2.652	1.944	2.756	2.838	2.35	2.427	3.052	1.938	3.077	2.7395	2.5075	0.0985	-0.1575
Mr1	12.386	9.698	13.794	14.752	11.042	14.273	6.187	6.569	9.082	3.459	6.378	6.2705	4.664	8.0025
Mr2	90.001	88.978	90.21	87.19	89.4895	88.7	90.635	89.533	89.866	86.893	90.084	88.3795	-0.5945	0.3205
A1	13.477	11.532	21.9	19.293	12.5045	20.5965	4.414	3.643	5.707	1.022	4.0285	3.3645	8.476	17.232
A2	15.116	14.613	9.516	17.649	14.8645	13.5825	11.366	15.971	9.822	20.167	13.6685	14.9945	1.196	-1.412

Table 3.6   Surface-measurement results for specimen D-3.5-300-Dry
Contact pressure p=300MPa

Parameters	R1						R2						Av1-Av1	Av2-Av2
	s1-d1	s1-d2	s2-d1	s2-d2	Av1	Av2	s1-d1	s1-d2	s2-d1	s2-d2	Av1	Av2		
Ra	2.824	2.768	2.538	2.663	2.796	2.6005	2.435	2.69	2.159	2.289	2.5625	2.36075	0.2335	0.23975
Rq	3.609	3.595	3.232	3.274	3.602	3.253	2.933	3.3	2.68	2.802	3.1165	2.89825	0.4855	0.35475
Rsk	0.256	0.571	0.185	0.212	0.4135	0.1985	-0.096	-0.33	-0.125	-0.205	-0.213	-0.169	0.6265	0.3675
Rku	3.281	3.807	2.946	2.823	3.544	2.8845	2.269	2.615	2.881	2.527	2.442	2.6615	1.102	0.223
Rp	9.86	10.538	8.431	8.706	10.199	8.5685	5.642	5.9	5.464	5.185	5.771	5.6175	4.428	2.951
Rv	9.589	8.81	7.644	7.855	9.1995	7.7495	6.599	8.511	7.451	7.318	7.555	7.503	1.6445	0.2465
Rz	19.448	19.347	16.075	16.562	19.3975	16.3185	12.241	14.411	12.915	12.504	13.326	13.1205	6.0715	3.198
Rt	23.932	26.38	20.041	18.373	25.156	19.207	14.622	17.729	16.353	14.628	16.1755	16.2643	8.9805	2.94275
Rc	11.425	10.94	10.538	10.184	11.1825	10.361	8.675	8.779	8.287	8.674	8.727	8.507	2.4555	1.854
RSm	0.136	0.157	0.15	0.126	0.1465	0.138	0.138	0.123	0.126	0.14	0.1305	0.12825	0.016	0.00975
Rdq	0.343	0.308	0.293	0.306	0.3255	0.2995	0.23	0.258	0.254	0.241	0.244	0.249	0.0815	0.0505
Rk	8.25	8.07	7.318	8.928	8.16	8.123	8.372	9.014	6.803	7.285	8.693	7.748	-0.533	0.375
Rpk	4.393	4.93	3.821	3.458	4.6615	3.6395	1.286	1.34	2.153	1.506	1.313	1.733	3.3485	1.9065
Rvk	3.728	3.432	3.108	2.439	3.58	2.7735	2.506	3.257	3.119	2.813	2.8815	3.00025	0.6985	-0.2268
Mr1	14.211	13.882	14.109	9.164	14.0465	11.6365	6.193	7.521	13.276	10.793	6.857	10.0665	7.1895	1.57
Mr2	90.304	90.218	88.185	92.359	90.261	90.272	90.845	88.722	91.427	89.78	89.7835	90.6053	0.4775	-0.3333
A1	31.218	34.22	26.955	15.842	32.719	21.3985	3.982	5.04	14.293	8.126	4.511	9.402	28.208	11.9965
A2	18.072	16.789	18.362	9.317	17.4305	13.8395	11.471	18.364	13.37	14.377	14.9175	14.1438	2.513	-0.3043

3.3.3 Measurement of lubricated surfaces

Two kinds of lubricants are used on the surfaces of the specimens, i.e. Turmlyb MDC and Rapid GT. They can be applied by spraying them onto the surfaces of the specimens. In order to form a uniform lubricant layer on a surface and an equal quantity between the surfaces of the specimens, pre-experiments have been undertaken. Table 3.7 shows an example of the pre-experiment for lubricant quantity.

Table 3.7   Test of lubricant quantity

Specimen No.	Lubricant	Spray Times	Specimen Weight (mg)	Specimen Weight +Lubricant(mg)	Lubricant Weight (mg)
1	GT	1	5956.8	5958.5	1.7
2	GT	2	8034.6	8036.8	2.2
3	GT	3	7996.4	8001	4.6
4	GT	4	7981.5	7990.5	9
5	MDC	1	7863.5	7865	1.5
6	MDC	2	7951.2	7953.8	2.6
7	MDC	3	8000.8	8004.6	3.8
8	MDC	4	8023.9	8029.3	5.4

The method for this experiment can be described as follows:

Step 1   Cleaning the surfaces of the specimen

Step 2   Marking the surface order and direction

Step 3   Measuring the surfaces roughness of the specimen

Step 4   Weighing the specimen using the Analysis Balance

Step 5   Spraying lubricant onto the surfaces of the specimen

Step 6   Weighing the specimen again

Step 7   Putting the specimen into the equipment

Step 8   Setting the control system

Step 9   Applying pressure up to the designated value

Step 10   Unloading

Step 11   Taking the specimen out of the equipment

Step 12   Measuring the surface of the specimen again

Step 13   Cleaning the lubricant remaining on the surface

Step 14   Measuring the surface of the specimen again

After Step 6, if the lubricant is not of equal quantity between the different surfaces, Steps 5 and 6 need to be repeated until the result conforms with the designated value.

3.3.4   Results for lubricated surfaces

Fig. A3.18 presents the bearing area curves (BAC) of the surface of specimen C-3-600-MDC: (a) is the result for the original surface of the specimen; and (b) is the result for the surface of the specimen after a contact pressure of 600MPa has been applied at an interfacial temperature of 100ºC with lubricant MDC being used. Fig. A3.19 shows the BAC of the surface of specimen C-4-600-MDC: (a) is the result for the surface of the specimen after a contact pressure of 600MPa has been applied at an interfacial temperature of 100°C, with lubricant MDC being used; and (b) is the measured result for the same specimen after the remaining lubricant MDC on the surface has been removed. Fig. A3.20 shows a comparison of the BAC between the surfaces before and after lubricant is removed: (a) is for the case of lubricant GT; and (b) is for the case of lubricant MDC.

3.4   Surface roughness measurement of the micro-stamping tool

Surface roughness is a major characteristic of the workpiece and the tool. It has a significant influence on the friction properties and thermal conductance of the contact surfaces and makes a contribution to the precision of the tool. At the beginning of the forming process, the tool is in contact with just the peaks of the asperities of the rough surfaces; therefore, the frictional properties depend on the distribution of the asperities, their height and their deformation during the forming process (Mumin, et al., 2007). With flattening of asperities of the surface of the workpiece the real contact area with the tool becomes larger, which results in varying

frictional properties between the workpiece and the tool (Dieter, 1984; Lange, 1985; Male and Cockroft, 1964). In micro-stamping tool design, contacts between components are involved. The frictional forces have a significant influence on the precision of the micro-stamping tool and the control system. The contacts between the components of the micro-stamping tool are as follows:

- Contact of the top plate and the ram
- Contact of the punch guide plate and the die plate
- Contact of the blank holder and the material
- Contact of the linear guides and the rollers
- Contact of the material with the die

In order to be able to choose a suitable value of the friction coefficient, the surface roughness of the components of a micro-stamping tool is measured. The results of measurement are listed in Table 3.8.

Table 3.8 Surface roughness of the components of the micro-stamping tool

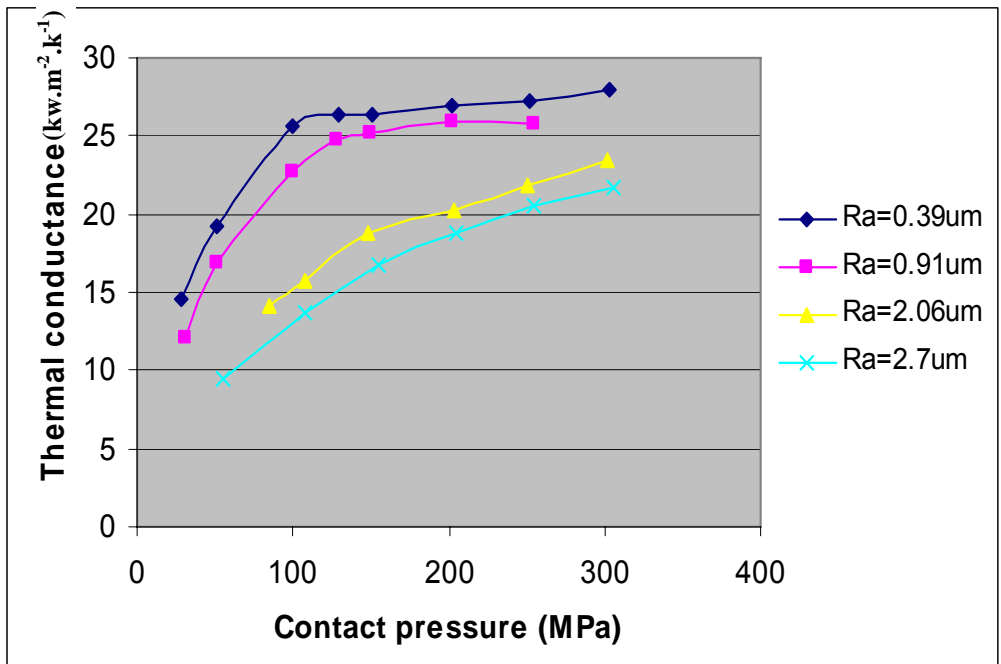| Components	Roughness (μm)
Top plate-1	1.105
Top plate-2	0.779
Punch guide plate-1	1.252
Punch guide plate-2	1.681
Die plate-1	1.252
Die plate-2	2.14
Blankholder-1	0.977
Blankholder-2	0.931
Die-1	0.316
Die-2	0.277
Material-1 (carbon-steel strip)	0.156
Material-2 (stainless-steel strip)	0.150
Scale guide plate (used for mounting the sensor for the experiments)	0.124

3.5   Thermal-conductance measurement

The thermal-contact resistance greatly reduces the heat flow in many machines, their elements, or other constructions (Piotr, Tomasz and Wisnieskki, 2002). The aim of this experiment is to investigate the influence of the contact-surface roughness and the lubricants on the thermal conductance of the contact surfaces under different contact pressures.

The differential equation of heat conduction is:

$$\nabla\left(k(T)\nabla T\right) + \varphi = \rho c \frac{\partial T}{\partial \tau} \qquad (3.1)$$

where:

τ is time

T, temperature

k, conductivity

ρ, mass density of the heat-transfer material

∇, Laplace operator

φ, rate of internal energy generation

For the steady temperature field $\dfrac{\partial T}{\partial \tau} = 0$. If there is no internal energy generation, then $\varphi = 0$. Therefore Eqn. (3.1) is simplified to Eqn. (3.2)

$$\nabla\left(k(T)\nabla T\right) = 0$$
$$k(T)\nabla T = q \qquad (3.2)$$

where q denotes heat flux density.

In the case of the present equipment, the heat flow is only along the axis of the tool. This means that Eqn. (3.2) can be further reduced to:

$$k(T)\frac{dT}{dz} = q \qquad (3.3)$$

where z is the direction of the axis of the tool. In the case of the heat flowing through the interface of the metal surfaces in contact, $\frac{dT}{dz}$ is recorded as ∇T, and $k(T)$ is recorded as $H(T)$. In order to obtain the thermal conductance $H(T)$, the values of ∇T and q should be known.

The tools in the equipment for thermal conductance measurement are made from steel N1019. The thermal conductivity is then:

$$
\begin{aligned}
k(T) &= a + bT + cT^2 \\
&= 19.2561 + 1.33 \times 10^{-2} T + 3.4699 \times 10^{-6} T^2
\end{aligned}
\tag{3.4}
$$

From Eqns. (3.3) and (3.4), Eqn. (3.5) can be deduced:

$$
aT + \frac{b}{2}T^2 + \frac{c}{3}T^3 = qz + c_0
\tag{3.5}
$$

Two groups of four thermocouples are installed in the upper tool and the lower tool. The arrangement of the thermocouples is shown in Fig. A3.2. Substituting the experimental results of temperature into Eqn. (3.5), Eqn. (3.6) is obtained:

$$
\begin{aligned}
aT_1 + \frac{b}{2}T_1^2 + \frac{c}{3}T_1^3 &= qz_1 + c_0 \\
aT_2 + \frac{b}{2}T_2^2 + \frac{c}{3}T_2^3 &= qz_2 + c_0 \\
aT_3 + \frac{b}{2}T_3^2 + \frac{c}{3}T_3^3 &= qz_3 + c_0 \\
aT_4 + \frac{b}{2}T_4^2 + \frac{c}{3}T_4^3 &= qz_4 + c_0
\end{aligned}
\tag{3.6}
$$

where z_i (i=1, 2, 3 and 4) are the positions of the thermocouples and T_i are the measured results of temperature. Quantities q and c_0 are solved using a regression method. It is easy to find the thermal conductance $H(T)$ using q, c_0, ∇T and Eqn. (3.3).

3.5.1 Thermocouple calibration

Eight K-type thermocouples are used. These thermocouples can be used in the range of temperature of between –200 and 1000ºC. This kind of thermocouple usually has a precision of about ±1.0ºC, or greater than ±1.0ºC at high temperature. The thermocouples need to be calibrated before they are installed in the equipment to be able to achieve such a high precision

The thermocouples are calibrated using the thermocouple-calibration equipment (see Section 3.2.6). The calibration method can be described as follows:

- Filling the tank with oil
- Covering the tank with insulating material
- Bundling the 8 thermocouples and reference thermocouples together
- Connecting the reference thermocouple with the temperature indicator
- Connecting the 8 thermocouples with the DAQ system
- Connecting the DAQ system to the computer
- Heating the oil to beyond the temperature range of the measurement
- Switching off the heater
- Starting to record as soon as the temperature field becomes uniform

The results of the calibration are analysed using a regression method. The relationship between the compensation temperature and the results of the calibration of the thermocouples were obtained as follows:

Thermocouple No.1 $\qquad \Delta T = 1.542 \times 10^{-2} T_{ref} - 1.168$

Thermocouple No.2 $\qquad \Delta T = 1.215 \times 10^{-2} T_{ref} - 1.341$

Thermocouple No.3 $\qquad \Delta T = 1.529 \times 10^{-2} T_{ref} - 1.495$

Thermocouple No.4 $\qquad \Delta T = 1.212 \times 10^{-2} T_{ref} - 1.141$

Thermocouple No.5 $\qquad \Delta T = 1.387 \times 10^{-2} T_{ref} - 1.004$

Thermocouple No.6 $\qquad \Delta T = 1.275 \times 10^{-2} T_{ref} - 0.888$

Thermocouple No.7 $\quad\quad\quad\quad \Delta T = 1.318 \times 10^{-2} T_{ref} - 0.713$

Thermocouple No.8 $\quad\quad\quad\quad \Delta T = 1.5.423 \times 10^{-2} T_{ref} - 0.104$

where ΔT is the compensation temperature and T_{ref} is the temperature of the reference thermocouple. The calibration results for the eight thermocouples are also shown in Figs. A3.21 to A3.28.

3.5.2 Dry contact surface

Four specimens with different surface roughness are used for the measurement of the thermal conductance of the contact surfaces. The details of the specimens are listed below:

Specimen with surface roughness grade A, Ra=0.39μm
Specimen with surface roughness grade B, Ra=0.91μm
Specimen with surface roughness grade C, Ra=2.06μm
Specimen with surface roughness grade D, Ra=2.7μm

The process of the experiment follows the same steps as were presented in Section 3.3.1. After the specimen is put into position, the contact pressure is increased continuously and held by the pressure-applying system when taking the readings. The results of measurement for the thermal conductance of the dry contact surfaces are given in Section 3.5.4.

3.5.3 Lubricated surfaces

Two kinds of lubricants are used in this experiment: namely lubricant MDC and lubricant GT. Specimens with surface roughness grade B and grade C are employed. Different quantities of the lubricants are designed to be used on the contact surfaces with different surface roughness. The details of the lubricated surfaces are listed below:

Lubricant	Surface roughness	Weight of lubricant (mg)
MDC	Grade B	6.4
MDC	Grade C	2.1
GT	Grade B	0.1
GT	Grade C	0.1

The process of the experiment follows the same steps as presented in Section 3.3.2. After the specimen is put into position, the contact pressure is increased continuously and held by the pressure-applying system when taking the readings. The results of measurement are given in Section 3.5.4.

3.5.4 Results and discussion

The results for the thermal conductance of dry contact surface with surface roughness grade A are shown in Fig. A3.29. Two specimens with surface roughness Ra=0.38μm and 0.39μm are used. The results for the thermal conductance of dry contact surface with surface roughness grade B (Ra=0.91μm), grade C (Ra=2.06μm) and grade D (Ra=2.7μm) are presented in Figs. A3.30, A3.31 and A3.32 respectively. A comparison of the results for different contact surfaces is shown in Fig. 3.1. The results of repeated tests of dry contact surface of a surface roughness grade A and surface roughness grade B are shown in Fig. A3.29 and Fig. 3.2 respectively.

The results for the thermal conductance of lubricated contact surface with surface roughness grade B and grade C are shown in Figs. 3.3 and 3.4. The quantities of lubricant MDC and GT used are presented in Section 3.5.3.

Measurement results of the surface roughness of the blankholder, the die plate and the materials are shown in Table 3.8.

The results of thermal conductance of the metal surfaces in contact were obtained based on the assumption that the thermal conductance at the upper and lower interfaces of the specimen is equal. But the temperature is different at the upper surface and the lower surface of the specimen due to the thickness of the specimen.

This may have a slight influence on the results. In further studies, if this influence can be considered the accuracy could be improved.

Table 3.8 Surface roughness of the components of the micro-stamping tool

Components	Roughness (μm)
Top plate-1	1.105
Top plate-2	0.779
Punch guide plate-1	1.252
Punch guide plate-2	1.681
Die plate-1	1.252
Die plate-2	2.14
Blankholder-1	0.977
Blankholder-2	0.931
Die-1	0.316
Die-2	0.277
Material-1 (carbon-steel strip)	0.156
Material-2 (stainless-steel strip)	0.150
Scale guide plate (used for mounting the sensor for the experiments)	0.124

Fig. 3.1   Comparison of the thermal conductance between different contact surface roughnesses
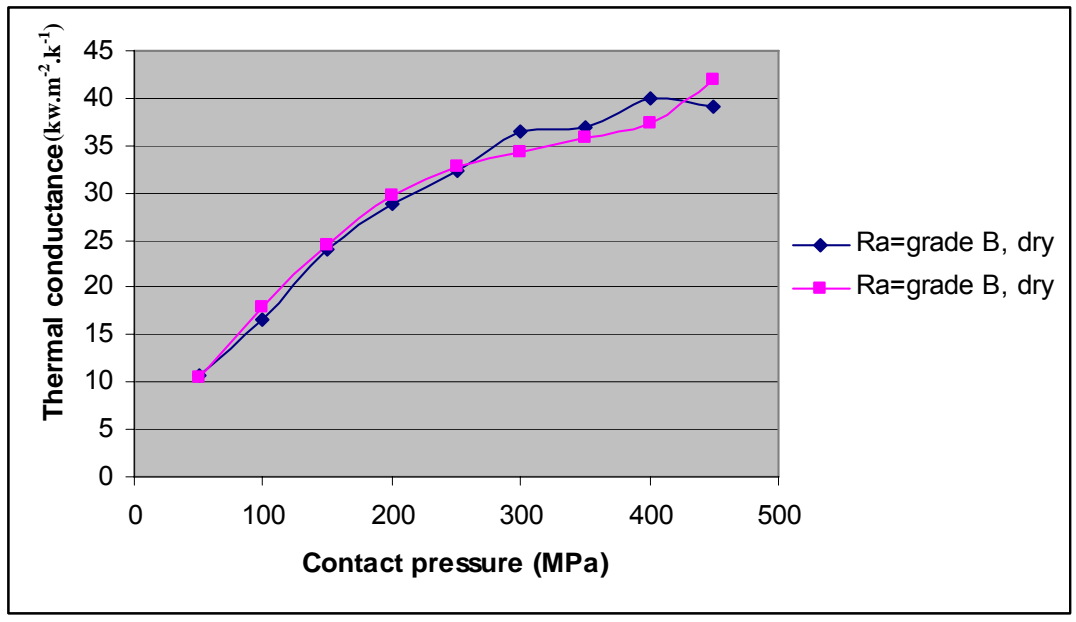
Fig. 3.2   Thermal conductance of dry contact surface with roughness grade B
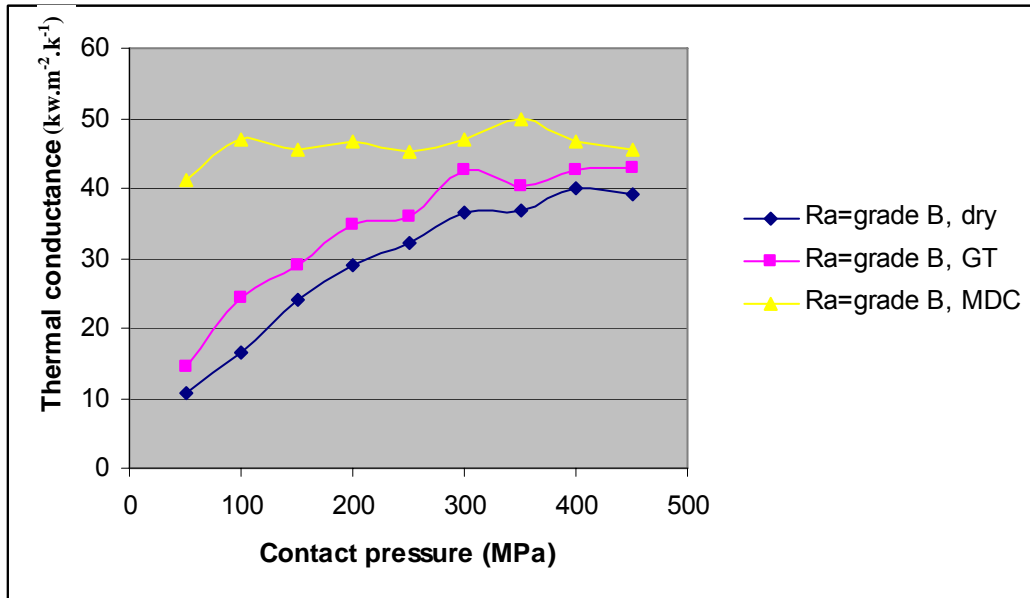
**Fig. 3.3   Comparison of thermal conductance between a dry surface
and a lubricated surface with roughness grade B**
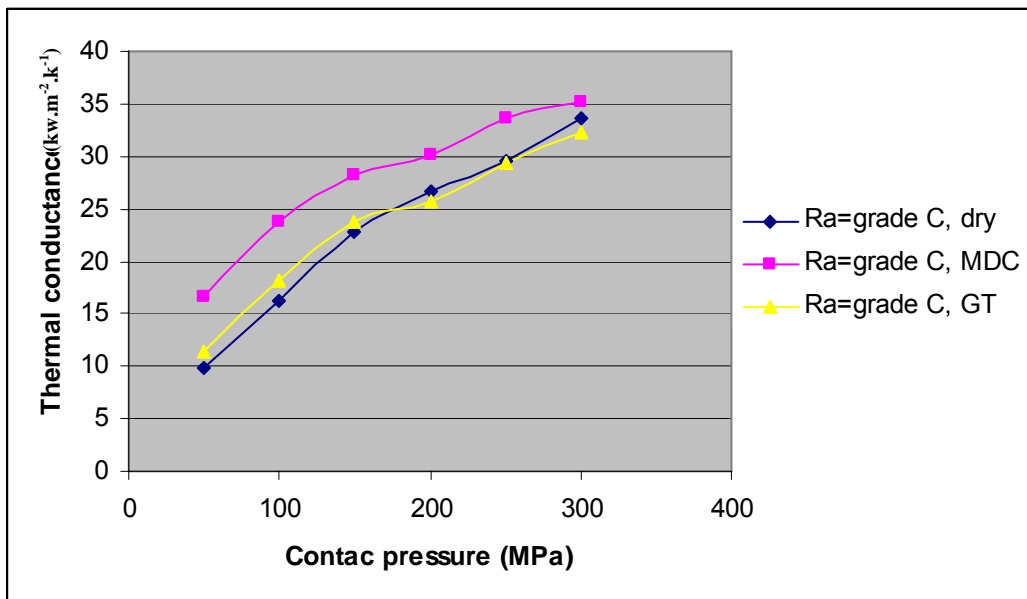
**Fig. 3.4   Comparison of thermal conductance between dry surface and
lubricated surface with roughness grade C**

3.6   Conclusions

- The quantity of lubricant used on the surface of the specimens has a significant influence on the thermal conductance of the solid contact surfaces. In Fig. 3.35, when 6.4mg lubricant MDC is used on the surface of the specimen the thermal conductance appears to be constant. The reason for this is that the lubricant nearly fully covers the surface of specimen. In this situation the thermal conductance of the contact surface is governed mainly by the thermal properties of the lubricant. However, in Fig. 3.36, when 2.1mg lubricant MDC is used on a surface of the specimen with surface-roughness grade C, the thermal conductance changes with the increase of the contact pressure, but is always greater than it is with dry contact surfaces. The reason for this is that the lubricant fills the valley of the rough surface, but does not completely cover the contact surface. The thermal conductance of the contact surface is only partly dependent on the thermal properties of the lubricant.

- Not only does the surface roughness have a significant influence on the thermal conductance of the metal surface in contact, but also the lubricant affects it. In the micro-stamping tool design the lubricant should be used to prevent the rollers and linear guide from over-heating. Therefore the thermal properties of a lubricant that will be used for micro-stamping tool is important.

- If two pieces of flat metal are made progressively smoother, a point will be reached where the resistance to relative movement increases. If their surfaces are very flat and smooth, and all of the surface contaminants are removed, the surfaces will actually adhere to each other (Friction, http://hyperphysics.phy-astr.gsu.edu/Hbase/frict.html#fri).

- In the design of the micro-stamping tool, the blankholder and lower die plate are used to hold the material strip during the stamping process. Therefore a greater friction force is expected. In order to obtain a greater friction force, the surface roughness of both the blankholder and the lower die plate should be small and close to that of the surface of the material strip. It can reduce the

danger of workpiece damage due to the strip loosing when the punch leaves the die.

3.7   References

Chen, X., (2002), 'Precision Cold Forming Modelling Interfacial Thermal Parameter Investigation and Tool Design Optimisation,' *University of Strathclyde,* PhD thesis.

Dieter GE, (1984), 'Mechanical metallurgy,' *Second ed, McGraw-Hill International Book Company.*

Friction, http://hyperphysics.phy-astr.gsu.edu/Hbase/frict.html#fri

Lange, K., (1985), 'Handbook of metal forming'. *McGraw-Hill International Book Company.*

Male AR, Cockroft MG, (1964), 'A method for the deformation of coefficient of friction of metals under bulk plastic deformation,' J. Ins. Met, pp 38-46

Piotr Furmanski, Tomasz, S. Wisniewski, (2002), 'Thermal Contact Resistance and Other Thermal Phenomena at Solid-Solid Interface,' *Institute of Heat Engineering Warsaw University of Technology.*

Rosochowska, M., Chodnikiewocz, K. and Balendra, R., (2004), 'A new method of measuring thermal contact conductance,' *Journal of Materials Processing Technology,* 145, pp 207-214.

Surface Profile Parameters,
http://www/parkafm.co.kr/c_board/upfile/surface%20Profiles.Pdf

Surface Roughness Profile Parameters,
http://www/Phase2pluse.com/surfaceroughnessteste/profile-parameter.htm

Varnier, F., Rasigni, G., Palmari, J.P., Lieberia, A. and Rasigni, M., (1984), 'Influence of some parameters on the surface profile restored from microdensitometer analysis of electron micrographs of surface replicas,' *Applied Optics,* Vol.23, No. 20, pp3705-3717.

3.8   Appendix A – Figures

Fig. A3.1 Surface-roughness measurement equipment SV-2000
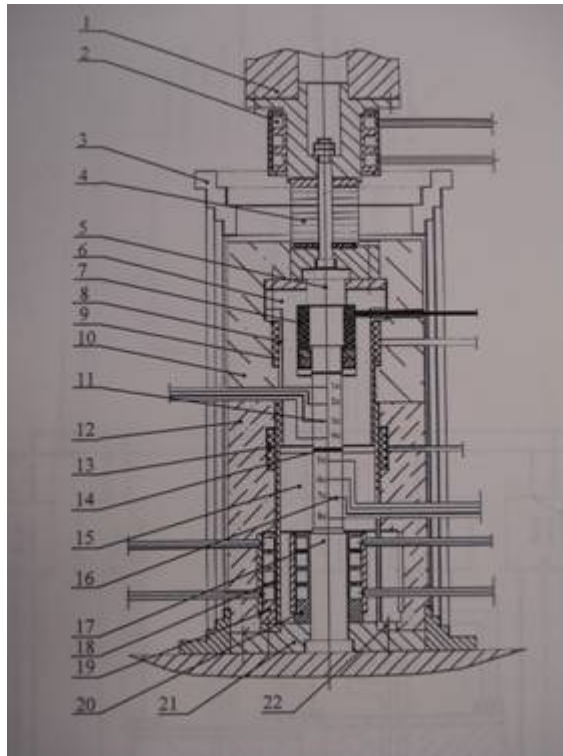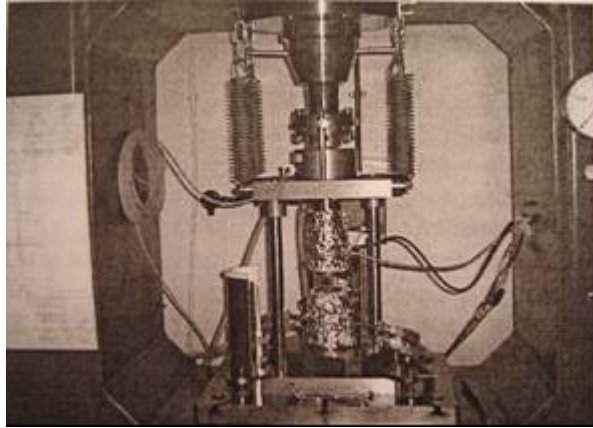
1. Load cell
2. Upper-cooler
3. Radiation shield
4. Insulator
5. Upper-tool
6. Upper insulator
7. Main heater
8. Upper frame
9. Upper compensation heater
10. Insulator
11. Thermocouples in upper tool
12. Insulator
13. Lower compensation heater
14. Specimen
15. Insulator
16. Thermocouples in lower tool
17. Lower tool
18. Lower frame
19. Outer cooler
20. Inner cooler
21. Seat
22. Lower frame

Fig. A3.2   Experimental equipment
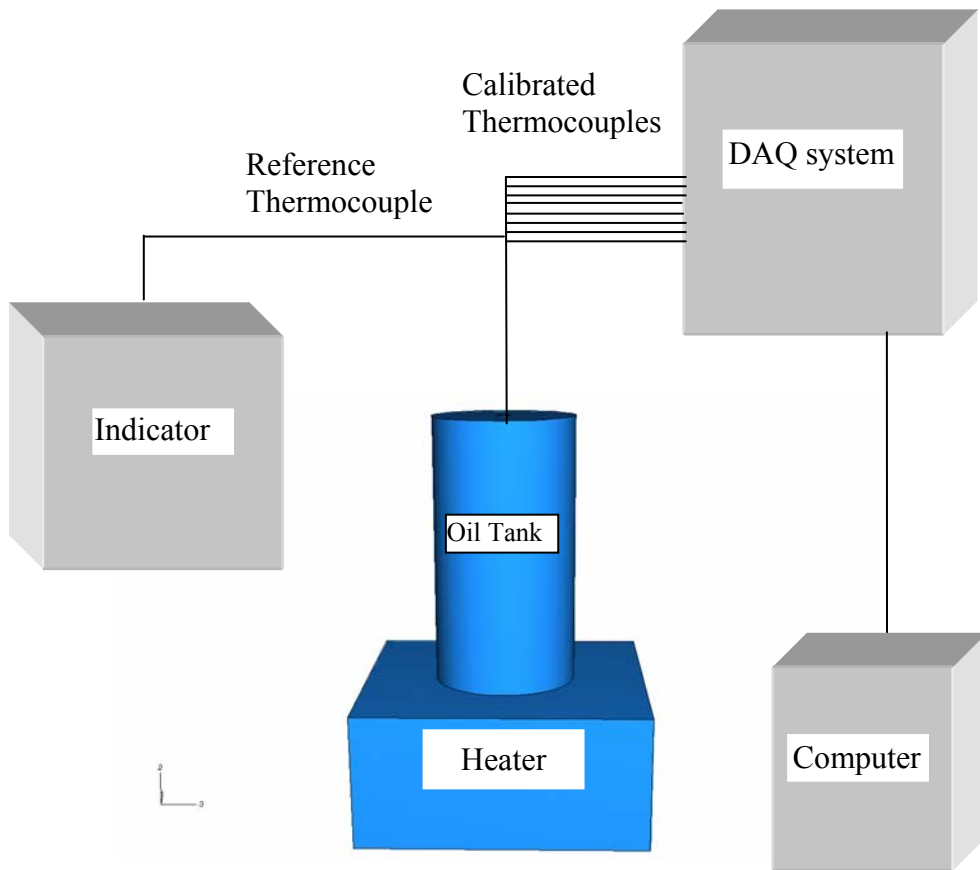
Fig. A3.3   System for calibrating the thermocouples

Fig. A3.4   Specimens

Contact pressure p=300MPa								
Ra	Δ Ra							
0.3685	0.0075							
0.8305	0.0305							
1.996	0.0575							
2.796	0.2335							
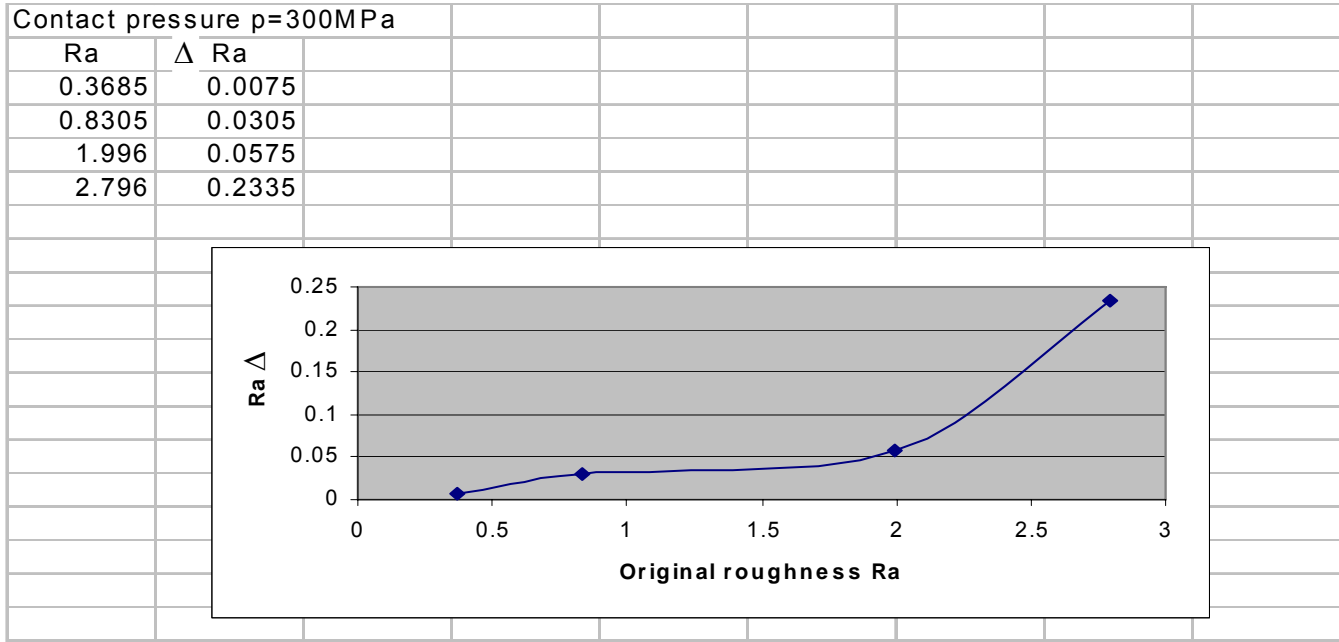
Fig. A3.5   ΔRa at interfacial pressure 300MPa

Contact pressure p=600MPa									
Ra	Δ Ra								
0.487	0.062								
0.988	0.103								
1.933	0.336								
2.01	0.337								
2.518	0.463								
3.01	0.817								
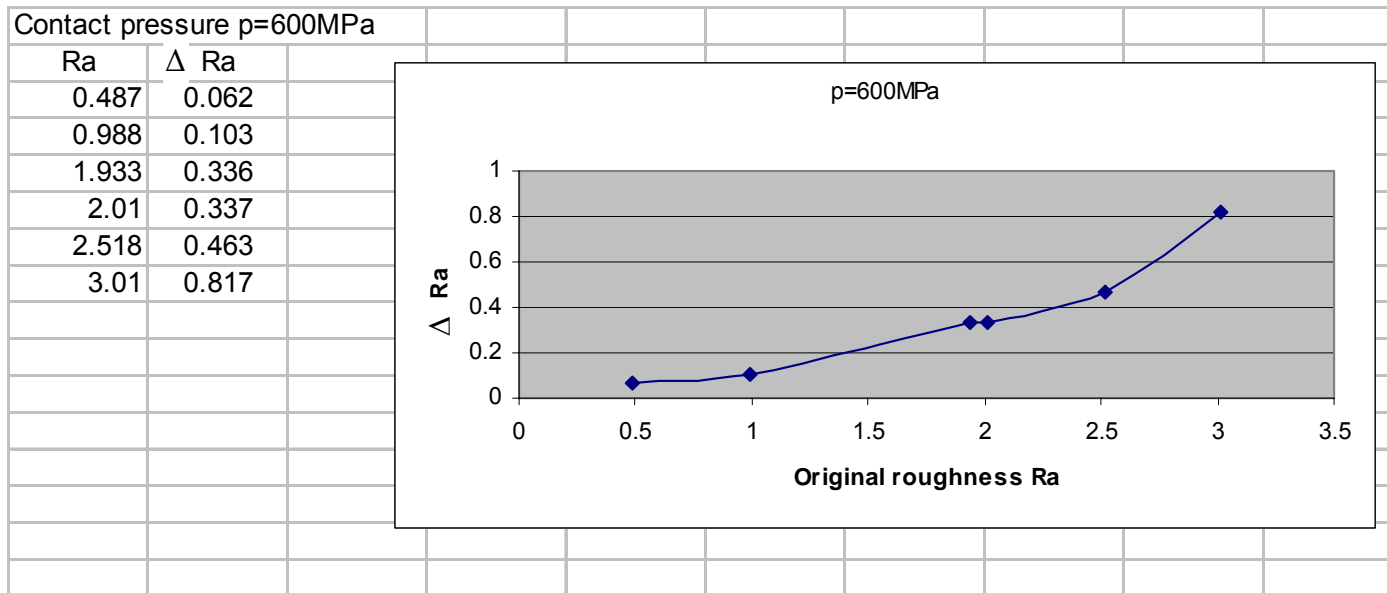
Fig. A3.6   ΔRa at interfacial pressure 600MPa

Contact pressure p=600MPa			Contact pressure p=300MPa		
Ra	Δ Ra		Ra	Δ Ra	
0.487	0.062		0.3685	0.0075	
0.988	0.103		0.8305	0.0305	
1.933	0.336		1.996	0.0575	
2.01	0.337		2.796	0.2335	
2.518	0.463				
3.01	0.817				
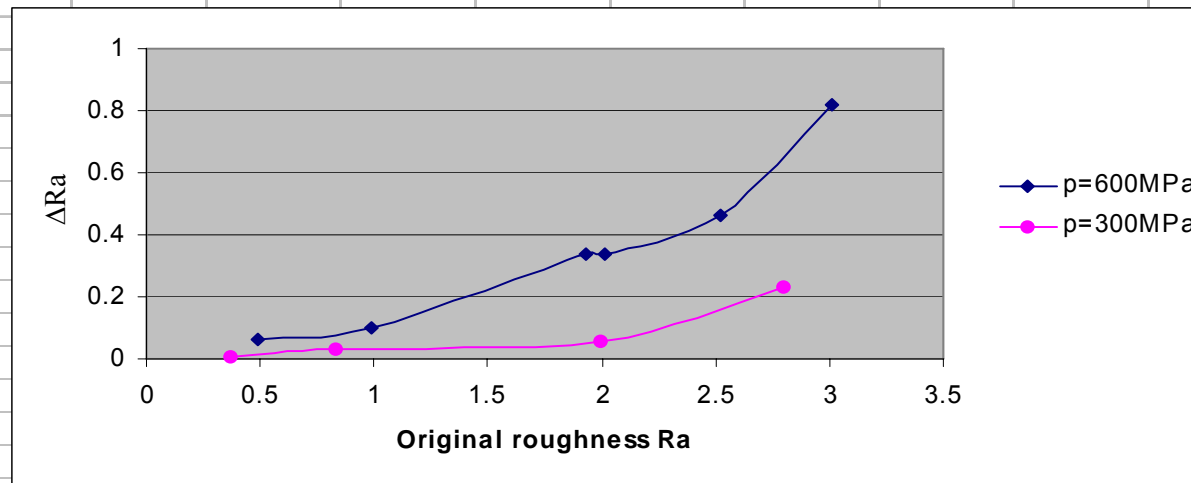
Fig. A3.7 ΔRa after the surface has been compressed

ΔA1after experiment p=300MPa , main heater setting 200 ºC and dry contact

A1	ΔA1
1.8575	1.0785
2.0915	1.2825
12.5045	8.476
32.719	28.208
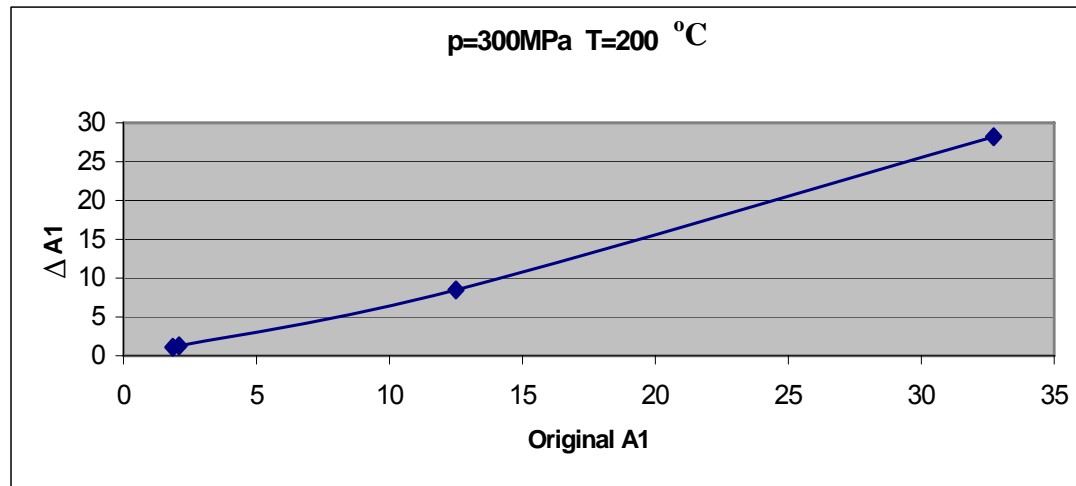
Fig. A3.8 ΔA1 after an experiment at an interfacial pressure of 300MPa, a main heater at 200ºC and dry contact

Δ A2 after experiment p=300MPa,main heater setting 200 ºC and dry contact		
A2	ΔA2	Ra
5.8295	-0.6165	0.368
13.9255	-0.3755	0.83
14.86	1.196	1.99
17.4305	2.513	2.79

p=300MPa T=200 ^{o}C

Fig. A3.9   ΔA2 as a function of original roughness Ra

$\triangle$ Rpk after experiment at p=300MPa, main heater setting 200 ^{o}C and dry contact												
Rpk	$\triangle$ Rpk											
0.469	0.223											
0.55	0.141											
2.277	1.009											
4.6615	3.3485											
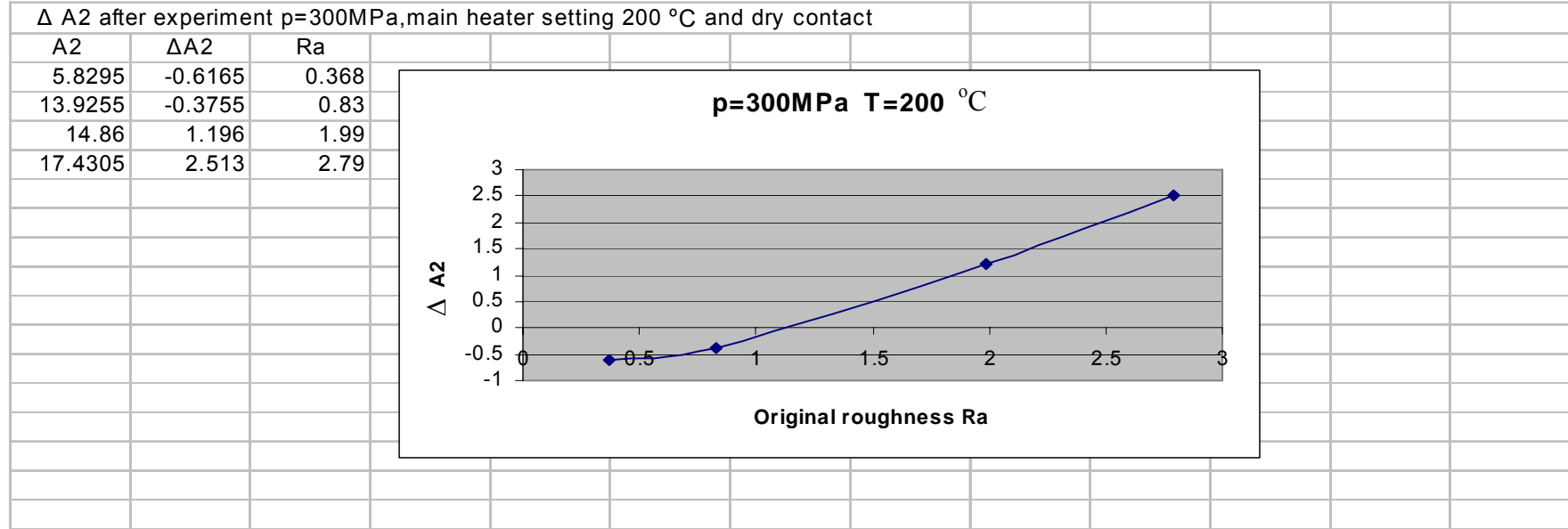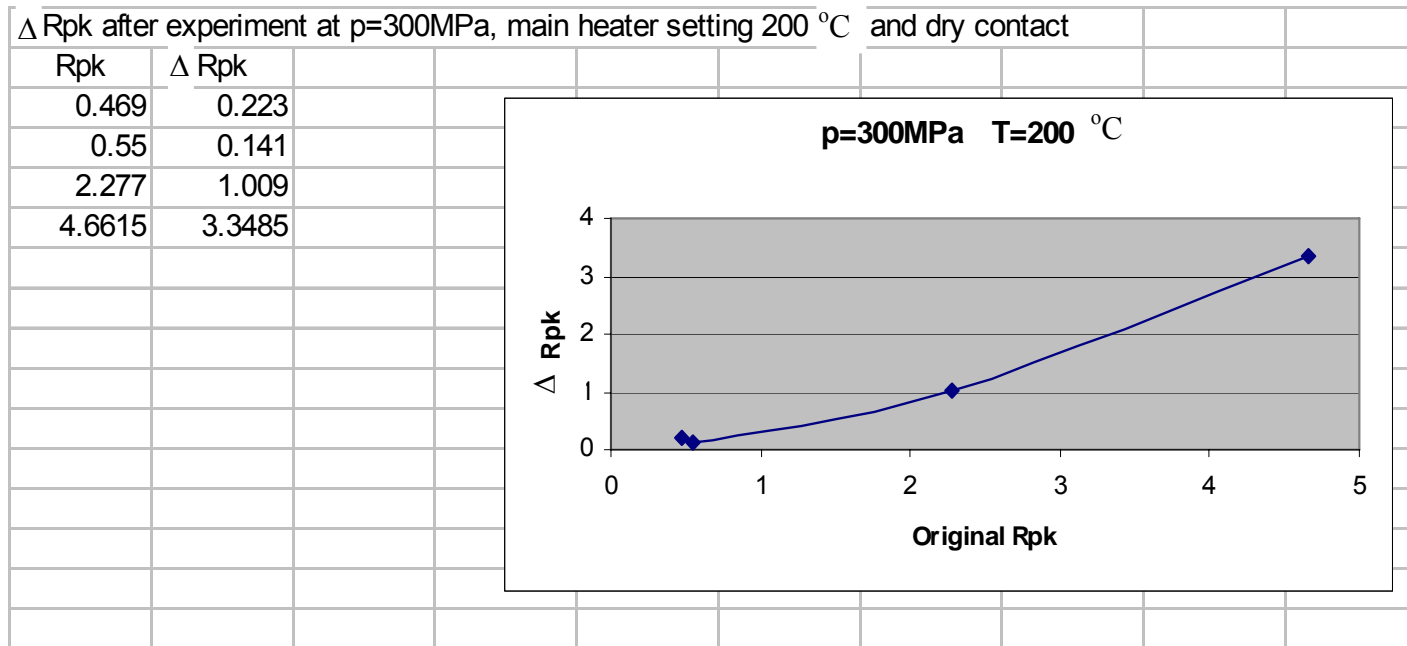
Fig. A3.10 ΔR_{pk} for an interfacial pressure of 300MPa, a main heater at 200ºC and dry contact

Δ Mr1after experiment at p=300MPa,main heater setting 200 °C and dry contact		
Ra	Δ Mr1	
0.39	2.41	
0.83	2.85	
1.99	4.66	
2.79	7.19	

p=300MPa T=200 °C
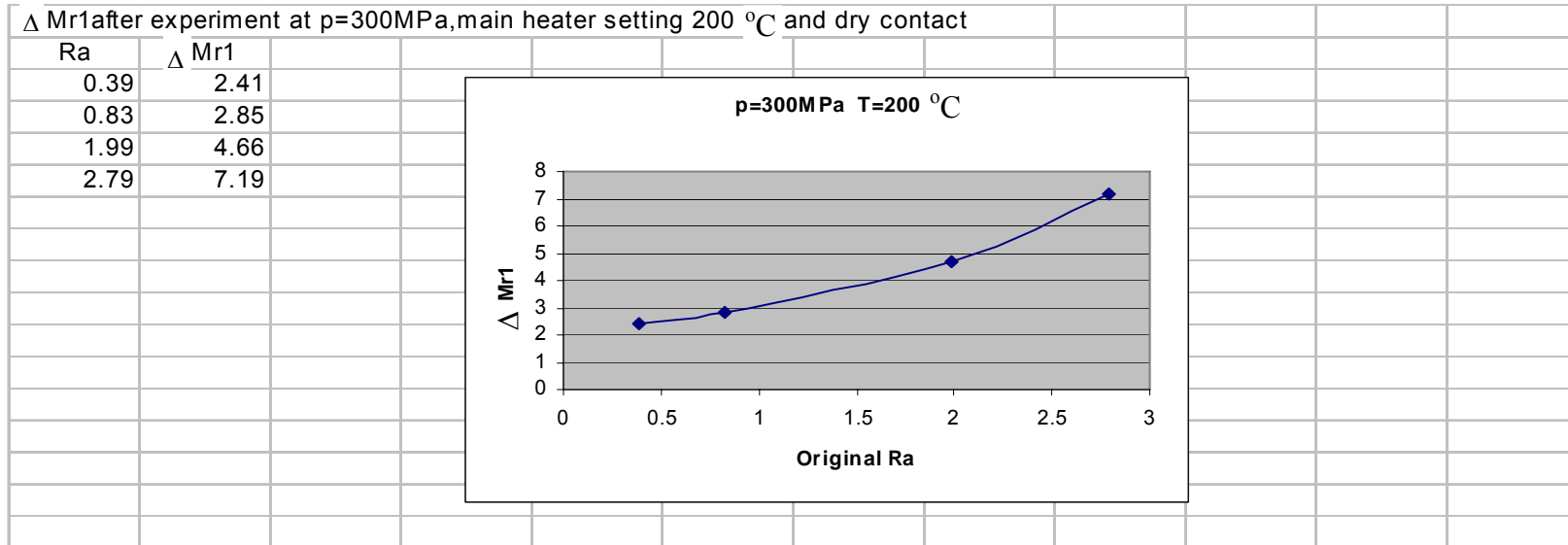
Fig. A3.11   ΔMr1 as a function of original roughness Ra

(a)

(b)

Fig. A3.12 **BAC comparison of the original surfaces and the compressed surfaces**
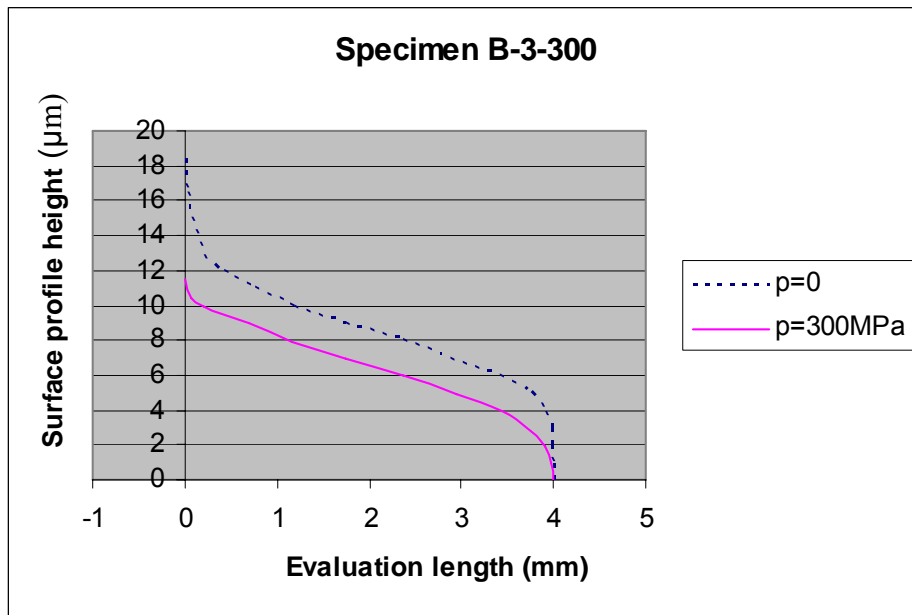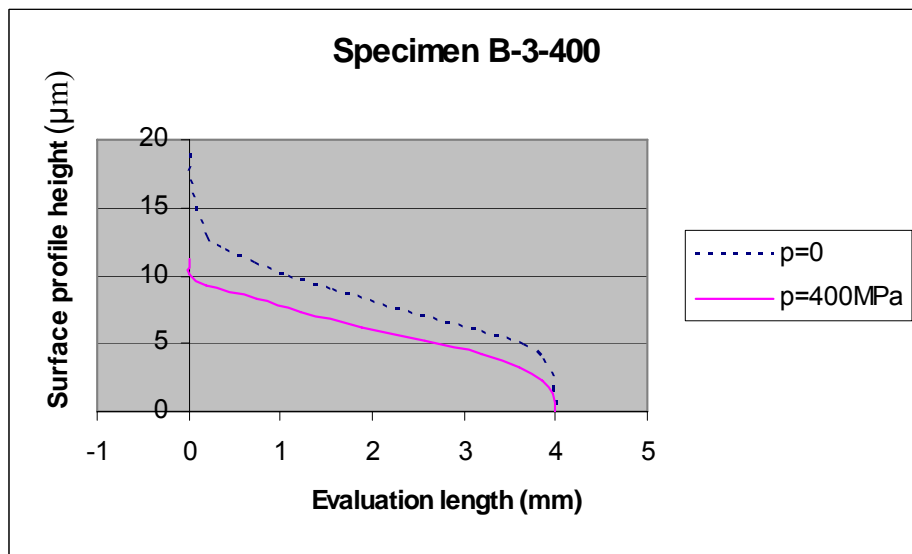
Specimen B-3-300

(c)

Specimen B-3-400

(d)

Fig. A3.12   BAC comparison of the original surfaces and the compressed surfaces

Specimen B-3-600

Height of Profile (µm) vs Evaluatipn Length (mm)

Legend:
- p=0
- p=600MPa

(e)

Fig. A3.12   BAC comparison of the original surfaces and the compressed surfaces

Graph[BAC]<<Profile=R_ISO - Section=[1]]>>

P=0

Depth 3.295um/cm, x3035.219
[um] 0.000
10.490
20.979

Density 0.382mm/cm, x26.184
0.000
2.000
[mm] 4.000

(a) Original surface

Graph[BAC]<<Profile=R_ISO - Section=[1]]>>

P=600MPa
T=100 ^{o}C

Depth 1.988um/cm, x5031.267
[um] 0.000
6.328
12.656

Density 0.382mm/cm, x26.184
0.000
2.000
[mm] 4.000

(b)

Surface after experiment at contact pressure p=600MPa and interfacial temperature T=100°C
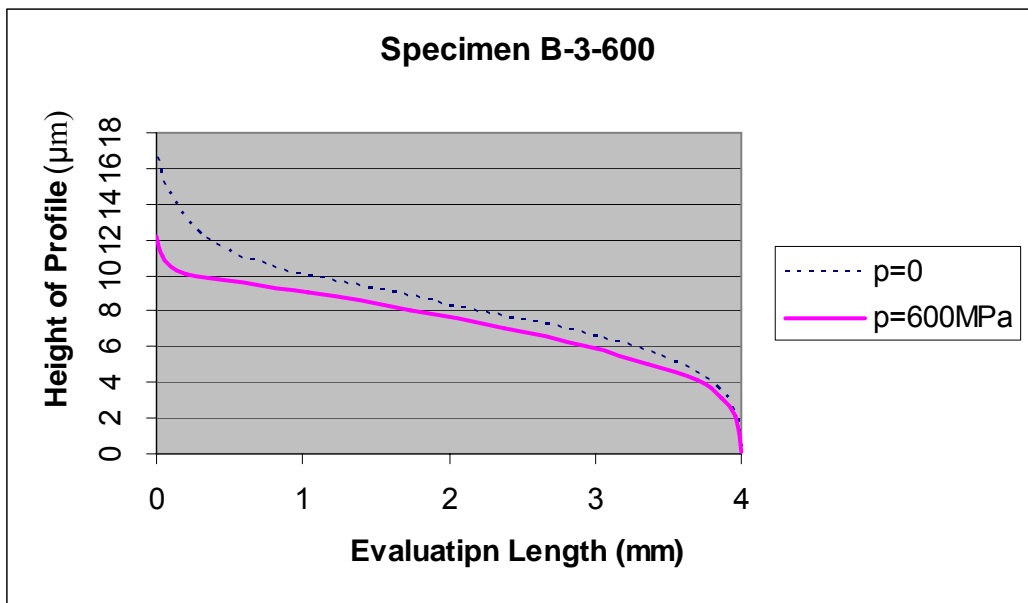
Fig. A3.13   BAC of the surface of specimen C-3-600
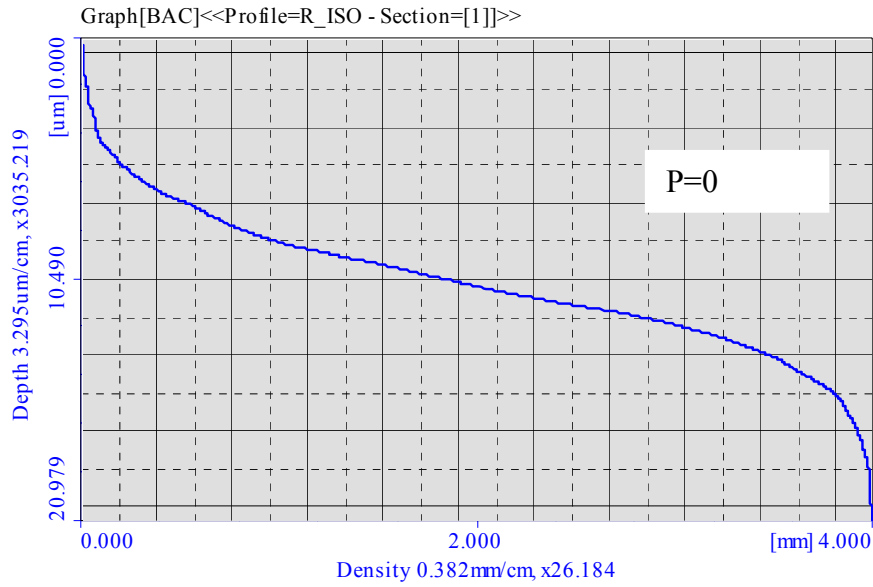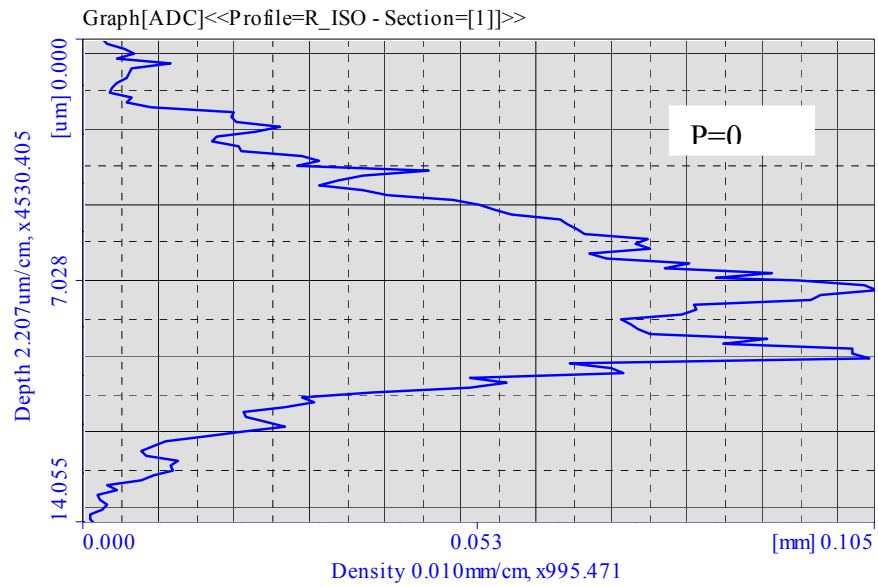
(a) Original Surface
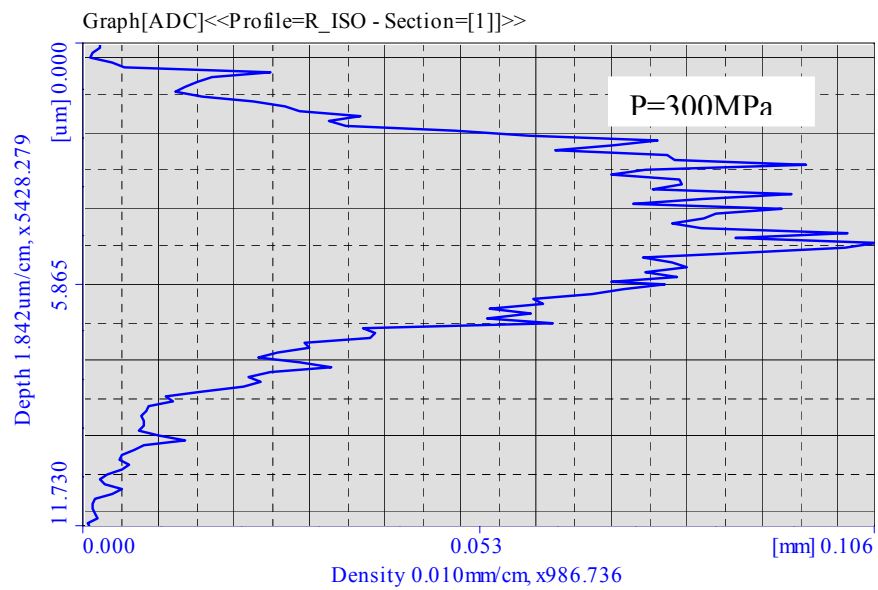
(b) Surface after an experiment at a contact pressure of p=300MPa

Fig. A3.14   ADC of the surface of specimen B-3-300

Graph[ADC]<<Profile=R_ISO - Section=[1]]>>

P=0

(a) Original Surface

Graph[ADC]<<Profile=R_ISO - Section=[1]]>>
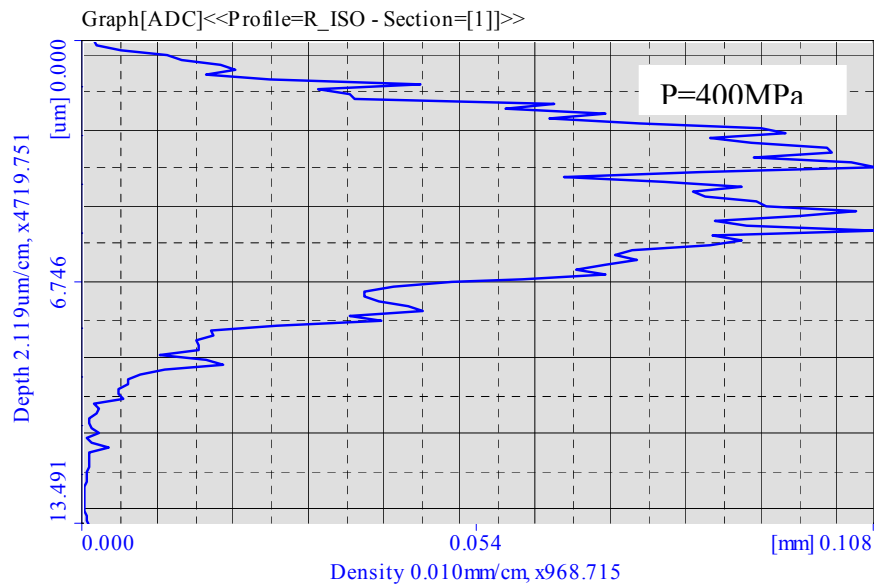
P=400MPa

(b) Surface after an experiment at a contact pressure of p=400MPa

Fig. A3.15   ADC of the surface of specimen B-3-400

Graph[ADC]<<Profile=R_ISO - Section=[1]]>>

P=0

Depth 2.764um/cm, x3617.951

[um] 0.000
8.800
17.600

0.000   0.070   [mm] 0.139
Density 0.013mm/cm, x753.263

(a) Original Surface

Graph[ADC]<<Profile=R_ISO - Section=[1]]>>

P=500MPa

Depth 1.939um/cm, x5157.932

[um] 0.000
6.173
12.345

0.000   0.057   [mm] 0.113
Density 0.011mm/cm, x925.724
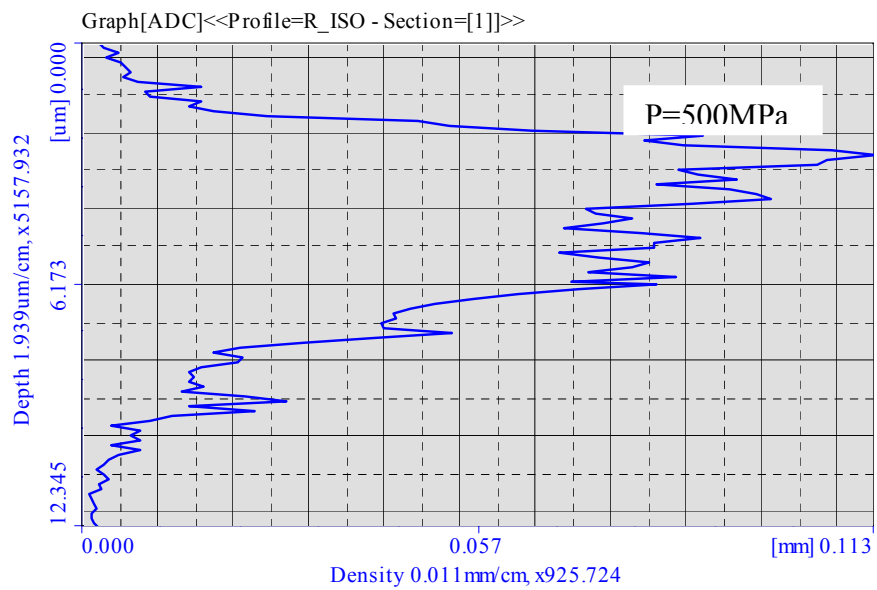
(b) Surface after an experiment at a contact pressure of p=500MPa

Fig. A3.16   ADC of the surface of specimen B-3-500

Graph[ADC]<<Profile=R_ISO - Section=[1]]>>

P=0

(a) Original Surface

Graph[ADC]<<Profile=R_ISO - Section=[1]]>>
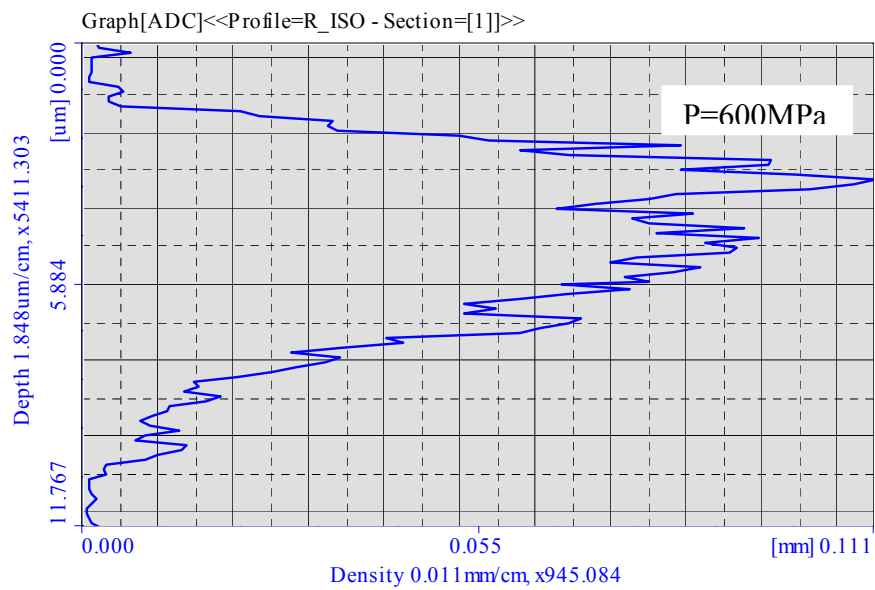
P=600MPa

(b) Surface after an experiment at a contact pressure of p=600MPa

Fig. A3.17   ADC of the surface of specimen B-3-600
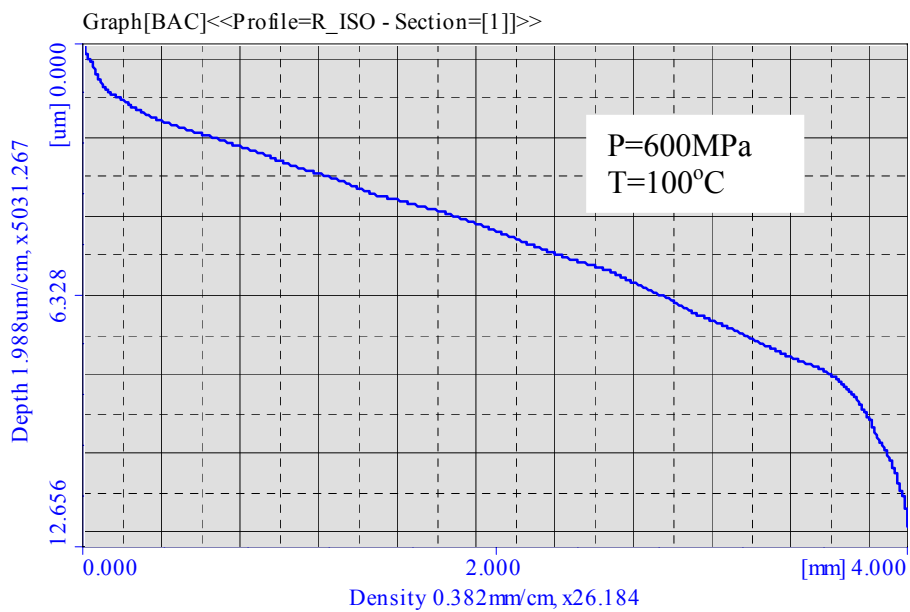
Graph[BAC]<<Profile=R_ISO - Section=[1]]>>

P=0
T=0

(a) Original surface

Graph[BAC]<<Profile=R_ISO - Section=[1]]>>

P=600MPa
T=100°C

(b) Surface after an experiment at a contact pressure of p=600MPa, an interfacial
temperature of T=100°C and lubricant MDC used

Fig. A3.18   BAC of the surface of specimen C-3-600-MDC
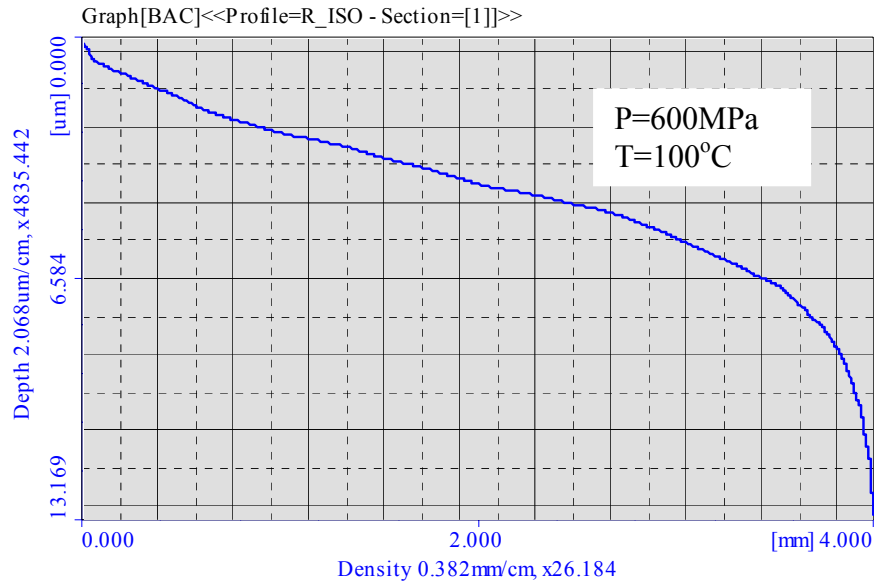
Graph[BAC]<<Profile=R_ISO - Section=[1]]>>

P=600MPa
T=100°C

Depth 2.068um/cm, x4835.442

Density 0.382mm/cm, x26.184

(a) Surface after experiment at a contact pressure of p=600MPa, an interfacial temperature of T=100°C and lubricant MDC used

Graph[BAC]<<Profile=R_ISO - Section=[1]]>>

P=600MPa
T=100°C

Depth 1.965um/cm, x5089.181

Density 0.382mm/cm, x26.184
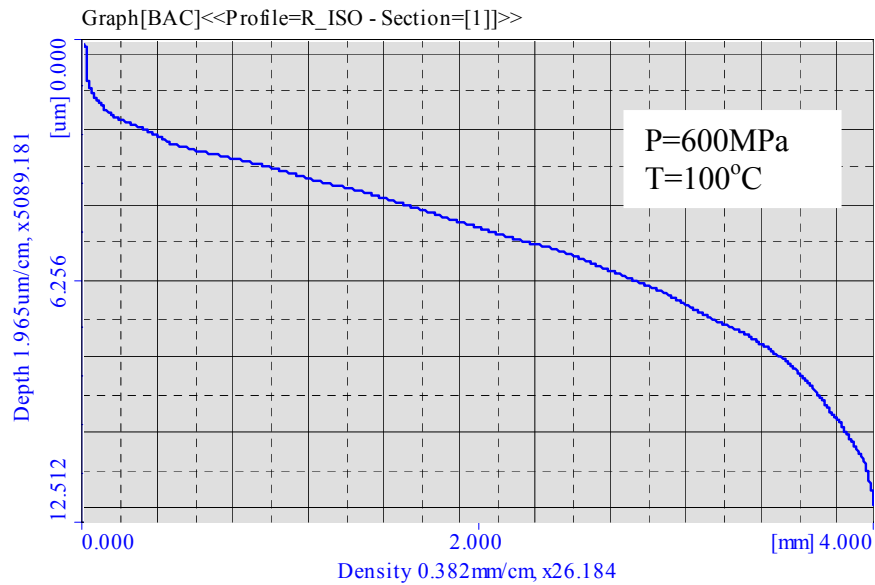
(b) Surface after experiment at a contact pressure of p=600MPa, an interfacial temperature of T=100°C and lubricant MDC removed after the experiment

Fig. A3.19   BAC of the surface of specimen C-4-600-MDC
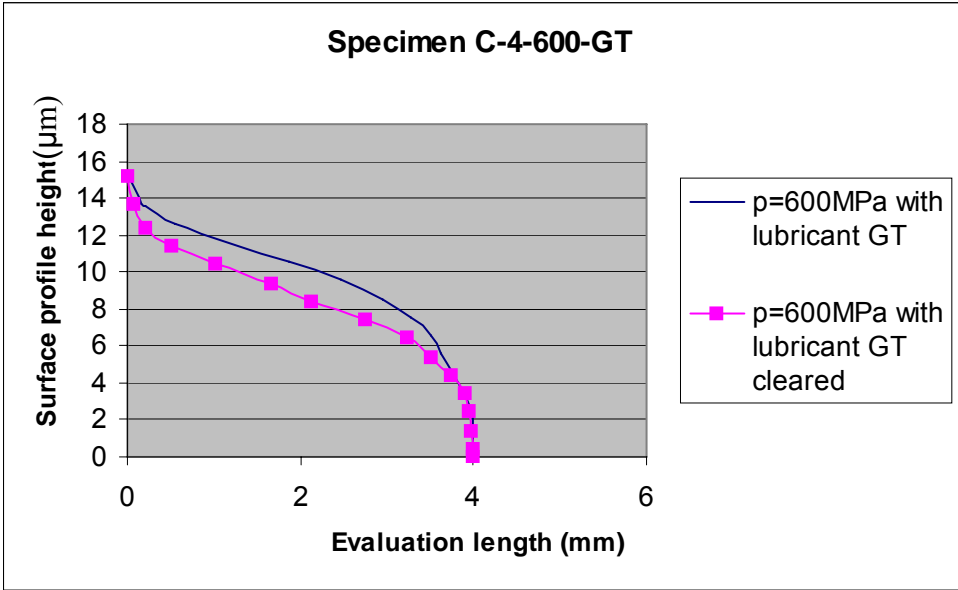
(a) Lubricant GT
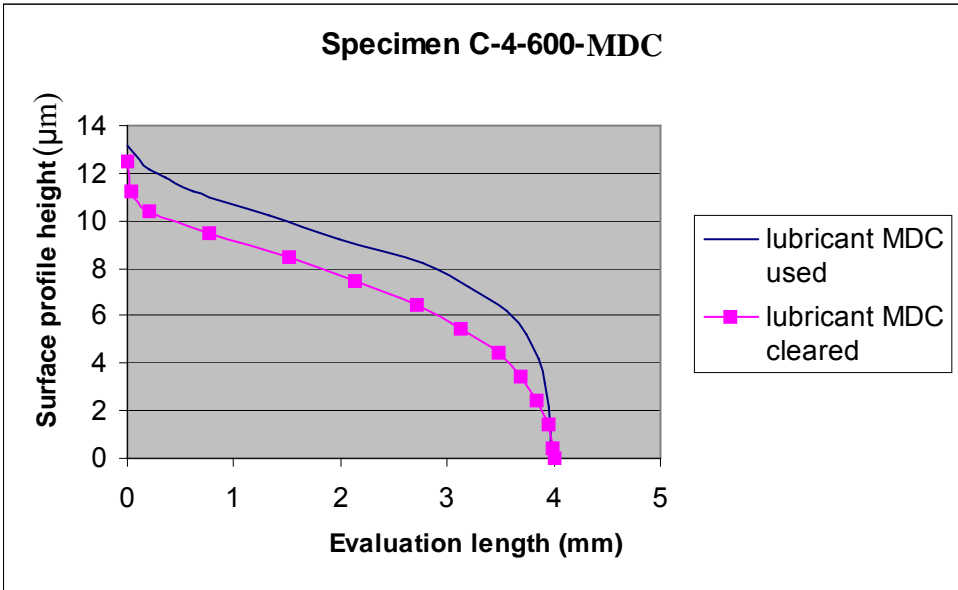
(b) Lubricant MDC

Fig. A3.20   BAC of surfaces with lubricant used and afterwards removed

Thermocouple No.1

$$\Delta T = 1.542 \times 10^{-2} T - 1.168$$

Standard Error = 0.062 ^{o}C
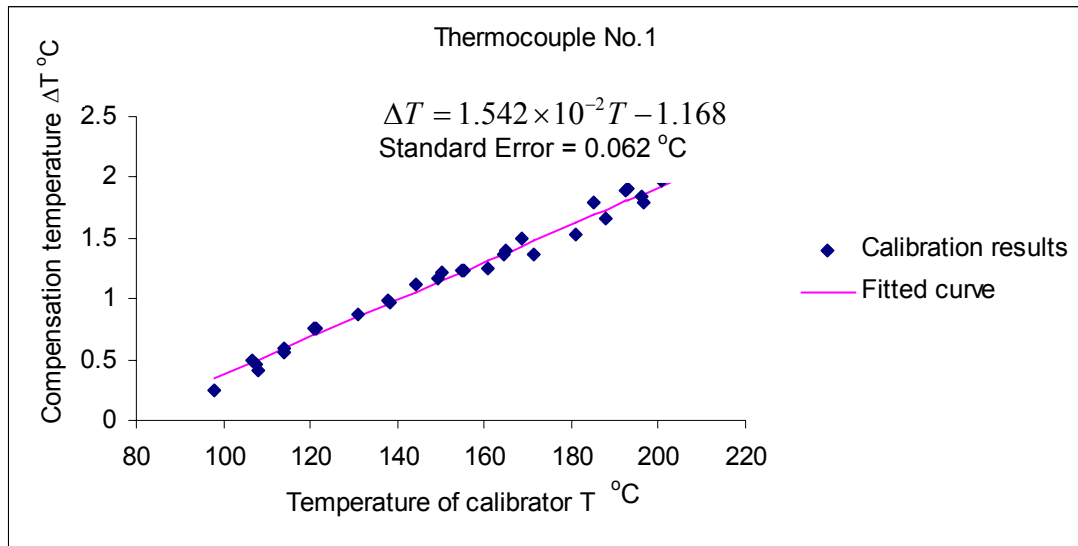
Fig. A3.21 Calibration result for thermocouple No. 1
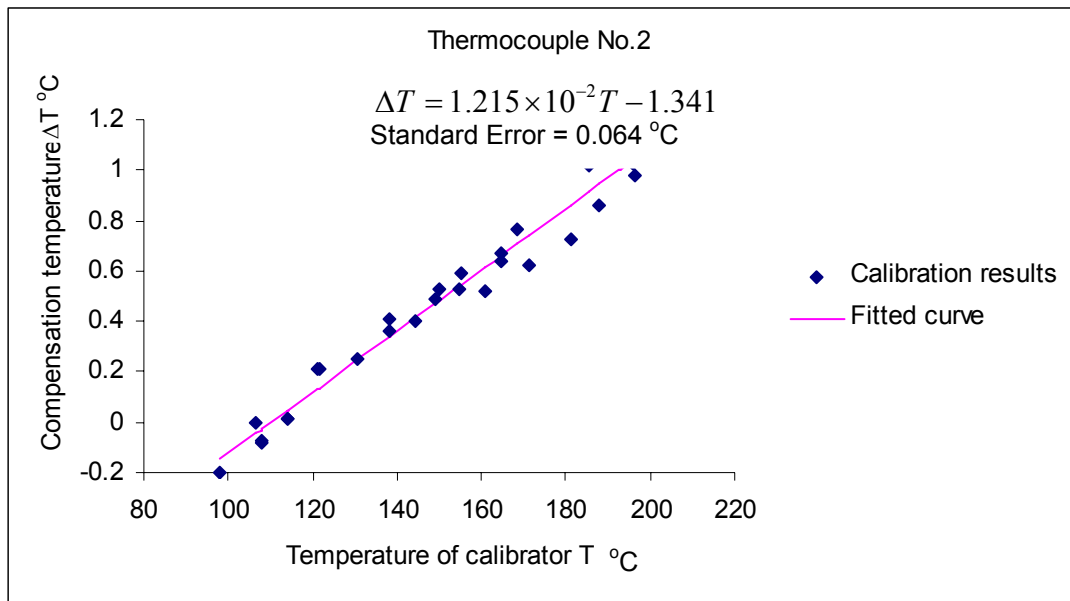
Fig. A3.22   Calibration result for thermocouple No. 2
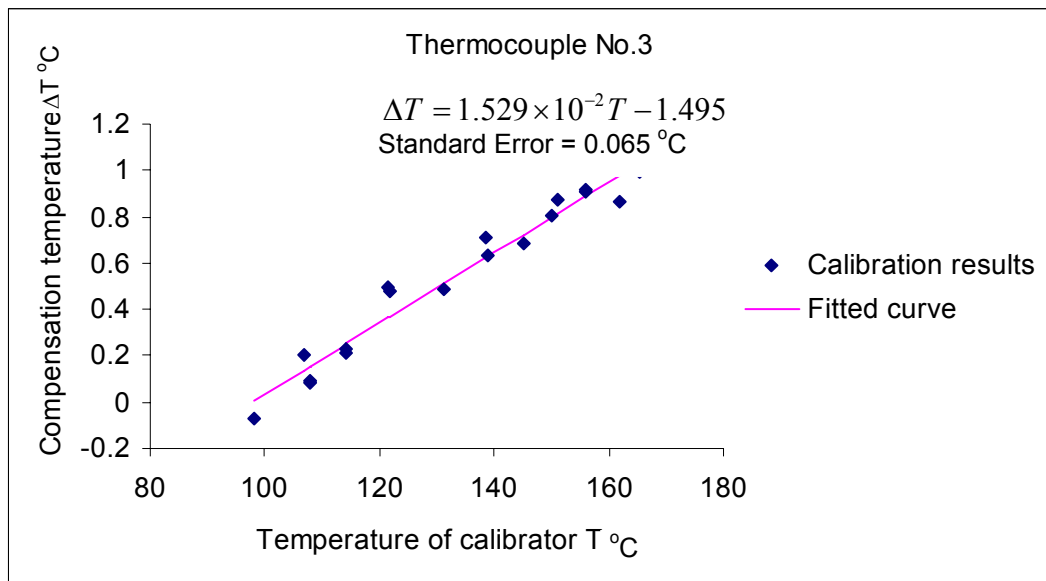
Fig. A3.23   Calibration result for thermocouple No. 3
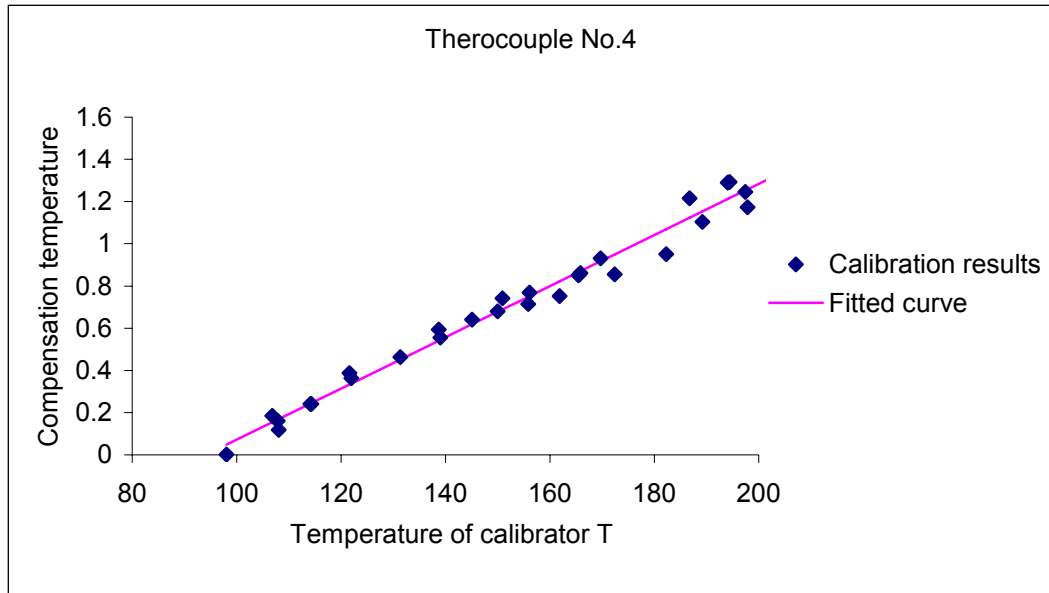
Fig. A3.24   Calibration result for thermocouple No. 4
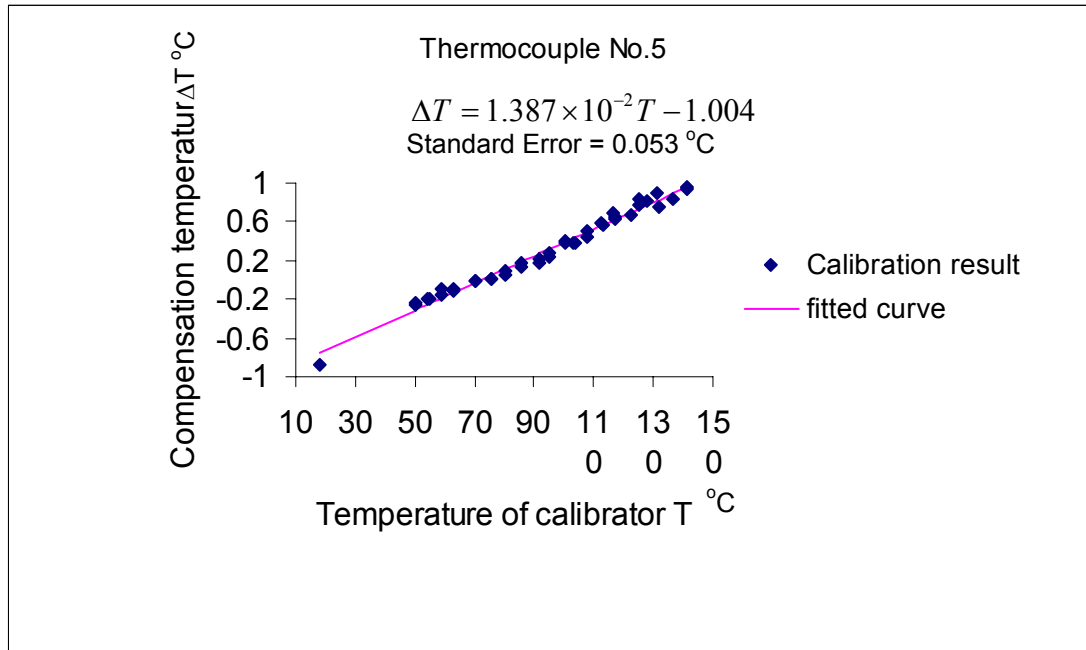
Fig. A3.25   Calibration result for thermocouple No. 5
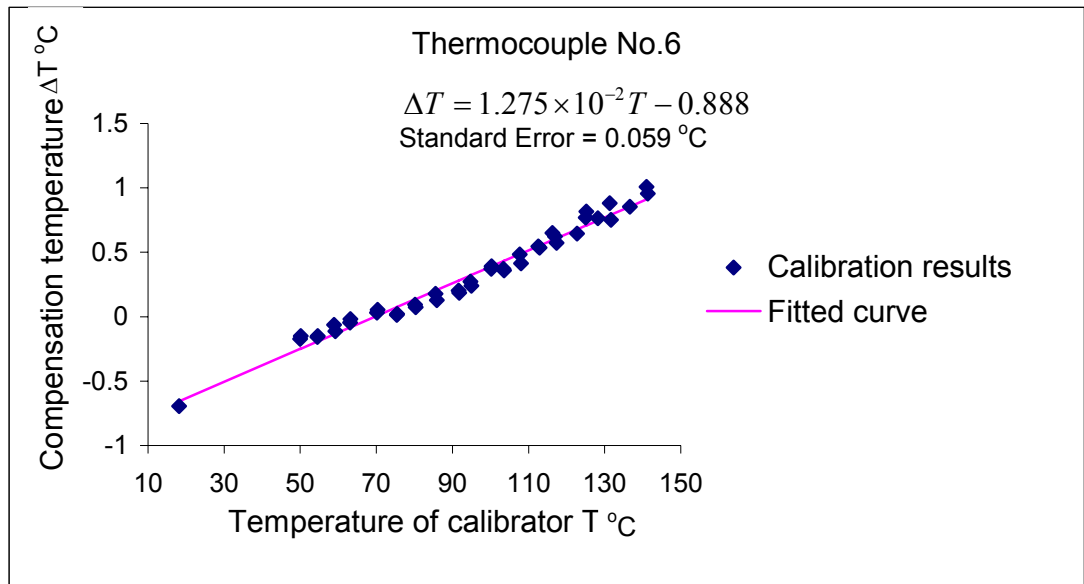
Fig. A3.26   Calibration result for thermocouple No. 6
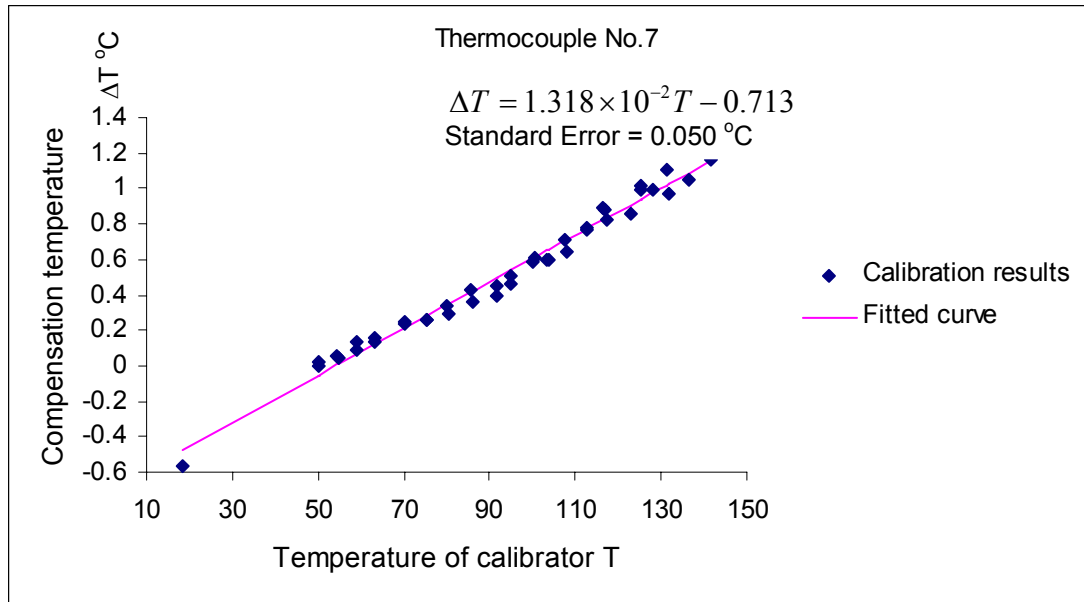
Fig. A3.27   Calibration result for thermocouple No. 7
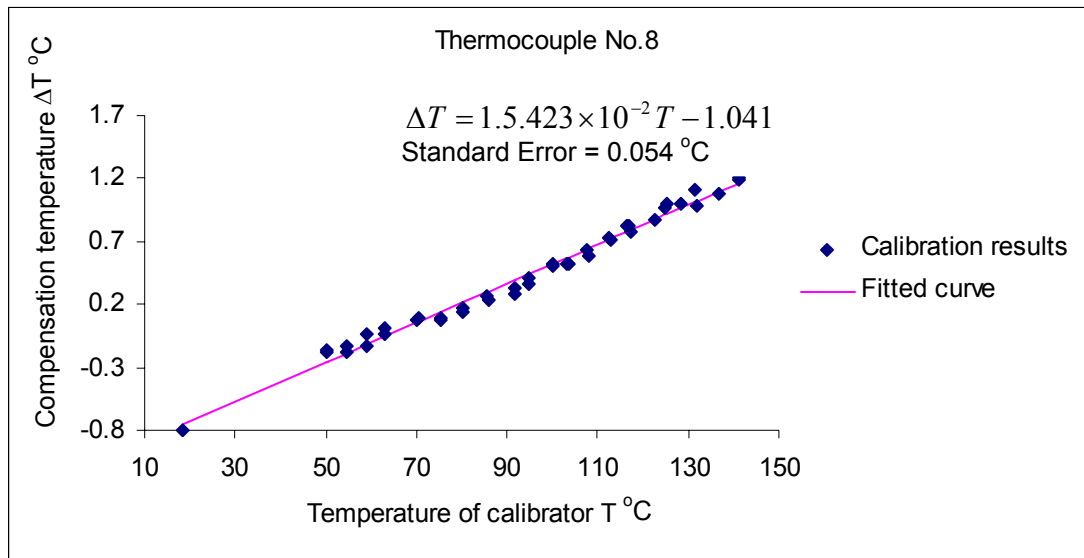
Fig. A3.28   Calibration result for thermocouple No. 8
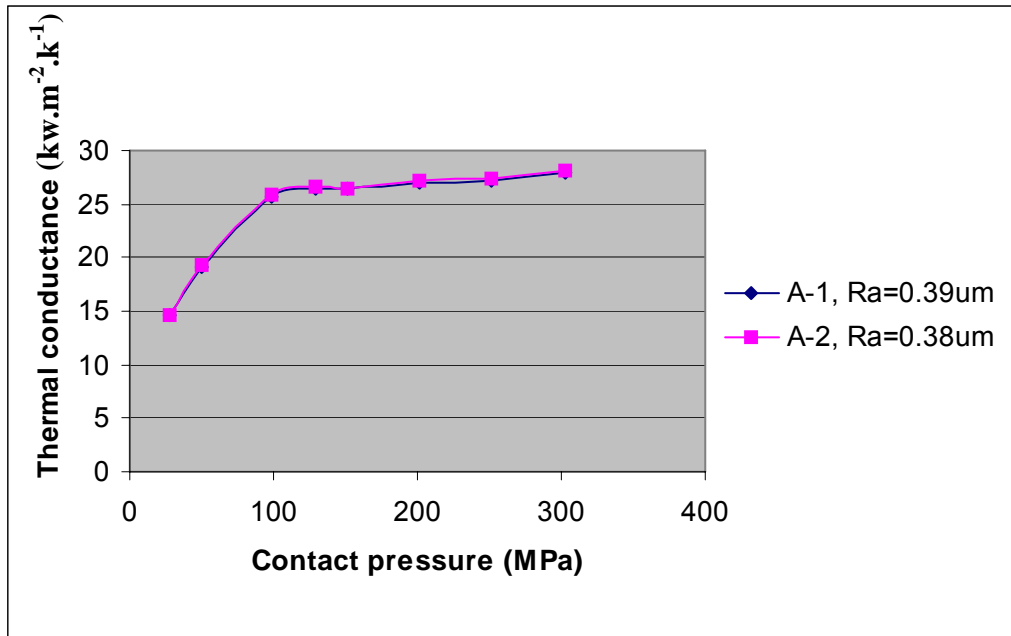
**Fig. A3.29 Thermal conductance of dry contact surfaces
with surface roughness grade A**
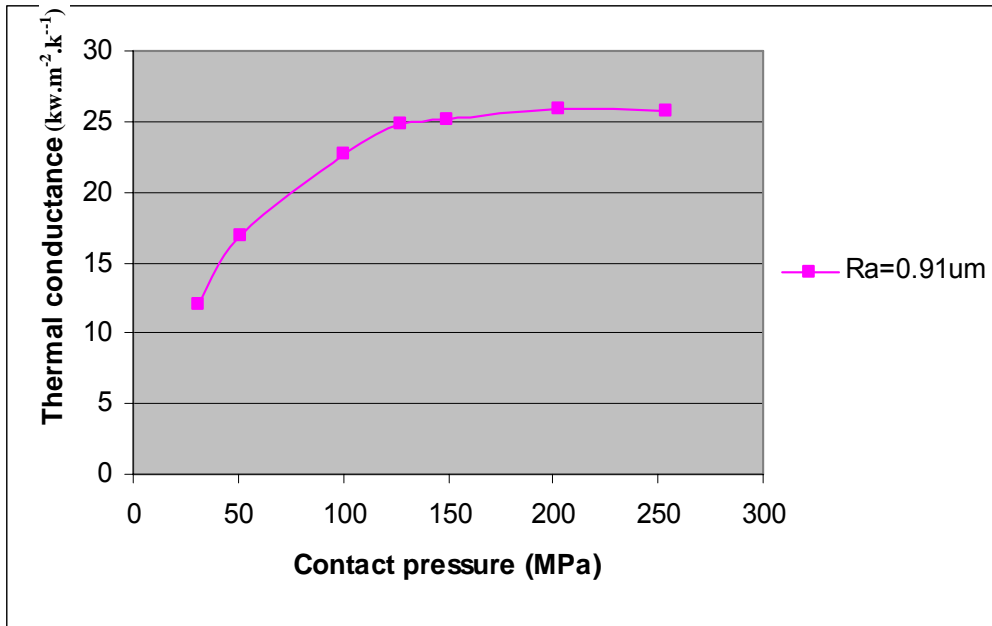
**Fig. A3.30   Thermal conductance of a dry contact surface
with surface roughness Grade B**
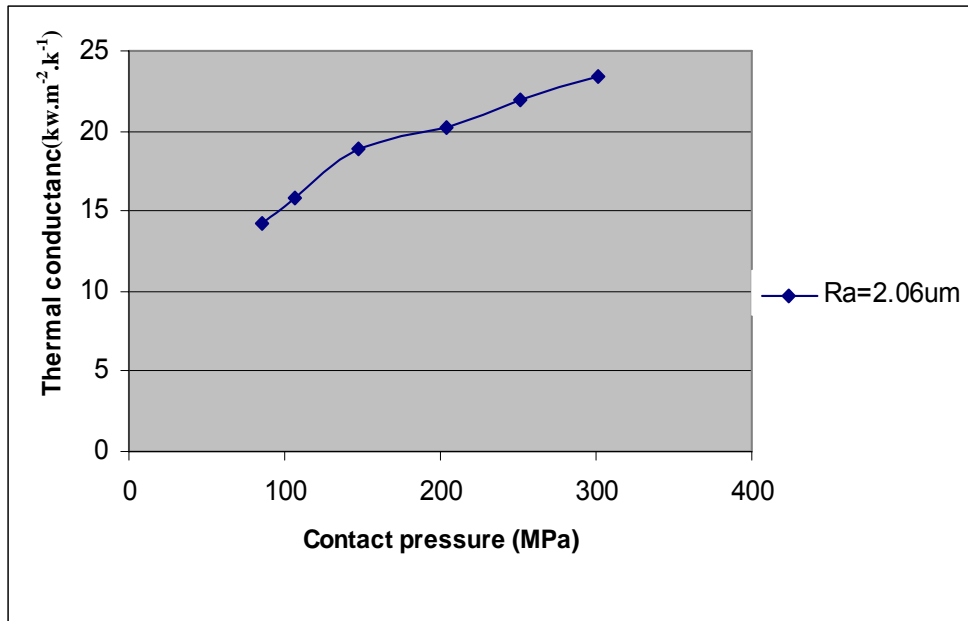
Fig. A3.31 **Thermal conductance of a dry contact surface with surface roughness Grade C**
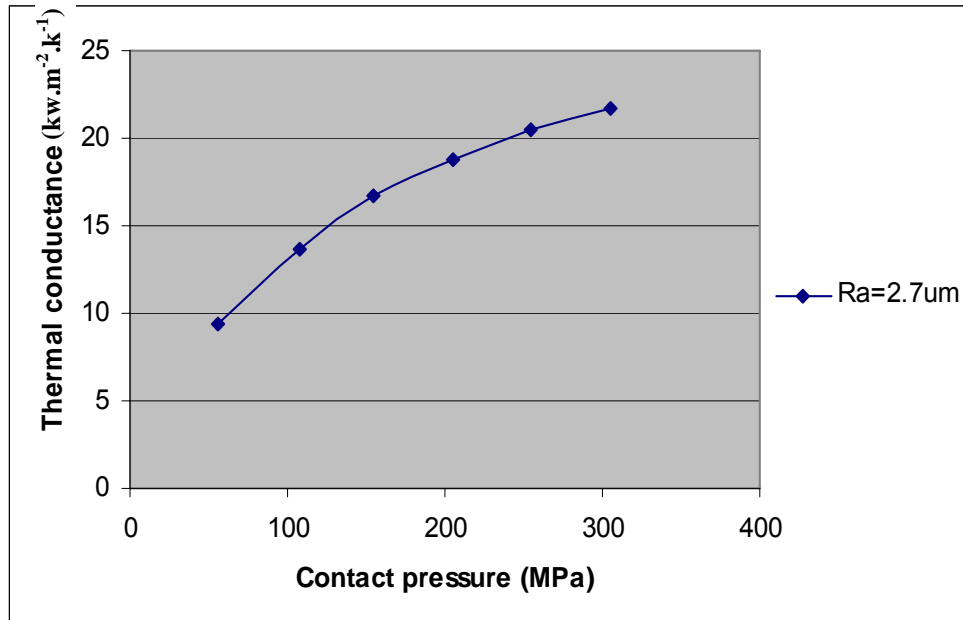
**Fig. A3.32   Thermal conductance of a dry contact surface
with surface roughness Grade D**

3.9 Appendix B – Surface Profile Parameters

1. Average Roughness R_a

Figure A-1 shows the plat of a measurement of a rough surface, where L is the evaluation length and l is a sample length. Normally the evaluation length contains five sample lengths with each sample length equal to one cut-off.
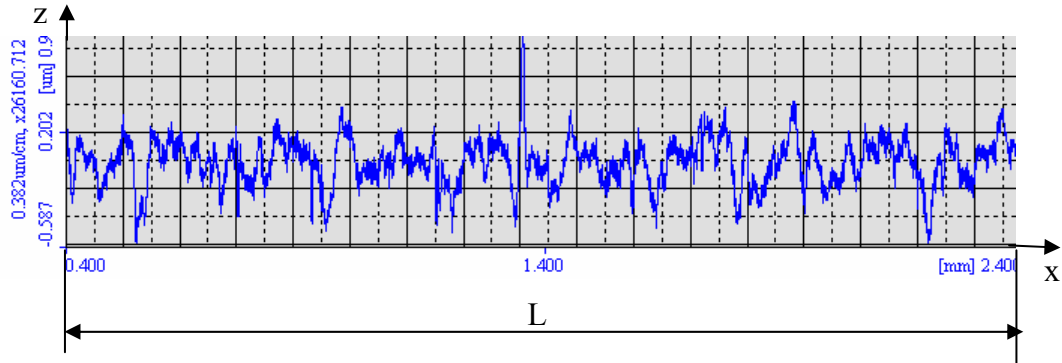
Fig. B-1   Output of rough surface measurement

The average roughness R_a, also known as the central line average, is the area between the roughness profile and its mean line divided by the evaluation length. It can be described by the integral of absolute value of the roughness profile height over the evaluation length:

$$R_a = \frac{1}{L}\int_0^L |z(x)|dx$$

where z(x) is the coordinate of the profile relative to its mean line.

When evaluated from digital data, the integral could normally be approximated by the following equation:

$$R_a = \frac{1}{N}\sum_{n=1}^{N}|z_n|$$

where N is the sum of the number of peaks and the number of valleys over the evaluation length.

The average roughness R_a is the most-commonly used parameter in surface measurement.

2. Root-mean-square-roughness R_q

The root-mean-square roughness of the surface is defined by another integral of the roughness profile:

$$R_q = \sqrt{\frac{1}{L}\int_0^L z^2(x)dx}$$

The digital-equivalent normally used is:

$$R_q = \sqrt{\frac{1}{N}\sum_{n=1}^N z_n^2}$$

3. Skewness R_{sk}

Skewness is a parameter that measures the symmetry of a profile about its mean line:

$$R_{sk} = \frac{1}{LR_q^3}\int_0^L z^3(x)dx$$

The digital-equivalent normally used is:

$$R_{sk} = \frac{1}{NR_q^3}\sum_{n=1}^N z_n^3$$

Surfaces with $R_{sk}>0$ have high peaks that protrude above a flatter average. Surface with $R_{sk}<0$ have deep valley in a smoother plateau.

4. The amplitude distribution function ADF

The amplitude distribution function is a probability density function that gives "how much " of the profile lies at a particular height.

The wider the ADF, the larger the value of R_{ku}, and the rougher the surface. This is shown in Fig.A-2.

5. Kurtosis R_{ku}

R_{ku} is a parameter of the ADF (amplitude distribution function). It is the degree of concentration around the mean value of an amplitude distribution curve:

$$R_{ku} = \frac{1}{LR_q^4} \int_0^L z^4(x)\,dx$$

The digital equivalent normally used is:

$$R_{ku} = \frac{1}{NR_q^4} \sum_{n=1}^{N} z_n^4$$
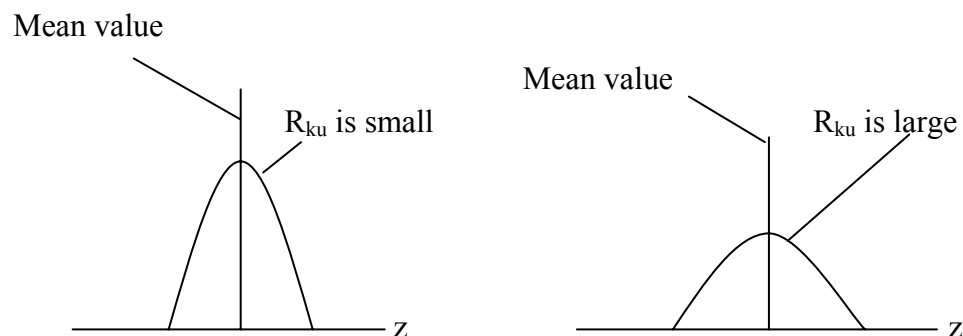
Fig. B-2   ADF curve of surface profile

6. Roughness R_p, R_v and R_t

The peak roughness R_p is the height of the highest peak in the roughness profile over the evaluation length. R_v is the depth of the deepest valley in the roughness profile over the evaluation length. R_t is the total roughness, i.e. the vertical distance from the highest peak to the lowest valley:

$$R_p = \left|\max[z(x)]\right|, \qquad 0 < x < L$$

$$R_v = \left|\min[z(x)]\right|, \qquad 0 < x < L$$

$$R_t = R_p + R_v$$

7. R_z is the distance between the average height of the five highest peaks and the average depth of the five lowest valleys within an evaluation length.

8. The bearing area curve BAC

The bearing area curve is the cumulative probability distribution corresponding to ADF. It is the integral of the amplitude distribution function.

9. Bearing ratio t_p

t_p is used generically as the abscissa of the BAC.

10. Parameters R_k, R_{pk} and R_{vk}

There is a significant amount of information encapsulated in the shape of the BAC for a surface. The R_k parameters are a simple approach where the knee-shaped BAC is approximated by a set of straight lines.

The R_k construction is designed to divide the BAC into three sections: the small peak above the main plateau, the plateau itself, and the deep valley below the plateau. These three sections can be determined as follows:

As illustrated in Fig. A-3, the first step is to slide a "window" across the BAC looking for the minimum secant slope. The window is 40% t_p wide. As the window slides across the curve it intersects two points on the curve. The goal is to find the position where the slope between the two points is minimum or, since the window has constant width, where the height H_{tp} between the two points is minimum

.
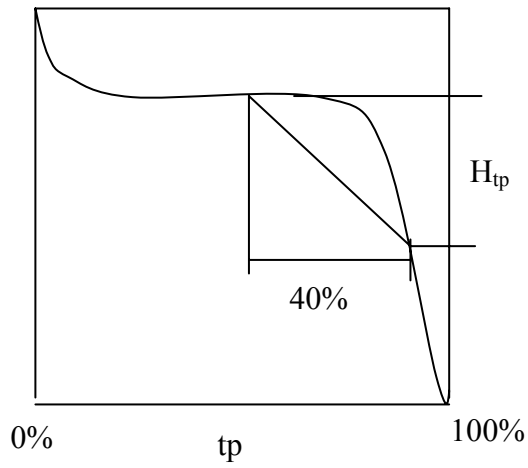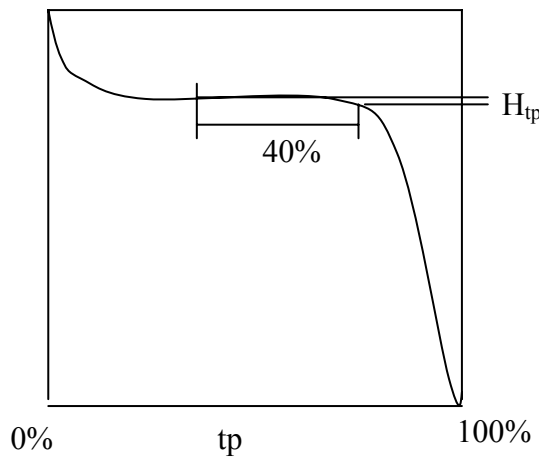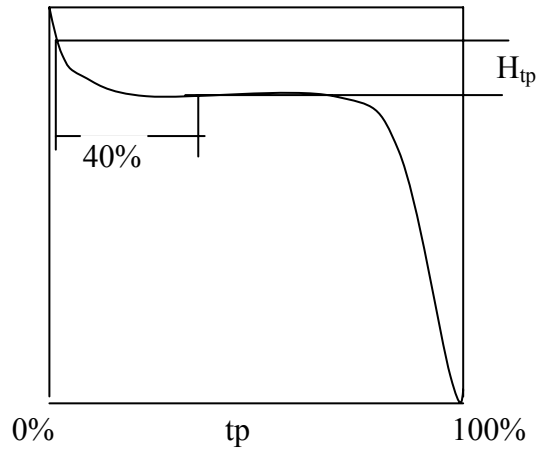
Fig. B-3   BAC analysis – determining H_{tp}

After the minimum slope window has been found, and also points A and B where the window intersects the BAC as shown in Fig. A-4, a line is then drawn through these two points to find the intercepts at 0% and 100%, points C and D. The vertical height between C and D is the first parameter, R_k. Drawing a horizontal line across from C to the BAC, point E is found. The area S_1 below the BAC and above the line CE (shaded area) is then computed. Next, R_{pk} is computed as the height of triangle CEG which has the same area as S_1. For the valleys, a horizontal line is drawn from D over to point F on the curve. The area S_2 below line DF and above the BAC (shaded area) is then computed. Next, R_{vk} is computed as the height of triangle DFH which has the same area as S_2.

The parameter R_k is the vertical height between the left and right intercepts of the line through the ends of the minimum H_{tp} 40% window.

R_k correlates with the depth of the working part of the surface, the flat part of the bearing area curve. After the initial run-in period, this part of the surface carries the load and most closely contacts the mating surface. Sometimes this part of the surface is called the "core roughness" or the "kernel".

R_{pk} is an estimate of the small peaks above the main plateau of the surface. These peaks will typically be worn off (or down) during the run-in period for a part. Generally, it would be desired to have a fairly small R_{pk}.

R_{vk} is an estimate of the depth of valleys that will retain lubricant on the surface

MR_1 is the fraction of the surface which consists of small peaks above the main plateau.

MR_2 is the fraction of the surface which will carry load during the practical lifetime of the part. Alternatively, 100%-MR_2 is the fraction of the surface that consists of deeper valleys that will retain lubricant.
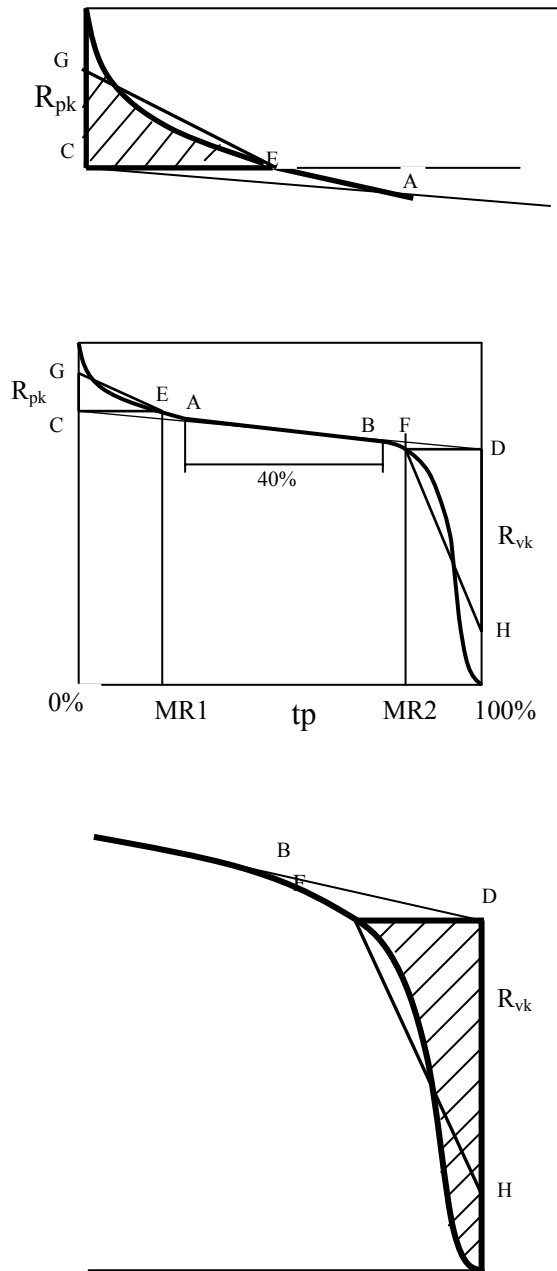
Fig. B-4   BAC analysis: determining R_{pk} and R_{vk}

The "area" of the peak portion of the bearing area curve is denoted by A_1. It is related to R_{pk} and M_{r1}:

$$A_1 = \frac{1}{2} \frac{R_{pk} M_{r1}}{100\%}$$

The "area" of the valleys in the Rv_k construction is denoted by A_2. It is related to R_{vk} and M_{r2}:

$$A_2 = \frac{1}{2} \frac{R_{vk}(100\% - M_{r2})}{100\%}$$

A_2 is also called V_o, the oil retention "volume" of the surface.

Chapter 4 FE Characterisation of Metal Surface Contact

4.1 Introduction

The contact area between solid contact surfaces is an important parameter in the thermal conductance of the surfaces. The real contact area is dependent on the situation of the surface roughness and the shape of the rough peaks as well as the deformation of the peaks.

The FE simulation method is often used to investigate micro deformation of the contact surfaces. In the early research, the investigations concentrated mainly on geometrical analysis (Ishigaki and Kawaguchi, 1979; Kucharski, et al., 1994). It is reported that displaced material rose at non-contact areas (Pullen and Williamson, 1972), Elastic-plastic surface-deformation models were proposed by M.R. Sridhar and Yovannovich (1994). Kucharski, et al. (1994) presented a finite element model of surface contact deformation, in which a spherical asperity was considered. An "equivalent asperity" model, which is a statistical representation of the surface, was developed by Chen, et al. (2004).

4.1.1 The aim of this study

The aim of this study is to investigate the influence of the deformation of peaks on the contact characteristic of the contact surfaces and the situation of lubricant retention after contact, through FE simulation. In this study, the micro deformation of solid contact surfaces has been analysed using single-peak model and multiple-peak model. The characteristics of the micro deformation of the contact surface and the temperature distribution in the range close to the contact surface have been investigated.

4.1.2 The problems to be investigated

The problems to be investigated in this chapter are listed as follows:

- What is the situation of the micro-deformation of the surface profile at different interface pressures?

- What is the temperature distribution in a rough surface near the interfaces from micro point view?

- What is the influence of the micro-deformation on the lubricant retained on the surface after being compressed?

4.2 Contact-surface deformation analysis

The deformation of a single peak is dependent on the contact pressure and the geometry of the peak of a specified material. In this study the geometry of a peak is determined by five parameters: the details of these parameters are given in Sub-section 4.2.2.1. The contact force is applied step-by-step. The deformation of the peak for each step has been achieved and used to analyse the situation of lubricant retention, the temperature field and the stress distribution.

4.2.1 Material model

En32C steel is used in this study for deformation analysis and temperature analysis. It is used widely in cold-forming operations such as heading, upsetting, and extrusion. The main properties of the material are listed in the following table.

Table 4.1   Material properties of En32C steel

Density	7.87g/cm^3
Tensile Strength, Ultimate	420MPa
Tensile Strength, Yield	350MPa
Elongation at Break	18%
Modulus of Elasticity	205GPa
Poisson's Ratio	0.29
Heat Capacity	0.481 J/g ºC from 50-100ºC 0.515 J/g ºC from 150-200ºC 0.595 J/g ºC from 350-400ºC
Thermal Conductivity	51.9 W/m-k (estimated based on similar materials)

Note: This information was obtained from the Internet 'MatWeb.com'.

4.2.2 Axisymmetric model of a single peak

The roughness of the surface and the geometries of the peaks are the major parameters in the surface-texture-deformation analysis of contact surfaces. The deformation of a single peak is first investigated by the FE simulation.

Four single-peak models are built for the micro-deformation analysis of single peaks. The details of the geometry and the FE modelling are given in the following sub-sections. The results are given in Section 4.4 along with those for other models.

4.2.2.1 Geometries of single peaks

Fig. 4.1 shows the parameters that define a single peak. The main dimensions of the four peaks are listed in Table 4.2 and are shown in Fig. A4.1. $R1$ increases from Model-1 to Model-4, while $R2$ decreases. R remains constant. The two arcs of radii $R1$ and $R2$ are tangential to a straight line. $H2$ is the vertical distance from the top to the lower tangential point. It can be seen from the figure that the models change gradually from sharp Model-1 to blunt Model-4. Fig. 4.2 shows the 2-dimensional models.
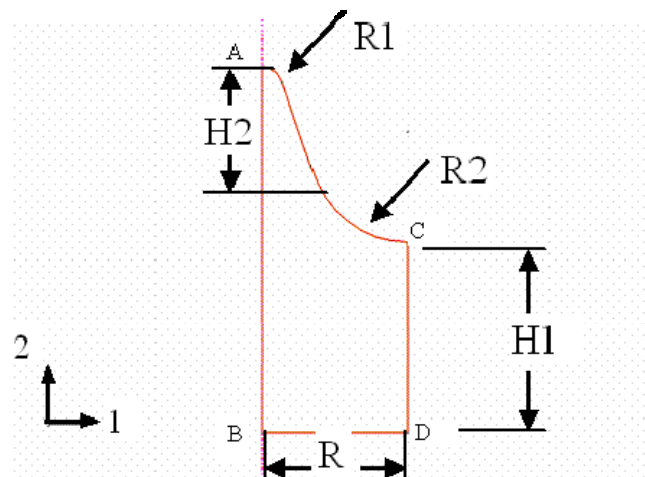
Fig. 4.1   Geometry of a single peak

Table 4.2   Dimensions of peaks

	R1 (μm)	R2 (μm)	H1 (μm)	H2 (μm)	R (μm)
Single-peak Model-1	1.50	7.0	12.0	5.30	10.0
Single-peak Model-2	2.07	6.0	12.0	6.24	10.0
Single-peak Model-3	3.07	5.0	12.0	5.90	10.0
Single-peak Model-4	5.07	3.0	12.0	6.04	10.0

4.2.2.2 Mechanical model

The mechanical model is a rigid plate contacted by a single peak. Axisymmetric characteristics are employed. 'Hard' contact with friction is considered in the contact model between the plate and the single peak. The details of the steps and loads are listed in Table 4.3, in which the pressure is equal to the concentrated force divided by the area of the base, namely πR^2.

Table 4.3   Steps and loads of FE simulation for single peaks

Single-peak models		Steps				
		1	2	3	4	5
1	Force (N)	5e-6	0.02	0.04	0.06	0.08
	Pressure (MPa)	0.016	63.7	127.3	191	255
2	Force (N)	5e-6	0.02	0.04	0.06	0.08
	Pressure (MPa)	0.016	63.7	127.3	191	255
3	Force (N)	5e-6	0.02	0.04	0.06	0.08
	Pressure (MPa)	0.016	63.7	127.3	191	255
4	Force (N)	5e-6	0.02	0.04	0.06	0.09
	Pressure (MPa)	0.016	63.7	127.3	191	287

4.2.2.3 Mesh

The meshes of the single peaks are shown in Fig. A4.2. The element type and the number of elements are listed in Table 4.4.

Table 4.4 Details of the elements of single-peak models

Single-peak model	1	2	3	4
Element type	CAX4H	CAX4H	CAX4H	CAX4H
Number of elements	825	825	924	591

CAX4H elements are used. The contact-pair approach is employed to model the contact between the top surface of the peak and the rigid surface of the plate. The mechanical interaction between the contact surfaces is assumed to be frictional, with the friction coefficient being 0.1.

4.2.2.4 Boundary conditions

Two kinds of boundary conditions are applied to investigate their influence on the deformation of the single peak (refer to Fig.4.1).

- BC-1 : edge CD free, edge BD fixed in direction 2
- BC-2 : edge BD fixed in direction 2, edge CD fixed in direction 1

4.2.3 Multiple-peak model

In order to build a model which is closer to the real situation of rough surfaces in contact, the measured results of surface roughness are used. The surface profile of the multiple-peak model is based on a part of a sample from experimental measurement. The peak points and valley points are taken from measured data. The influence of the deformation of the peaks on the material flow is considered in this model.

4.2.3.1 Geometry of the multiple-peak model

The geometry of the multiple-peak model is shown in Fig. 4.2. The dimensions of the model are 1000μm×800μm. AB is the rough surface.

4.2.3.2 Mechanical model

The mechanical model is that of a rigid plate contacted by a two-dimensional rough surface. Hard and frictionless contact is considered in the contact model between the rigid plate and the rough surface.

4.2.3.3 Mesh

The meshes of the multiple-peak models are shown in Fig. A4.12. The numbers of elements of these models are listed in Table 4.5.

Table 4.5   Details of the elements of the multiple-peak models

Models	1	2	3
Element type	CAX4R	CAX4R	CAX4R
Number of elements	8429	10487	8625

4.2.3.4 Boundary conditions

The boundary conditions are presented in Table 4.6. These boundary conditions include the displacement constraints applied to the boundary lines AC, CD and BD and the enforced vertical displacements (applied via the rigid plate) on the rough surface in each step.
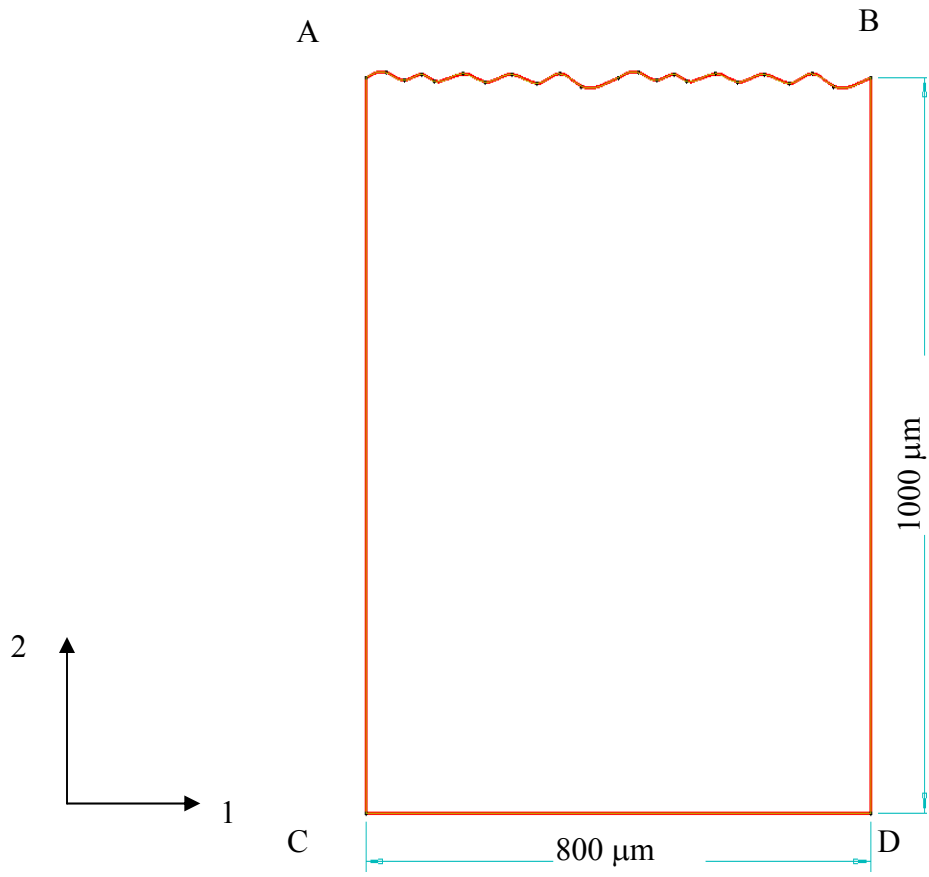
Fig. 4.2   Geometry of the multiple-peak model

Table 4.6   Multiple-peak FE simulation models

Model	Steps	1	2	3	4	5	6	7	8	9	10	11	12	13	14	15
1	Boundary Conditions	AC and BD edges free in direction 1 and CD edge fixed in direction 2														
	Displacement of the rigid plate(μm)	-1	-2	-3	-4	-5	-6	-7	-8	-9	-10	-12	-14	-16	-18	-23
2	Boundary Conditions	AC edge fixed in direction 1 and CD edge fixed in direction 2														
	Displacement of the rigid plate(μm)	-1	-2	-3	-4	-5	-6	-7	-8	-9	-10	-12	-14			
3	Boundary Conditions	AC and BD edges fixed in direction 1, CD edge fixed in direction 2														
	Displacement of the rigid plate(μm)	-1	-2	-3	-4	-5	-6	-7	-8	-9	-10	-12	-14	-16	-18	-23

4.3   Contact-surface temperature-field analysis

Analytical, experimental and numerical models have been developed to predict thermal contact resistance (Bahram, et al., 2003). The real area of contact is typically a small fraction of the nominal contact area (Greenwood and Williamson, 1966). Heat flow experiences two stages of resistance: macroscopic- and microscopic-constriction resistance; and the radiation heat-transfer remains small and can be neglected for surface temperatures of up to 700k (Clausing and Chao, 1963; Yovannovich, 1969).

Temperature-field analysis is performed based on FE simulation of the micro-deformation of contact surfaces. The surface roughness is still an important parameter here. Simplified model are used to investigate the temperature-field characteristics near to the interface.

The analysis model is that of a smooth surface contacted by a rough surface, as shown in Figs. 4.3. In this situation, the tool surface is absolutely smooth and the surface of the specimen is rough. The real contact area is just a portion of the nominal surface and the contacting parts are in perfect contact. Two models are employed. Model-2 (Fig. A4.28) has greater real contact area than model-1 (Fig. A4.27). The real contact area is 50% of the nominal surface in model-2 and 30% of the nominal surface in model-1.

The following basic assumptions are made:

(a) The temperature distribution is uniform at the end of the tool.
(b) The temperature field is one-dimensional in direction 2 in parts that are distant from interface. The heat flows from the tool to the specimen.
(c) The contact is perfect in the real contact area, so the temperatures are the same in both of the contact surfaces at the real contact area.
(d) No heat is transferred through non-contacting surfaces.

800.00 µm

Tool

1000.00 µm

2000.00 µm

A ——————— A

Specimen

gap
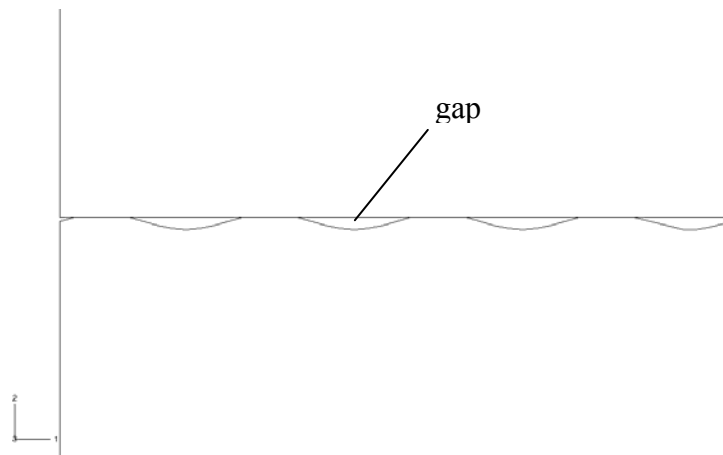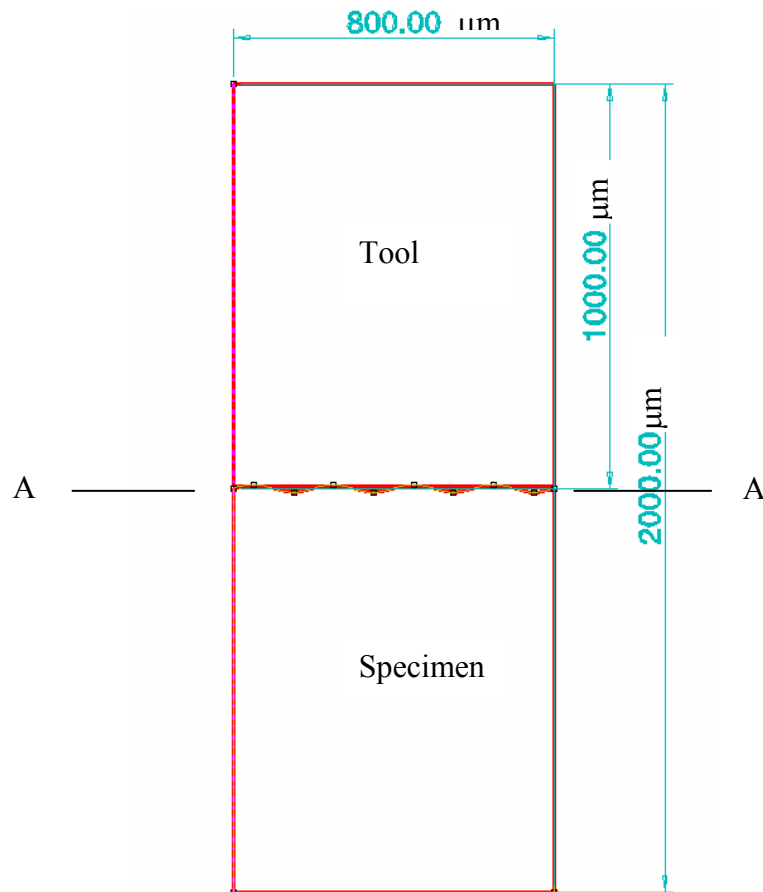
Zoom-in of the section A-A

Fig. 4.3   Geometry of the temperature-analysis model

4.4 Results and discussion

Results for the FE simulation of surface-contact characteristics have been acquired for the different models described in previous sections: details are presented in the following sections.

4.4.1 Results of single-peak models

The details of real contact areas are listed in Table 4.8, in which AC-1 and AC-2 are the real contact area for boundary condition BC-1 and boundary condition BC-2, respectively. AC-0 is the original section-width at the real contact positions of the steps. (AC-2-AC-0)/AC-0 gives the ratio of deformation relative to the original section.

Figs. A4.3 to A4.10 show all deformations of single peaks at each step. The deformations of the sharp peaks appear to retain lubricant more easily than do the blunt peaks. Fig. 4.11 shows the stress distributions of four single-peak models for a fixed boundary at edge CD (see Fig. 4.1). All of the models exhibit the same phenomena; that is, the position of the lowest stress occurs below the surface of the valley.

Table 4.8 Results of FE simulation for the deformation of single-peak models

		Step 2	Step 3	Step 4	Step 5
Single-peak model 1					
Original section	AC-0	2.577	3.448		
Real contact section	AC-1	3.285	4.997	6.058	6.887
	AC-2	3.416	4.869		
	$\frac{AC\text{-}2\text{-}AC\text{-}0}{AC\text{-}0}$	0.325	0.412		
Single-peak model 2					
Original section	AC-0	2.577	3.447	3.965	4.286
Real contact section	AC-1	3.285	4.997	6.058	6.887
	AC-2	3.285	4.998	6.065	6.873
	$\frac{AC\text{-}2\text{-}AC\text{-}0}{AC\text{-}0}$	0.275	0.450	0.529	0.604

Single-peak model 3					
Original section	AC-0	2.790	3.627	4.223	4.628
Real contact section	AC-1	3.037	4.648	5.889	6.962
	AC-2	3.037	4.649	5.896	6.966
	AC-2-AC-0 AC-0	0.088	0.282	0.396	0.505
Single-peak model 4					
Original section	AC-0	2.551	3.915	4.712	5.386
Real contact section	AC-1	2.769	4.244	5.388	6.717
	AC-2	2.792	4.281	5.388	6.886
	AC-2-AC-0 AC-0	0.095	0.094	0.144	0.279

4.4.2 Results for multiple-peak models

Figs. A4.13 to A4.19 and A4.24 to A4.26 show the deformations u1, u2 and u of the specimen near to the contact interface under different boundary conditions and for different steps. It is seen clearly that the material at the valleys have moved up relative to the original surface. This is shown in Fig. A4.26.

The stress distributions near to the interface are shown in Fig. A4.20 for free boundaries. Figs. A4.21, A4.22 and A4.23 show the stress distribution for fixed boundaries at step 6, step 10 and step 15, respectively. The stress is the greatest in the compressed peaks and the lowest below the surface at the valley position. In some places the lower stress area is surrounded by the higher stress area.

4.4.3 Results of temperature-field analysis

- Both model-1 and model-2 are a smooth tool surface contacted by a rough specimen surface. Figs. A4.27 and A4.28 give the temperature distribution near to the interface. In both of the figures, (b) is the enlargement of the area near to the interface to reveal the temperature variation more clearly.
- There is a greater real contact area in model-2 than in model-1. The two models show the same phenomenon in that the temperatures are the greatest

in the contact area such as point A and are the lowest on the specimen surface at the valley of the gaps such as point B (see Fig. A4.28).

- In model-1, the surfaces are not in contact at their ends. The temperature at point C is greater than the temperature at other gap locations. Contrary, the temperature at point D is lower than at other gap locations on the specimen surface (Fig. A4.27).

4.5 Conclusions

Based on the analysis, the following conclusions can be drawn.

- Depending on the deformation of single peaks, the material flow in a sharp single peak produces a rough surface that seems to retain the lubricant more easily for carrying out micro-forming with the lubricant used and makes it less easy to remove after micro-forming. The material flow in the blunt single peak makes the surface at the position of the valley move up relative to the original surface.

- After analysing the results obtained from the multiple-peak model, the conclusion is that the stress distribution is not uniform near to the interface and that there are local lower-stress areas under the surface at the position of the valleys. The non-uniform stress distribution near to the surface may have an influence on the precision of a micro-formed product.

- Rough surface contact also produces a non-uniform temperature field near to the interface. It may have an influence on the micro-expansion of the material near to the interface and make the non-uniform stress distribution more severe.

- The surface roughness of material to be used for micro-forming should be as low as possible and blunt rough peaks are better than sharp rough peaks.

The results of the micro-deformation were obtained based on some simplification. In future study, more complex boundary conditions and the friction force in the interface may be considered in the finite element simulation to investigate the influence of those parameters on the micro-deformation.

4.6   References

Bahrami M., Culham J. R., Yovanovich M. M. and Schneider G. E. (2003), ' Review of thermal joint resistance model for non-conforming rough surfaces in a vacuum,' *Proceeding of HTC'03, ASME Summer Heat Transfer Conference,* HT2003-47051.

Chen X., Qin, Y. and Balendra, R. (2004), 'Development of a statistical parameter-based surface model for the simulation of variation of surface roughness with contact pressure,' *Joural of Materials Technology 145,* pp 247-255

Clausing, A. M. and Chao, B. T. (1963), 'Thermal contact conductance in a vacuum environment,' *University of Illinois, Urbana, Illinois, Report ME-TN-242-1.*

Francis, H.A. (1977), 'Application of spherical indentation mechanics to reversible and irreversible contact between rough surfaces,' *Wear 45,* pp 221-269.

Greenwood, J. A. and Williamson, B. P. (1966), 'contact of nominally flat surfaces,' *Proc., Roy. Soc., London, A295*, pp 300-319.

Ishigaki, H. and Kawaguchi, I. (1979), 'A simple estimation of the elastic-plastic deformation of contacting asperities,' *Wear 54,* pp 157-164.

Kucharski, S., Klimczak, T., Polijaniuk, A. and Kaczmarek, J. (1994), 'Finite-element model for the contact of rough surfaces,' *Wear 177,* pp 1-13.

Pullen, J. and Williamson, J.B.P. (1972), 'On the plastic contact of rough surfaces,' *Proc. R. Soc. London A 327.* pp 159 173.

Sridhar, M.R. and Yovannovich M.M. (1994) 'Review of elastic and plastic contact conductance models: comparison with experiment,' *J. Thermaophys, Heat Transfer 8* (4), pp 633-641.

Yovannovich, M. M. (1969), 'Overall constriction resistance between contacting rough, wavy surfaces,' *Int. J. Heat Mass Transfer 12,* pp 1517-1520.

4.7 Appendix A – Figures
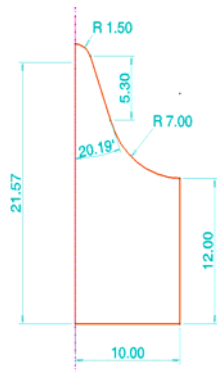
Single-peak model-1
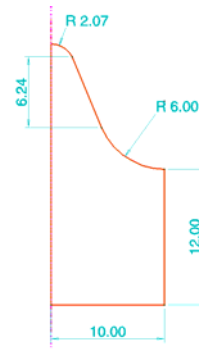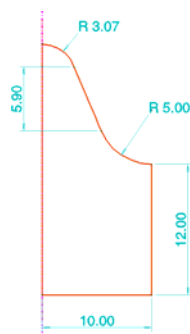
Single-peak model-2
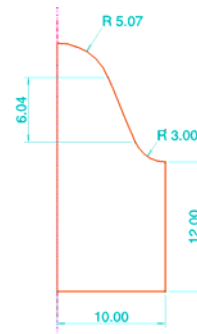
Single-peak model-3

Single-peak model-4

Fig. A4.1 Geometry of single peaks
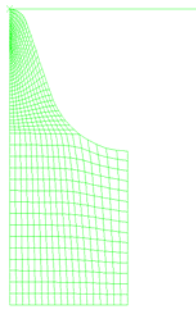
Singl-peak model-1
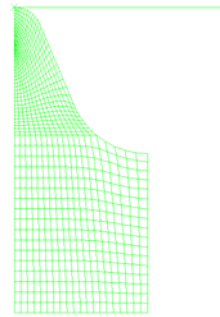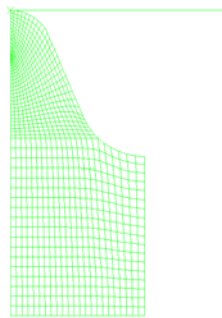
Single-peak model-2
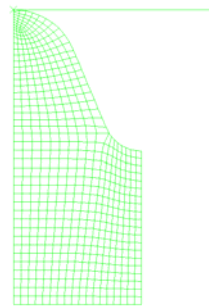
Single-peak model-3

Single-peak model-4

Fig. A4.2   Meshes of single peaks
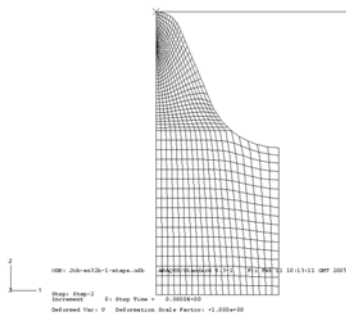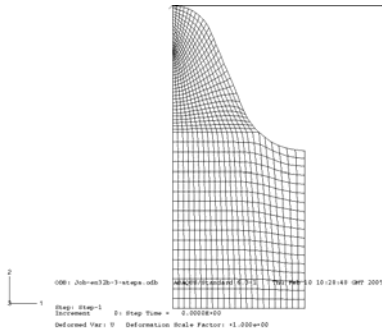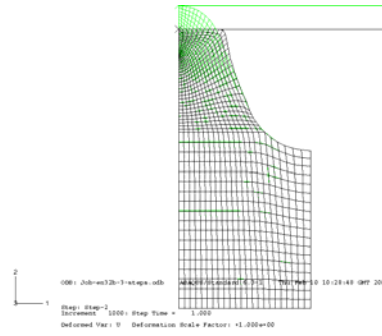
Step 1
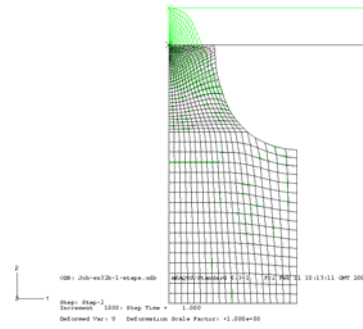
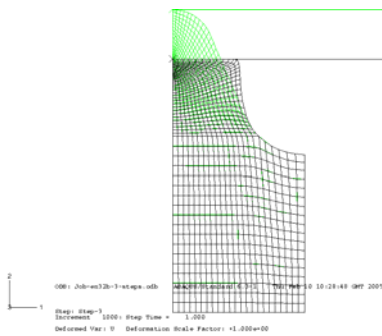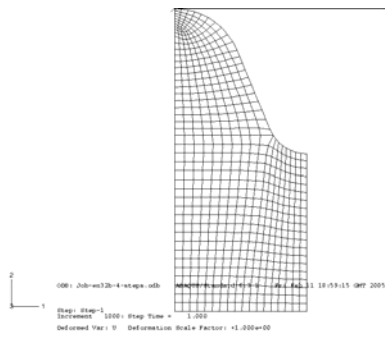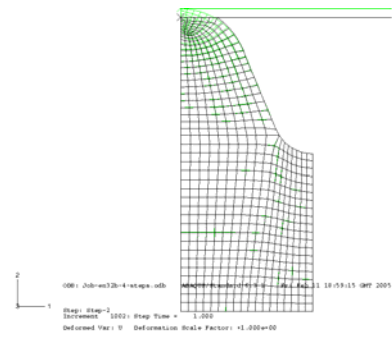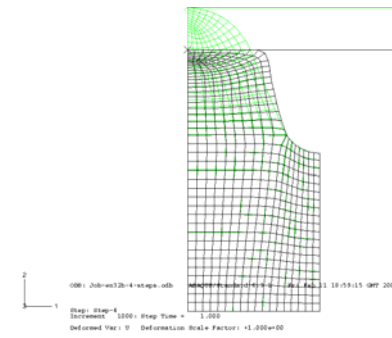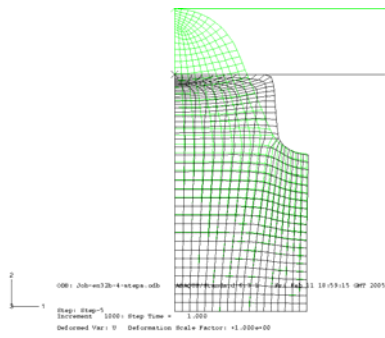**Step 2**
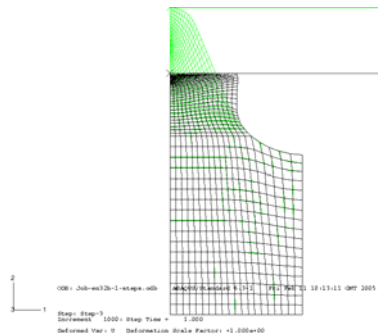
Step 3
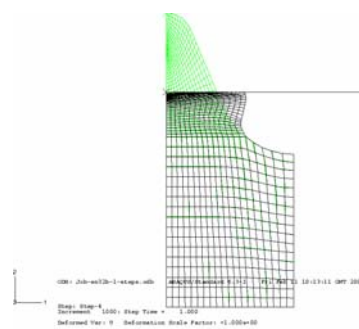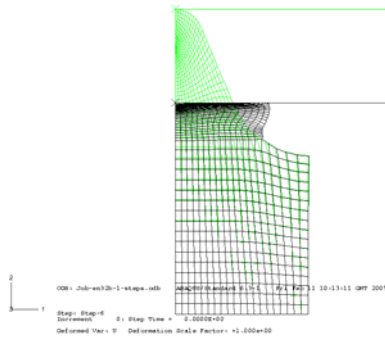
Step 4

Step 5

Fig. A4.3   Deformation of Single-peak model-1 for a free boundary at edge CD
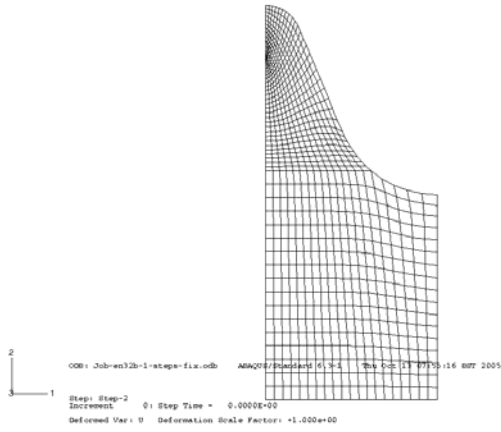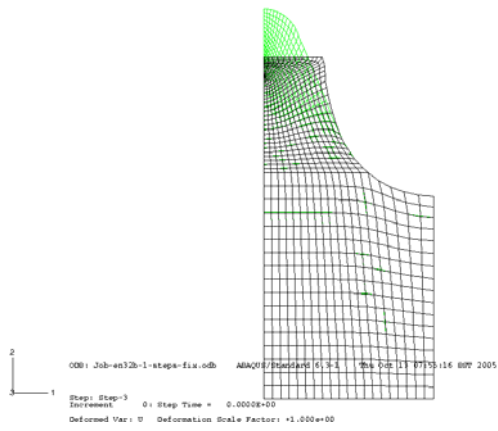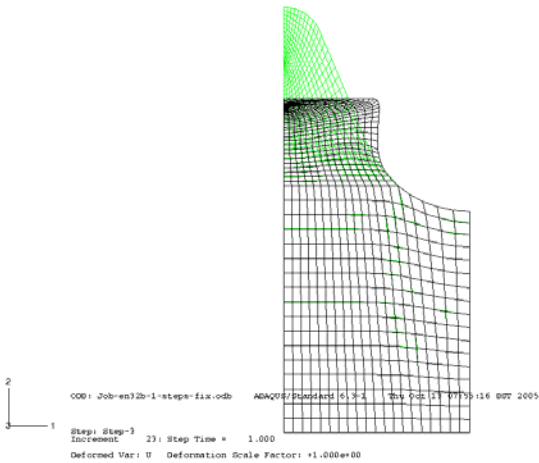
Step 1

Step 2

Step 3

Fig. A4.4   Deformation of Single-peak model-1 for a fixed boundary at edge CD
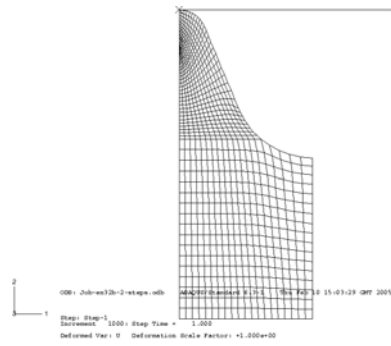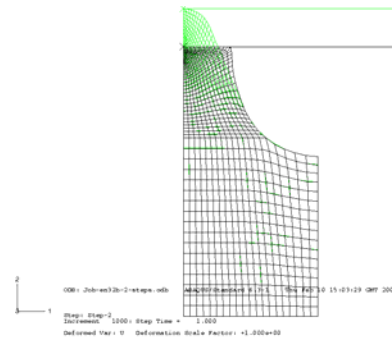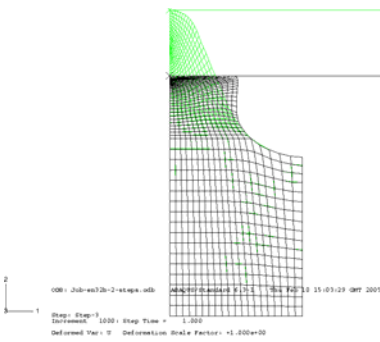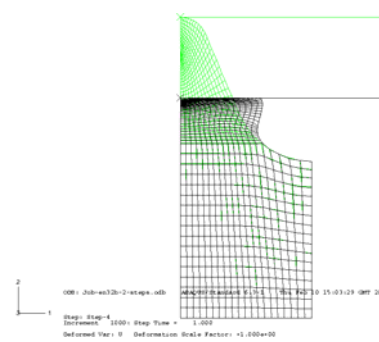
Step 1
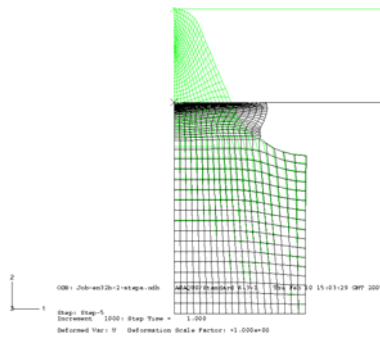
Step 2

Step 3

Step 4

Step 5

Fig. A4.5   Deformation of Single-peak model-2 for a free boundary at edge CD
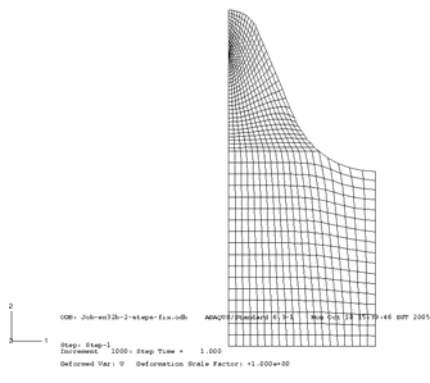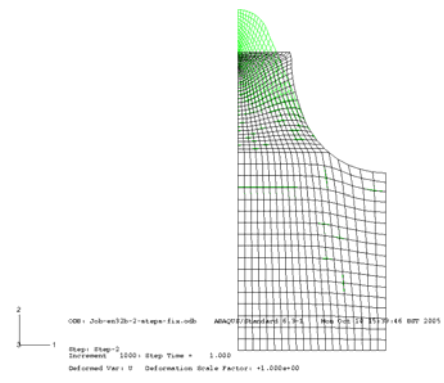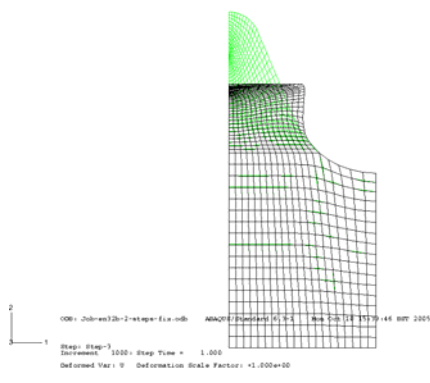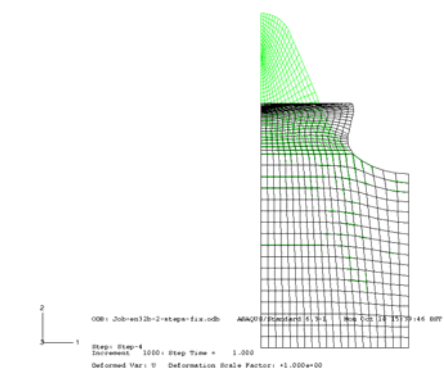
Step 1
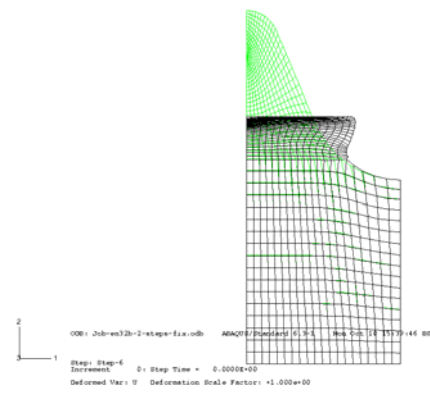
Step 2

Step 3

Step 4

Step 5

Fig. A4.6   Deformation of Single-peak model-2 for a fixed boundary at edge CD
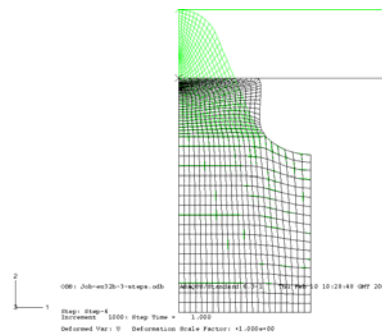
Step 1
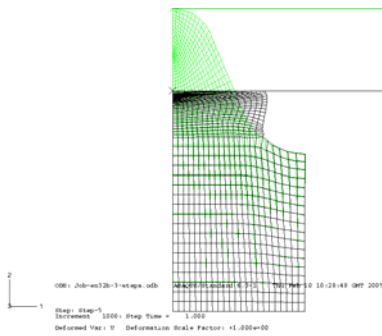
Step 2

Step 3

Step 4

Step 5

Fig. A4.7   Deformation of Single-peak model-3 for a free boundary at edge CD

Step 1

Step 2

Step 3

Step 4

Step 5

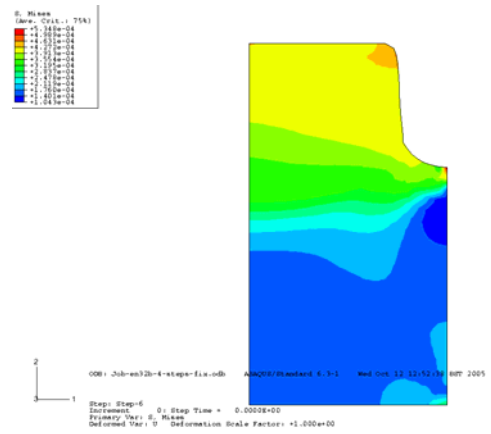**Fig. A4.8   Deformation of Single-peak model-3 for a fixed boundary at edge CD**

Step 1

Step 2
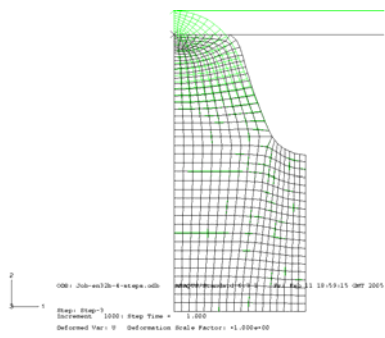
Step 3

Step 4

Step 5

Fig. A4.9   Deformation of Single-peak model-4 for a free boundary at edge CD

Step 1

Step 2

Step 3

Step 4

Step 5
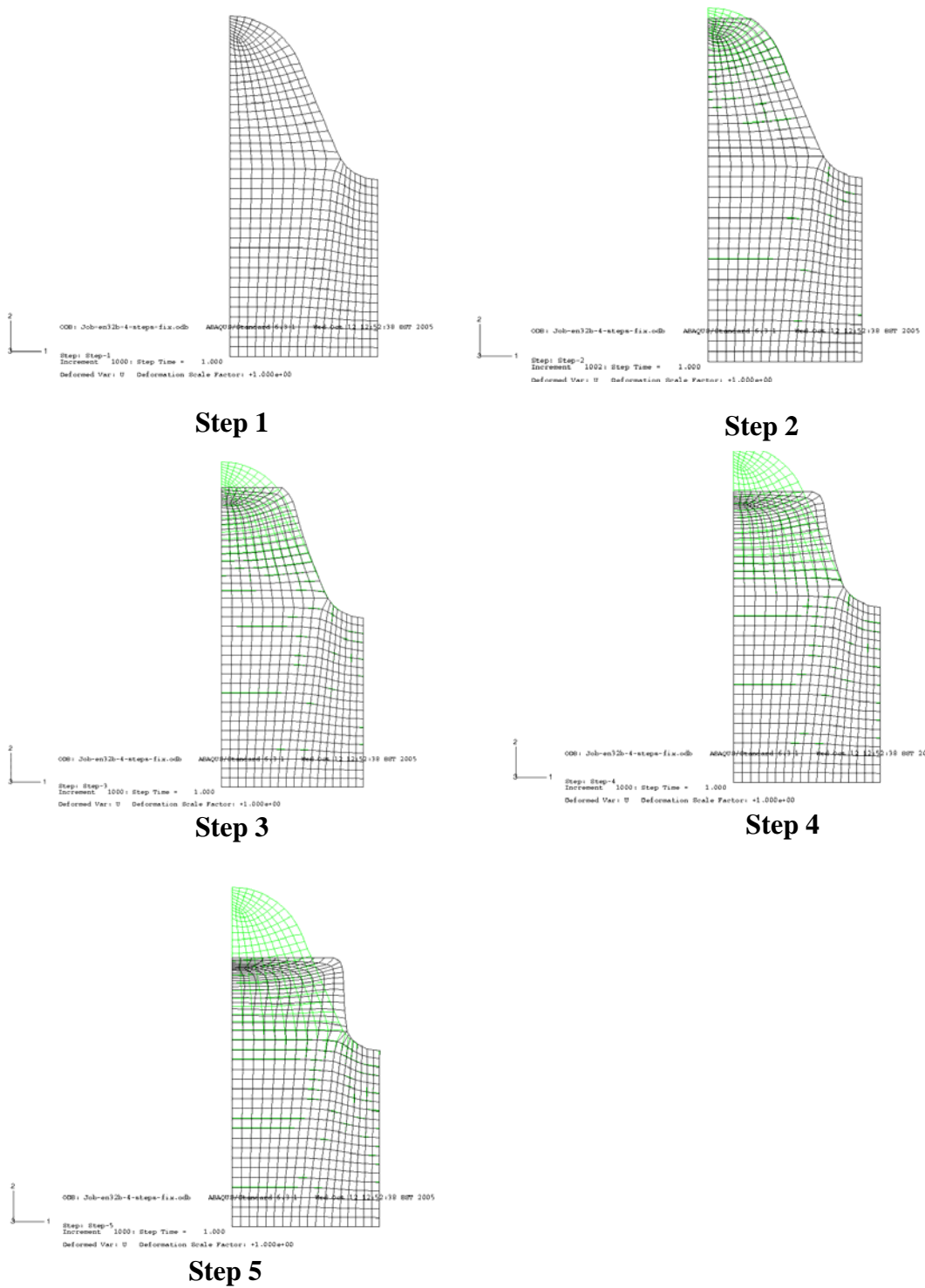
Fig. A4.10   Deformation of Single-peak model-4 for a fixed boundary at edge CD
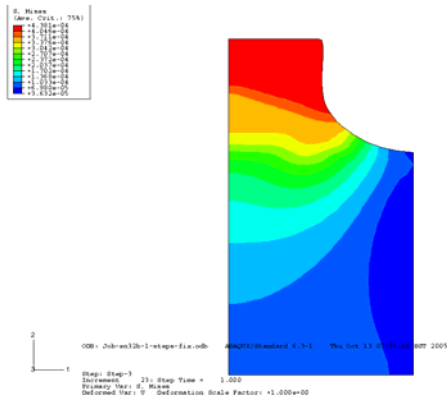
Single-peak model-1
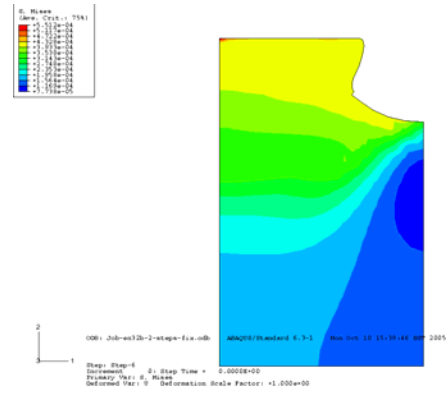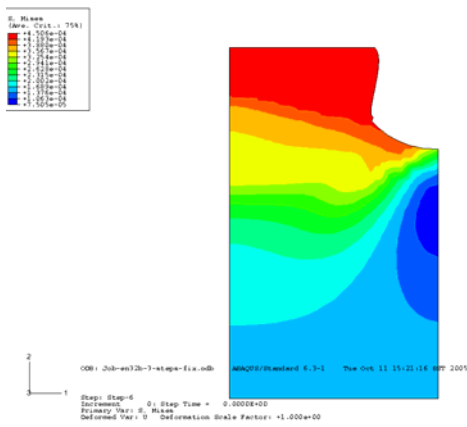
Single-peak model-2

Single-peak model-3

Single-peak model-4

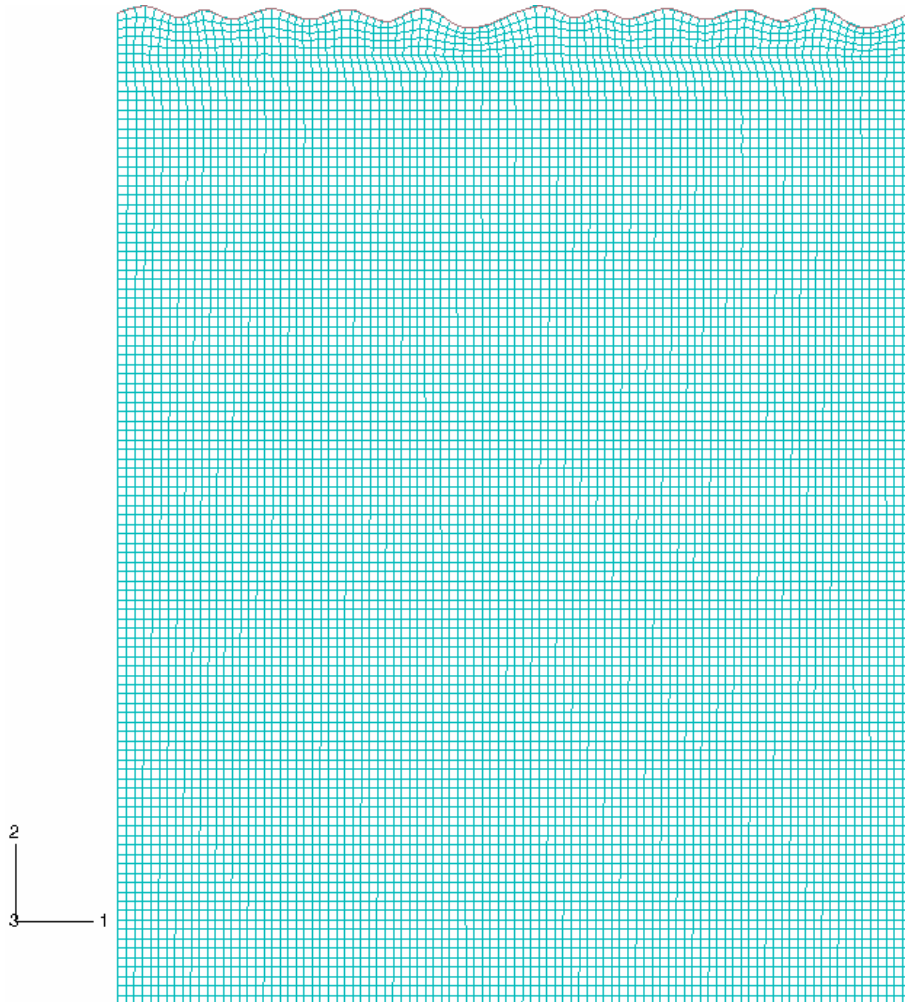**Fig. A4.11   Stress of Single-peak models for a fixed boundary at edge CD**
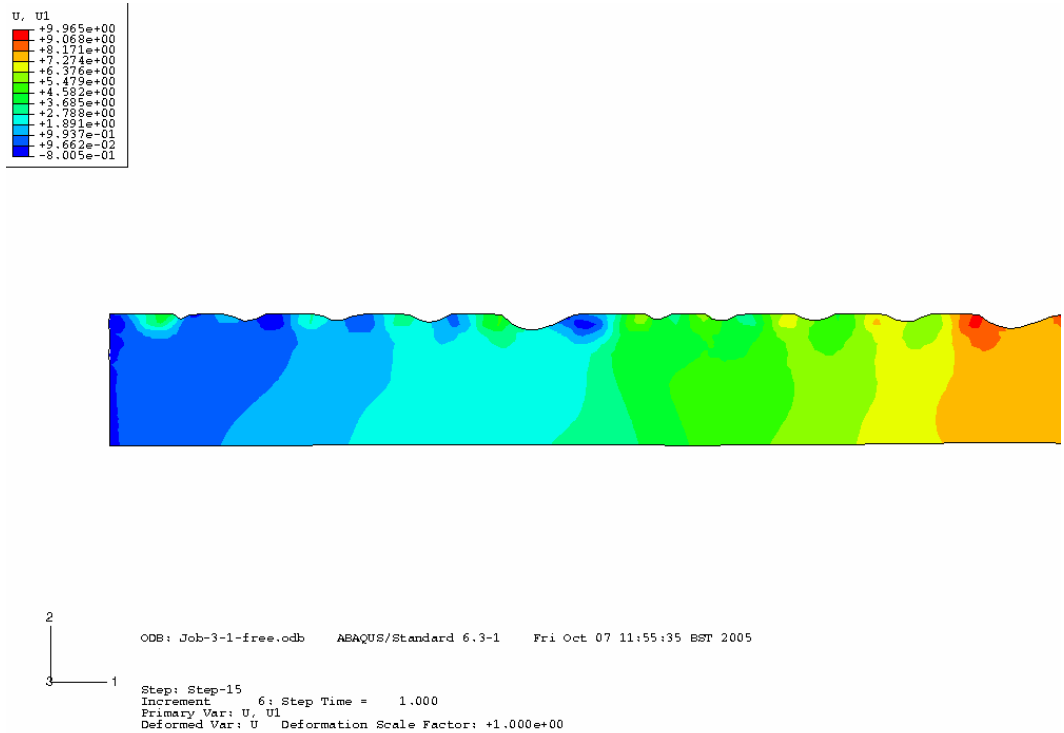
Fig. A4.12   The mesh of the multiple-peak model

U, U1
+9.965e+00
+9.068e+00
+8.171e+00
+7.274e+00
+6.376e+00
+5.479e+00
+4.582e+00
+3.685e+00
+2.788e+00
+1.891e+00
+9.937e-01
+9.662e-02
-8.005e-01

ODB: Job-3-1-free.odb   ABAQUS/Standard 6.3-1   Fri Oct 07 11:55:35 BST 2005

Step: Step-15
Increment   6: Step Time =   1.000
Primary Var: U, U1
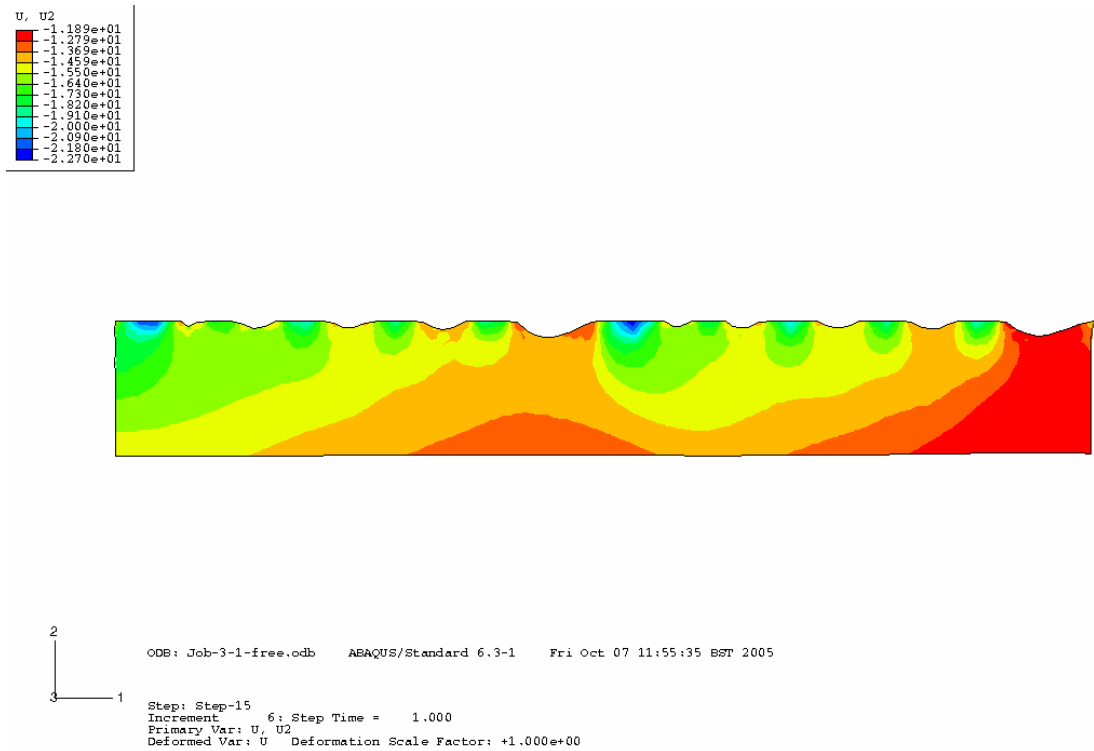Deformed Var: U   Deformation Scale Factor: +1.000e+00

Fig. A4.13   Deformation u1 of the 2D model (strip near the interface) for a free boundary at edges AC and BD

U, U2
-1.189e+01
-1.279e+01
-1.369e+01
-1.459e+01
-1.550e+01
-1.640e+01
-1.730e+01
-1.820e+01
-1.910e+01
-2.000e+01
-2.090e+01
-2.180e+01
-2.270e+01

ODB: Job-3-1-free.odb   ABAQUS/Standard 6.3-1   Fri Oct 07 11:55:35 BST 2005

Step: Step-15
Increment   6: Step Time =   1.000
Primary Var: U, U2
Deformed Var: U   Deformation Scale Factor: +1.000e+00

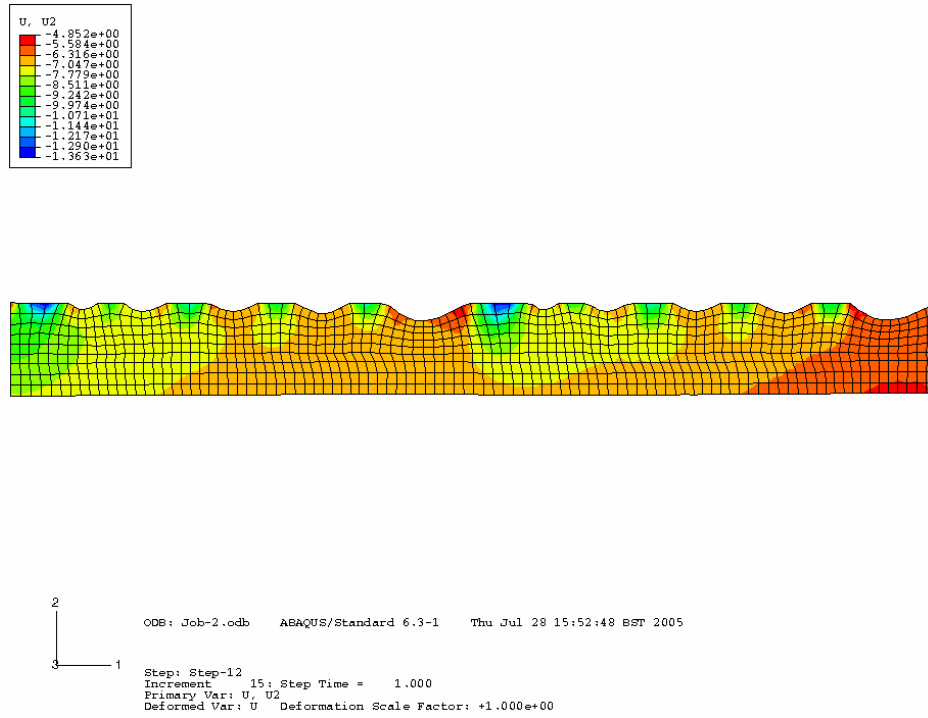**Fig. A4.14   Deformation u2 of the 2D model (strip near the interface) for a free boundary at edges AC and BD**

```
U, Magnitude
    +2.283e+01
    +2.200e+01
    +2.117e+01
    +2.034e+01
    +1.951e+01
    +1.868e+01
    +1.785e+01
    +1.703e+01
    +1.620e+01
    +1.537e+01
    +1.454e+01
    +1.371e+01
    +1.288e+01
```

```
ODB: Job-3-1-free.odb    ABAQUS/Standard 6.3-1    Fri Oct 07 11:55:35 BST 2005

Step: Step-15
Increment      6: Step Time =    1.000
Primary Var: U, Magnitude
Deformed Var: U   Deformation Scale Factor: +1.000e+00
```
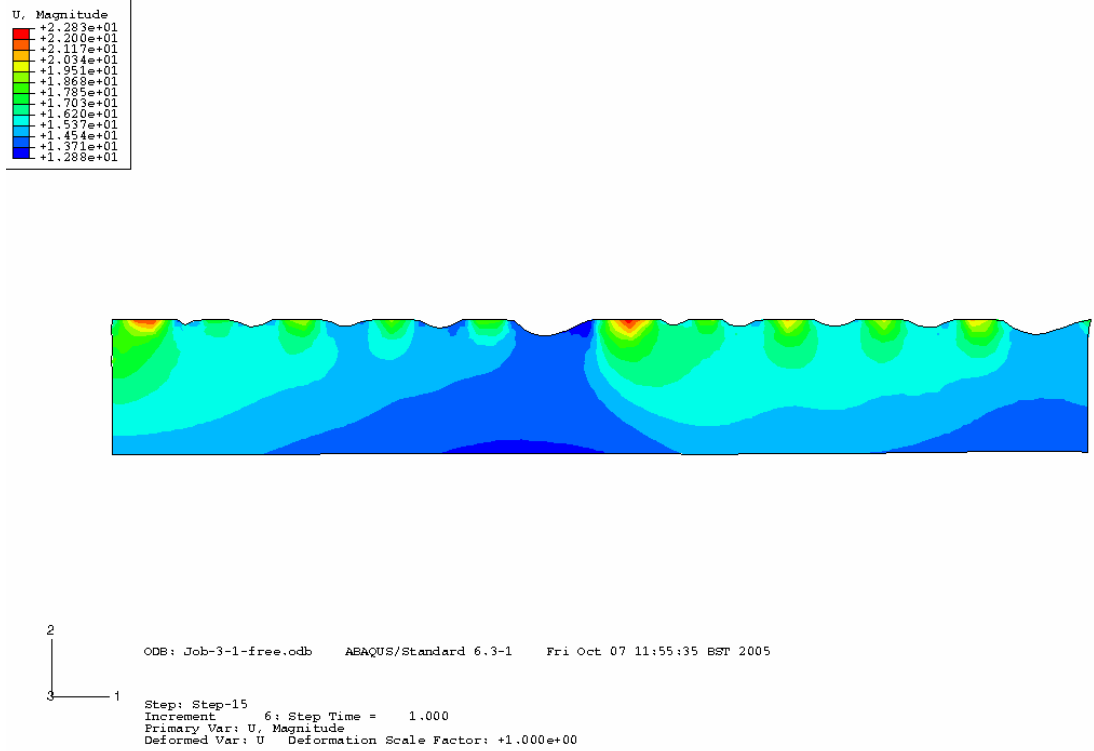
Fig. A4.15   Deflection u (magnitude) of the 2D model (strip near the interface) for a free boundary at edges AC and BD

Fig. A4.16 **Deformation u1 of the 2D model (strip near the interface) for a fixed boundary at edges AC and BD**
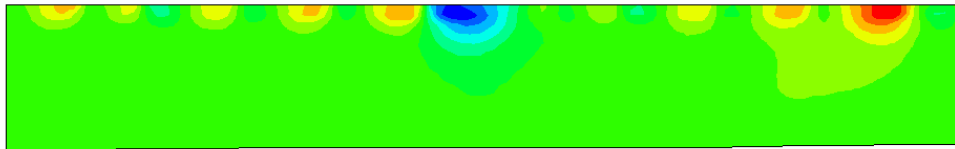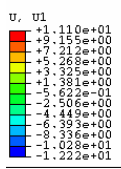
Fig. A4.17   Deformation u2 of the 2D model (strip near the interface) for a fixed boundary at edges AC and BD

Fig. A4.18   Deformation u1 of the 2D model (strip near the interface) for a fixed boundary at edges AC and BD

Fig. A4.19   Deformation u2 of the 2D model (strip near the interface) for a fixed boundary at edges AC and BD

S, Mises
(Ave. Crit.: 75%)
+4.200e-04
+4.143e-04
+4.086e-04
+4.029e-04
+3.972e-04
+3.915e-04
+3.858e-04
+3.801e-04
+3.744e-04
+3.687e-04
+3.630e-04
+3.573e-04
+3.516e-04
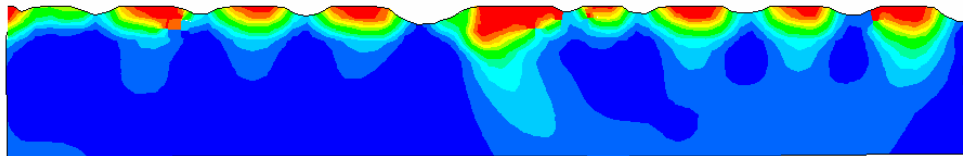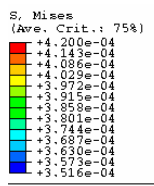
ODB: Job-3-1-free.odb   ABAQUS/Standard 6.3-1   Fri Oct 07 11:55:35 BST 2005

Step: Step-15
Increment   6: Step Time =   1.000
Primary Var: S, Mises
Deformed Var: U   Deformation Scale Factor: +1.000e+00

Fig. A4.20   Mises stress near to the interface of the 2D model (strip near the interface) for a free boundary at edges AC and BD

Step 6

Low stress area

Mises
ve. Crit.: 75%)
+4.200e-04
+3.854e-04
+3.508e-04
+3.162e-04
+2.816e-04
+2.471e-04
+2.125e-04
+1.779e-04
+1.433e-04
+1.087e-04
+7.412e-05
+3.954e-05
+4.948e-06

ODB: Job-3-1-fix.odb   ABAQUS/Standard 6.3-1   Mon Oct 10 10:02:00 BST 2005

Step: Step-6
Increment   18: Step Time =   1.000
Primary Var: S, Mises
Deformed Var: U   Deformation Scale Factor: +1.000e+00
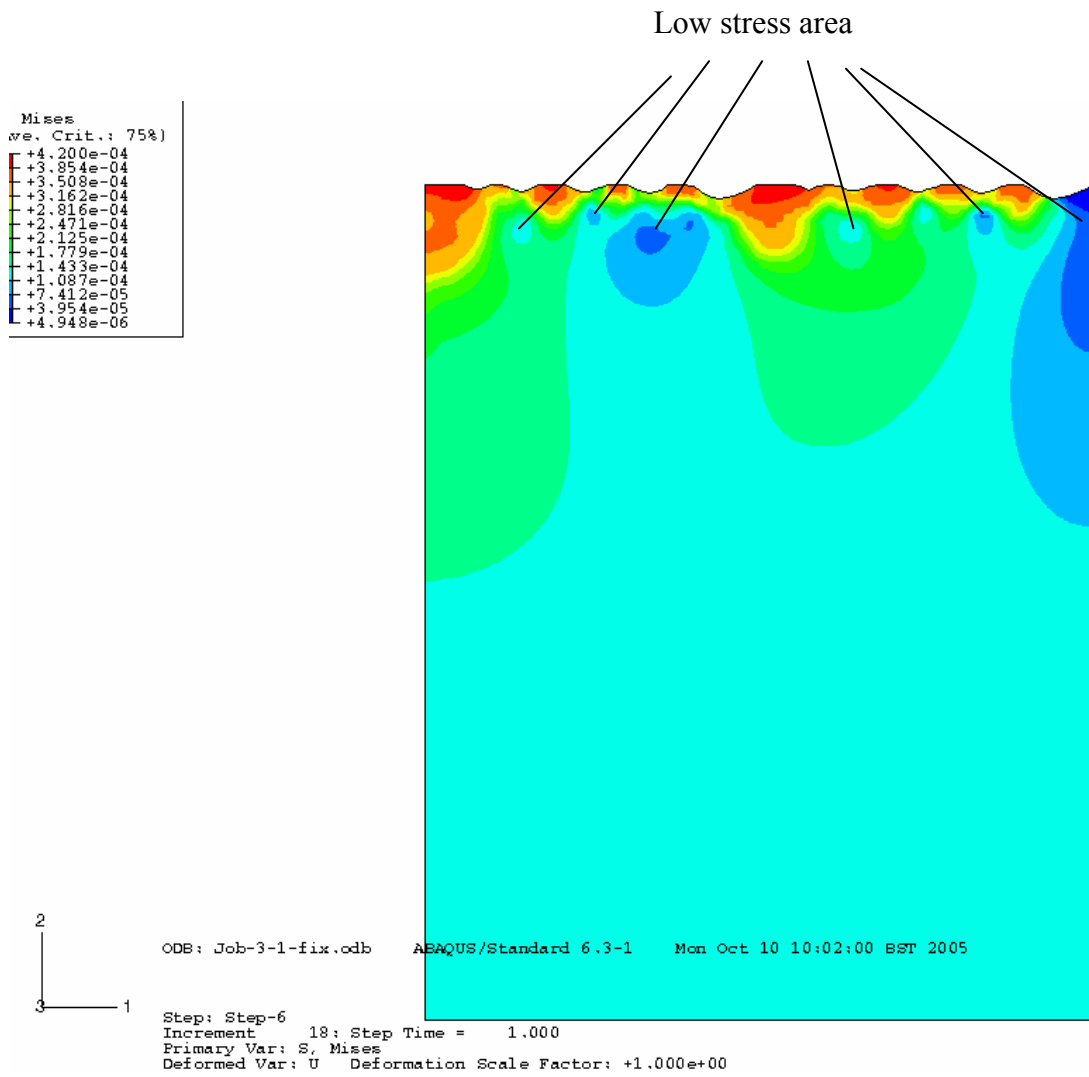
Fig. A4.21   Mises stress for the 2D model at step 6 for a fixed boundary at edges AC and BD

Step 10

Low stress area

S, Mises
(Ave. Crit.: 75%)
+4.200e-04
+3.928e-04
+3.657e-04
+3.385e-04
+3.114e-04
+2.842e-04
+2.571e-04
+2.299e-04
+2.027e-04
+1.756e-04
+1.484e-04
+1.213e-04
+9.412e-05

ODB: Job-3-1-fix.odb   ABAQUS/Standard 6.3-1   Mon Oct 10 10:02:00 BST 2005

Step: Step-10
Increment   17: Step Time =   1.000
Primary Var: S, Mises
Deformed Var: U   Deformation Scale Factor: +1.000e+00
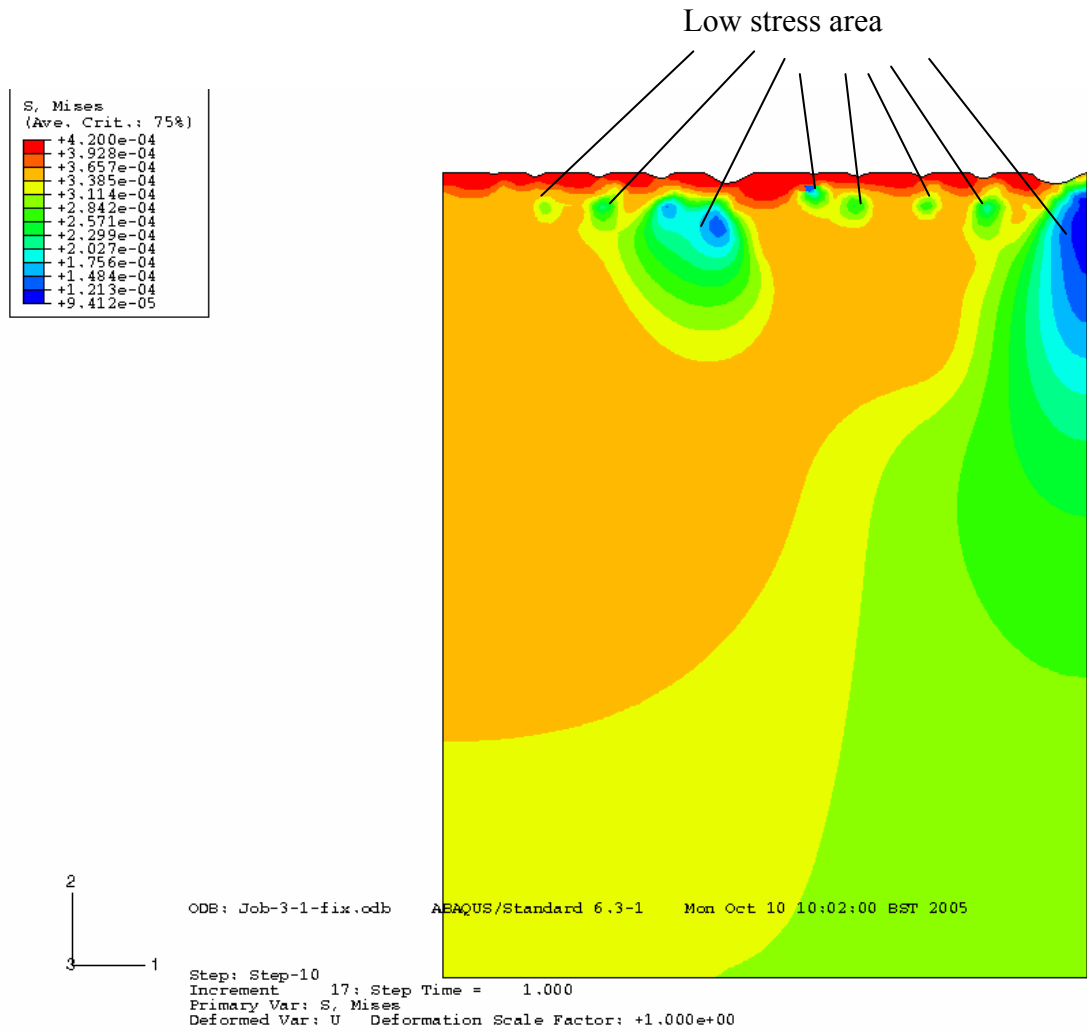
Fig. A4.22   Mises stress for the 2D model at step 10 for a fixed boundary at edges AC and BD

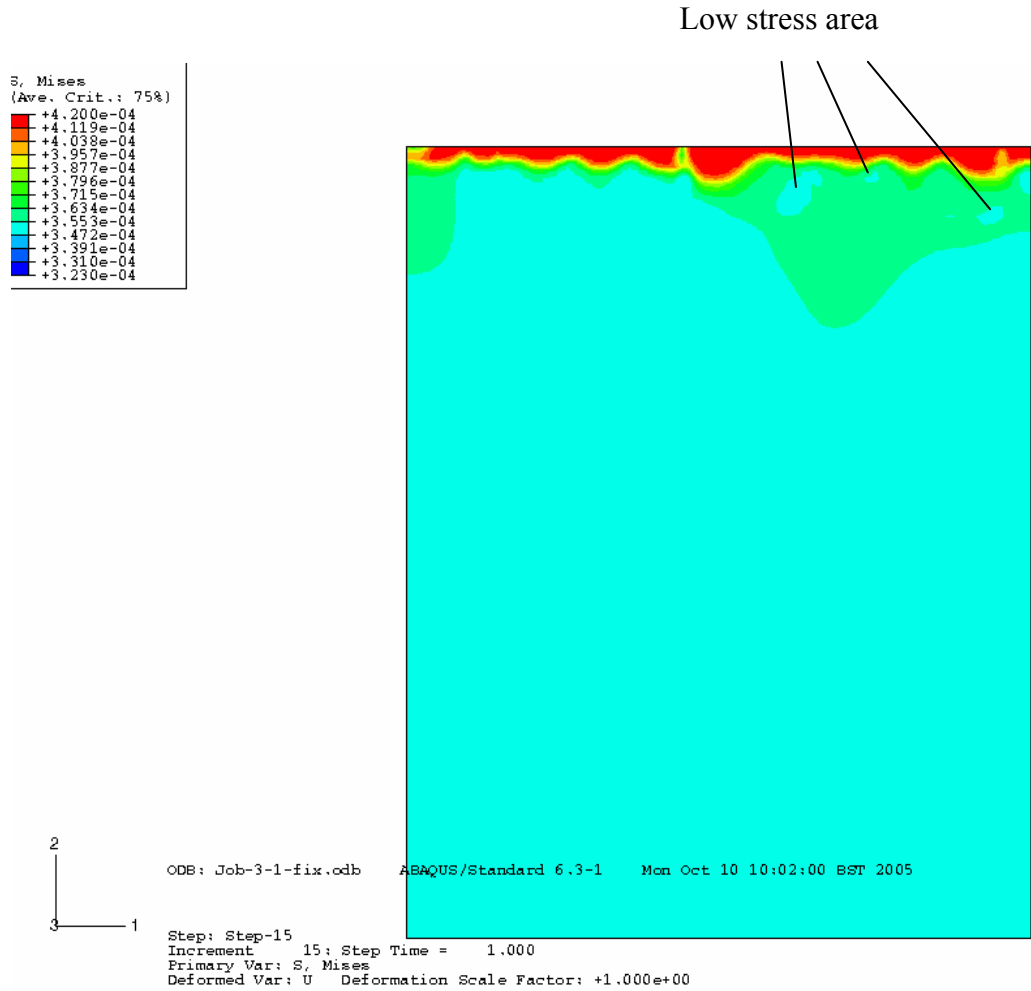**Step 15**

Low stress area

Fig. A4.23   Mises stress for the 2D model at step 15 for a fixed boundary at edges AC and BD

**Fig. A4.24   Deformation of U1 of the multiple-peak model for a
fixed boundary at edge AC and free at BD**

**Fig. A4.25   Deformation of U2 of the multiple-peak model
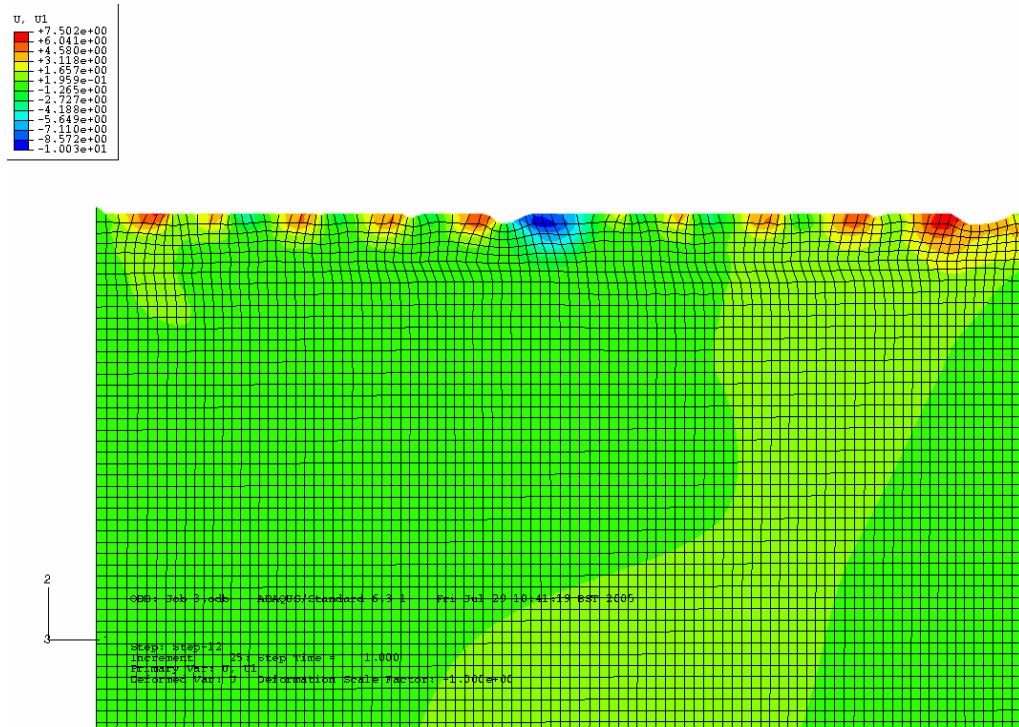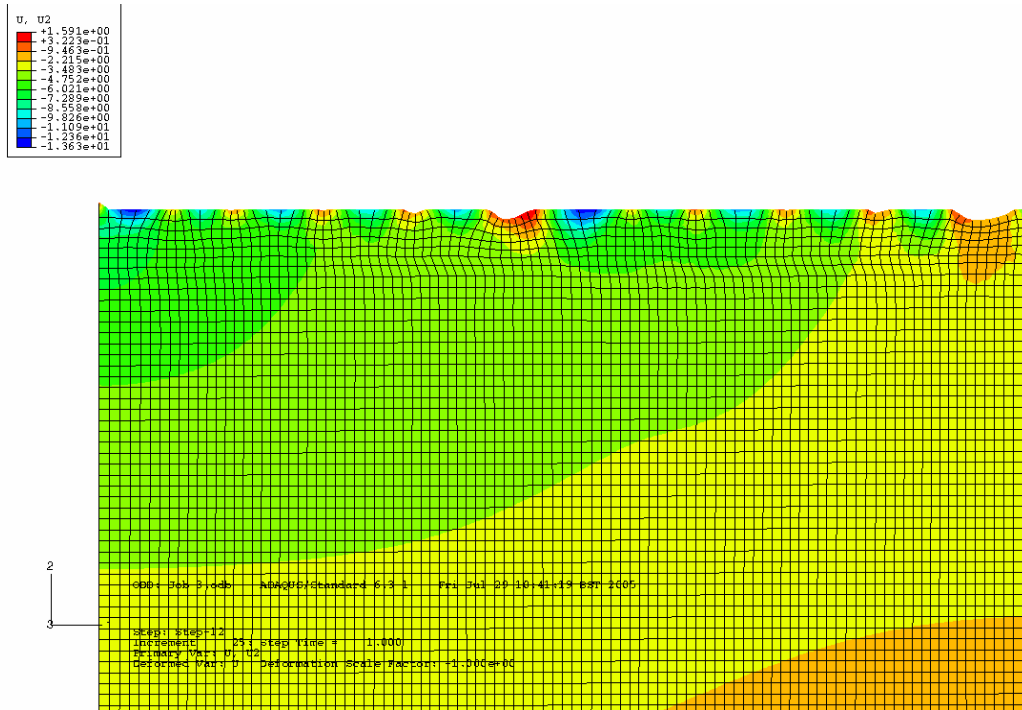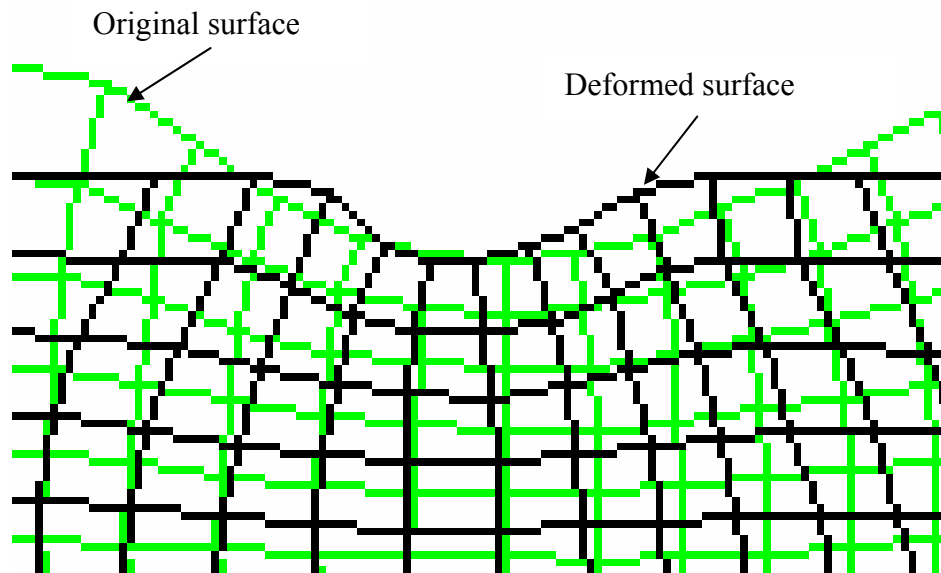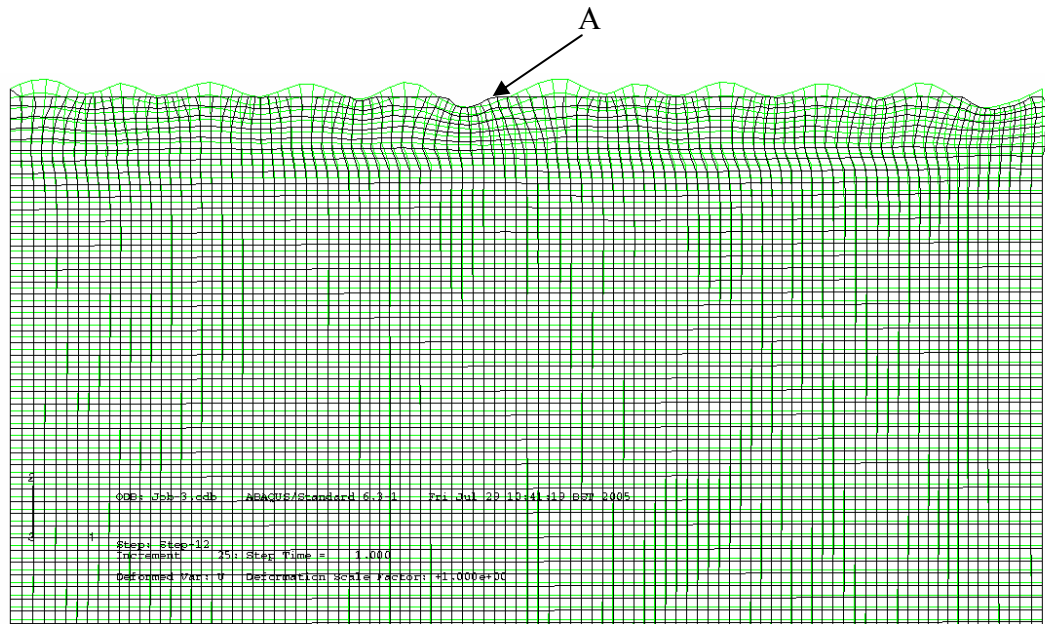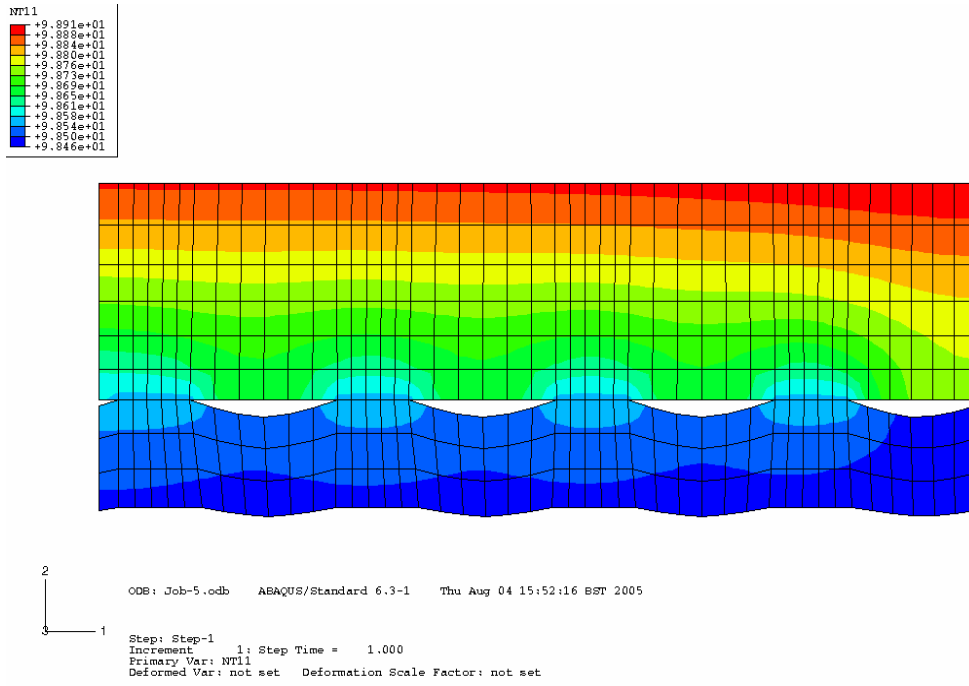for a fixed boundary at edge AC and free at BD**
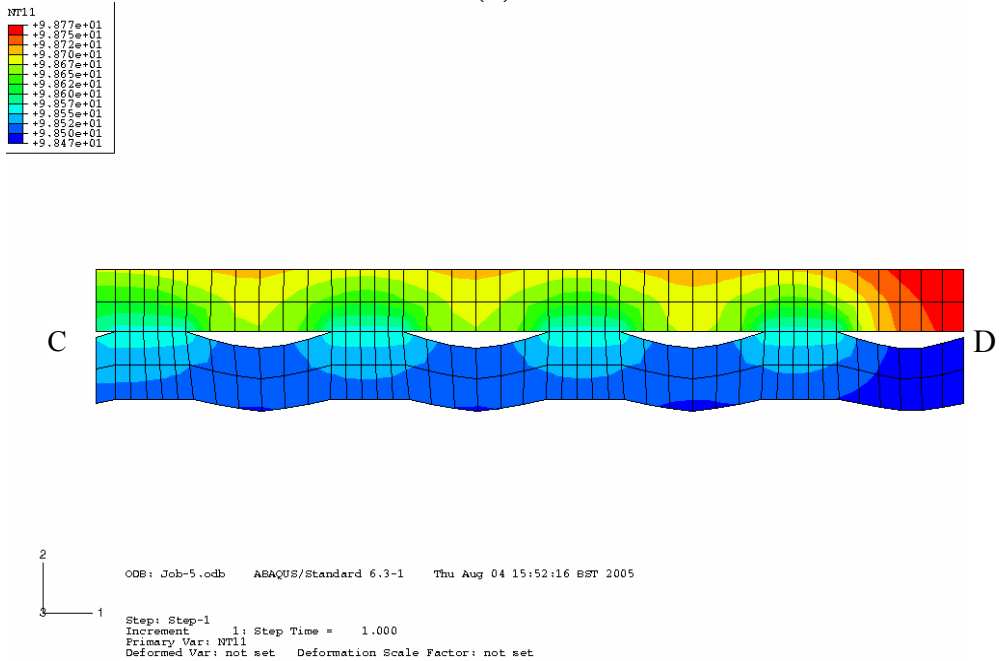
Zoom A

**Fig. A4.26   Deformation of U of the multiple-peak model
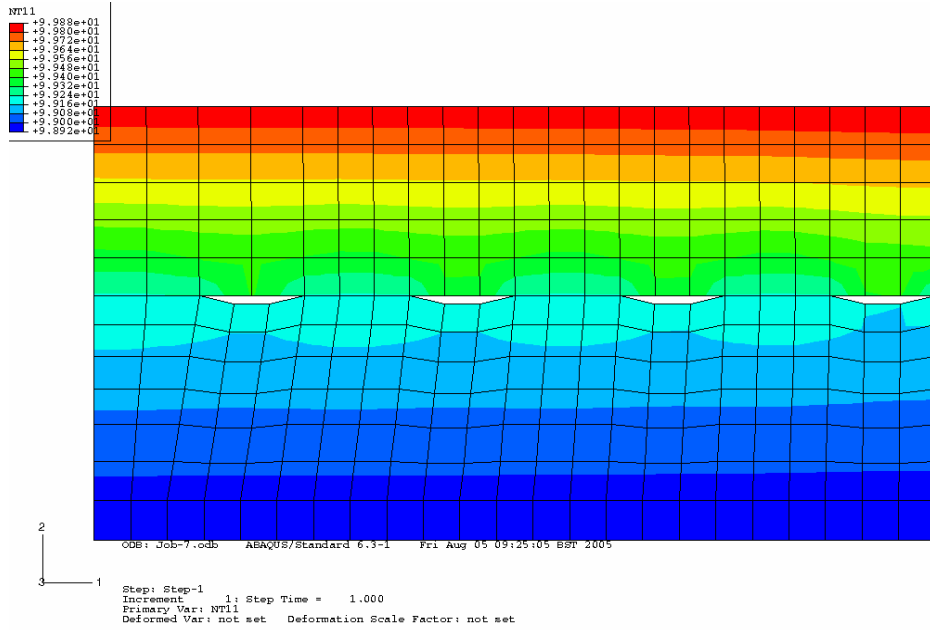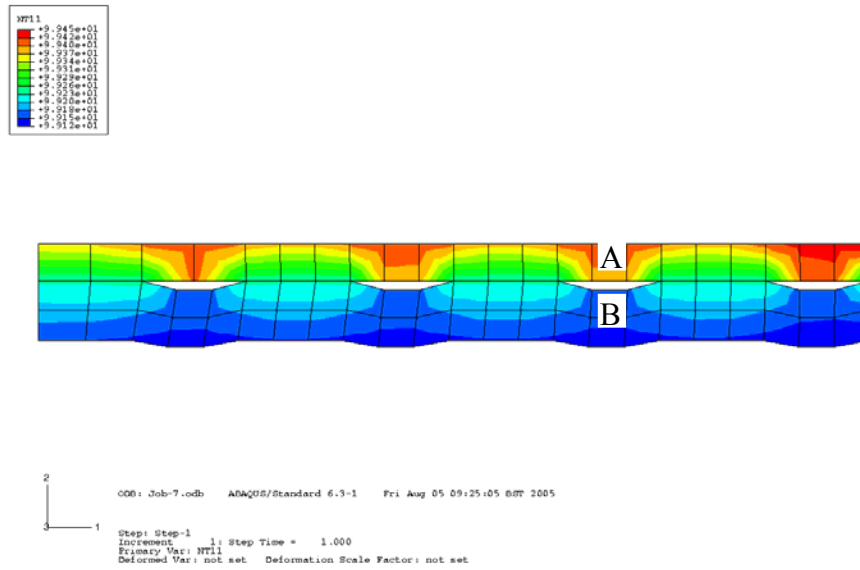for a fixed boundary at edge AC and free at BD**

(a)

(b)

Fig. A4.27   Temperature distribution of model-1

(a)

(b)

Fig. A4.28   Temperature distribution of model-2

Chapter 5 Conceptual Design of the Frame of a Micro-Stamping Machine

5.1   Introduction

Integral design of the machine frame structure and the whole machine system will become more important in the development of future generations of machines (Zaeh and Oertli, 2004). Despite many achievements in the development of micro-forming machine systems, some problems still exist, such as large conventional geometry, high maintenance cost, and low flexibility (Geiger, 2001; Groche and Schneider, 2004; Hess, 2000). New methods in the development of micro-forming machine systems are being investigated through numerical analysis and experimentation (Proche and Schneider, 2004)

High precision, mass manufacture and light-weight structure are the main targets in the design of a micro-stamping manufacturing system. In order to improve the design, macro-analysis and micro-analysis have been undertaken through numerical studies and experimental measurement. The investigation in the foregoing chapters is focused on the analysis of the contact characteristics of rough contact surfaces. In the present chapter, dynamics analysis of the manufacturing system is performed for purposes of concept design and improved design of a micro-stamping manufacturing system. The findings from micro-analysis are used for building the models for the dynamics analysis of a micro-stamping machine and a micro-stamping tool.

The aim of the study in this chapter is to design a micro-stamping machine in conceptual design stage and use it for further study.

The first stage of micro-stamping machine design is the concept design. During this stage, six concepts of micro-stamping machines have been designed by working in a group and the dynamic behaviour of the structures of these six concept machines have been investigated through finite element analysis using the general-purpose FE Code ABAQUS. Based on the critical elements of the micro-stamping machine and

information obtained from the investigation during this stage, further optimised design of the micro-stamping machines will be explored, the details of the improved design and analysis being described in subsequent chapters.

5.2   Concepts of the micro-stamping machine

The functional requirements of the machine include requirement for forces, speed of stroke, precision, vibration frequency, a feeding and handling system, and so on. The machine should be able to supply a force which ranges from several hundred Newtons to a few tonnes to meet the force required for micro-forming processes. The strokes produced by the machine tool should be able to meet displacements from several tens of microns for micro-stamping to 1 to 2 mm for micro deep-drawing or extrusion. A rate of around 1000 parts per minute is proposed with a view to meeting mass-production requirements. Precision of the machine to be developed was expected to be high. In other words, geometrical errors of the micro-components caused by the machine-errors may be within a few microns. Special devices, such as a vacuum system, should also be adopted for handling the material and workpiece. In order to meet mass manufacture, the machine should be facilitated to their maximum extent of the automation, such as automatic control, monitoring, and data acquisition of the forming process.

5.3   Structural design of the micro-stamping machine

In the stage of concept design, the structure of the machine is focused on: forming-force generation, a linear guidance system, the working table and the machine frame. The main parameters involved in the design are:

- Stiffness of the structure
- Natural frequency
- An adjustable structure for different tools
- Easy connection with material-feeder and workpiece-handing devices
- A large working space
- Light weight

The main components of the six concepts for micro-forming machines are listed in Table 5.1; and the six micro-forming machines are shown in Figs. 5.1 to 5.8.

Table 5.1 Main components of the conceptual micro-forming machines

Concepts	Main components	Driving force
Concept 1	A machine frame, four lead-screw shafts, four ball-screw nuts, four linear guides, a movable ram, a rotary table for the lower rotational working table.	motors
Concept 2	A machine frame, four linear shafts as the linear guides, four linear bearings, a movable ram, a piston rod, a hydraulic cylinder for the movable ram, and a (ART300) rotary table for the lower rotational working table.	A hydraulic cylinder
Concept 3	A machine frame, two magnetic tracks, two linear-motor moving forcers (BLMX382), a movable ram connected to the forcers, and upper as well as lower dies in turn fixed on the movable ram and the lower working table.	Two linear motors
Concept 4	A machine frame, four magnetic tracks, linear-motor moving forcers, a movable ram connected to the forcers and upper/lower dies, which in turn are fixed onto the movable ram and the lower working table.	Four linear motors
Concept 5	A rectangular machine frame with three locations for fixing six magnetic tracks and six linear-motor moving forcers, by means of which three rams would be attached to the three locations separately.	Six linear motors
Concept 6	A rectangular machine frame with four locations for fixing eight magnetic tracks and eight linear-motor moving forcers, by means of which four rams would be attached to the four locations separately.	Eight linear motors

Machine
frame

Four lead-screw
shafts

Movable ram

Four linear
guides

Rotary table

**Fig. 5.1 Concept 1(a) of the micro-stamping
machine**

Enhanced
machine
columns
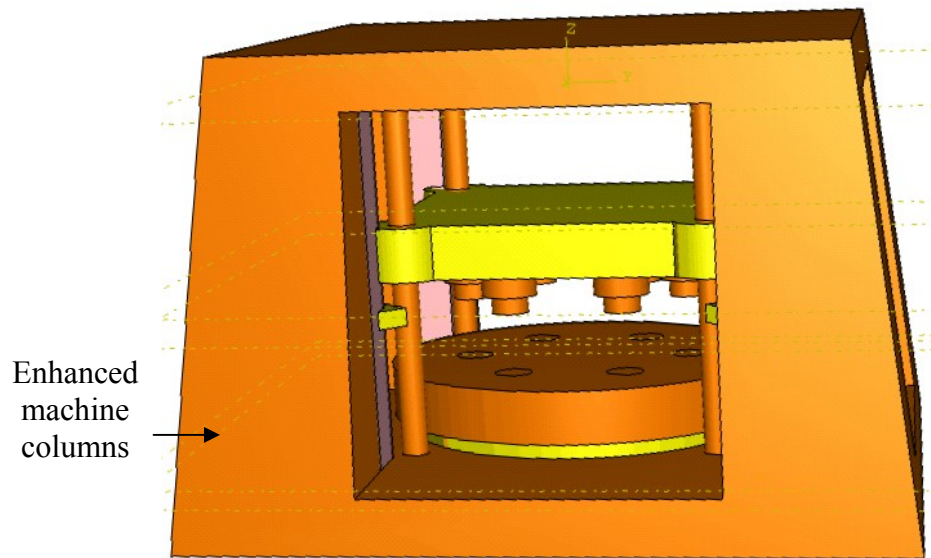
Fig. 5.2 Concept 1(b) of the micro-stamping machine

(The machine columns are enhanced. Other parts are the same as concept 1(a))

Hydraulic cylinder

Piston rod

Machine frame

Four linear bearing

Four linear shafts
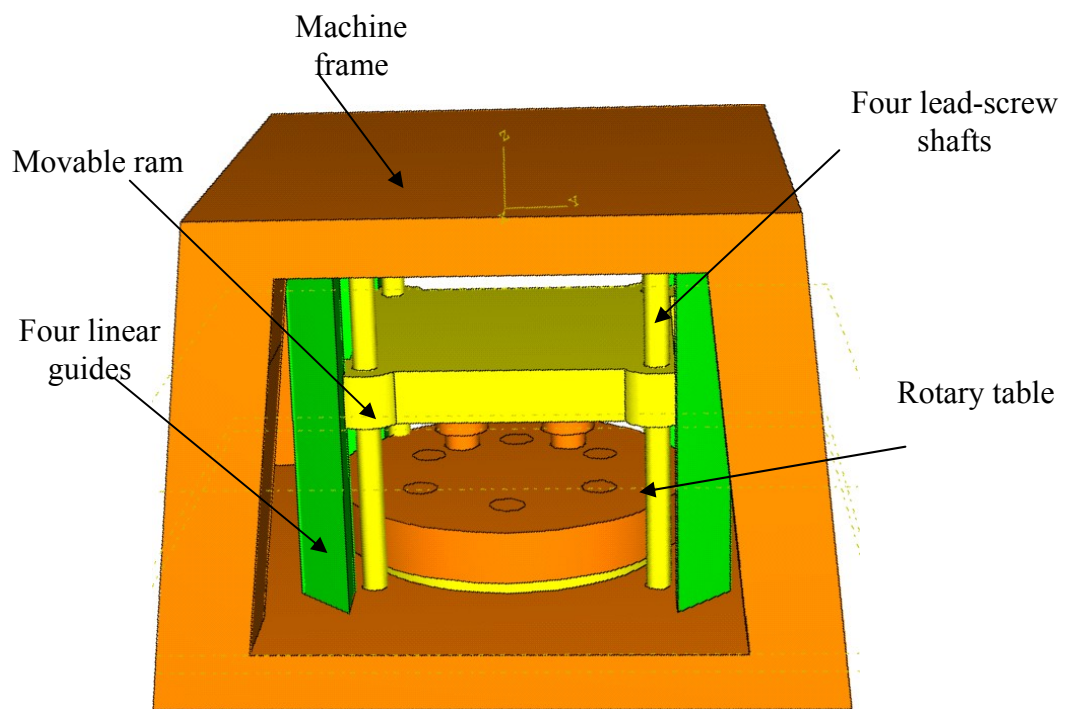
Movable ram

Rotary table
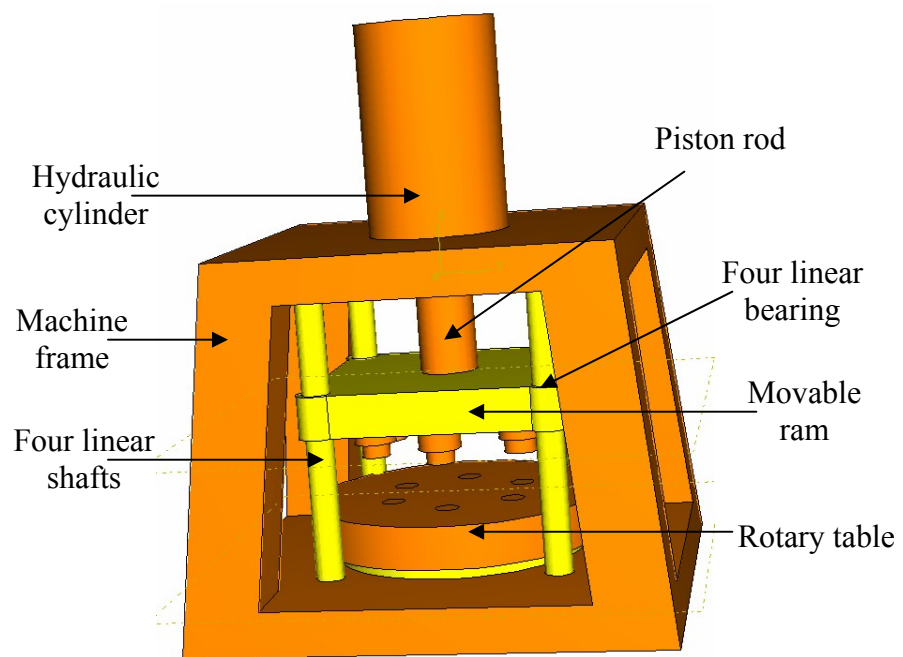
Fig. 5.3 Concept 2 (a) of the micro-stamping machine
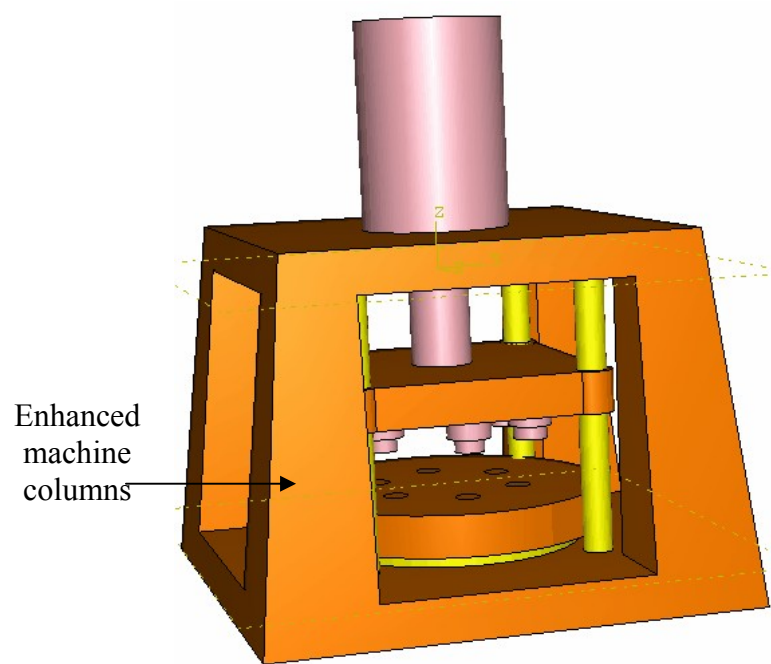
Fig. 5.4 Concept 2 (b) of the micro-stamping machine

(The machine columns are enhanced. Other parts are the same as concept 2(a))

Machine
frame

Movable ram

Stable
working table
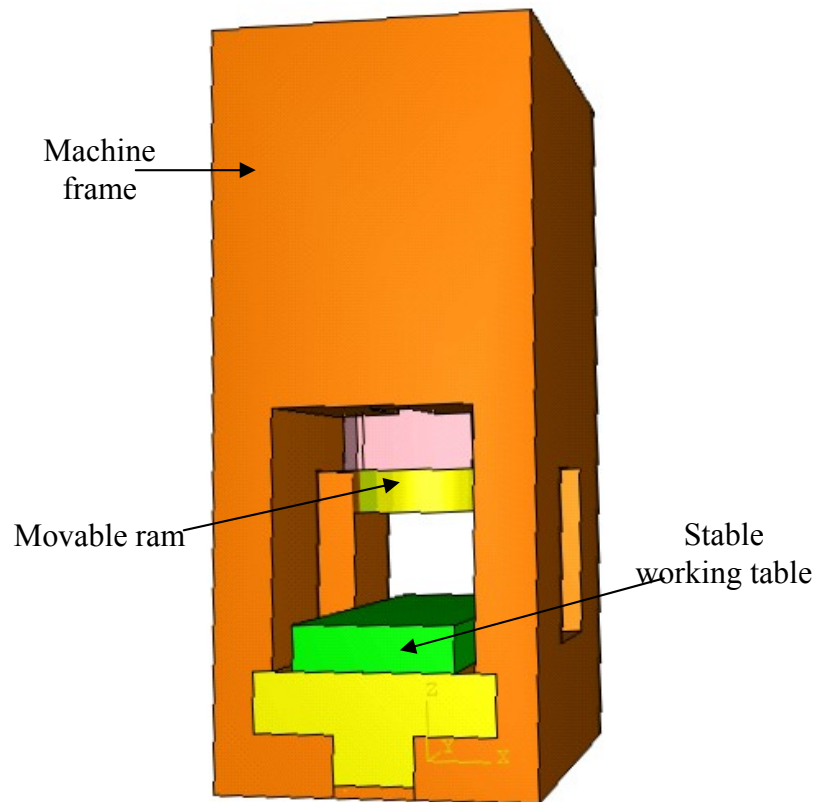
Fig. 5.5 Concept 3 of the micro-stamping machine
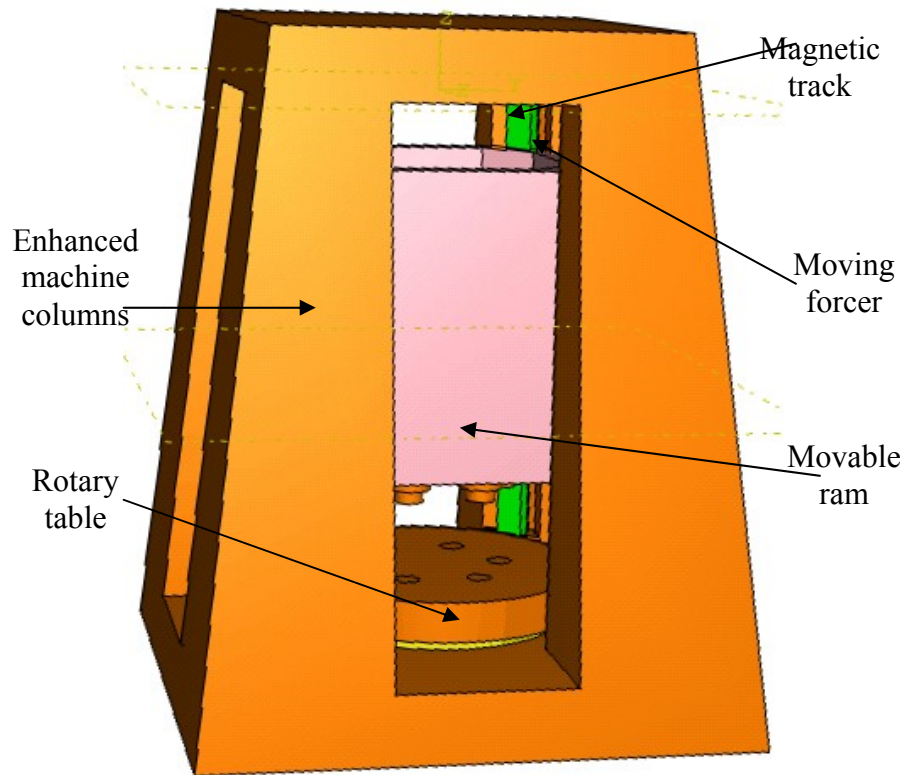
(a) The four-linear-motor driven micro-stamping machine

(b) The movable ram (left) and the machine frame (right)

Fig. 5.6 Concept 4 of the micro-stamping machine

Machine frame

Moving forcer

Magnetic track

Movable ram

Stable working table

Fig. 5.7 Concept 5 of the micro-stamping machine
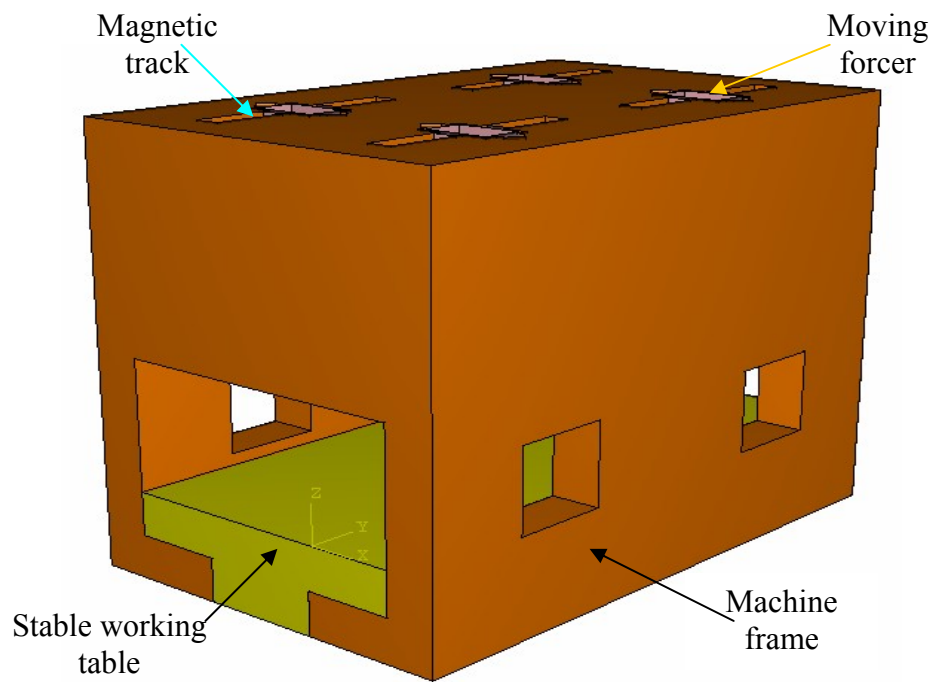
Fig. 5.8 Concept 6 of the micro-stamping machine

5.4 Dynamics analysis of the conceptual models of the micro-stamping machine

For the dynamics analysis of the structures of the conceptual micro-stamping machines, six models are used to obtain results for natural frequency. The material properties used in all models are as described in Sub-section 5.4.1. The details of the six models are presented in Sub-sections 5.4.2 to 5.4.7.

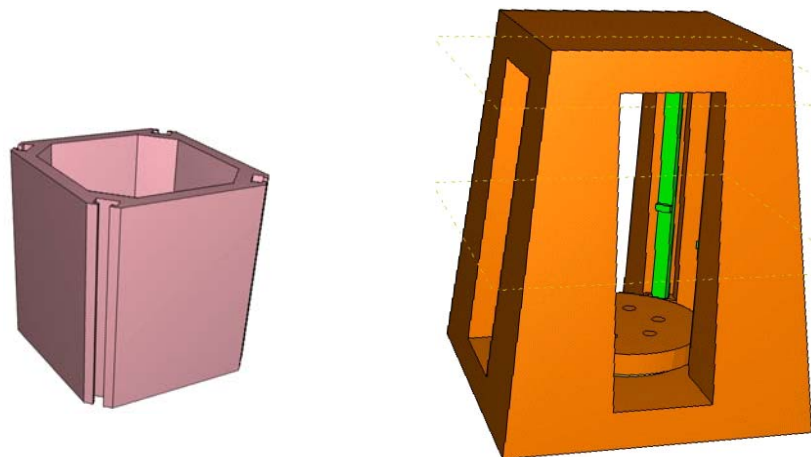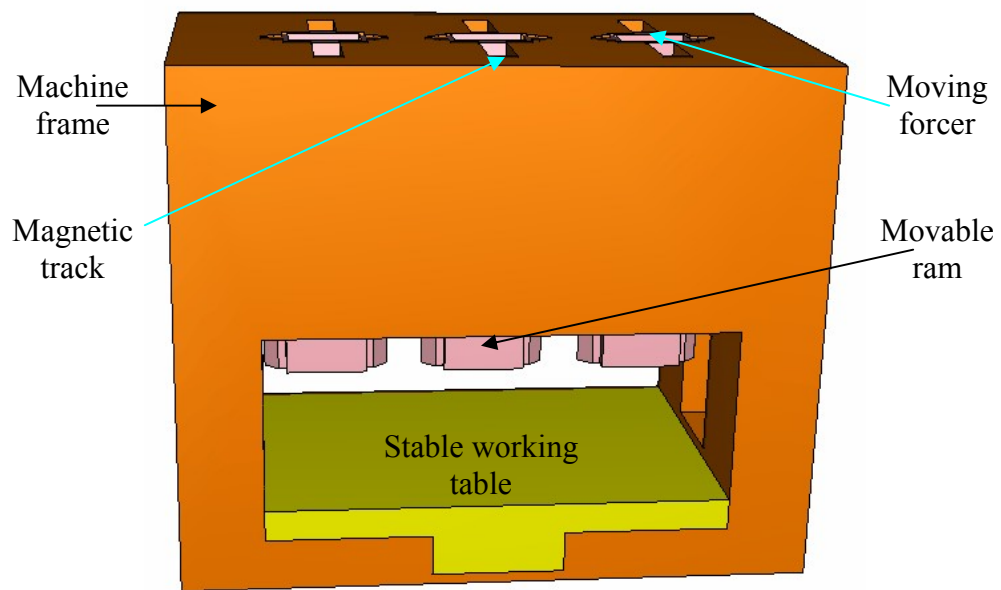### 5.4.1 Materials

The material properties used for the FE simulation of the conceptual micro-stamping machines are as follows:

Young's modulus = 210000MPa

Poisson's ratio = 0.3

Mass density = 7.8×10^{-9} tonne/mm^3

5.4.2 Conceptual micro-stamping machine model 1

The model for conceptual micro-stamping machine 1 contains a machine frame, four lead-screw shafts, four ball screw nuts, four linear guides, a ram, and a rotary table. There are two designs for concept 1. One is the micro-stamping machine that is shown in Fig. 5.1 and the other is the machine with enhanced columns that is shown in Fig. 5.2. The mesh details are listed in Table 5.2 and shown in Figs. A5.1 and A5.2, respectively.

Table 5.2   Mesh details for concept 1

Models	Element type	Number of elements
Model (a)	C3D4	68980
Model (b)	C3D4	112438

The natural frequencies are obtained by FE analysis. The first-mode frequency is 397.69Hz for model 1(a) and 512.71Hz for model 1(b). The first-frequency mode

shapes are shown in Figs. A5.3 and A5.4 for models 1(a) and 1(b), respectively. The fundamental frequency of the enhanced design is 29% greater than that of the base design.

5.4.3 Conceptual micro-stamping machine model 2

The model for concept 2 contains a machine frame, four lead-screw shafts, four linear bearings, a movable ram, a rotary table, a hydraulic cylinder and a piston rod. There are two designs for concept 2. One is the micro-stamping machine that is shown in Fig. 5.3, and the other is the machine with enhanced columns as shown in Fig. 5.4. The mesh details are listed in Table 5.3 and shown in Figs. A5.5 and A5.6 for model concept 2(a) and 2(b), respectively.

Table 5.3   Mesh details for concept 2

Models	Element type	Number of elements
Model (a)	C3D4 and C3D8R	70582
Model (b)	C3D4 and C3D8R	60564

The natural frequencies are obtained by FE analysis. The frequency of the first mode is 469.05Hz for model 2(a) and 533.65Hz for model 2(b); and contour plots of mode 1 of the micro-stamping machine are shown in Fig. A5.7 for model 2(a) and Fig. A5.8 for model 2(b). In this concept design, the fundamental frequency of the enhanced design is 14% greater than that of the base design.. On the other hand, both models in concept 2 have greater fundamental frequencies than those in concept 1.

5.4.4 Conceptual micro-stamping machine model 3

The model for concept 3 contains a machine frame, a movable ram, a stable working table, two magnetic tracks, and two linear-motor moving forcers (BLMX382). The movable ram is connected to the forcers, and the upper as well as the lower dies, which in turn are fixed onto the movable ram and the lower working table. The mesh details are listed in Table 5.4 and shown in Fig. A5.9.

Table 5.4   Mesh details for concept 3

Models	Element type	Number of elements
Model 1	C3D4 and C3D8R	55000

The natural frequencies are obtained by FE analysis. The lowest modal frequency is 537.54 Hz. A contour plot of mode 1 of the micro-stamping machine is shown in Fig. A5.10. The fundamental frequency is similar to that of concept 2.

5.4.5 Conceptual micro-stamping machine model 4

The model for concept 4 contains a machine frame, a movable ram, a rotary table, four magnetic tracks, and linear-motor moving forcers. The movable ram is connected to the forcers and upper/lower dies, which in turn are fixed onto the movable ram and the lower working table The mesh details are listed in Table 5.5 and shown in Fig. A5.11.

Table 5.5   Mesh details for concept 4

Models	Element type	Number of elements
Model 1	C3D4	50581

The natural frequencies are obtained by FE analysis. The lowest mode frequency is 629.49Hz, which is greater than that of the previous 3 design models. A contour plot of mode 1 of the micro-stamping machine is shown in Fig. A5.12.

5.4.6 Conceptual micro-stamping machine model 5

The model for concept 5 contains a machine frame, a movable ram, a stable working table, and magnetic tracks. A rectangular machine frame has three locations for fixing six magnetic tracks and six linear motor moving forcers, by means of which three rams would be attached to the three locations separately. The mesh details are listed in Table 5.6 and shown in Fig. A5.13.

Table 5.6   Mesh details for concept 5

Models	Element type	Number of elements
Model 1	C3D8R	88151

The natural frequencies are obtained by FE analysis. The frequency of the first mode is 397Hz. A contour plot of the first mode of the micro-stamping machine is shown in Fig. A5.14. In terms of fundamental frequency, this model is not very satisfactory.

5.4.7 Conceptual micro-stamping machine model 6

The model for concept 6 contains a machine frame, a stable working table, and magnetic tracks. A rectangular machine frame has four locations for fixing eight magnetic tracks and eight linear-motor moving forcers, by means of which four rams would be attached to the four locations separately. The mesh details are listed in Table 5.7 and shown in Fig. A5.15.

Table 5.7 Mesh details for concept 6

Models	Element type	Number of elements
Model 1	C3D4 and C3D8R	350968

The natural frequencies are obtained by FE analysis. The frequency of the first mode is 483.04Hz. A contour plot of mode 1 of the micro-stamping machine is shown in Fig. A5.16.

5.5   Summery of results

The main parameters and the dynamic-analysis results for the conceptual micro-stamping machines are listed in Table 5.8. According to the results of dynamics analysis, the frequencies of the fundamental mode of all of the conceptual micro-stamping machines are located well away from the frequency of excitation forces, which is about 16 Hz. Thus the design can be further optimised to reduce its scale and its weight. From the view of dynamics analysis, the frequency and magnitude of

the excitation force should be as small as possible. The improved design should consider the basic elements as follows:

- Reducing the scale and weight of the machine frame.
- Keeping the natural frequency high enough to avoid the frame being excited by the load forces.
- Improving the structure of the frame to be as flexible (adaptable) as possible
- Keeping the work-space big enough to be able to change the machine tool
- Enabling the structure of the frame to be easily connected with the feeder and the handling device.
- All of the changes have to secure high precision.

Depending on the above considerations, further micro-stamping machine frames are to be designed. The details of the final conceptual micro-stamping machine are given in Section 5.6.

Table 5.8   **Main parameters and dynamics analysis results for the conceptual micro-stamping machines**

Concepts	Main Dimensions (mm)	Weight (kg)	Excitation Forces	Lowest Mode Frequency (Hz)
Concept 1-a	900*900*700	743	motors	397.69
Concept 1-b	900×900×700	919	A hydraulic cylinder	521.71
Concept 2-a	900×900×700	667	motors	469.05
Concept 2-b	900×900×700	718	A hydraulic cylinder	533.65
Concept 3	520×720×1240	1470	Two linear motors	537.54
Concept 4	900×900×1180	2012	Four linear motors	629.49
Concept 5	600×1240×1400	3815	Six linear motors	397.20
Concept 6	1000×1200×1240	5941	Eight linear motors	483.04

5.6   Conclusions

It was stated above that a large working space, light weight, high precision and high natural frequency are major targets in the design of a micro-stamping machine. The structure should be flexible and easy to connect with the material feeder and the workpiece handing device.

- **Vibration**. The micro-stamping machine works at high speed. The range of frequency is from 1Hz to 16Hz. The range of the first mode of the six conceptual models is from 397Hz to 629Hz. The range of the working frequency lies well away from the range of the natural frequencies of the first mode of the conceptual micro-stamping machines: however the exiting source is complex. Excitation may come from the forming-force supplying device, e.g. the linear motor or other moving components. Therefore the exiting sources should be as few as possible. One linear-motor control should be better than the use of multiple linear-motor control.
- **Weight**. Among the 8 designs, conceptual model 1 and model 2 have a lighter structure than the others. Concept 2 models are lighter than concept 1 models, and have higher frequencies.
- **Working space.** Conceptual model 1 and model 2 have good working space and the structure is easy to adjust and connect with other devices.

Comparing the results between the conceptual micro-stamping machine models, conceptual model 2(a) is the best. As a result, some improvements are made based on this model and a final conceptual micro-stamping machine is designed and used for further investigations: this is shown in Fig. A5.17. The main dimensions of the machine are 496×496×845 (mm). The main components involved in the machine are as follows:

- A power supplying unit - a linear motor
- A top plate. The top plate and two motor mounting plates as well as four motor-mounting bolts are used for fixing the linear motor.

- A base plate. The base plate has T-slots for fixing the stamping tool and making the structure of machine more flexible/adaptable for fitting with different tools.

- Four machine columns. The four columns are position-adjustable for making up different working spaces for examining different micro-forming processes

A FE analysis model has been built for dynamics analysis. The first mode is 344Hz and the contour plot is shown in Fig. A5.18. A prototype based on this design has been built. Detailed analyses have been carried out and are reported in Chapter 6.

The FE model used for the vibration analysis of the conceptual micro-stamping machine did not include the driving force components, such as linear motor. These may have some influence on the results. The model including a linear motor has been used for a test micro-stamping machine analysis, which is addressed in Chapter 6.

5.7 References

Geiger, M. (2001) 'Micro-forming,' CIRP Annals 2001, Vol.50, p445-462.

Groche, P. and Schneider, R. (2004), 'Method for the Optimization of Forming Press for the manufacturing of micro parts,' CIRP Annals 2004, Vol. 53/1, p281-284.

Hess, A. (2000), 'Pizeoelectric driven press for production of metallic micro parts by forming,' Actuator 2000, 7th Int. Conf. pp 19-21.

Zaeh, M.F. and Oertli, Th. (2004), 'Finite element modelling of ball screw feed drive systems,' CIRP Annals - Manufacturing Technology 2004, Vol. 53, pp 289-292.
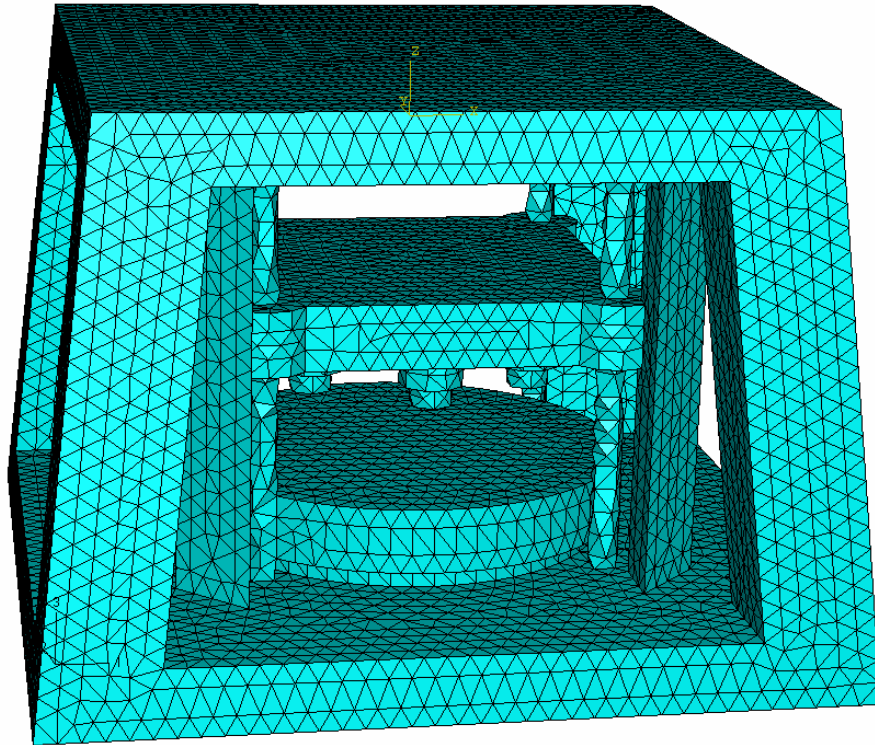
5.8   Appendix A – Figures

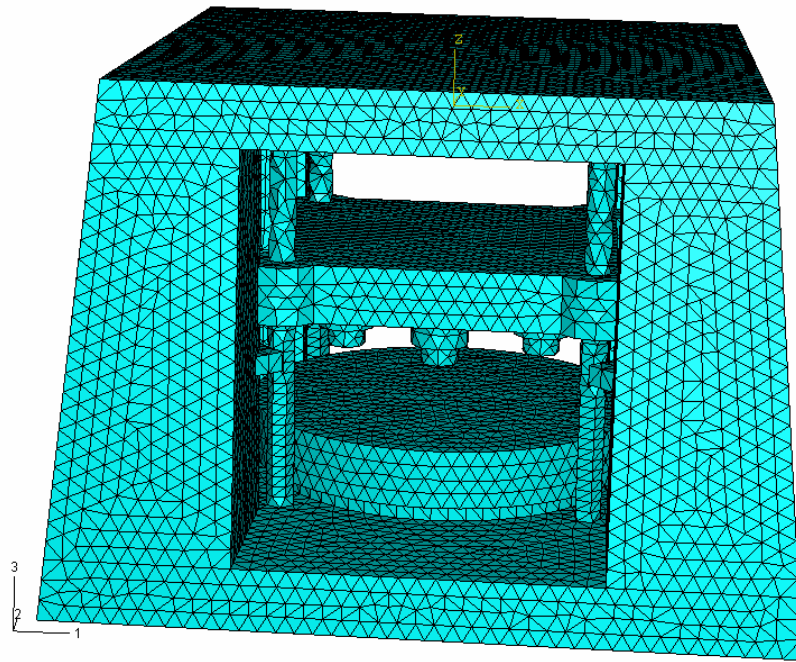**Fig. A5.1 The mesh of micro-stamping machine concept 1 (a)**

Fig. A5.2 The mesh of micro-stamping machine concept 1 (b)

U, Magnitude
+1.114e+00
+1.023e+00
+9.316e-01
+8.403e-01
+7.490e-01
+6.577e-01
+5.665e-01
+4.752e-01
+3.839e-01
+2.926e-01
+2.013e-01
+1.100e-01
+1.877e-02

Step: Step-1
Mode   7: Value = 6.24370E+06 Freq =   397.69   (cycles/time)
Primary Var: U, Magnitude
Deformed Var: U   Deformation Scale Factor: +5.000e+01

**Fig. A5.3 Contour plot of mode 1 of micro-stamping machine
concept 1 (a)**

U, Magnitude
+1.185e+00
+1.087e+00
+9.894e-01
+8.917e-01
+7.940e-01
+6.963e-01
+5.986e-01
+5.009e-01
+4.031e-01
+3.054e-01
+2.077e-01
+1.100e-01
+1.230e-02

Step: Step-1
Mode   7: Value = 1.07455E+07 Freq =   521.71   (cycles/time)
Primary Var: U, Magnitude
Deformed Var: U   Deformation Scale Factor: +5.000e+01

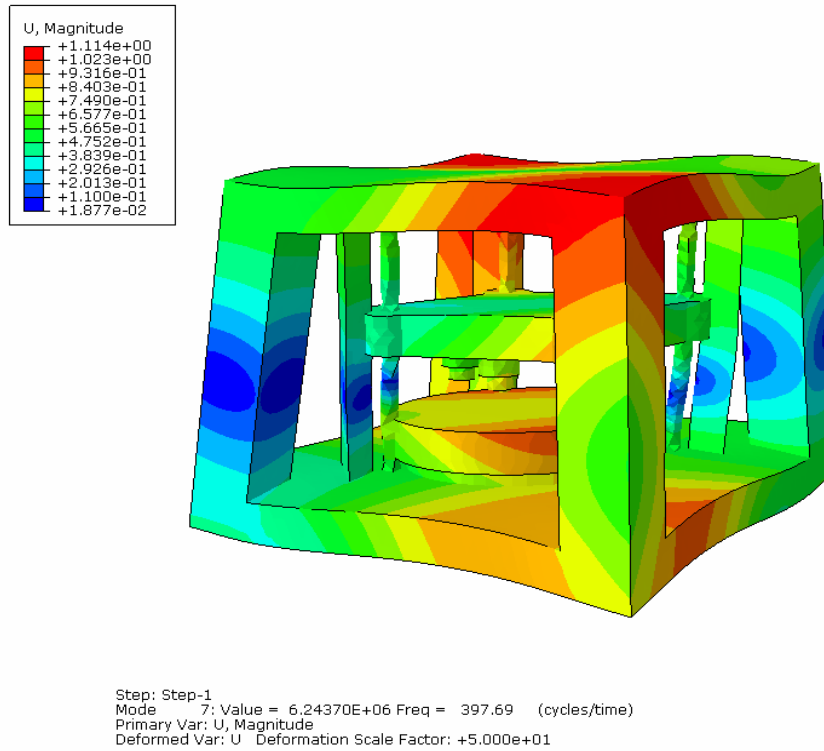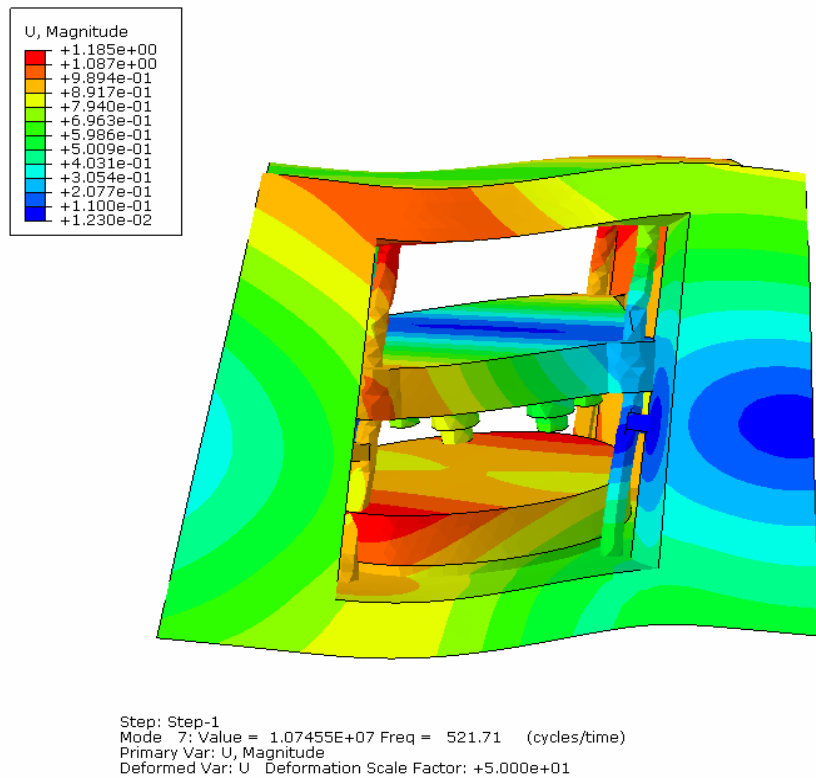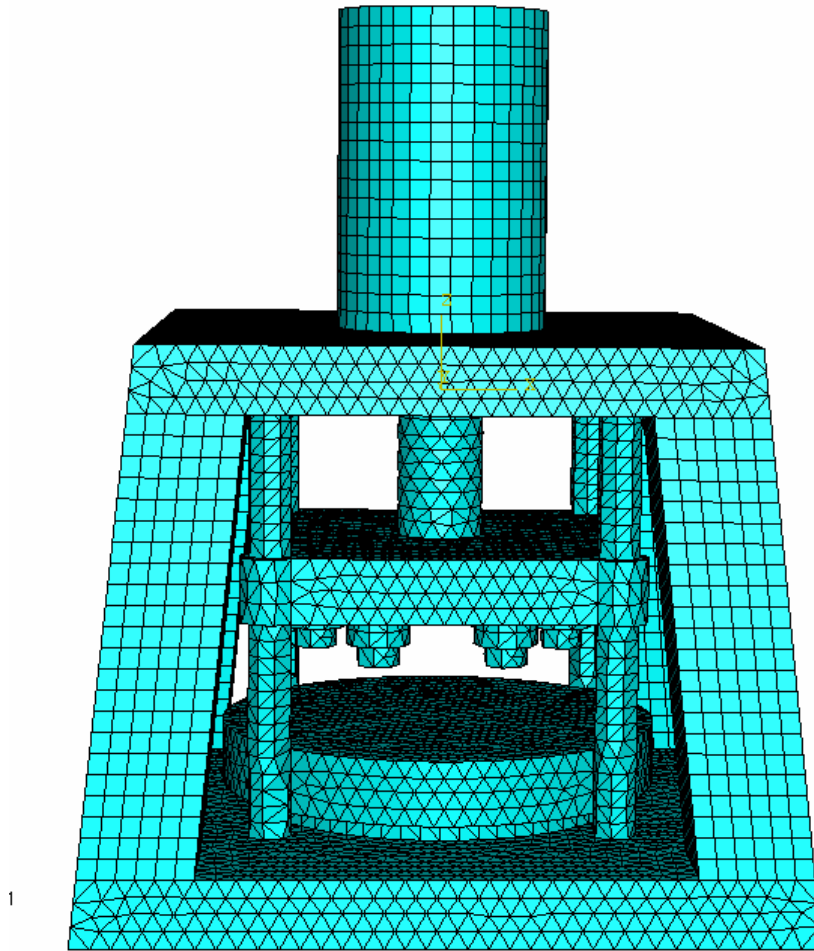**Fig. A5.4 Contour plot of mode 1 of micro-stamping machine concept 1 (b)**

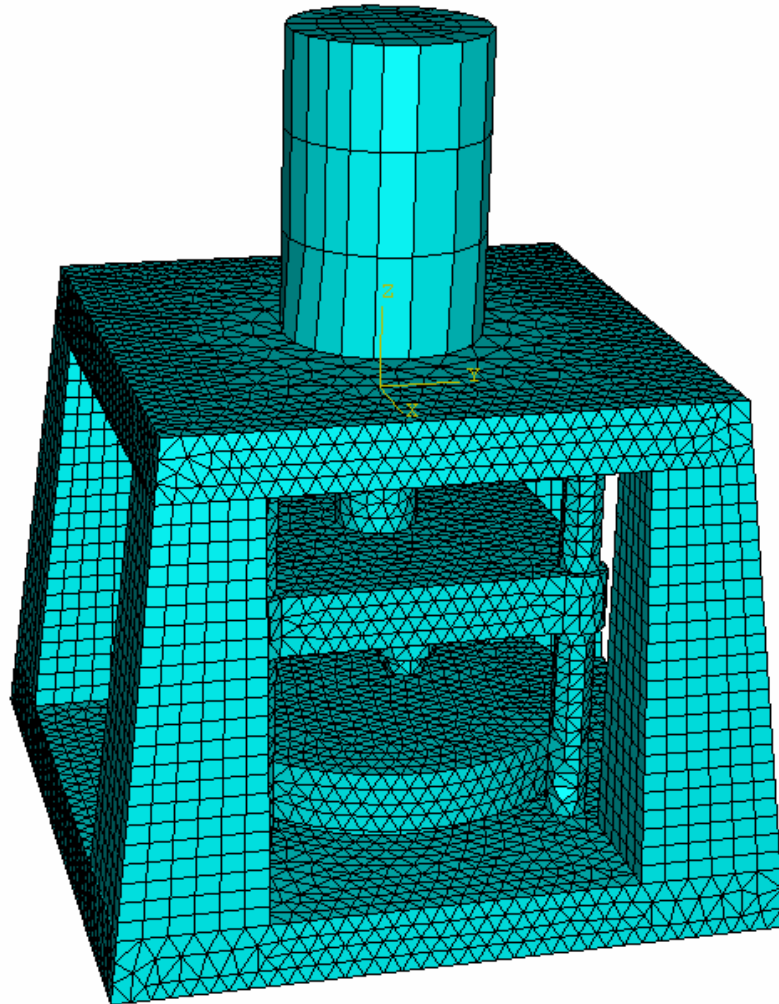**Fig. A5.5 The mesh of micro-stamping machine concept 2 (a)**
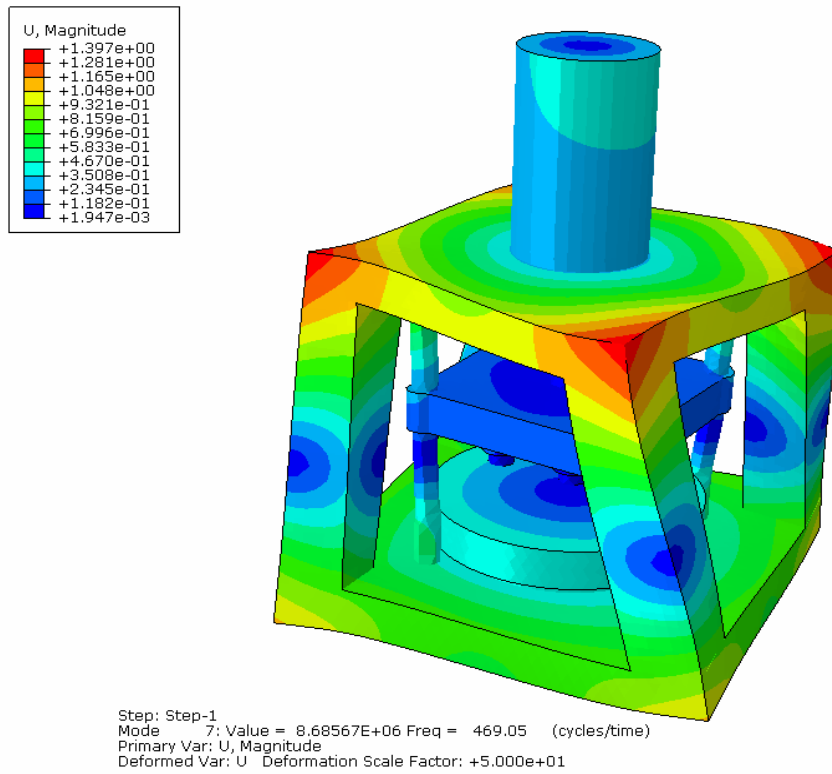
Fig. A5.6 The mesh of micro-stamping machine concept 2 (b)

U, Magnitude
+1.397e+00
+1.281e+00
+1.165e+00
+1.048e+00
+9.321e-01
+8.159e-01
+6.996e-01
+5.833e-01
+4.670e-01
+3.508e-01
+2.345e-01
+1.182e-01
+1.947e-03

Step: Step-1
Mode   7: Value = 8.68567E+06 Freq =   469.05   (cycles/time)
Primary Var: U, Magnitude
Deformed Var: U   Deformation Scale Factor: +5.000e+01

Fig. A5.7 Contour plot of mode 1 of micro-stamping machine concept 2 (a)

U, Magnitude
+1.101e+00
+1.013e+00
+9.249e-01
+8.371e-01
+7.492e-01
+6.614e-01
+5.736e-01
+4.858e-01
+3.979e-01
+3.101e-01
+2.223e-01
+1.344e-01
+4.662e-02

Step: Step-1
Mode   7: Value = 1.12429E+07 Freq =   533.65   (cycles/time)
Primary Var: U, Magnitude
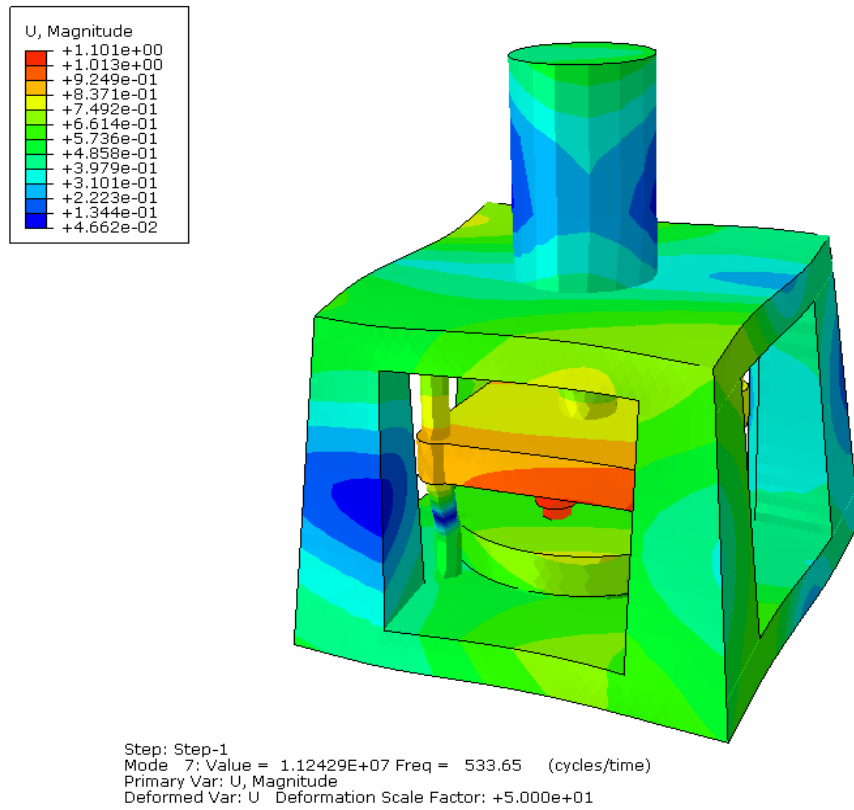Deformed Var: U   Deformation Scale Factor: +5.000e+01

Fig. A5.8 Contour plot of mode 1 of micro-stamping machine concept 2 (b)
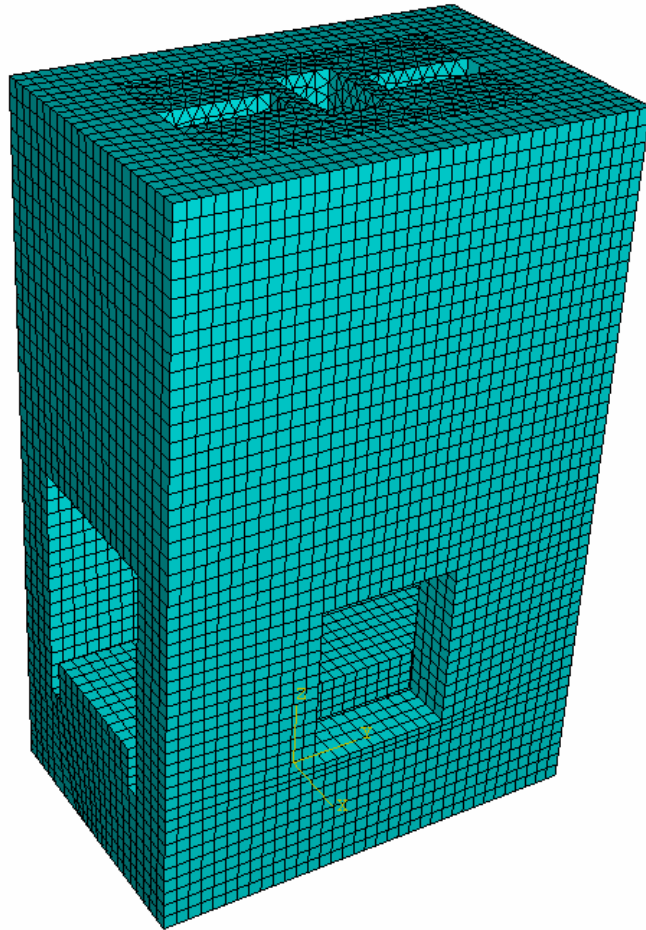
Fig. A5.9 The mesh of micro-stamping machine concept 3

U, Magnitude
+1.029e+00
+9.441e-01
+8.589e-01
+7.738e-01
+6.886e-01
+6.034e-01
+5.183e-01
+4.331e-01
+3.480e-01
+2.628e-01
+1.776e-01
+9.247e-02
+7.312e-03

Step: Step-1
Mode   7: Value =   1.14073E+07 Freq =   537.54   (cycles/time)
Primary Var: U, Magnitude
Deformed Var: U   Deformation Scale Factor: +5.000e+01

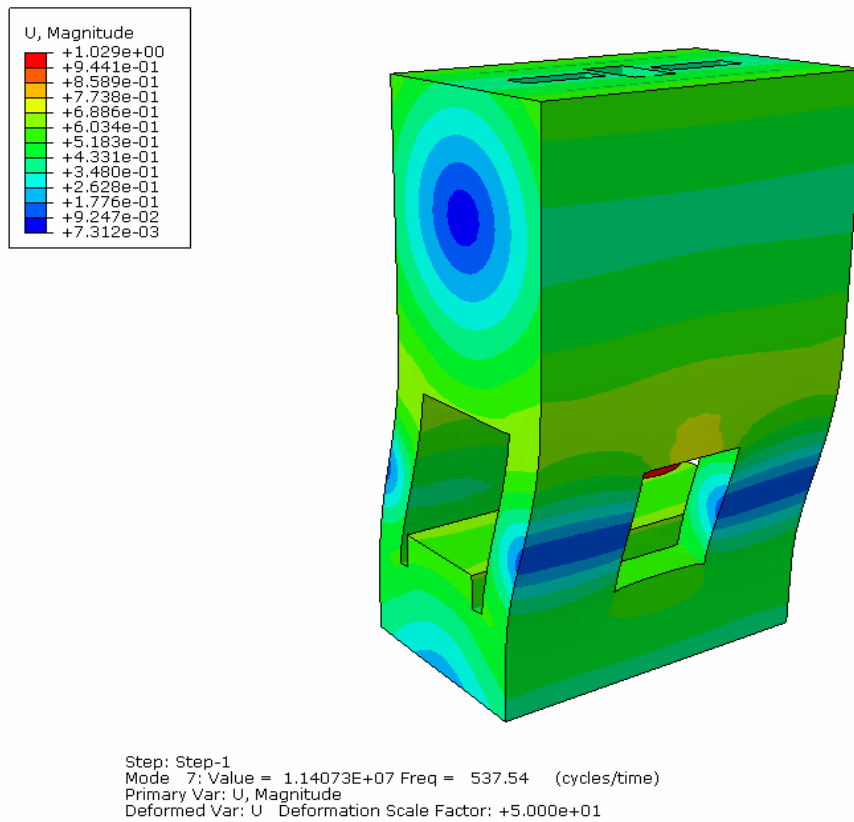**Fig. A5.10 Contour plot of mode 1 of micro-stamping machine concept 3**

Fig. A5.11 The mesh of micro-stamping machine concept 4

U, Magnitude
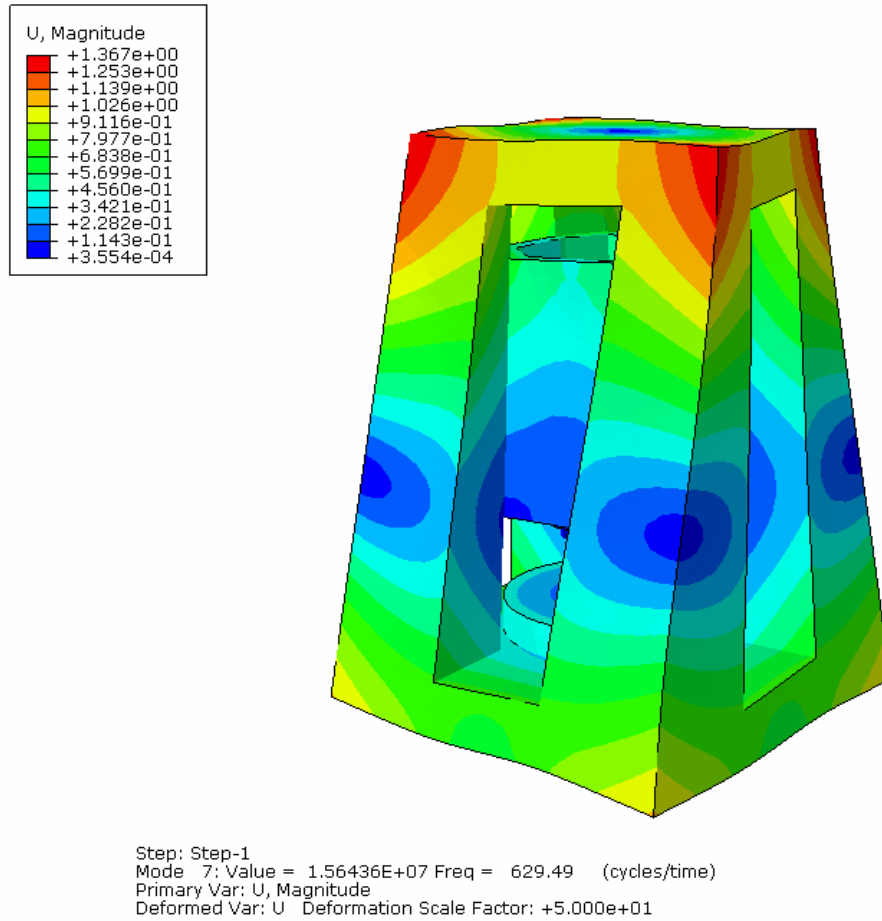+1.367e+00
+1.253e+00
+1.139e+00
+1.026e+00
+9.116e-01
+7.977e-01
+6.838e-01
+5.699e-01
+4.560e-01
+3.421e-01
+2.282e-01
+1.143e-01
+3.554e-04

Step: Step-1
Mode 7: Value = 1.56436E+07 Freq = 629.49 (cycles/time)
Primary Var: U, Magnitude
Deformed Var: U Deformation Scale Factor: +5.000e+01

Fig. A5.12 Contour plot of mode 1 of micro-stamping machine concept 4
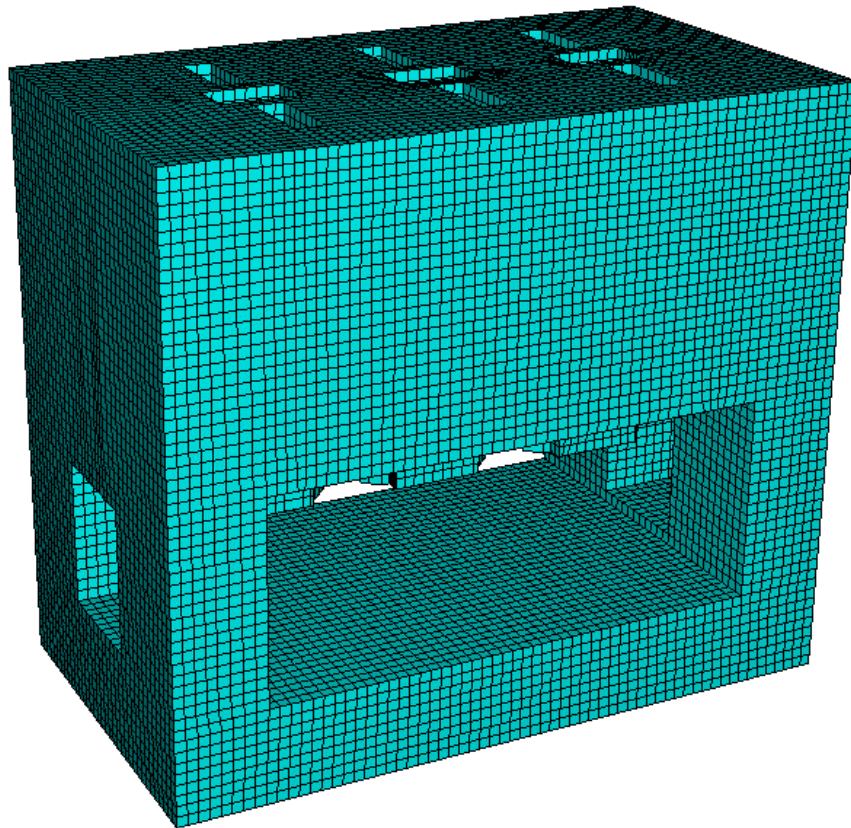
Fig. A5.13 The mesh of micro-stamping machine concept 5

U, Magnitude
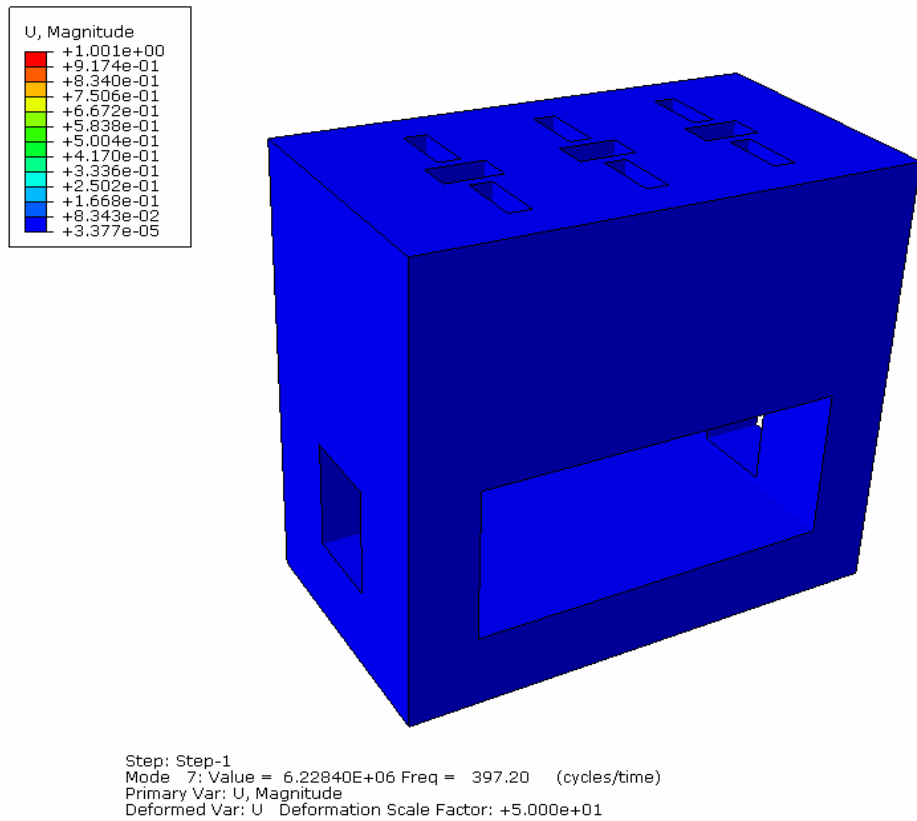
+1.001e+00
+9.174e-01
+8.340e-01
+7.506e-01
+6.672e-01
+5.838e-01
+5.004e-01
+4.170e-01
+3.336e-01
+2.502e-01
+1.668e-01
+8.343e-02
+3.377e-05

Step: Step-1
Mode   7: Value = 6.22840E+06 Freq =   397.20   (cycles/time)
Primary Var: U, Magnitude
Deformed Var: U   Deformation Scale Factor: +5.000e+01

Fig. A5.14 Contour plot of mode 1 of micro-stamping machine concept 5
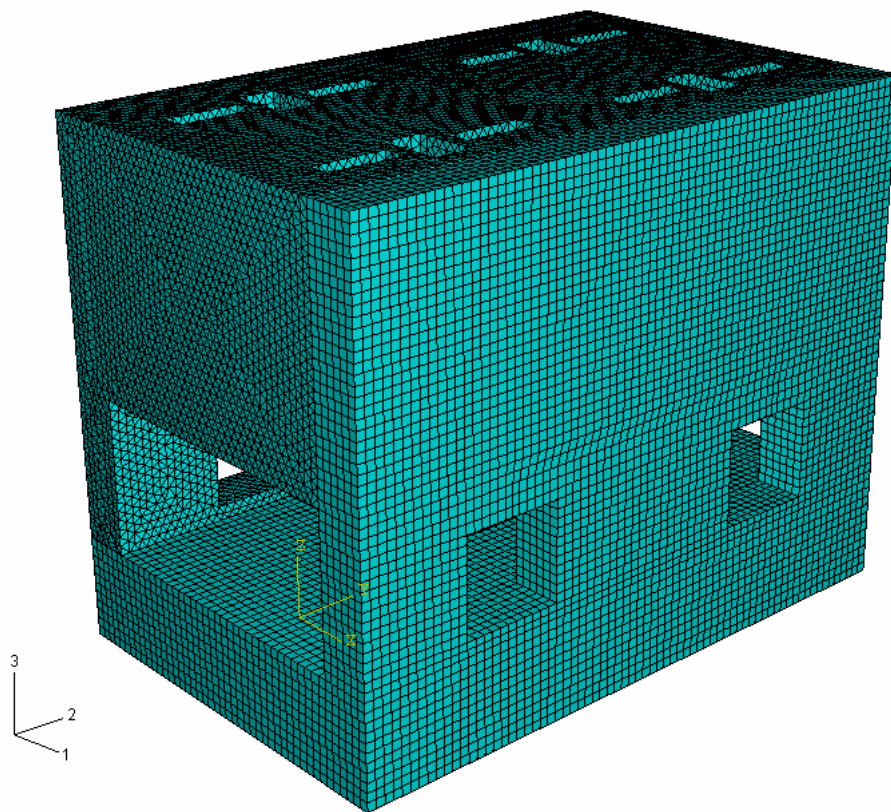
Fig. A5.15 The mesh of micro-stamping machine concept 6

U, Magnitude
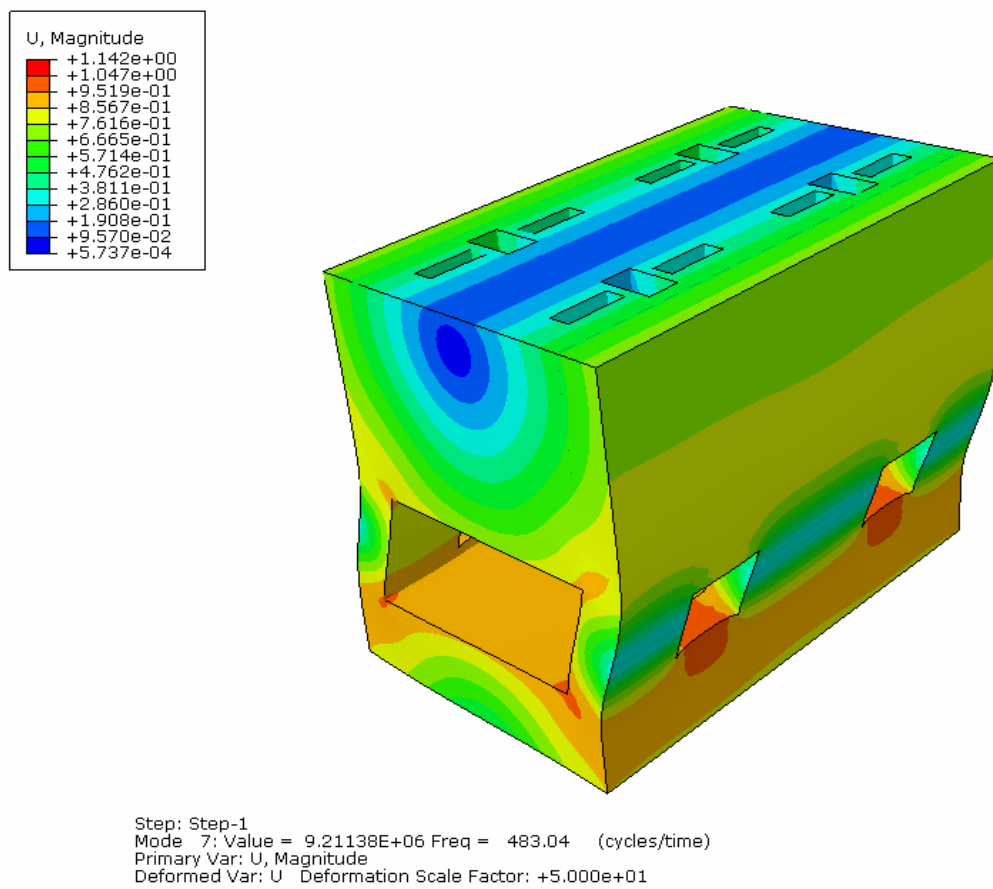+1.142e+00
+1.047e+00
+9.519e-01
+8.567e-01
+7.616e-01
+6.665e-01
+5.714e-01
+4.762e-01
+3.811e-01
+2.860e-01
+1.908e-01
+9.570e-02
+5.737e-04

Step: Step-1
Mode   7: Value = 9.21138E+06 Freq =   483.04   (cycles/time)
Primary Var: U, Magnitude
Deformed Var: U   Deformation Scale Factor: +5.000e+01

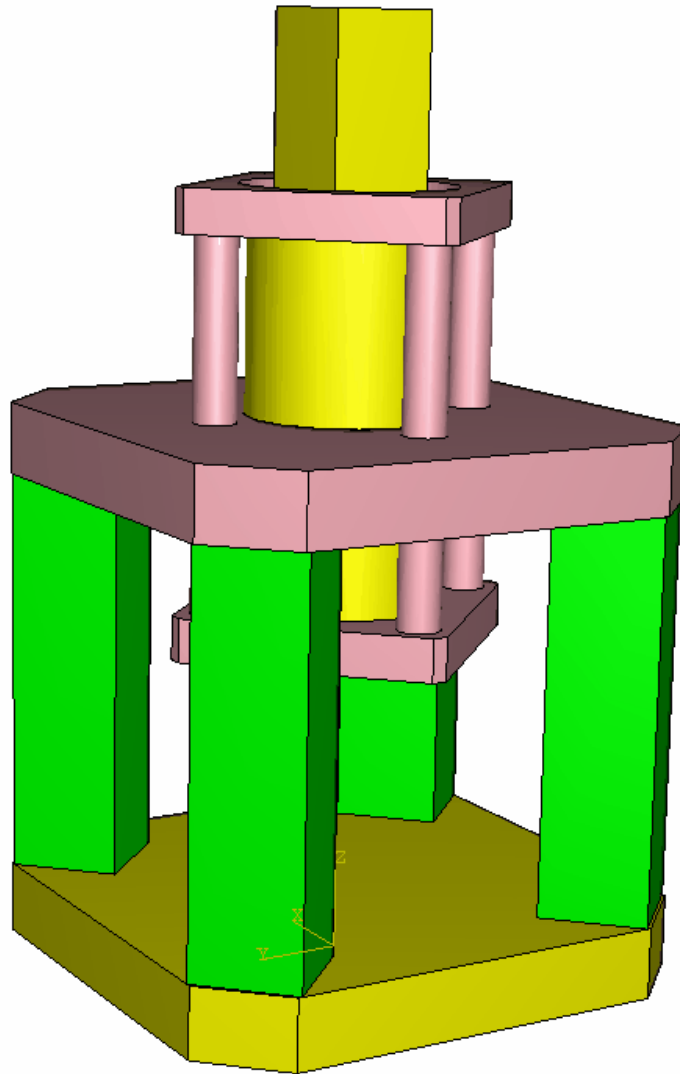**Fig. A5.16 Contour plot of mode 1 of micro-stamping machine concept 6**

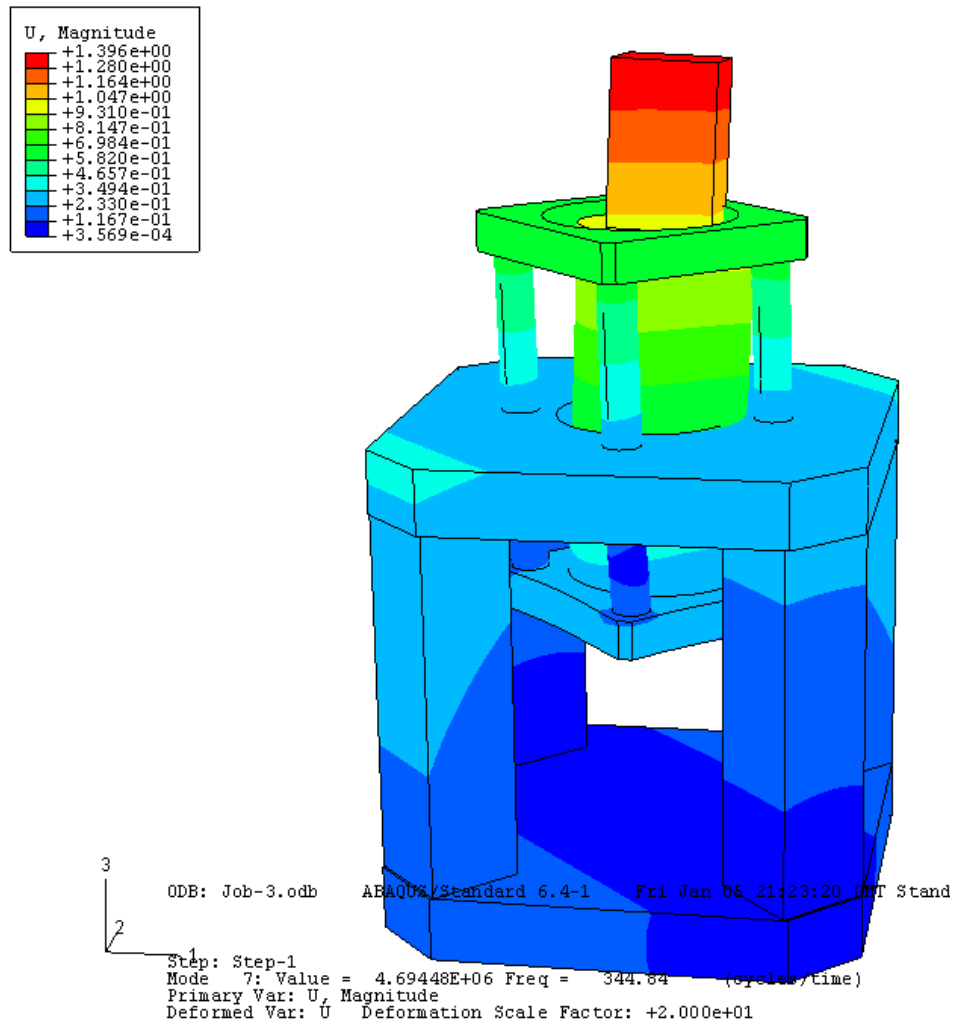**Fig. A5.17 The geometry of the micro-stamping machine**

Fig. A5.18 Contour plot of mode 1 of the micro-stamping machine

Chapter 6 Dynamics analysis of the Micro-Stamping Machine

6.1   Introduction

For the micro-stamping machine, vibration is undesirable, but is not avoidable. Vibration can lead to machine- or tool-damage. The micro-stamping system includes exiting forces. These are forming forces coming from the linear motor, the vibration of components or the reaction force between the tool and the machine bed. In order to be able to protect the micro-stamping machine from resonance, the natural frequencies in different situations are investigated.

Depending on the concept design in Chapter 5, a real micro-stamping machine has been designed by the research group within the university and manufactured by Pascoe Engineering Ltd., Scotland, for test. The machine is shown in Fig. 6.1. It contains a machine frame, a linear motor, a set of linear-motor support components and a linear guide. The machine frame has a top plate, a base plate, and four columns. The adjustable top plate and the base plate enable the work-space to be changed easily. Especially, the base plate enables different stamping tools to be mounted on it, e.g. a single-stamping tool or a multi-stamping tool. However, this makes it difficult to form the FE mesh model of the structure. Four motor-support bolts are used to combine the motor-support top plate and bottom plate as well as to connect with the machine frame. The linear guide is used to guide the ram during the stamping process. Two linear guide columns and a linear guider bride for guiding the movable ram were also fabricated and fitted separately from the top plate and the four machine columns of the frame, so that the forming-forces applied during the micro forming processes would not have significant effects on the deflection of the linear guides. In other words, the precision and accuracy of the micro-stamping machine was enhanced and secured with such a design and an arrangement of the linear guide bride. The linear motor is fixed onto the motor-support bottom plate. The main components and assemblies are shown in Figs.A6.1 to A6.4. The micro-stamping machine is connected with the feeder and the workpiece handing device. The design range of the working frequency of the micro-stamping machine is from

1Hz to 16 Hz. It is clear that with the flexible set-up, i.e., changeable working area, changeable forming-force, and the changeable strokes, micro sheet forming can be examined under the different conditions.

The following are the problems to be investigated in this chapter:

- What is the influence of the linear motor assembly on the vibration of the micro-stamping machine?

- What is the influence of the micro-stamping machine base on the vibration of the micro-stamping machine?

- What is the influence of the ram position relative to the linear guide plate on the vibration of the micro-stamping machine?

Improvements have been made step-by-step by taking advantage of a linear guide and in the assembly of the ram. FE analysis of the natural frequency of the machine frame with the linear motor, the linear guide, and the ram assembled, has been performed using ABAQUS. The results of FE simulations provide useful information for improving the design of the micro-stamping machine. Natural frequencies of nine cases of three models are investigated for: different assemblies between the linear-motor support plate and the linear guide; and for different contact conditions between the ram and linear guide, and the adjustable structure. The influence of a flexible structure on the natural frequency has been analysed also. Assessing the results obtained from these three models, an improved design has been obtained. The details of the geometry of the micro-stamping machine are presented in Section 6.2.1. The geometries of four models are shown in Figs. 6.2 to Fig. 6.5, respectively. The main dimensions and weight of the models are listed in Table 6.1. The FE simulation models contain a geometric model, a material model, a mesh model, a contact model and a connection model, as well as boundary conditions: all of these are presented in Section 6.3. Analysis of the micro-stamping machine base is described in Sub-section 6.3.6. The findings are given in Section 6.4 and an improved design is described in Section 6.5. Conclusions are drawn in Section 6.6.

Fig. 6.1   Micro-stamping machine

Table 6.1   Dimensions and weight of the models

Models	Length (mm)	Width (mm)	Height (mm)	Weight (kg)
Model-1	496	496	868	417
Model-2	496	496	868	417
Model-3	496	496	948	432
Model-4	496	496	828	378

6.2   FE model of micro-stamping machine

FE models of the micro-stamping machine for different geometrical shapes, different materials, and different boundaries are built in a sequential way so as to be able to choose an efficient and high-precision mesh. Relevant details are provided in the following sections.

6.2.1 Geometric models

The first geometric model is depicted in Fig. 6.2. It contains a machine frame, a linear motor, a set of linear-motor support components, and a linear guide. The ram and the four legs are not included in this model. Model-1 is used to investigate the influence of different assemblies on the natural frequencies of the micro-stamping machine. Two cases of the assembly between the linear-motor bottom support plate and the linear guide plate are computed. Case one is called Model-1-case-1, in which the linear-motor bottom support plate is in contact with the linear-guide plate. Case two is called Model-1-case-2, in which the linear-motor support plate and the linear guide plate are locked together.

The second geometric model, Model-2, is shown in Fig. 6.3. Model-2 is based on Model-1, but enables the adjustment of the positions of the four columns by means of the adjustable structure of the bed plate and the top plate. Model-2 is used to investigate the influence of change of the work-space on the natural frequencies of

the micro-stamping machine. Two cases of Model-2 are the same as that of Model-1: Model-2-case-1 and Model-2-case-2.

The third geometrical model, called Model-3, is shown in Fig. 6.4. Model-3 is designed to simulate the real micro-stamping machine, which has been improved based on the results of FE analysis and experiment. Five cases of contacts between the ram and the linear guide are analysed. The details of the contact positions are presented in Table 6.2 and shown in Fig. A6.5.

Table 6.2 Contact positions between the linear guide and the ram

Cases	Case 1	Case 2	Case 3	Case 4	Case 5
Contact positions	No contact	2,4,6,8	1,3,5,7	1,5	3,7

The fourth geometrical model, called Model-4, is shown in Fig. 6.5 (b). After analysing the results of FE simulation, Model-4 was designed and the natural frequencies were obtained by the FE simulation. In this model the structure of the micro-stamping machine is simplified. The set of motor-support items is removed. The motor is supported directly by the frame and the linear guide, which latter is slightly different from the original linear guide. This linear guide is shown in Fig. 6.5 (a).
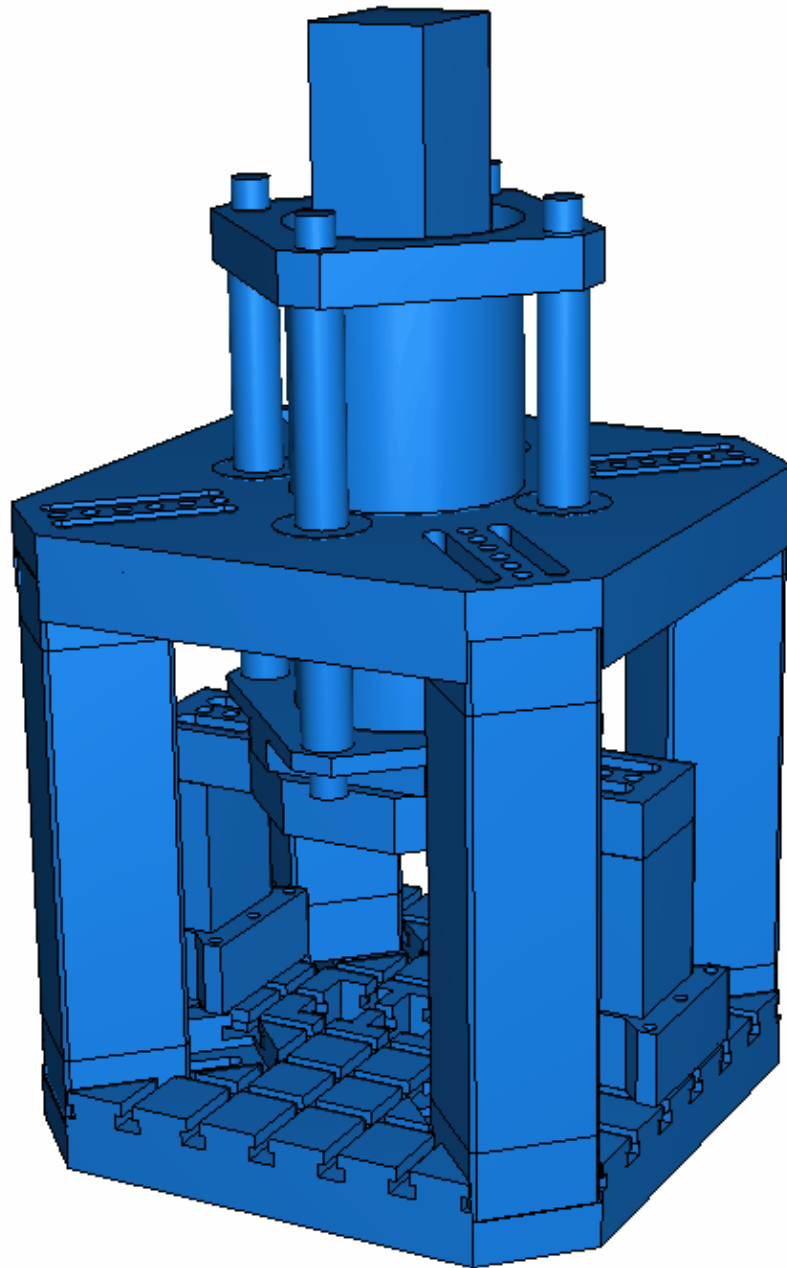
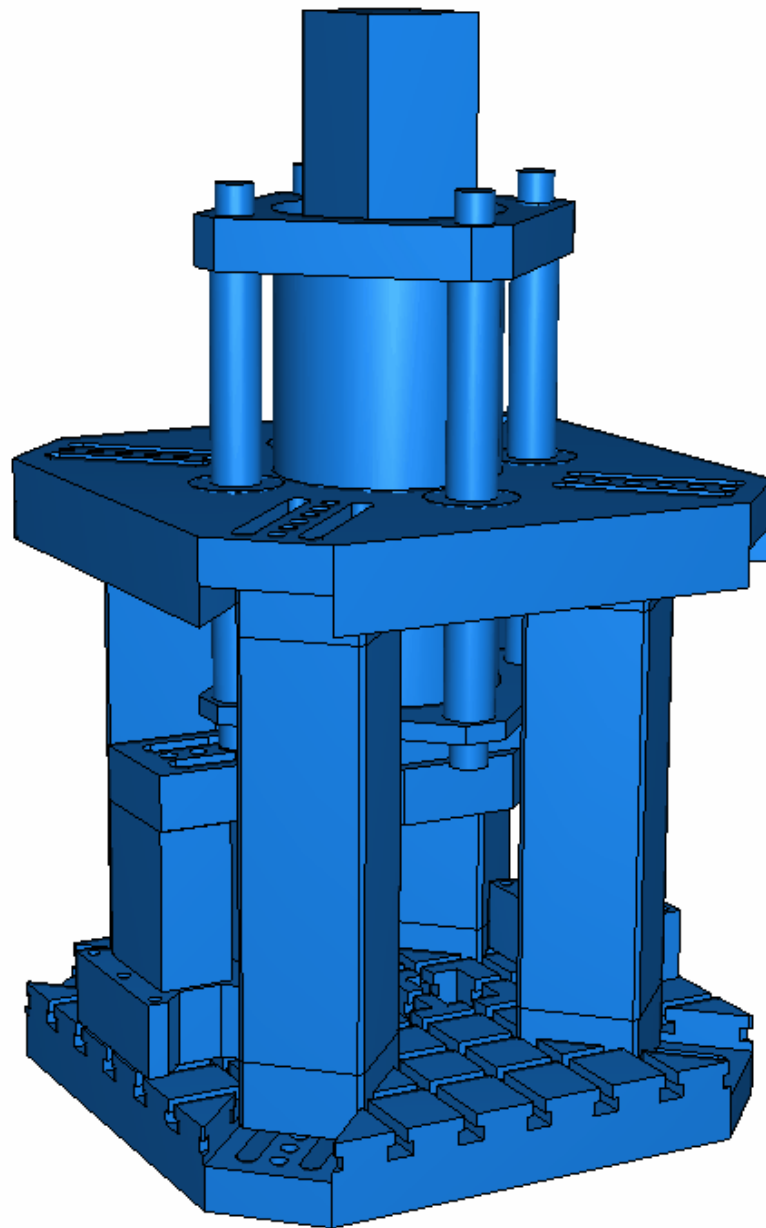**Fig. 6.2   Model-1 of the micro-stamping machine**
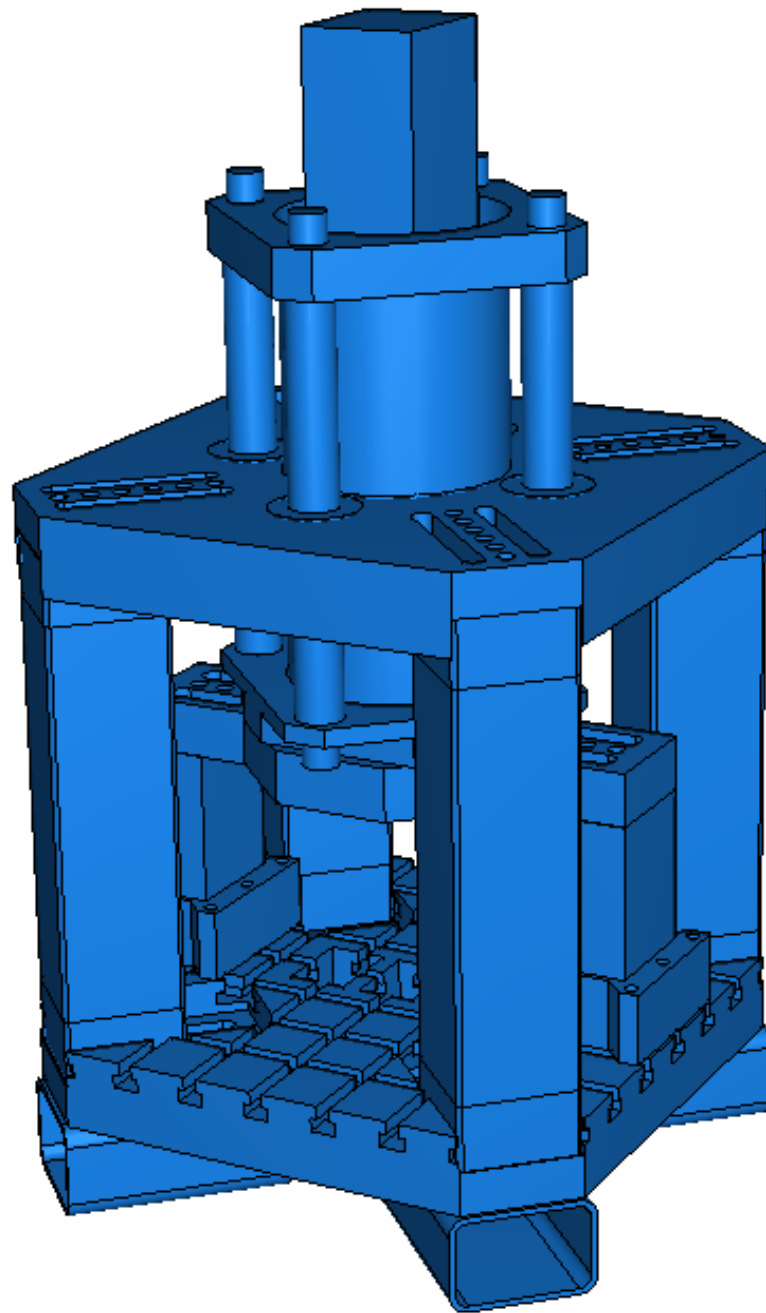
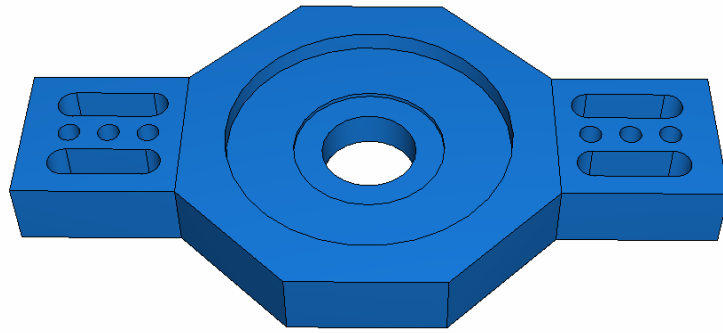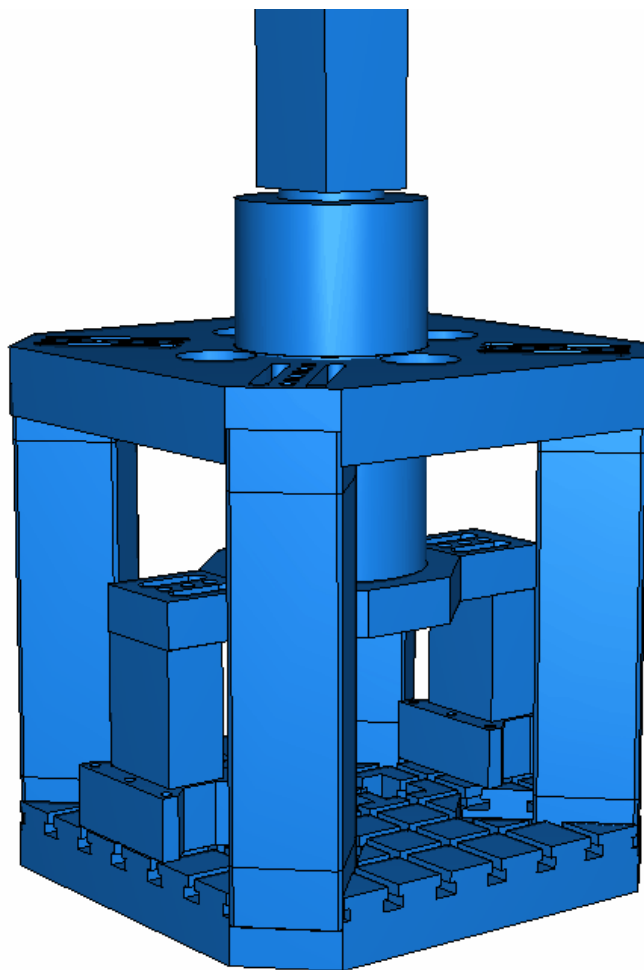**Fig. 6.3   Model-2 of the micro-stamping machine**

Fig. 6.4   Model-3 of the micro-stamping machine

(a) Linear guide of model-4

(b) Micro-stamping machine

Fig. 6.5   Model-4 of the micro-stamping machine

6.2.2 Material model

An isotropic linear material model is used in the FE simulation. In this model, the elastic properties are completely defined by giving Young's modulus, *E*, and Poisson's ratio, ν. The shear modulus, G, can be expressed in terms of E and ν, namely $G=E/(2(1+v))$. The stability criterion requires that E>0, G>0, and 0<ν<0.5. A value of Poisson's ratio approaching 0.5 results in nearly incompressible behaviour and generally require the use of "hybrid" element (ABAQUS Analysis User's manual). The properties of the materials are listed in Table 6.3.

Table 6.3 Material properties

Material	Density (ton/mm^3)	Young's Modulus (MPa)	Poisson's Ratio
Medium-carbon steel	7.8e-9	205000	0.29
Rubber	1.3e-9	4	0.45
		Stress	Plastic Strain
		7 (Yield Stress)	0
		20	8
Nitrile 641		Test data:	
		Biaxial test data	
		Planar test data	
		Uniaxial test data	
Nitrile 642		Test data:	
		Biaxial test data	
		Planar test data	
		Uniaxial test data	

The material properties were taken from website http://www.efunda.com/materials and http://www.matweb.com. The non-linear material properties of rubber can be obtained from the biaxial-tension test (Kurkin, et al., 1973 and Qin and Juster, 2003).

The test data used in the material model for Nitrile 641 and Nitrile 642, are taken from the thesis "Fundamental and Engineering Application Studies of Pressure-Assisted Injection Forging of Thick-Walled Tubular Components", University of Strathclyde, (Ma, 2004).

6.2.3 Mesh model

Four types of elements, C3D4, C3D6, C3D8R and C3D8RH are used in the FE analysis. C3D4 is a 4-node linear tetrahedron element, C3D6 is a 6-node linear triangular-prism element, and C3D8R and C3D8RH are 8-node linear brick elements that use reduced integration with hourglass control: the latter is a hybrid formulation. The first-order tetrahedral element C3D4 is a constant-stress tetrahedron, which should be avoided as much as possible; the element exhibits slow convergence upon mesh refinement. This element provides accurate results only in general cases with very fine meshing. Therefore, C3D4 is recommended only for filling-in regions of low stress-gradient in meshes of C3D8 or C3D8R elements, when the geometry precludes the use of C3D8 or C3D8R elements throughout the model. Similarly, the linear version of the wedge-element C3D6 should generally be used only when necessary to complete a mesh, and, even then, the element should be far from any areas where accurate results are needed. This element provides accurate results only with very fine meshing.

Suitable transition of element density is made to achieve high-accuracy at a relatively low cost. Partition skills are used to achieve better meshes. Six mesh models are explored. Details of the models and the results are presented in Table 6.4. Finer C3D4 and C3D6 elements are used in Mesh-model-1. From Mesh-model-2 to Mesh-model-6, elements C3D8R have been used nearly throughout the whole structure. The range of related error between all mesh models is from 0.046% to 2.09%. Considering efficiency and accuracy, Mesh-model-5 is better to be used in further analysis. Mesh model-1 and mesh model-5 are shown in Fig. A6.7 and Fig. A6.8, respectively. The mesh model of the micro-stamping machine base is shown in Fig. A6.9.

Within the area of connected components, it is necessary that finer elements are used. Finer elements can obtain results of greater precision, but require greater computing time. The design of a proper density of element is very important.

Table 6.4 Mesh models

Mesh Models	Type of Element	No of Elements	Mode 1 of Model-1 Case 1 (Hz)	Notes
Mesh-model-1	C3D4, C3D6, C3D8R	231931	281	Finer C3D4, C3D6 and C3D8R elements are used
Mesh-model-2	C3D4, C3D6, C3D8R	242366	276.78	C3D8R elements are used nearly for whole structure
Mesh-model-3	C3D4, C3D6, C3D8R	222418	275.12	C3D8R elements are used nearly for whole structure
Mesh-model-4	C3D4, C3D6, C3D8R	180228	276.14	C3D8R elements are used nearly for whole structure and finer element used within connect areas of components
Mesh-model-5	C3D4, C3D6, C3D8R	154433	276.71	C3D8R elements are used nearly for whole structure
Mesh-model-6	C3D4, C3D6, C3D8R	151714	276.58	C3D8R elements are used nearly for whole structure

Hourglassing can be particularly troublesome in eigenvalue extraction problems: the low stiffness of the hourglass modes may create many unrealistic modes with low eigenfrequencies. In the case of incompressible material behaviour, such as hyperelasticity at finite strain, mixed-formulation elements with reduced integration should be used. When large strain-gradients or strain discontinuities are expected in the solution - such as in plasticity analysis at large strains, limit-load analysis, or analysis of severely loaded rubber components - the first-order elements are usually recommended. Reduced integration can be used with such elements, but because the hourglass controls are not always effective in severely non-linear problems, caution should be exercised (ABAQUS Theory manual)

6.2.4 Contact model

When the micro-stamping machine is working during a stamping process, the ram and linear-guide plate, and the motor-support bottom plate are in contact. A contact model has been used to simulate these situations. The details of the contact model are as follows:

- Tangential behaviour includes rough contact, frictionless contact, and penalty with different friction coefficients.
- Normal behaviour is 'Hard' contact. The surfaces in contact can not penetrate each other and allow separation after contact.
- A finite-sliding formulation is used.
- Different contact positions are investigated.

6.2.5 Connect model

Eighteen components are connected together using the tie technique at the positions of screws. This makes the FE model easy to change and also makes the mesh model easy to generate.

6.2.6 Machine base

All of the above models for computing natural frequencies are free at all boundaries. Different machine bases are simulated and analysed in this section. Mesh-model-5 is used to analyse the influence of the machine base on the frequencies of vibration of the micro-stamping machine. Seven different base conditions are examined. Different number of rubber plates with different thicknesses, of dimensions 120mm×190mm, are used to make different bases. The thicknesses of the rubber plates are 2mm, 6mm and 12.7mm. Three kinds of the material properties are used for the rubber plates for the calculation of the natural frequencies of the machine. The details of seven models of the base of the micro-stamping machine are listed and shown in Table 6.5. Results are given in Table 6.6 for three different materials. Contour plots for Mode 1, Mode 2 and Mode 3 are shown in Figs. A6.20, A6.21 and A6.22, respectively. The results from all base conditions are very close.

The Comparison between the finite element analysis and the vibration test is presented in Section 8.6.

6.3 Findings of the dynamics analysis

Some findings are obtained from micro-stamping machine base analysis, linear motor assembly analysis and contact analysis.

6.3.1 Findings on the machine base

The rubber base causes the natural frequency of micro-stamping machine to decrease dramatically and the lowest frequency is very close to the range of the working frequency of the micro-stamping machine. This is of great importance in the design of the base of a micro-stamping machine with a high working speed. The results are very sensitive to the material properties of the rubber: a harder rubber is more suitable for the base of micro-stamping machine than a softer rubber. The natural frequency of the micro-stamping machine decreases with the increase of the thickness of the rubber, and increases with the increase of the contact area.

6.3.2 Findings on the linear-motor assembly

As described in Sub-section 6.2.1, Model-1 and Model-2 were devised to show the effects of contact (case 1) and tied (case 2) between the linear motor and the linear guide. The results are listed in Table 6.6, and reveal that different assemblies between the linear motor and the linear guide have a significant influence on the vibration frequency of the micro-stamping machine. The tied connection gives a much greater natural frequency of the first mode, the reason for this being that the linear-guide columns contribute directly to supporting the linear motor. Details of the results, Model-1, are presented in Table6.6.

6.3.3 Findings on the contact position between the ram and the linear guide

Model-3 has five different contact positions between the ram and the linear guide, as shown in Table 6.2 and Fig. A6.5. The results for the natural frequencies of the model are listed in Table 6.6. The case of non-contact, Model-3-case-1, has the least natural frequencies, whilst the case of the contact position being at 1,3,5,7 points,

Model-3-case-3, has the greatest natural frequencies. As expected the natural frequency is fairly sensitive to the contact position.

6.4   Improved design of the micro-stamping machine

Depending on the dynamics analysis of the micro-stamping machine, the design can be improved from four aspects: the first is motor mounting; the second is contact between the ram and the linear guide; the third is the base of the machine; and the fourth is the weight of the machine. The improved motor-mounting is dependent on the results of Model-4, which are listed in Table 6.6. The motor-mounting set is simplified and the top plate is made to support the motor directly. Therefore the force can be transferred directly to the main frame of the machine. This is an improvement, because the main frame of the machine is much stronger than the motor-support set.

Different contact positions between the ram and the linear guide have been analysed. After comparing the results between five cases, the results of case 3 are seen to be the best. This case is employed in the improved design. The contact points are 1, 3, 5 and 7, as shown in Fig. A6.5(a).

The base of the machine is a crucial factor that influences the frequency of vibration of the micro-stamping machine. If rubber is utilised as a kind of vibration damper at the base of a machine that works at high stamping speed, the contact area should be as large as possible and the thickness of rubber should be as small as possible. The mechanical properties of the rubber are more important than other factors: greater frequency can be achieved when harder rubber is used. In the improved design, the four legs are removed and the micro-stamping machine is put directly onto the rubber plate. The motor-mounting set is simplified, and the weights of the linear-guide column and main frame columns are reduced. The model of improved design is shown in Fig. A6.6. The weight of machine is 378kg.

6.5   Conclusions

Based on the analysis of the results obtained to date for all models, the following conclusions can be drawn.

- Contact between the ram and the linear guide significantly increases the natural frequency of the micro-stamping machine. Therefore, investigating the contact positions and reducing the contact area are both necessary during the design of a micro-stamping machine.

- When a linear motor is used to control the process of the stamping for the micro-stamping machine, it is better that the main frame can contribute to support the linear-motor assembly. This can make the linear motor more stable, and help to achieve high precision.

- When rubber is used beneath the machine base, a group of lower natural frequency modes develop, which are close to the working frequency of the micro-stamping machine. All of the parameters of the rubber plates have a significant influence on the results. Therefore, when the rubber is used as a damper at the base of the micro-stamping machine, especial care should be taken in choosing the dimensions of the rubber plates and the contact area. Reducing the thickness and increasing the contact area will increase the natural frequency of a micro-stamping machine employing a rubber base. Accurate material properties of the rubber used are important in micro-stamping machine base-design. In the design of a micro-stamping machine system, attempt should be made to minimise exiting force in the xy plane generated by the feeder and the workpiece-handling device, because the lowest mode occurs in that plane.

The model of the micro-stamping machine did not include the micro-stamping tool. The upper part of the micro-stamping tool moves down and comes into contact with the lower part of the micro-stamping tool during the process of the stamping. Therefore it can be taken as an exciting force applied to the structure of the micro-stamping machine. The lower half of the micro-stamping tool is fixed on the micro-stamping machine base plate. It should not have big influence on the vibration of the micro-stamping machine. The results obtained in this chapter have been validated by the comparison with the results obtained from the experimental measurement in Chapter 8.

The pre-stressing will influence the stiffness of the structure of the micro-stamping machine. As a result, the fundamental frequency of the structure also will be influenced. The contribution of the pre-stressing to the vibration frequency of the structure will be different for different structures, especially depending on the location of the pre-stress applied and the mode of the natural frequencies of the structure. In the FE analysis of the vibration of the micro-stamping machine, the analysis models have not included the pre-stress applied at the connection of the micro-stamping machine. The "tie" technique was used to simulate different connections, e.g. screws, pusher, and so on, by setting different parameters. When two components are tied together for all nodes on the contact surfaces, the stiffness of the connection is quite high. Therefore the results obtained from FE analysis should be close to the real solution. This has been verified by the good agreement between the results obtained from the FE analysis and those obtained from experimental measurement. Of course, a new FE model including the pre-stressing could be built to investigate the influence of the pre-stressing of the structure on the natural frequencies of the structure in the future.

Table 6.5   Machine base

	No. of Rubber Plates	Dimension of Rubber plates (mm)	Structure
BC-1	4	190×120×12.7	
BC-2	8	190×120×12.7	
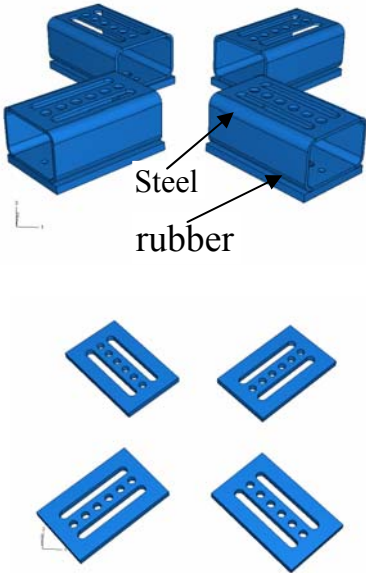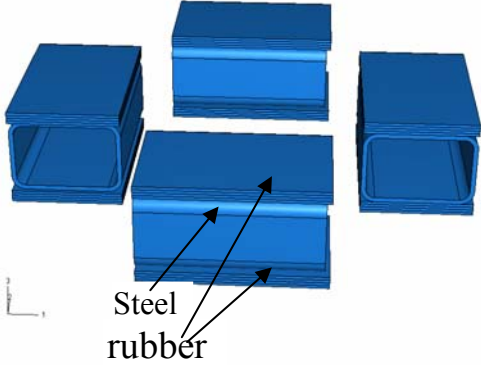
Table 6.5   Machine base - cont'd

	No. of Rubber Plates	Dimension of Rubber plates (mm)	Structure
BC-3	4	190×120×12.7	Steel Rubber
BC-4	4	190×120×6	Same as BC-3
BC-5	4	190×120×2	Same as BC-3
BC-6	8	190×120×12.7	Steel Rubber
BC-7	16	190×120×12.7 190×60×12.7	Steel Rubber
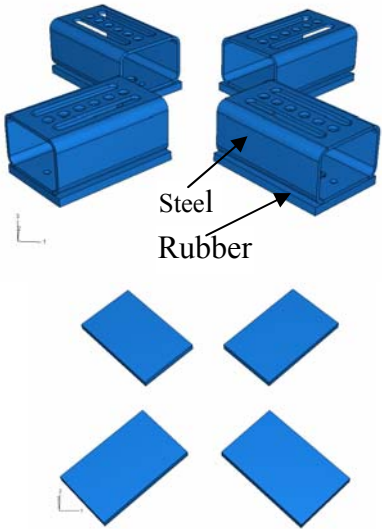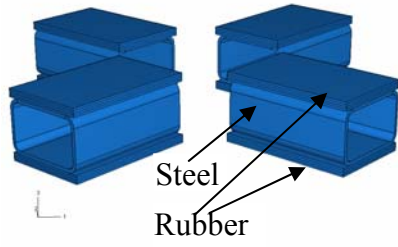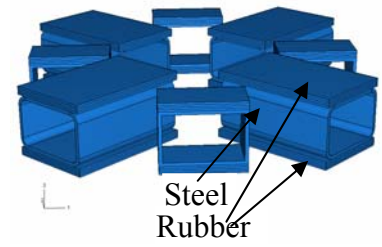
Table 6.6 Results of natural frequencies analysis (Hz) (Without rubber base)

| Modes | Model-1 | | Model-2 | | Model-3 | | | | | Model-4 |
	Case 1	Case 2	Case 1	Case 2	Case 1	Case 2	Case 3	Case 4	Case 5	Case 1
Mode 1	281.6	435.7	378.8	454.6	291.5	322.6	381.6	291.5	322.6	530.2
Mode 2	299.9	445.4	390.8	471.1	322.5	383.9	432.0	379.3	379.9	562.2
Mode 3	339.2	463.9	403.7	504.6	372.8	431.7	439.5	433.0	431.7	735.8
Mode 4	358.5	532.3	453.4	615.0	432.6	439.5	516.0	442.0	439.5	781.0
Mode 5	376.1	621.1	473.6	735.0	442.0	5 34.4	5 65.3	516.08	534.3	921.5
Mode 6	516	643.4	555.9	771.2	5 34.4	5 74.7	7 57.4	565.2	575.4	961.7

BC	Material	Mode 1	Mode 2	Mode 3	Mode 4
Table 6.7 Results of different machine bases (Hz)					
BC-1	Rubber	13.7	20.8	45.3	51.1
	Nitrile641	13.6	16.9	44.5	63.1
	Nitirle642	16.0	20.5	51.8	70.8
BC-2	Rubber	9.9	16.1	31.2	37.6
	Nitrile641	10.5	13.6	34.6	50.9
	Nitirle642	11.9	16.1	38.1	53.9
BC-3	Nitirle641	16.45	16.51	18.56	
	Nitirle642	20.55	20.66	21.73	
BC-4	Nitirle642	27.93	28.19	29.19	
BC-5	Nitirle642	41.22	41.76	42.65	
BC-6	Nitirle642	14.88	14.91	17.28	
BC-7	Nitirle642	16.84	17.10	19.83	

6.6 References

ABAQUS Analysis User's Manual. 'Linear elastic behavior, Section 10.2.1.

ABAQUS Theory Manual. 'solid isoparametric quadrilaterals and hexahedra' Section 3.2.4, Version 6.3.

Kurkin, S.A., Lukyanov, V.F. and Krumboldt, M.N. (1973), 'Design of biaxial tensile testing machines,' *Strength of Material,* Volume 5, Number 12, pp 1519-1524.

Ma, Y. (2004), 'Fundamental and Engineering Application Studies of Pressure-Assisted Injection Forging of Thick-Walled Tubular Components,' University of Strathclyde PhD Thesis, Volume 2, p 299-330.

Qin, Y. and Juster, N.P. (2003), 'Advances in manufacturing technology XVII,' The 1st International Conference on Manufacturing Research (ICMR 2003), pp 329-335.

http://www.efunda.com/materials visited in Jun 2007

http://www.matweb.com visited in October 2006

http://www.reliabilityweb.com visited in June 2008

6.7 Appendix A – Figures
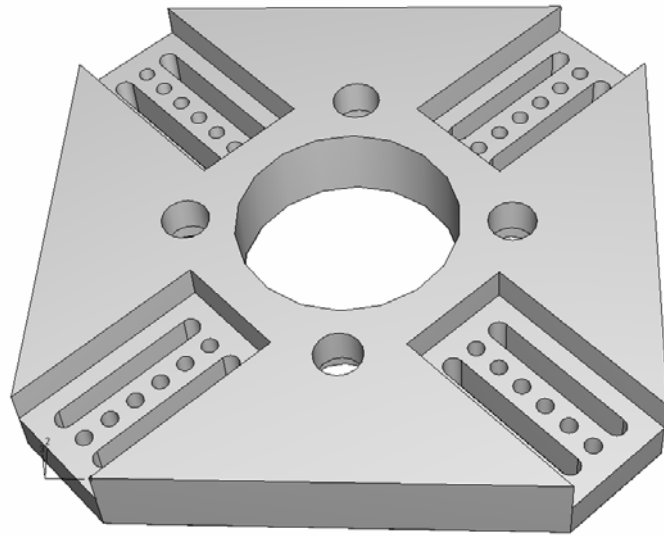
(a) Top plate
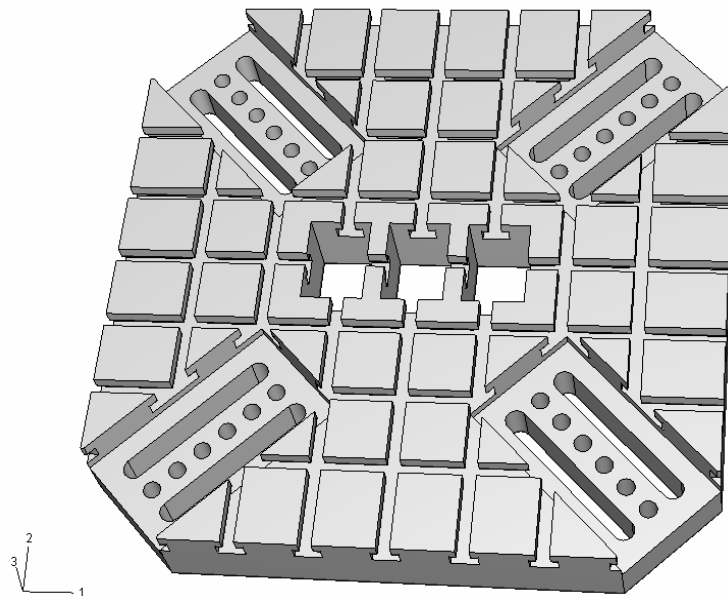
(b) Base plate

Fig. A6.1 Main components of the micro-stamping machine
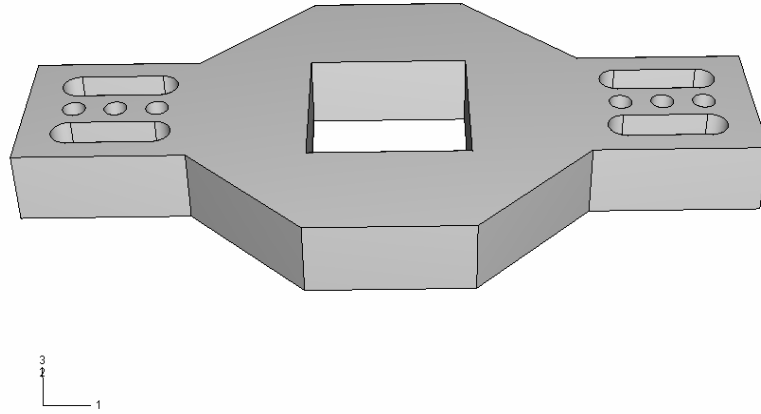
(a) Linear guide plate
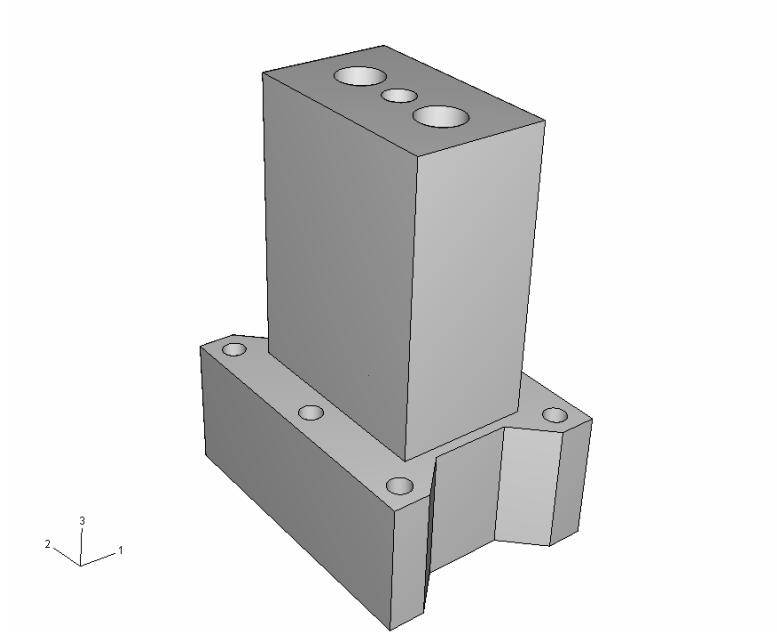
(b) Linear guide column

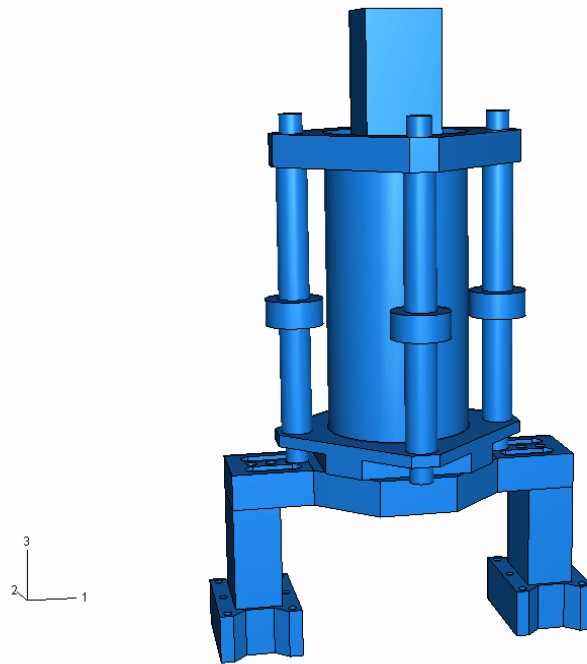**Fig. A6.2   Main components of the micro-stamping machine**
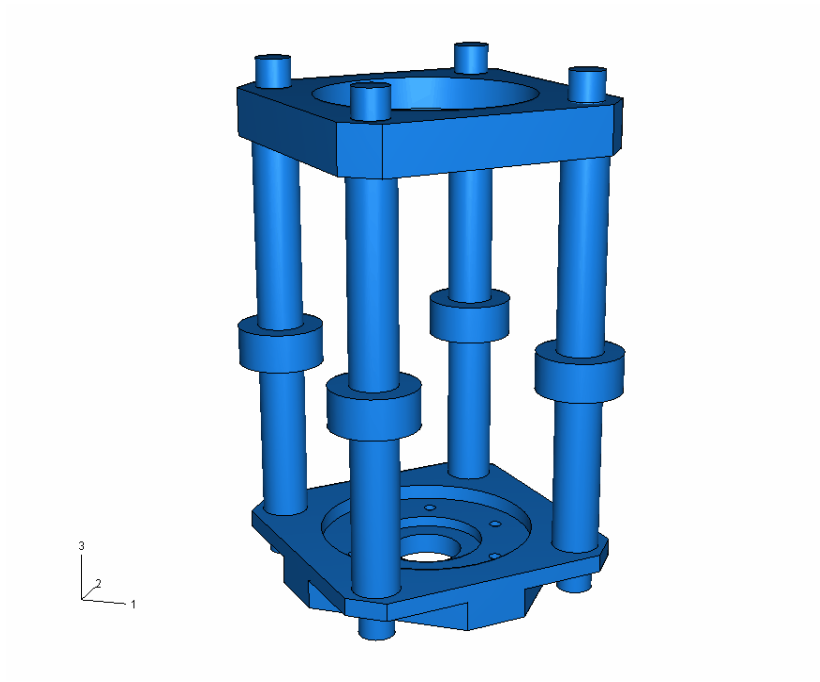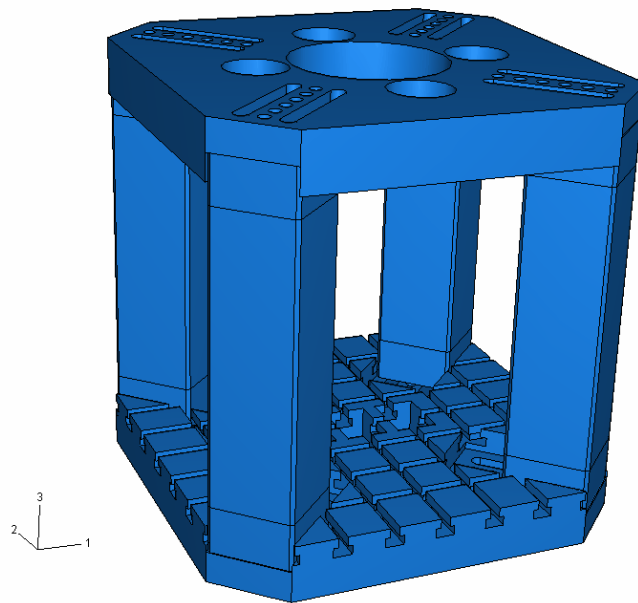
(a)   Set of linear-motor supports
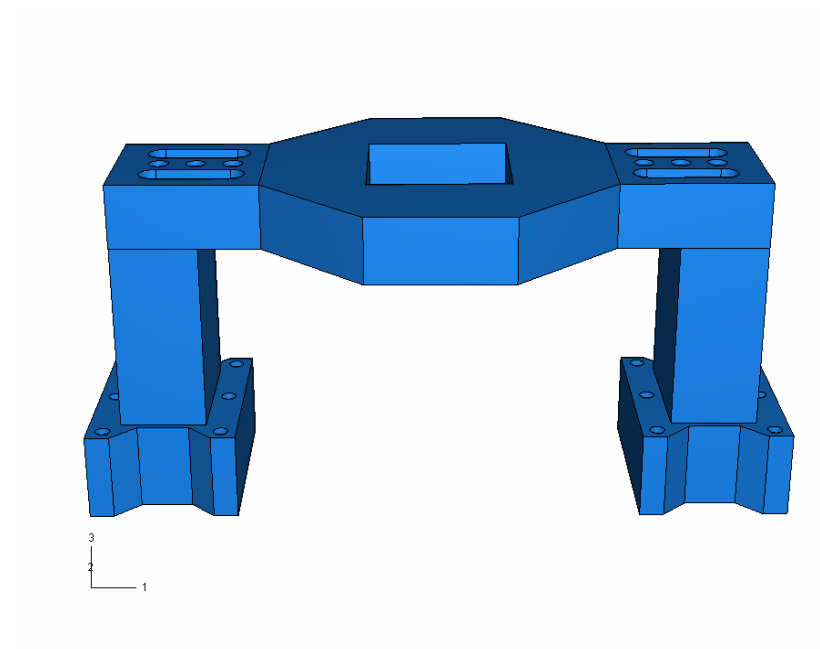
(b)   Linear guide
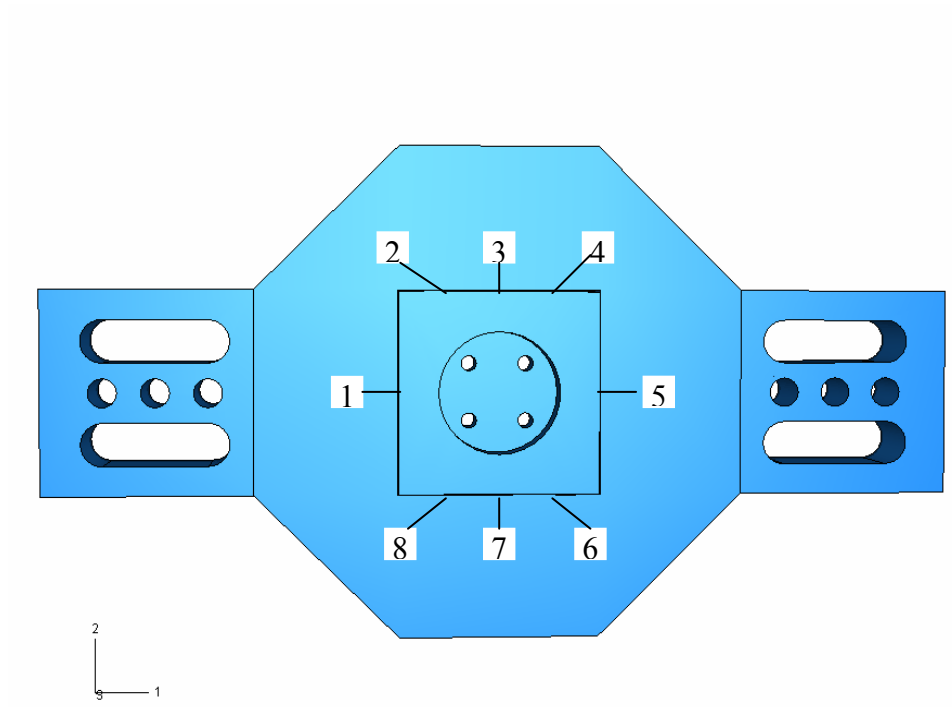
Fig. A6.3   Main assemblies of the micro-stamping machine
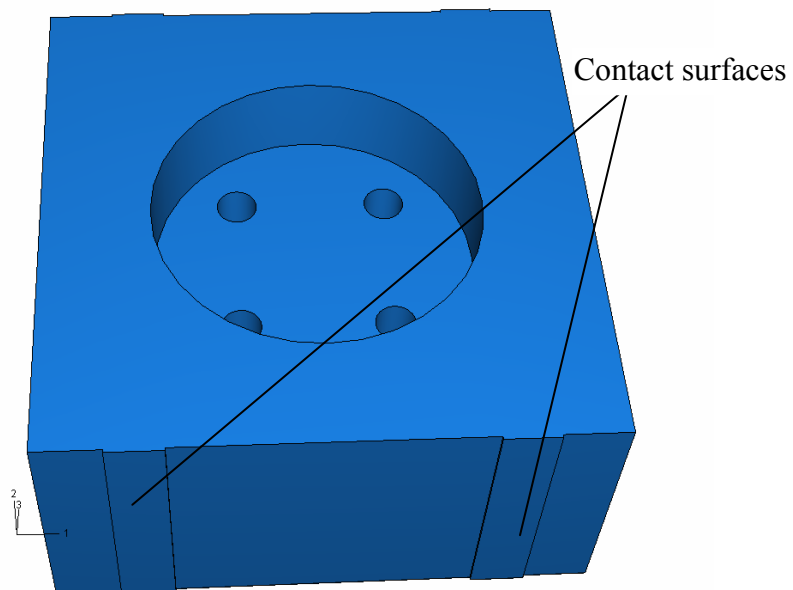
(a) Linear motor and linear guide

(b) Frame of the micro-stamping machine

Fig. A6.4   Main assembly of the micro-stamping machine

(a) Contact positions

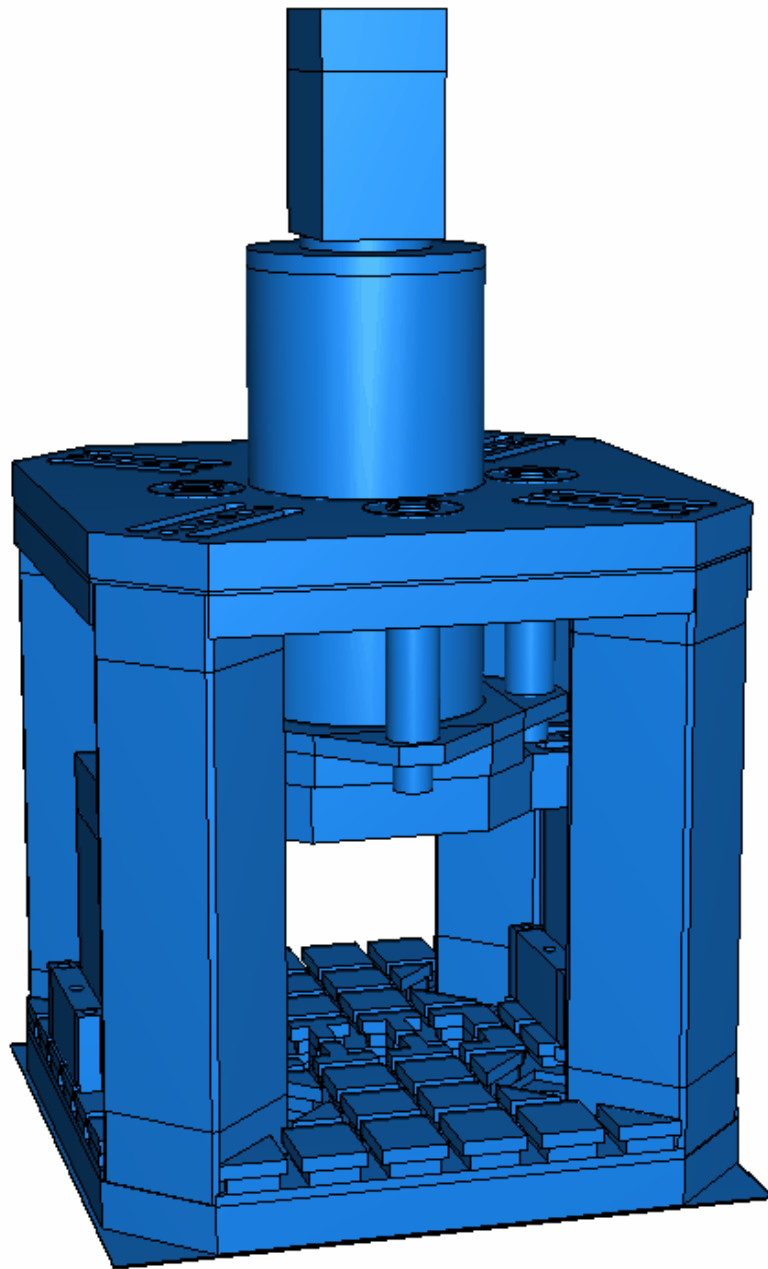**(b) Ram**

Fig. A6.5 Contact of the linear guide and the ram

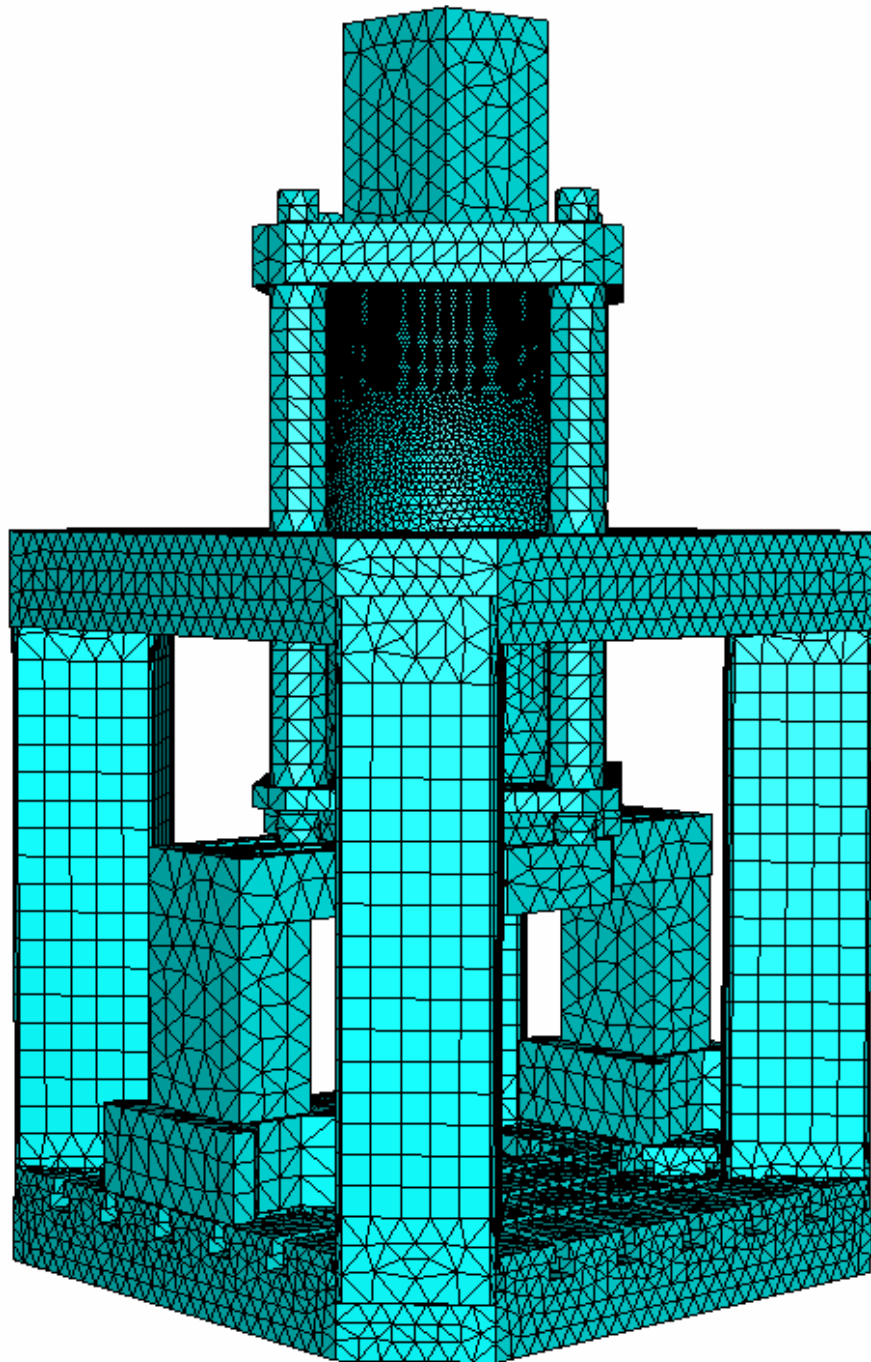**Fig. A6.6   Improved design of the micro-stamping machine**

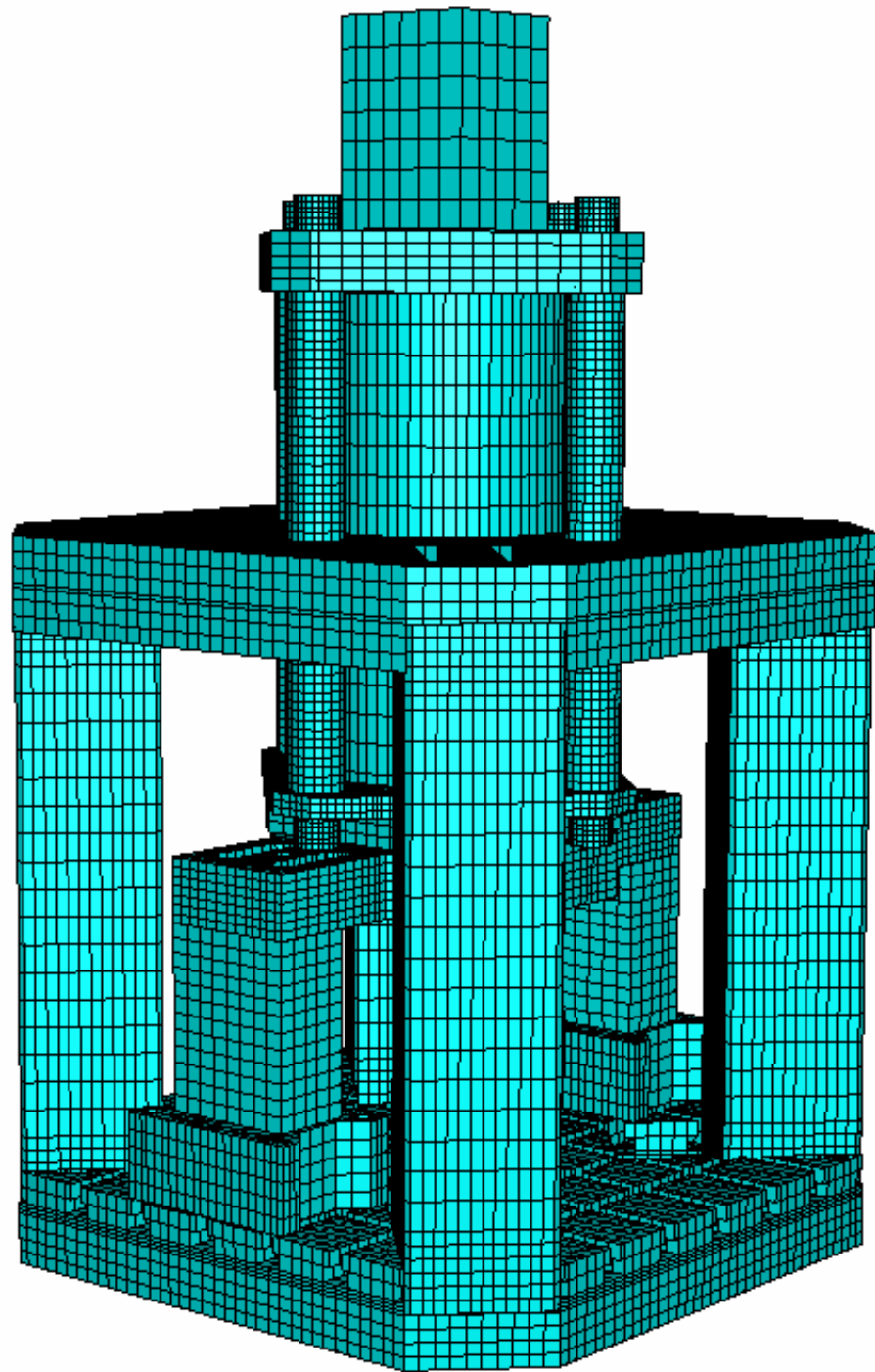**Fig. A6.7   Mesh-1 of the micro-stamping machine**

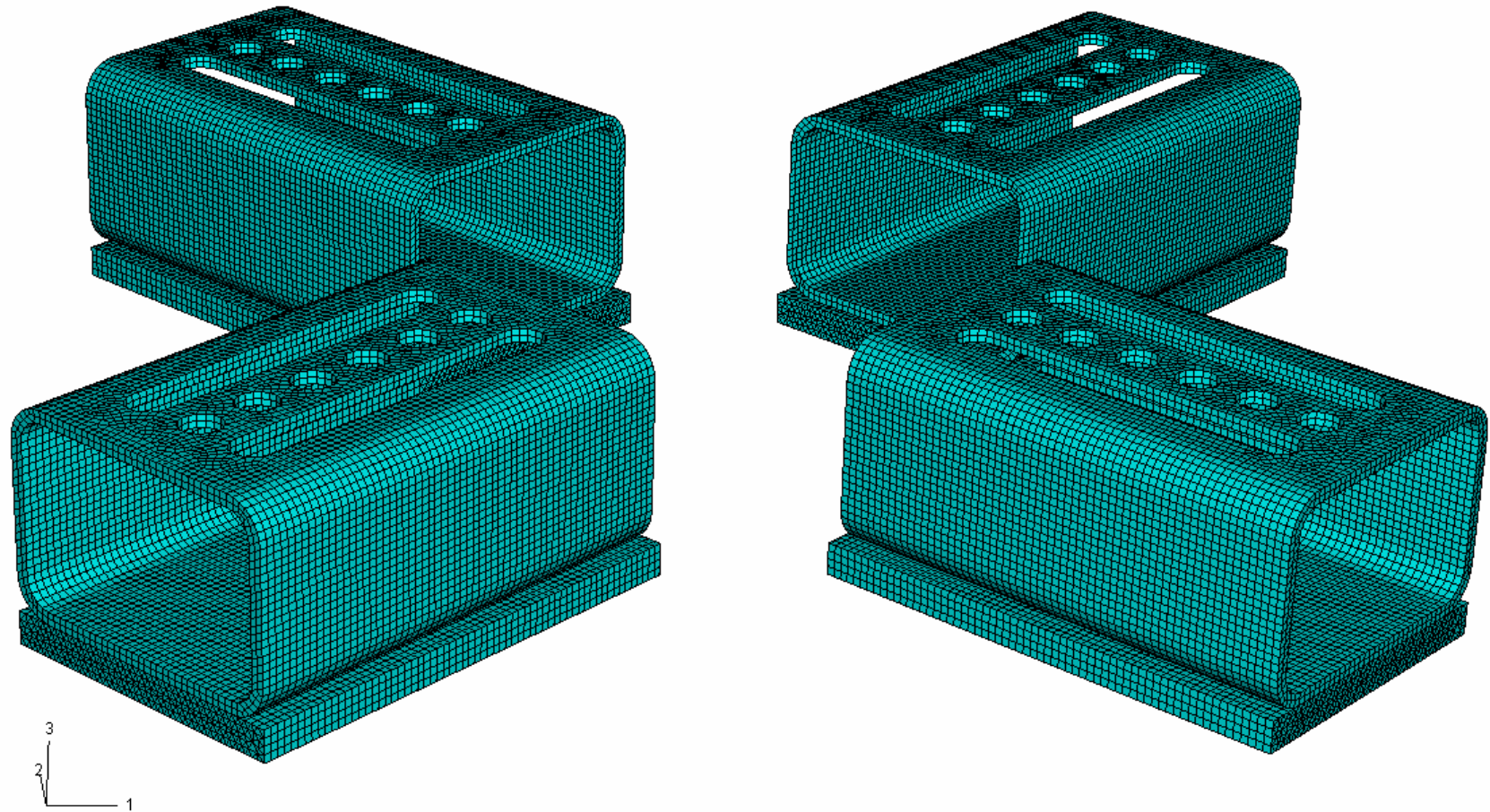**Fig. A6.8   Mesh-5 of the micro-stamping machine**

Fig. A6.9   Mesh of the micro-stamping machine base

Fig. A6.10   Contour plot of mode 1 of the micro-stamping machine (model-1 case 1)

Fig. A6.11 Contour plot of mode 1 of the micro-stamping machine (model-1 case 2)
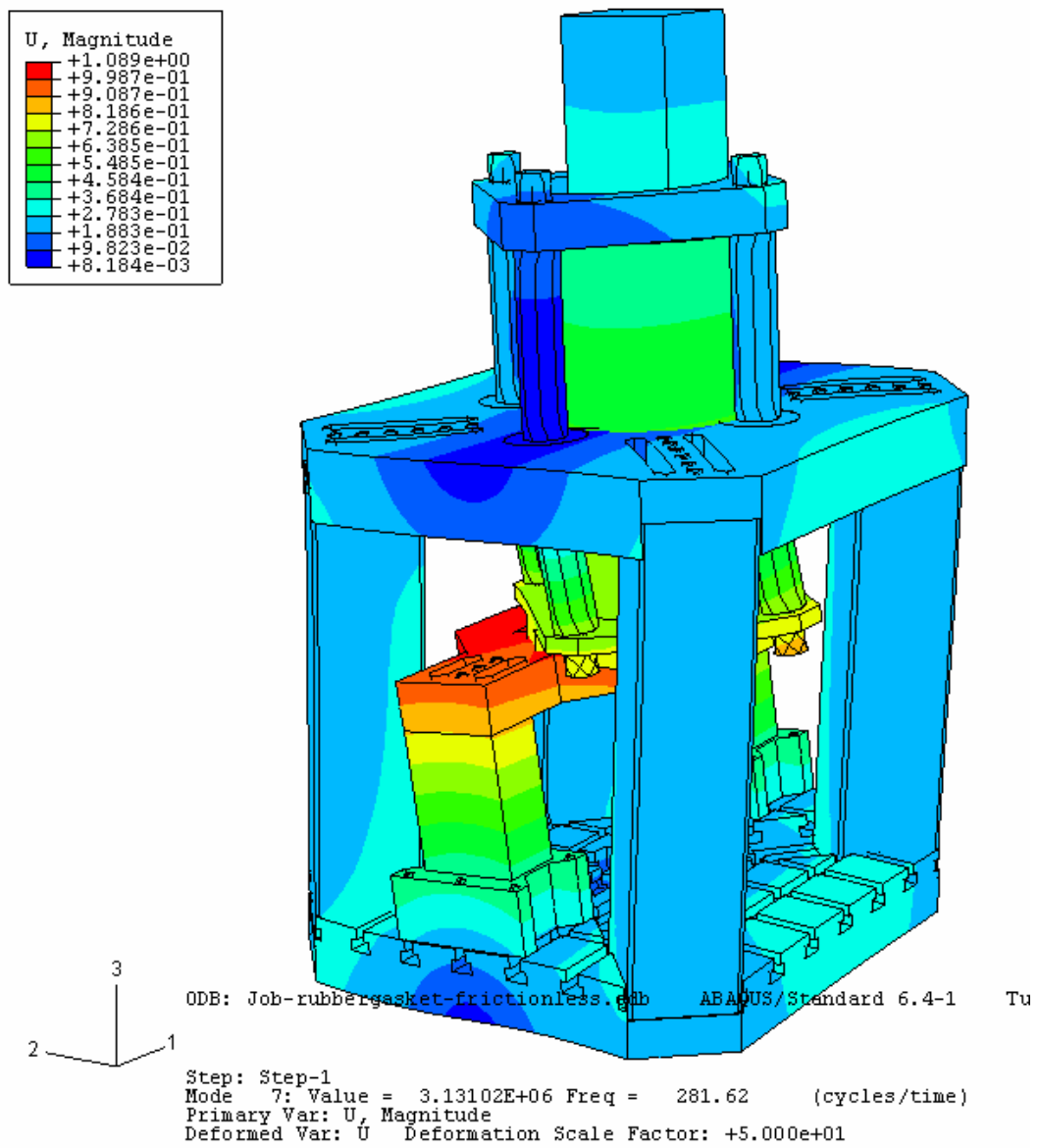
**Fig. A6.12   Contour plot of mode 1 of the micro-stamping machine
(model-2 case 1)**

Fig. A6.13 Contour plot of mode 1 of the micro-stamping machine (model-2 case 2)

**Fig. A6.14   Contour plot of mode 1 of the micro-stamping machine
(model-3 case1)**
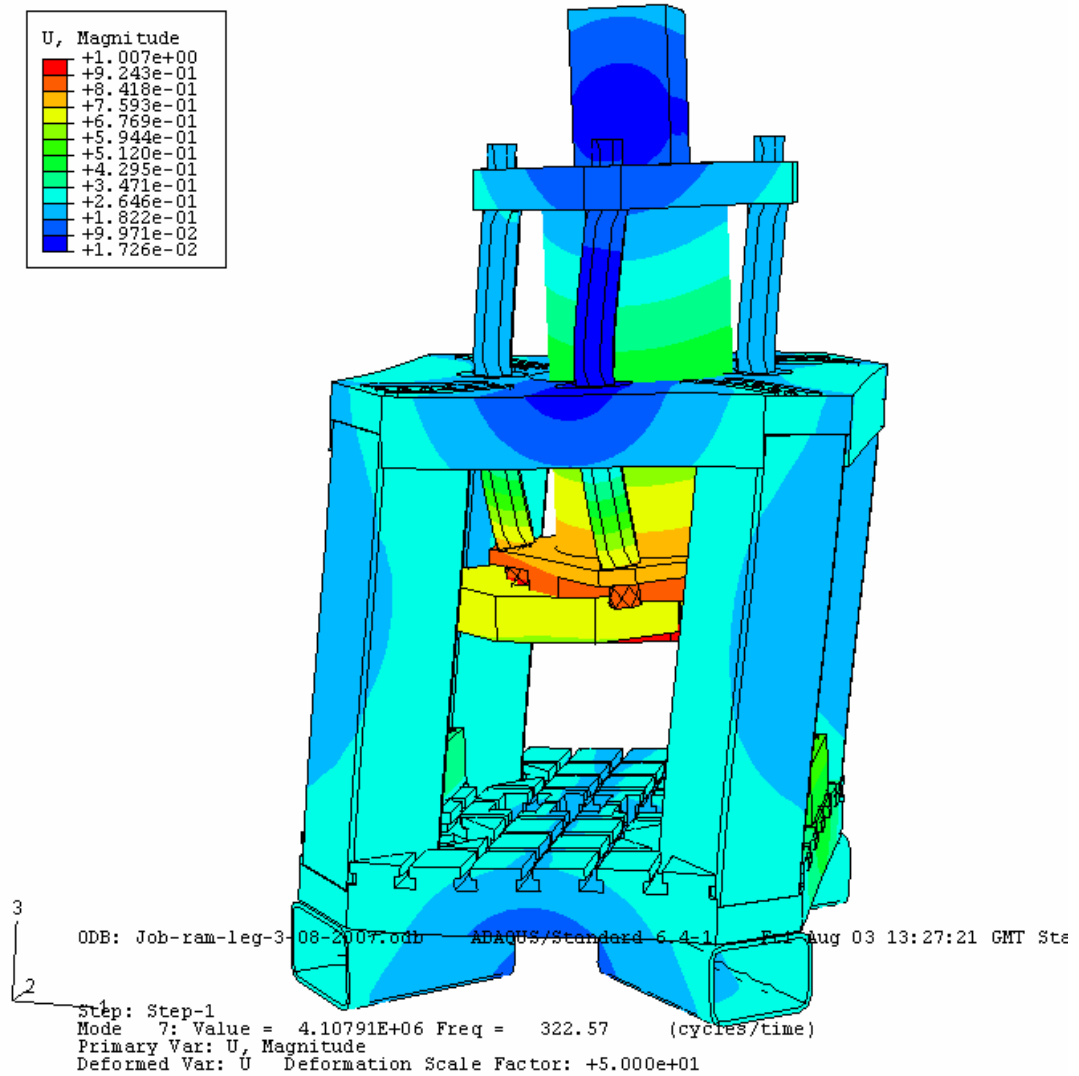
Fig. A6.15   Contour plot of mode 1 of the micro-stamping machine (model-3 case 2)
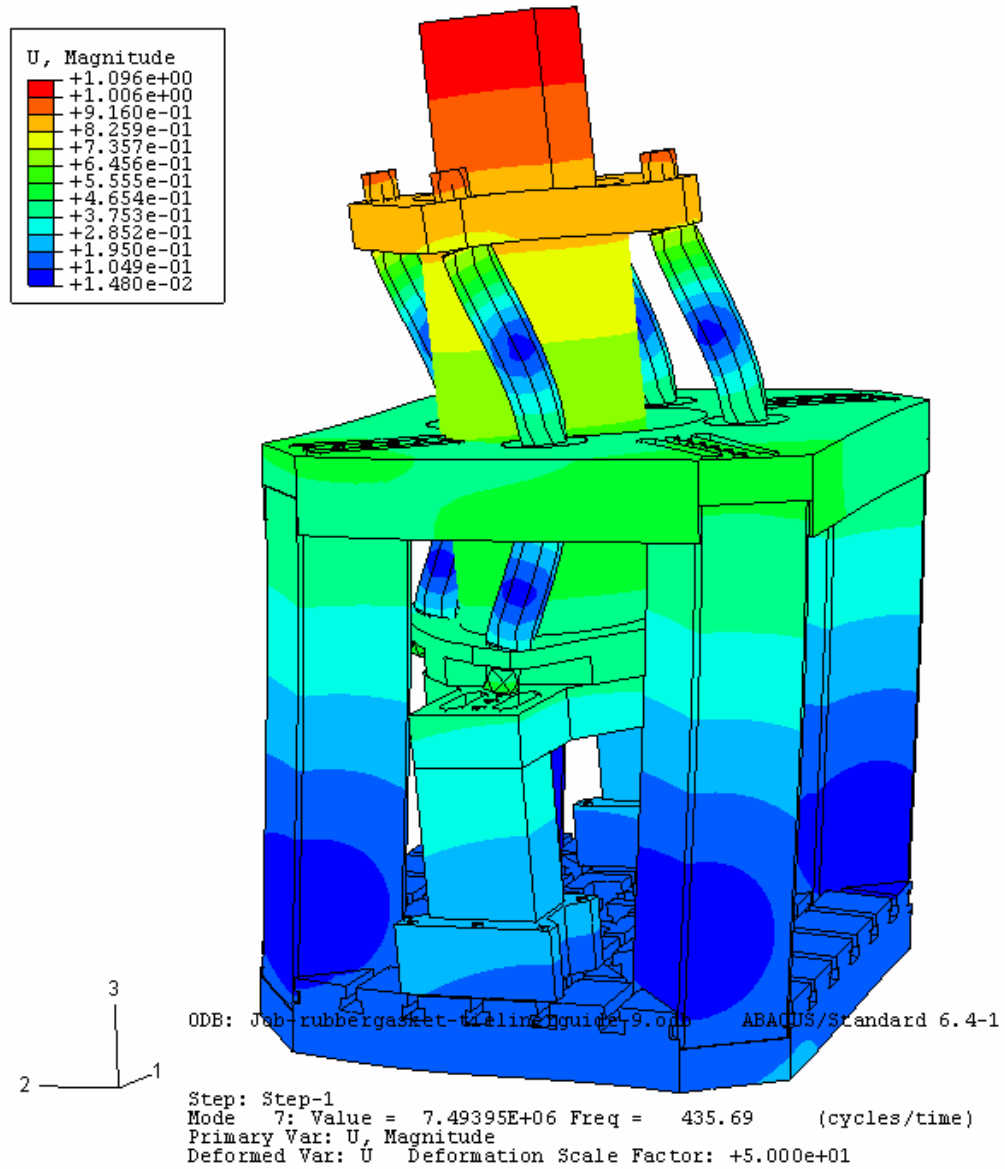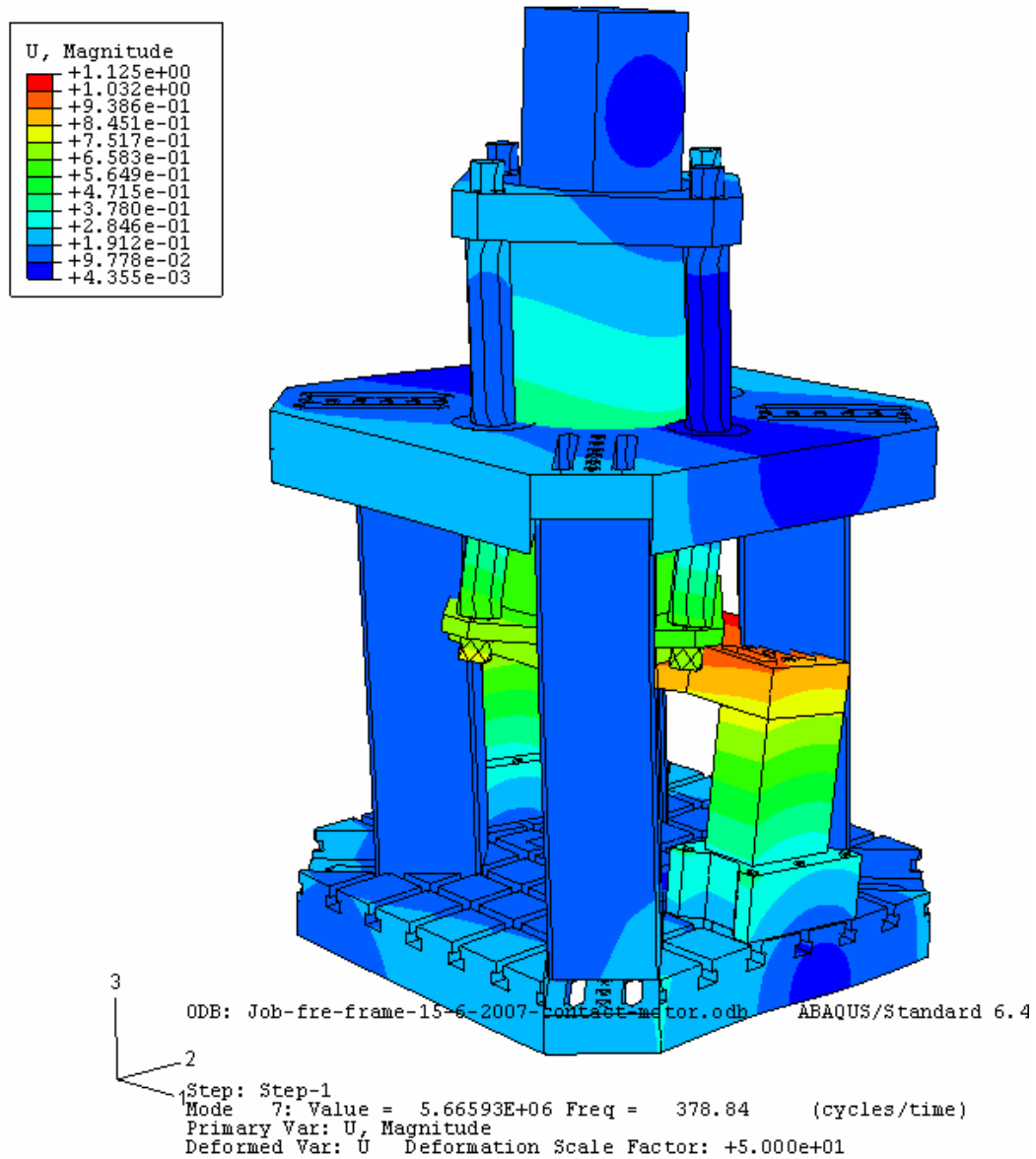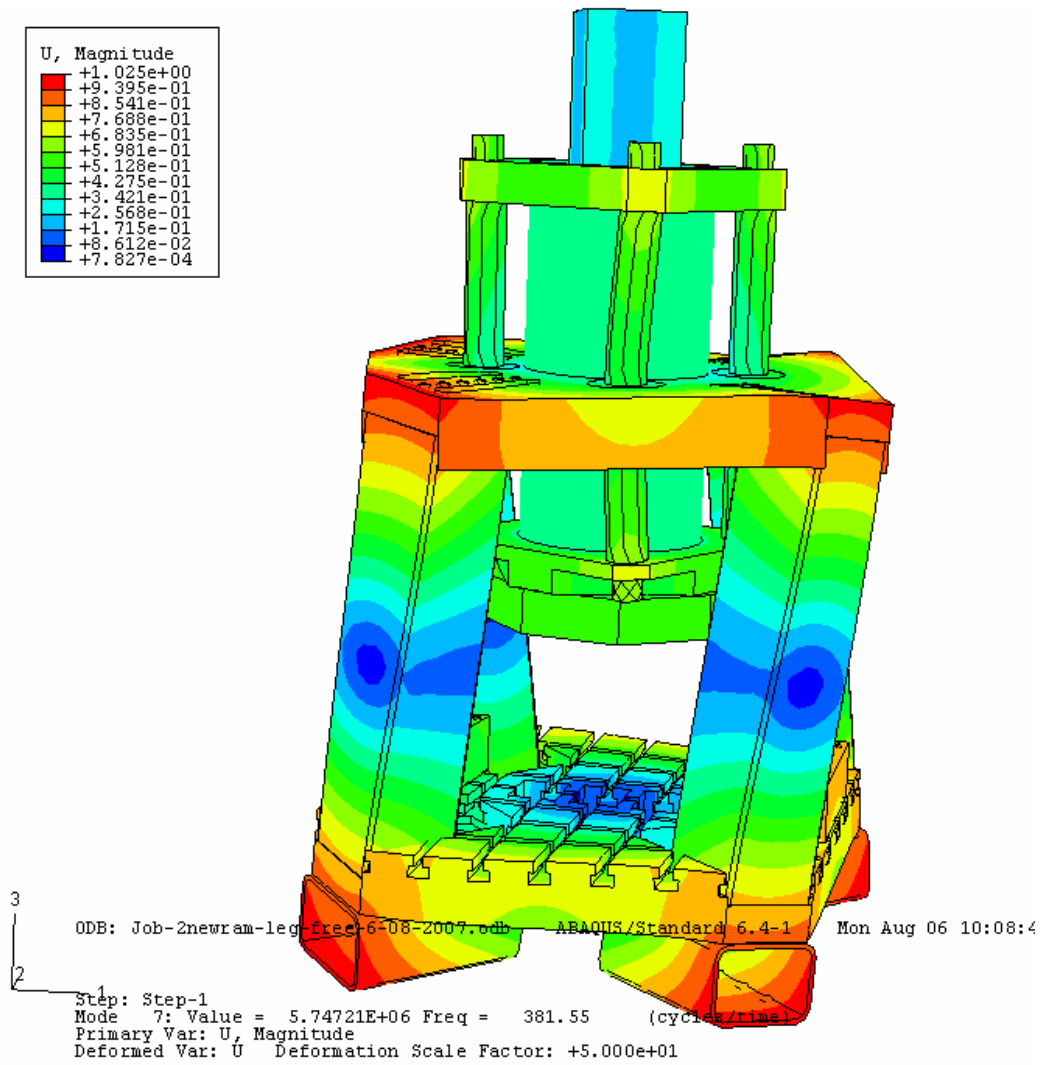
Fig. A6.16   Contour plot of mode 1 of the micro-stamping machine (model-3 case 3)
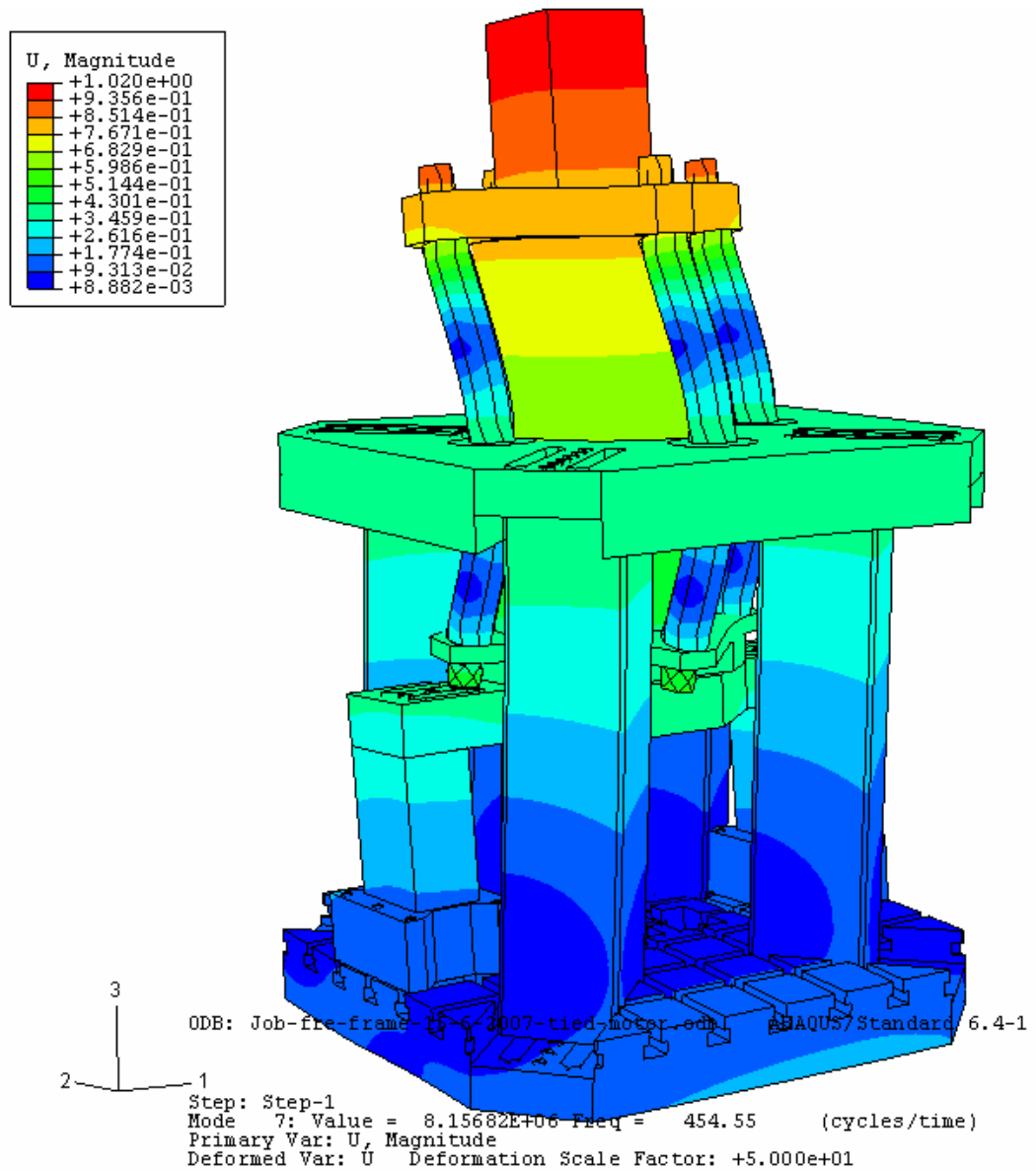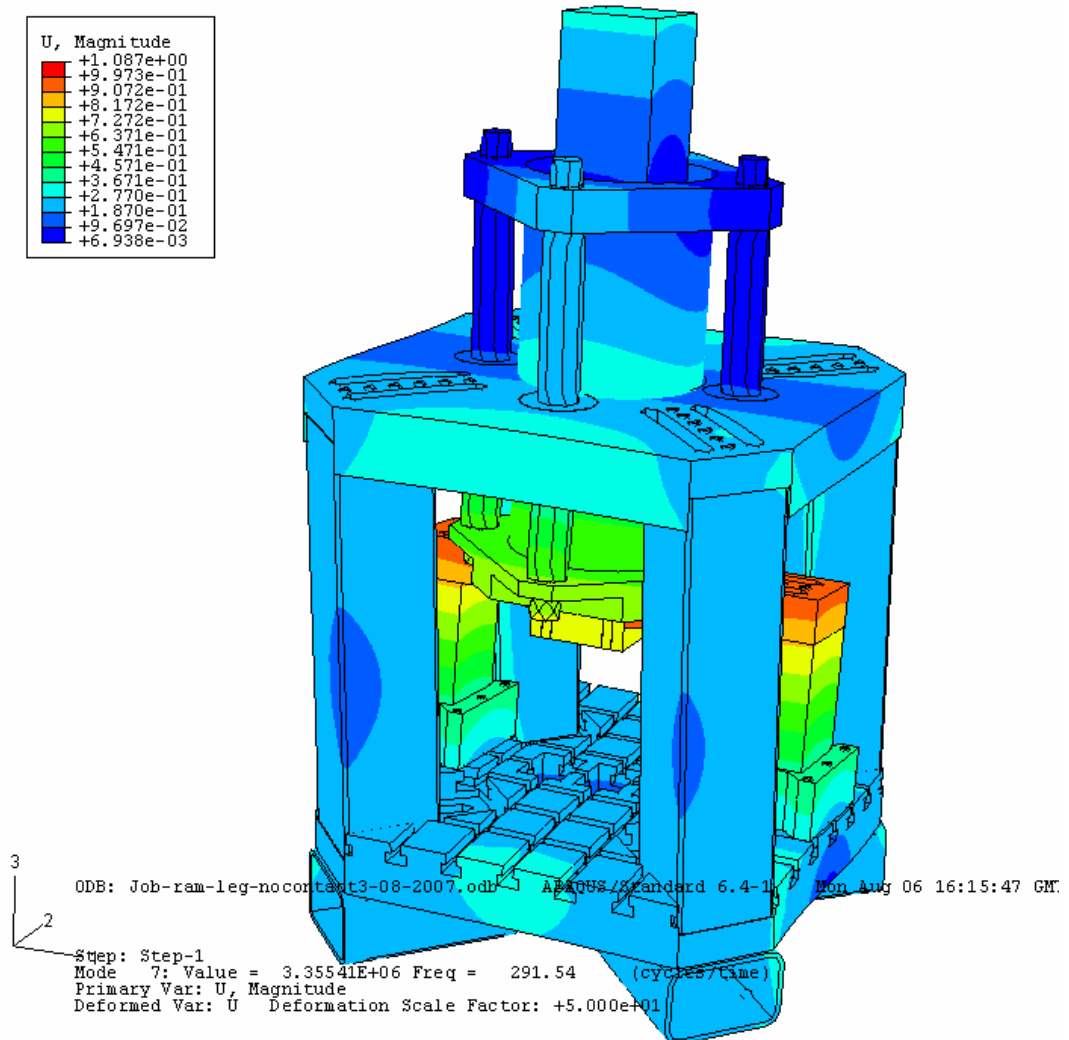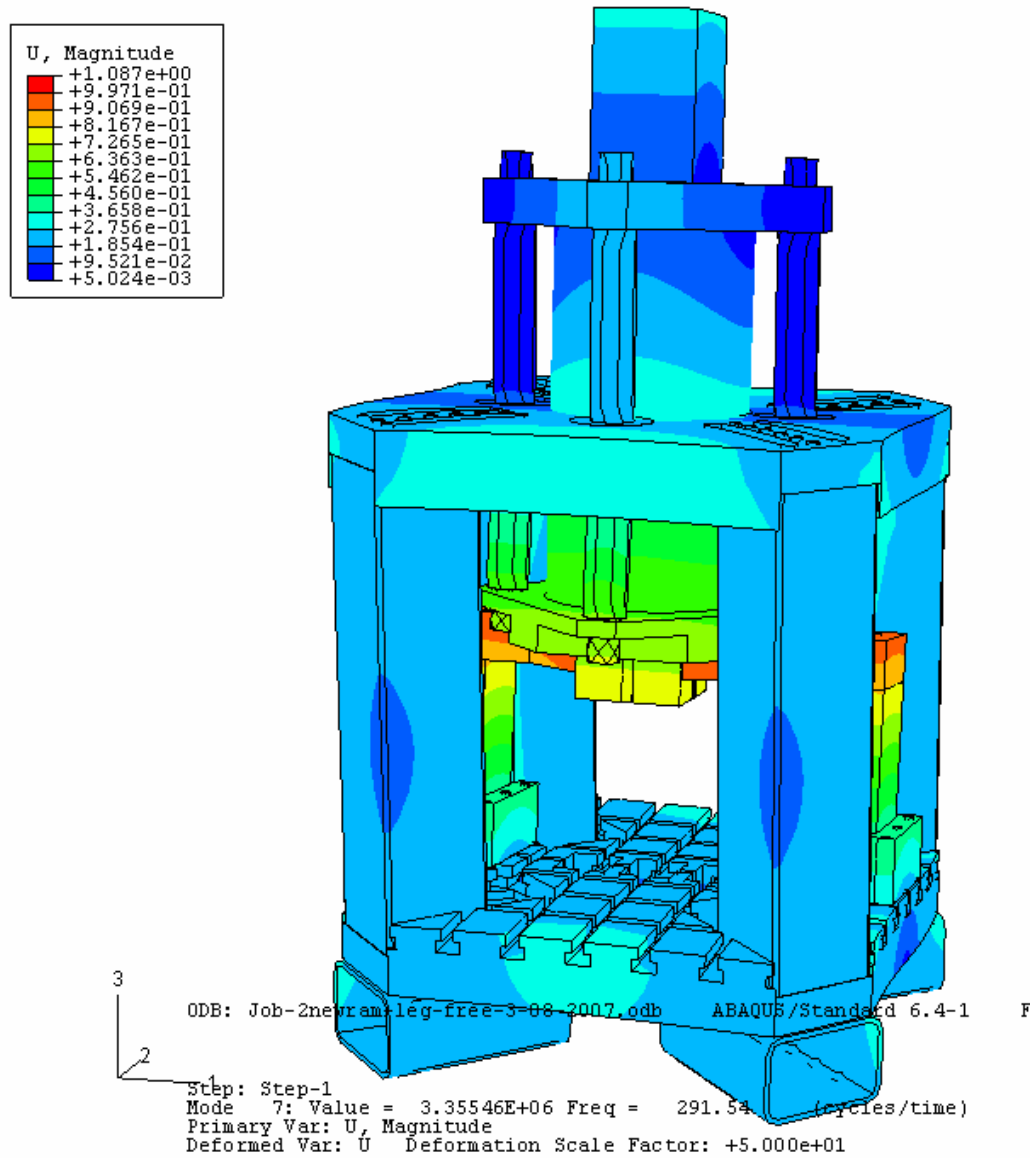
**Fig. A6.17   Contour plot of mode 1 of the micro-stamping machine
(model-3 case 4)**

**Fig. A6.18   Contour plot of mode 1 of the micro-stamping machine
(model-3 case 5)**

U, Magnitude
+1.202e+00
+1.102e+00
+1.002e+00
+9.021e-01
+8.020e-01
+7.019e-01
+6.019e-01
+5.018e-01
+4.017e-01
+3.016e-01
+2.015e-01
+1.014e-01
+1.366e-03

ODB: Job-12-model3ease1.odb   ABAQUS/Standard 6.4-1   Tue Aug 14 14

Step: Step-1
Mode   7: Value =   1.10977E+07 Freq =   530.20   (cycles/time)
Primary Var: U, Magnitude
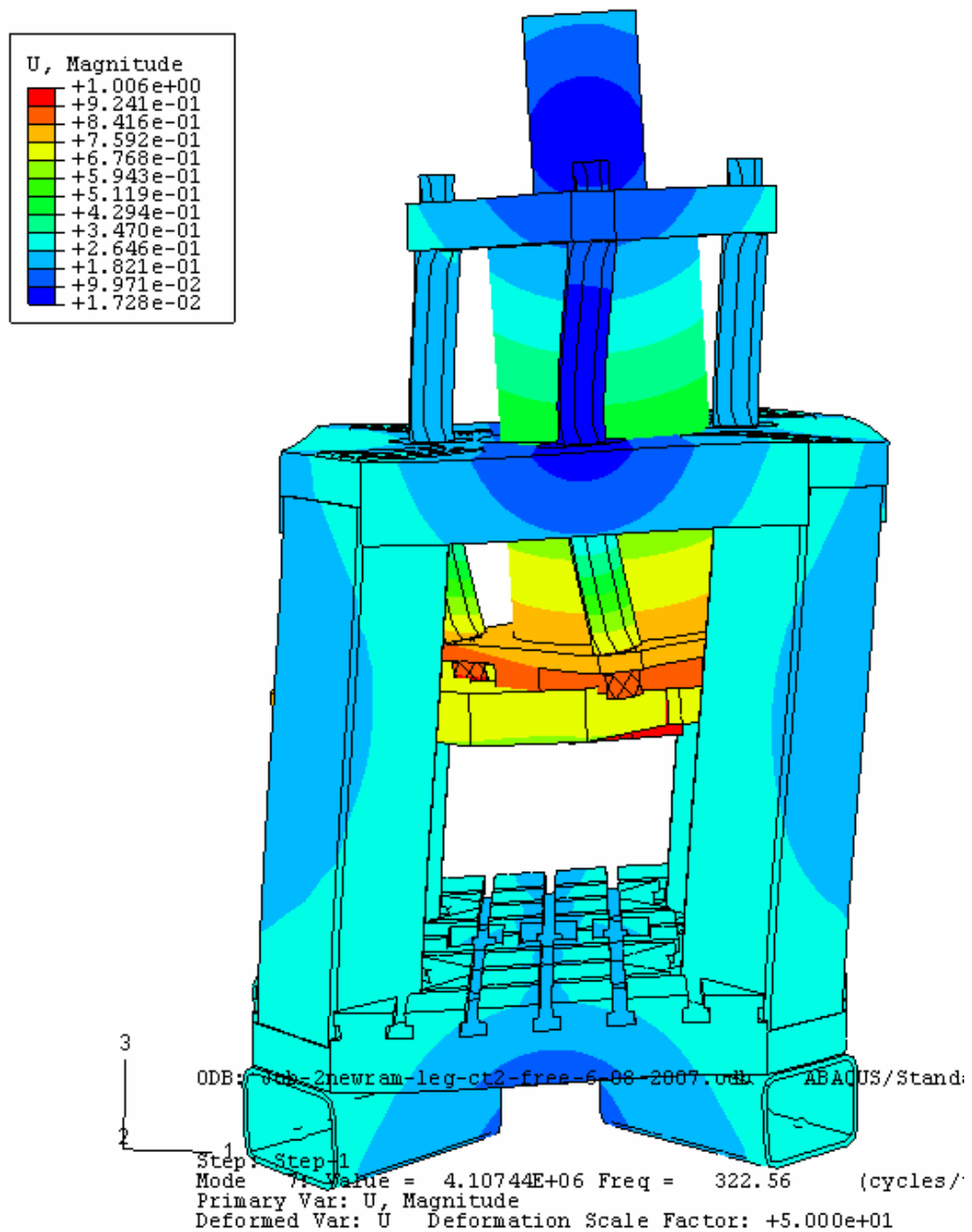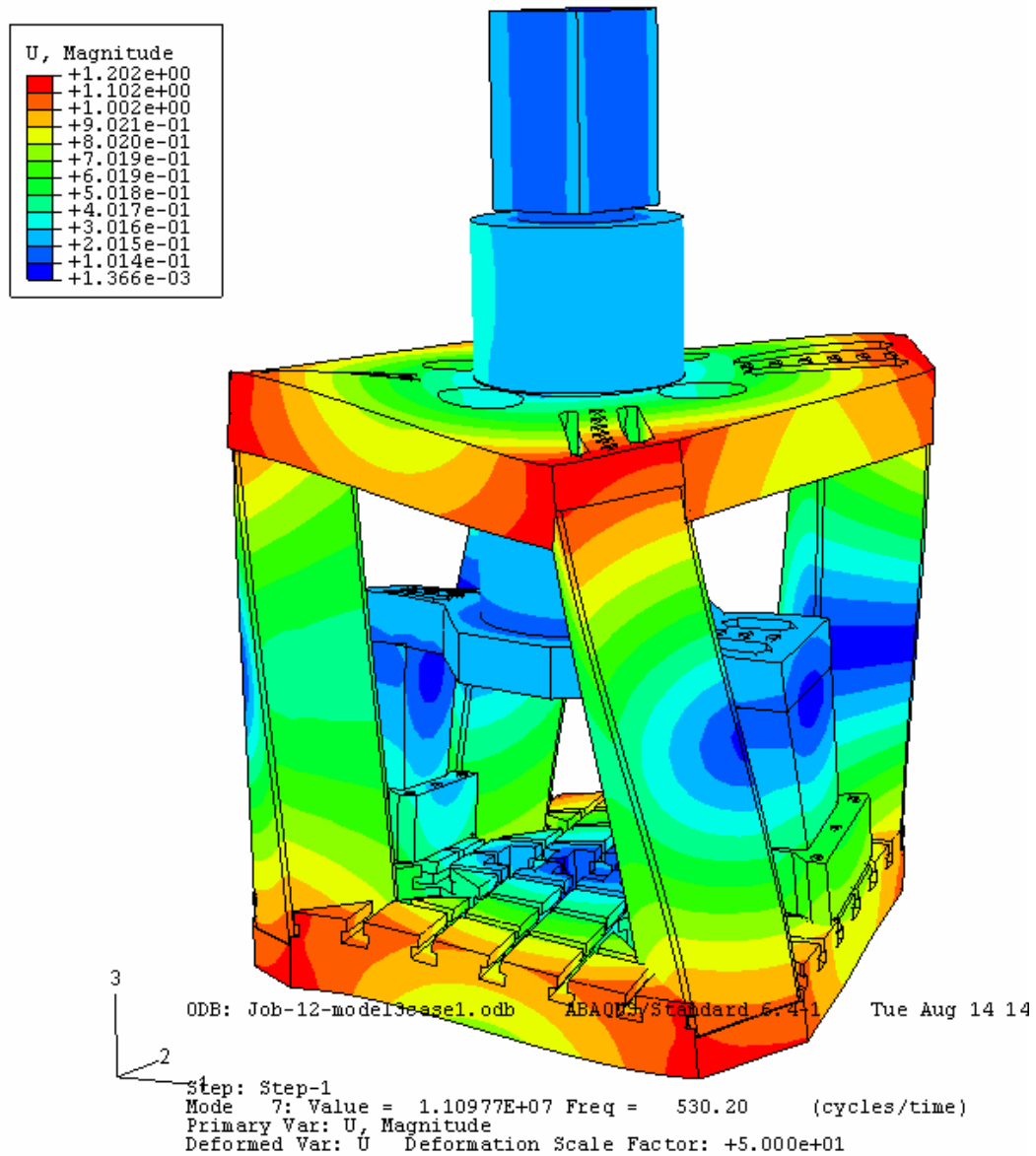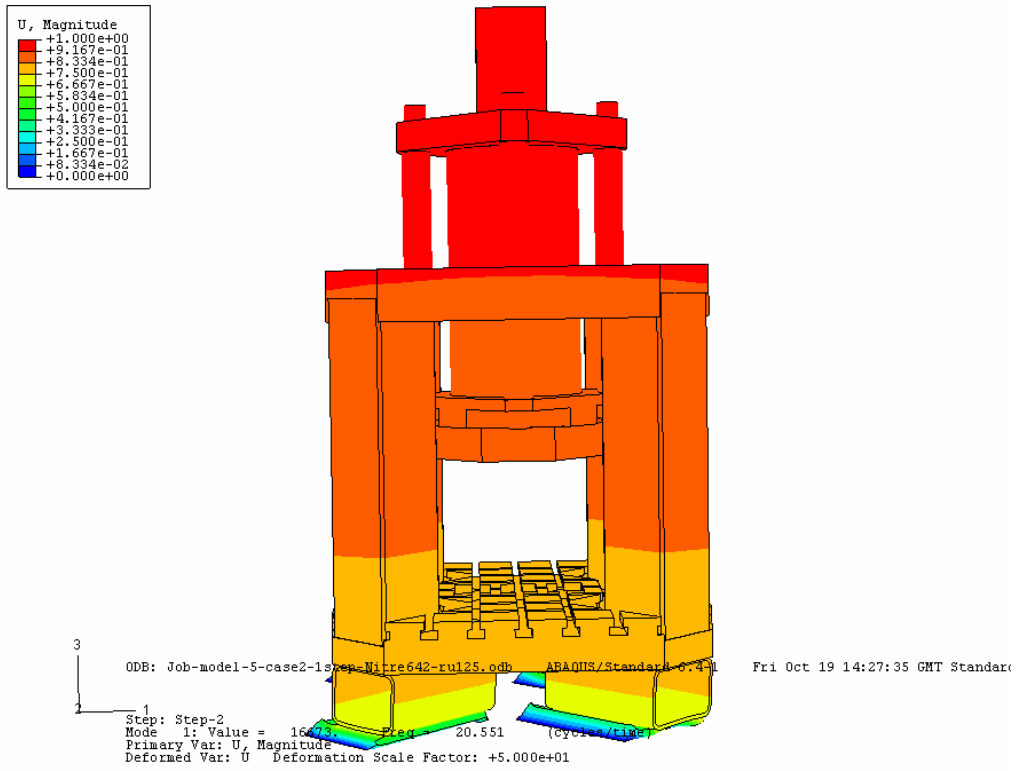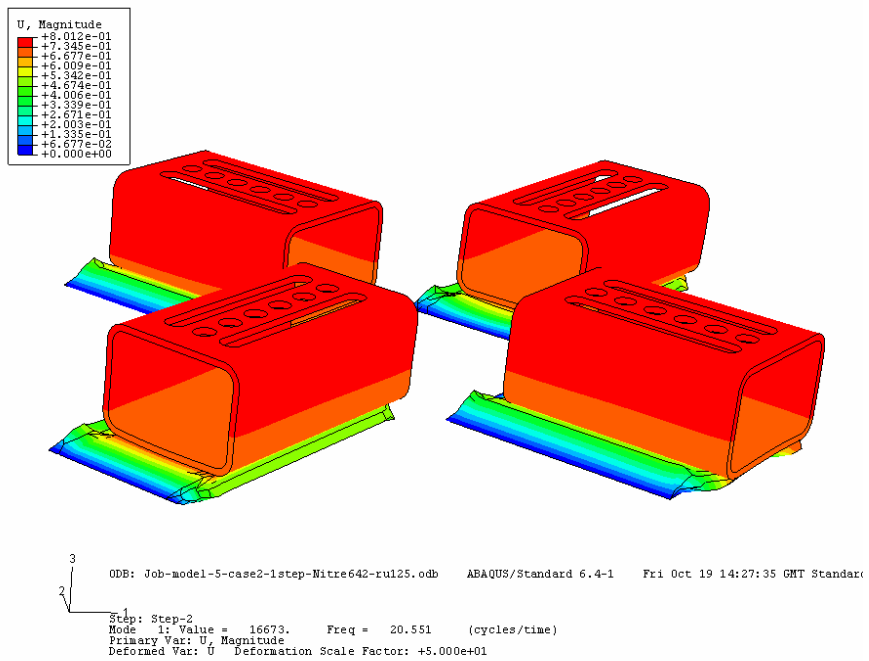Deformed Var: U   Deformation Scale Factor: +5.000e+01

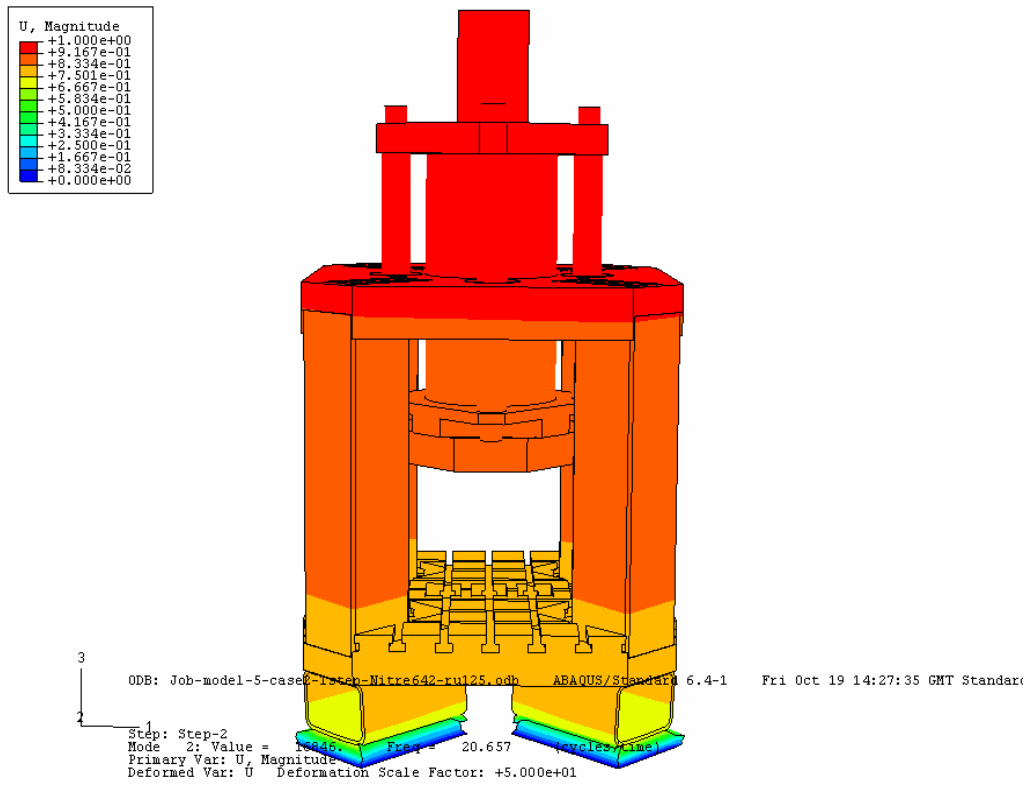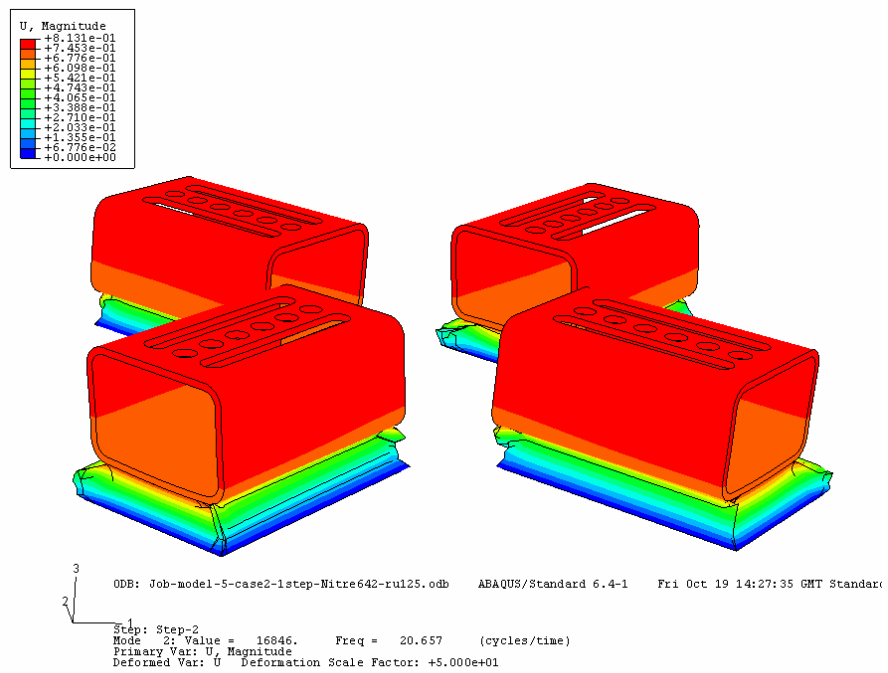**Fig. A6.19   Contour plot of mode 1 of the micro-stamping machine (model-4)**

(a) Machine

(b) Base

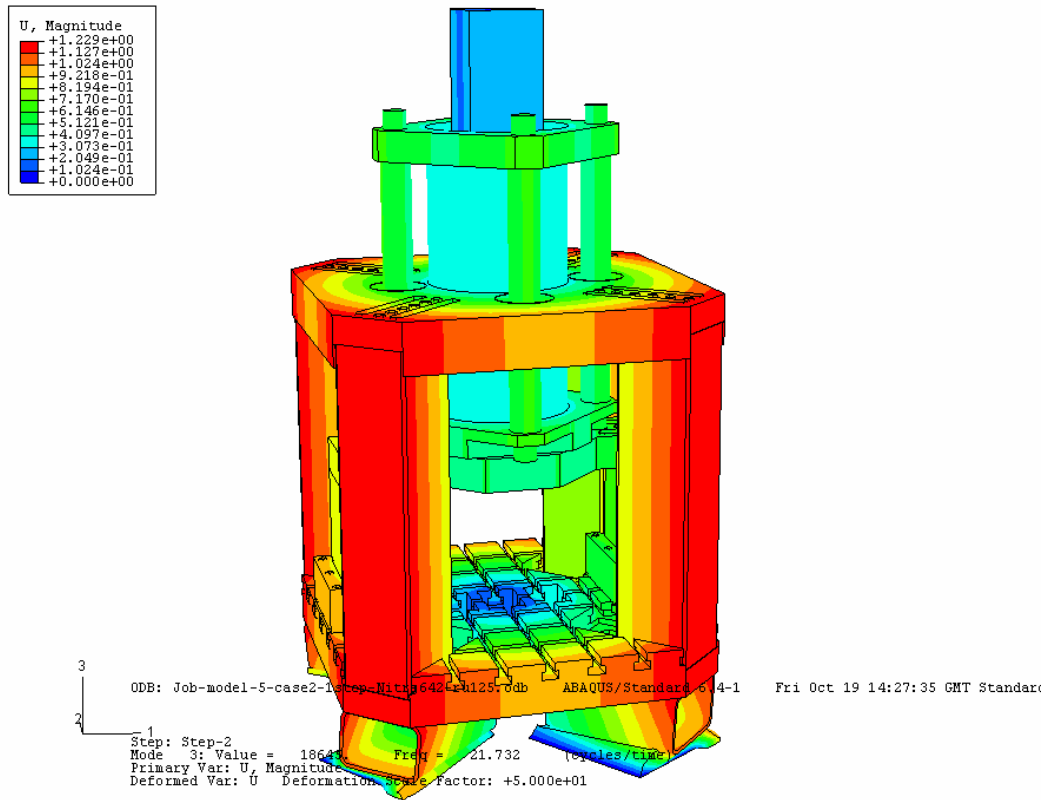**Fig. A6.20   Mode 1 of model BC-1**
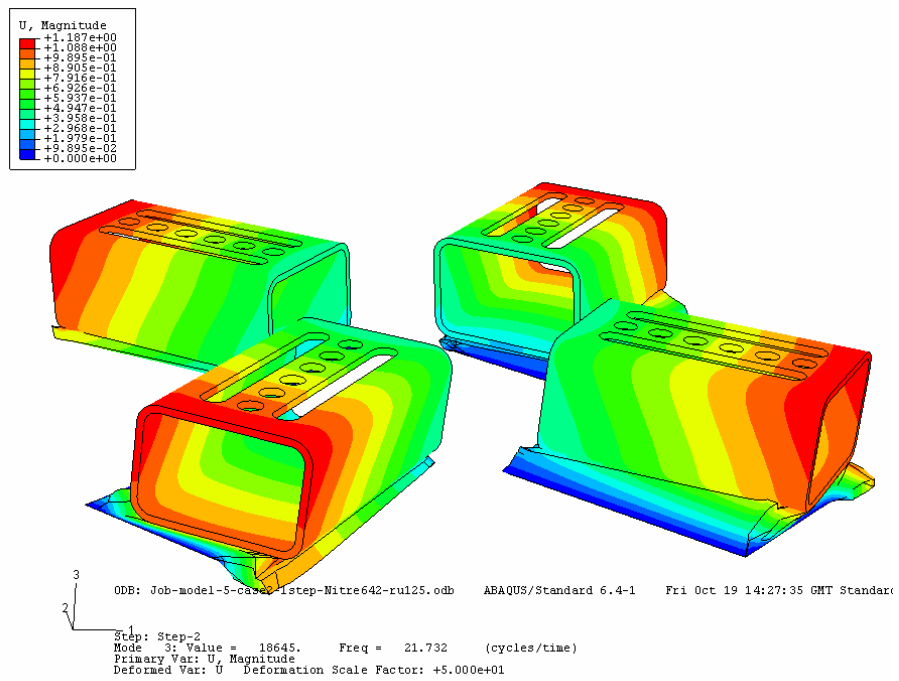
(a) Machine

(b) Base

Fig. A6.21   Mode 2 of model BC-1

(a) Machine

(b) Base

Fig. A6.22   Mode 3 of model BC-1

Chapter 7 Dynamic-Behaviour Analysis of a Micro-Stamping Tool

7.1   Introduction

As demands for the forming of micro-products increase, ensuring high-quality design of machine-tool systems becomes increasingly more important. This is particularly due to a need to address smaller geometries and stricter tolerance requirements, compared to those of conventional forming. The finite element simulation of the dynamic behaviour of machines and tools is particularly useful for supporting design optimisation. Detailed finite element modelling of stamping tool systems has, however, not been addressed previously. Difficulties tend to arise when many tool parts need to be considered in the modelling. In this chapter, the dynamics analysis of a micro-sheet-forming system driven by a linear motor is presented. The analysis was performed using ABAQUS. Parameters that influence the dynamic behaviour of the micro-stamping tool were investigated. The findings provide useful information for the improvement of micro-stamping tool design as well as micro-forming machine-system design.

Damage to the punches of the stamping tools is one of the major problems during high-speed stamping. In order to avoid punch damage and to achieve high precision during high-speed stamping, the dynamic response of the tools is taken as a critical factor (Groche and Schneider, 2004). At the same time, for a stamping-tool that holds multi-punches, the influence of the asymmetrical cutting-forces generated from different punches on the precision has also been taken as a target of investigation. Especially for improving the performance of the whole forming-machine system, the exciting forces transferred from the stamping tool to the machine system have to be analysed. These are particularly important for micro-forming, since precision is a key issue to be addressed in the forming of micro-products (Qin, 2006).

The problems to be investigated in this chapter are listed as follows:

- What is the appropriate model for an efficient and accurate FE analysis of the dynamic characteristics of the micro-stamping tool?

- What is the dynamic response of the moving components of the micro-stamping tool?

- What is the influence of the lubricant on the dynamic responses of the micro-stamping tool?

- What is the influence of the micro-stamping tool on the vibration of the micro-stamping machine?

In the micro-stamping tool considered, springs are the connectors of the moving components. The influence of the stiffness of the springs on the dynamic behaviour of the micro-stamping tool has been investigated.

7.2 Finite element method for dynamics analysis

When a structure is subjected to dynamic loads such as impact or enforced displacements, the additional inertia forces are equal to the mass multiplied by the acceleration. Hence, dynamical analysis is a simple extension of the static analysis of the structure. Moreover, the damping effect can be significant and needs to be taken into consideration in structural dynamic-analysis. In dynamics analysis by the finite element method, the force equilibrium of a real physical structure can be expressed as an equation of time:

$$[M]\{\ddot{u}(t)\} + [C]\{\dot{u}(t)\} + [K]\{u(t)\} = \{F(t)\} \tag{7.1}$$

where $[M]$ is the mass matrix of the structure

$[C]$, the damping matrix of the structure,

$[K]$, the stiffness matrix of the structure,

$\{u(t)\}$, the vector of nodal displacements,

$\{\dot{u}(t)\}$, the vector of nodal velocities,

$\{\ddot{u}(t)\}$, the vector of nodal accelerations, and

$\{F(t)\}$, the vector of applied forces.

In linear analysis the matrices in Eqn. (7.1) are constant but the vectors are time-dependent, so it is a second-order, linear differential equations. Various methods have been developed to solve this equation numerically, each having its advantages and limitations. In addition, the general equation will simplify to a particular form if some term takes on a special form or is removed (ignored) from the equation. A review is presented in the following sub-sections prior to the finite element analysis of the dynamic characteristics of stamping tools.

7.2.1 Undamped free vibration

If the structure is free of damping and there is no external force acting on the structure, the equilibrium equation is simplified to:

$$[M]\{\ddot{u}(t)\} + [K]\{u(t)\} = \{0\} \tag{7.2}$$

Mathematically, this is an eigenvalue problem. The deformation of the undamped, free vibration is in harmonic form, namely:

$$\begin{aligned} \{u(t)\} &= \{\overline{u}\}\sin(\omega t) \\ \{\ddot{u}(t)\} &= -\omega^2\{u(t)\} \end{aligned} \tag{7.3}$$

where ω is the natural frequency and $\{\overline{u}\}$ is a time-independent vector representing the mode shape of the structure when it vibrates.

Substituting Eqn. (7.3) into Eqn. (7.2), the eigenvalue characteristic function is obtained:

$$\left([K] - \omega^2[M]\right)\{\overline{u}\} = \{0\} \tag{7.4}$$

in which $\{\overline{u}\}$ is known as the eigenvector, ω^2 is known as the eigenvalue, and ω is known as the natural frequency or circular frequency.

If the structure has n degrees of freedom, there will be n natural frequencies and associated mode shapes - including the zero frequencies corresponding to the rigid-body modes. Therefore a normal mode analysis is much more expensive

computationally than a static analysis. In principle, the eigenvalues can be found by solving the following equation:

$$\text{Det}\left([K] - \omega^2 [M]\right) = 0 \tag{7.5}$$

However, in the case of large structural problems, this approach will be very time-consuming. This eigenvalue problem can be solved by many other numerical methods, for example the Jacobi iteration method.

On the other hand, it is very rare in practical applications that all the eigenvalues are needed. Instead, only a number of the lowest eigenpairs are appropriate in analysing a problem. Again, several methods have been developed to calculate a specified number of eigenvalues and eigenvectors of the lowest frequencies (or frequencies falling into a specified region). The Lanczos and sub-space algorithms are among those that are used frequently.

7.2.2 Undamped harmonic response analysis

The steady-state harmonic loads take the form:

$$\{F(t)\} = \{\overline{F}\}\sin(\overline{\omega}t) \tag{7.6}$$

where the vector $\{\overline{F}\}$ represents the amplitudes and spatial distribution of the loads and is not a function of time, and $\overline{\omega}$ is the frequency of the applied loads. Therefore, in the case where the damping is ignored, the force equilibrium equation for the structure system becomes:

$$[M]\{\ddot{u}(t)\} + [K]\{u(t)\} = \{\overline{F}\}\sin(\overline{\omega}t) \tag{7.7}$$

The solution of this differential equation is simply:

$$\{u(t)\} = \{\overline{u}\}\sin(\overline{\omega}t) \tag{7.8}$$

The amplitudes of displacement response $\{\overline{u}\}$ can be found by solving the following equation:

$$([K] - \bar{\omega}^2 [M]) \{\bar{u}\} = [\bar{K}] \{\bar{u}\} = \{\bar{F}\} \tag{7.9}$$

Obviously, the solution procedure is nothing but that employed for a static problem. As a result, the various methods developed for static analysis can be employed for harmonic response analysis.

7.2.3 General dynamic-response problem

7.2.3.1 Modal methods

The modal method, or the mode-superposition method, can transform Eqn. (7.1) so that the displacement vector $\{u\}$ is replaced by $\{z\}$, where $\{z\}$ is a vector of modal amplitudes. The transformed equations are uncoupled in the case where the damping matrix is orthogonal. The solutions of these modal equations are superimposed to yield the solution of the original problem (Bathe and Wilson, 1976; Clough and Penzien, 1975; Zienkiewicz, 1978):

$$\{u(t)\} = [\Phi]\{z(t)\}, \quad \{\dot{u}(t)\} = [\Phi]\{\dot{z}(t)\}, \quad \{\ddot{u}(t)\} = [\Phi]\{\ddot{z}(t)\} \tag{7.10}$$

Because the columns of $[\Phi]$ contain eigenvectors, it satisfies the following orthogonality conditions:

$$\{\Phi_i\}^T [M]\{\Phi_j\} = \{\Phi_i\}^T [K]\{\Phi_j\} = 0, \quad i \neq j \tag{7.11a}$$

If the orthogonal vectors are normalised w.r.t. the mass matrix; that is:

$$\{\Phi_i\}^T [M]\{\Phi_i\} = 1 \tag{7.11b}$$

Then:

$$\{\Phi_i\}^T [K]\{\Phi_i\} = \omega_i^2 \tag{7.11c}$$

where ω is the natural frequency of the ith mode.

The above equation can be written in matrix form:

$$[\Phi]^T[M][\Phi]=[I] \qquad\qquad (7.12a)$$

$$[\Phi]^T[K][\Phi]=[\Omega] \qquad\qquad (7.12b)$$

where $[I]$ is an identity matrix and $[\Omega]$ is a diagonal spectrum matrix that contains squares of n natural frequencies:

$$[\Omega]=\mathrm{diag}(\omega_i^2) \qquad\qquad (7.12c)$$

Substituting Eqn. (7.10) into Eqn. (7.1) and pre-multiplying by $[\Phi]^T$, and noting Eqn. (7.12), n ordinary differential equations are obtained:

$$\ddot{z}_i+2\zeta_i\,\omega_i\dot{z}_i+\omega_i^2 z_i=p_i, \quad i=1,2,\cdots,n \qquad\qquad (7.13a)$$

where n is the number of degrees of freedom in the structural system, and:

$$p_i=[\Phi_i]^T\{F(t)\} \qquad\qquad (7.13b)$$

In driving Eqn. (7.13a) it has been assumed that the damping matrix $[C]$ is orthogonal with respect to $[\Phi]$. In this situation, the coefficient matrix of $\{\dot{z}\}$ becomes diagonal. The ith diagonal term is replaced by $2\zeta_i\omega_i$, where ζ_i is the ratio of damping in mode i to the critical damping in mode i. A simple but useful orthogonal damping matrix is a linear combination of the mass matrix and the stiffness matrix, i.e.:

$$[C]=\alpha[K]+\beta[M] \qquad\qquad (7.14)$$

This damping is called proportional damping or Rayleigh damping. The combination coefficients α and β can be calculated from two modes of vibration. If $\alpha = 0$ the higher modes are lightly damped; if $\beta = 0$, the higher modes are heavily damped.

The modal method is efficient if the response of the structure can be expressed in terms of a relatively small number of eigenmodes of the system. Orthogonality of the

eigenmodes uncouples this system. Furthermore, only eigenmodes that are close to the frequency of interest are usually involved in the solution. For example, only the lowest few frequencies are usually required to obtain an accurate estimate of a structure's linear dynamic response to relatively slow loading.

7.2.3.2 Direct integration method

The most general approach to the dynamic response of structural systems is the direct numerical integration of the dynamic equilibrium equations. Many methods for direct integration have been developed over the past half century. All of these methods can be classified into explicit and implicit integration methods.

The explicit methods do not involve the solution of a set of linear equations at each step, so the time spent in each step is short. However, the time step must be very small in order to obtain a stable solution. The implicit methods require the solution of a set of linear equations at each time step; however, relatively large time steps may be used. All explicit methods are conditionally stable; the implicit methods can be conditionally or unconditionally stable.

(1) Newmark family of methods

Since Newmark proposed the single-step integration methods for solving structural dynamic problems in 1959, modifications and improvements have been proposed by many other researchers. Among them, E. L. Wilson's work has been celebrated.

Newmark presented a direct-integration formulation by modifying the truncated Taylor's series of Eqn. (7.1) into the form:

$$\mathbf{u}_t = \mathbf{u}_{t-\Delta t} + \Delta t \dot{\mathbf{u}}_{t-\Delta t} + \frac{\Delta t^2}{2}\ddot{\mathbf{u}}_{t-\Delta t} + \beta \Delta t^3 \dddot{\mathbf{u}} \qquad (7.15a)$$

$$\dot{\mathbf{u}}_t = \dot{\mathbf{u}}_{t-\Delta t} + \Delta t \ddot{\mathbf{u}}_{t-\Delta t} + \gamma \Delta t^2 \dddot{\mathbf{u}} \qquad (7.15b)$$

If the acceleration is assumed to be linear within the time step, hence constant $\dddot{\mathbf{u}}$, Newmark's equations have the standard form:

$$\mathbf{u}_t = \mathbf{u}_{t-\Delta t} + \Delta t \dot{\mathbf{u}}_{t-\Delta t} + \left(\frac{1}{2} - \beta\right)\Delta t^2 \ddot{\mathbf{u}}_{t-\Delta t} + \beta \Delta t^2 \ddot{\mathbf{u}}_t \qquad (7.16a)$$

$$\dot{\mathbf{u}}_t = \dot{\mathbf{u}}_{t-\Delta t} + (1-\gamma)\Delta t \ddot{\mathbf{u}}_{t-\Delta t} + \gamma \Delta t \ddot{\mathbf{u}}_t \qquad (7.16b)$$

Newmark solved these equations along with Eqn. (7.1) by iteration.

In 1962, Wilson formulated the Newmark's method in matrix notation, added stiffness and mass proportional damping, and eliminated the need for iteration by introducing the direct solution of equations in each time step. In his formulation, Eqn. (7.16) is rewritten in the following form:

$$\ddot{\mathbf{u}}_t = b_1\left(\mathbf{u}_t - \mathbf{u}_{t-\Delta t}\right) + b_2 \dot{\mathbf{u}}_{t-\Delta t} + b_3 \ddot{\mathbf{u}}_{t-\Delta t} \qquad (7.17a)$$

$$\dot{\mathbf{u}}_t = b_4\left(\mathbf{u}_t - \mathbf{u}_{t-\Delta t}\right) + b_5 \dot{\mathbf{u}}_{t-\Delta t} + b_6 \ddot{\mathbf{u}}_{t-\Delta t} \qquad (7.17b)$$

where the constants b_1 to b_6 can be expressed by Newmark's constants and time step.

Substituting Eqn. (7.17) into Eqn. (7.1) gives the equation in matrix form:

$$\begin{aligned}
(b_1\mathbf{M} + b_4\mathbf{C} + \mathbf{K})\mathbf{u}_t &= \mathbf{F}_t + \mathbf{M}(b_1\mathbf{u}_{t-\Delta t} - b_2\dot{\mathbf{u}}_{t-\Delta t} - b_3\ddot{\mathbf{u}}_{t-\Delta t}) \\
&+ \mathbf{C}(b_4\mathbf{u}_{t-\Delta t} - b_5\dot{\mathbf{u}}_{t-\Delta t} - b_6\ddot{\mathbf{u}}_{t-\Delta t})
\end{aligned} \qquad (7.18)$$

For zero damping, Newmark's method is conditionally stable if:

$$\gamma \geq \frac{1}{2}, \quad \beta \leq \frac{1}{2} \quad \Delta t \leq \frac{1}{\omega_{max}\sqrt{\dfrac{\gamma}{2} - \beta}} \qquad (7.19)$$

where ω_{max} is the maximum frequency in the structural system. Newmark's method is unconditionally stable if:

$$2\beta \geq \gamma \geq \frac{1}{2} \qquad (7.20)$$

However, if $\gamma > \dfrac{1}{2}$, errors are introduced. Those errors are associated with "numerical damping" and "period elongation".

It can be shown that, when $\gamma = 1/2$ and $\beta = 1/4$, Newmark's method is identical with the average acceleration method for $\tau = \Delta t$ (Wilson, 2002).

(2) Wilson's θ factor

In 1973, the general Newmark method was made unconditionally stable by Wilson by the introduction of a θ factor. Wilson modified Newmark's method by using a time step defined by:

$$\Delta t' = \theta \Delta t \tag{7.21}$$

and a load defined by:

$$\mathbf{F}_{t'} = \mathbf{F}_{t-\Delta t} + \theta (\mathbf{F}_t - \mathbf{F}_{t-\Delta t}) \tag{7.22}$$

where $\theta \geq 1$.

Apparently, if $\theta = 1$ Wilson's method reverts to Newmark's method. After the acceleration vector $\ddot{\mathbf{u}}_{t'}$ has been found using Newmark's method at the integration time step $\theta \Delta t$, values of accelerations, velocities and displacements are calculated from the following fundamental equations:

$$\ddot{\mathbf{u}}_t = \ddot{\mathbf{u}}_{t-\Delta t} + \dfrac{1}{\theta}(\ddot{\mathbf{u}}_{t'} - \ddot{\mathbf{u}}_{t-\Delta t}) \tag{7.23a}$$

$$\dot{\mathbf{u}}_t = \dot{\mathbf{u}}_{t-\Delta t} + (1-\gamma)\Delta t \ddot{\mathbf{u}}_{t-\Delta t} + \gamma \Delta t \ddot{\mathbf{u}}_t \tag{7.23b}$$

$$\mathbf{u}_t = \mathbf{u}_{t-\Delta t} + \Delta t \dot{\mathbf{u}}_{t-\Delta t} + \Delta t^2 \left(\dfrac{1}{2} - \beta\right)\ddot{\mathbf{u}}_{t-\Delta t} + \beta \Delta t^2 \ddot{\mathbf{u}}_t \tag{7.23c}$$

The use of the θ factor tends to numerically damp out the high modes of the system. For problems where the high mode response is important, the error introduced can be

large. In addition, the dynamic equilibrium equations are not exactly satisfied at time *t*. At the time of the introduction of the θ factor, Wilson's method solved all the problems associated with the stability of the Newmark method. However, during the past twenty years, new and more accurate numerical methods have been developed. As a result, the author frankly stated that he no longer recommends the use of the θ factor (Wilson, 2002).

7.3   Micro-stamping tool

The photo and the geometry model of the micro-stamping tool are shown in Fig. 7.1(a) and Fig. 7.1(b) respectively.

7.3.1 Structure of the stamping tool

The stamping tool and coordinate system are shown in Fig. 7.1(b). Tens of components are connected together by bolts, bearings, springs and push-fit assemblies. This tool set may be separated into two parts: the upper half and the lower half.

The structure of the upper half is shown in Fig. 7.2, and includes a top plate, a punch holder plate, a punch guide plate, a blank holder, two stoppers, two guide pins, and eight pairs of spring and spring bolt. Four springs are used to connect the top plate and the punch guide plate and the other four springs are used to connect the punch hold plate and the blank holder. Two punches with different geometry are fixed to top plate, and are the key parts of a single-stage stamping-tool set. The roller guide bearing is used into the micro-stamping tool.

The structure of the lower half is shown in Fig. 7.3. It includes a lower die plate, a base plate, a support plate, two linear guides, two dies, and a workpiece container. The internal structure of the micro-stamping tool is shown in Fig. 7.4.

The micro-stamping tool is driven by a linear motor via a ram. The ram, which is controlled by the linear motor, contacts with the top plate of the tool and is guided using a guiding bridge that is connected with the micro-stamping machine frame.

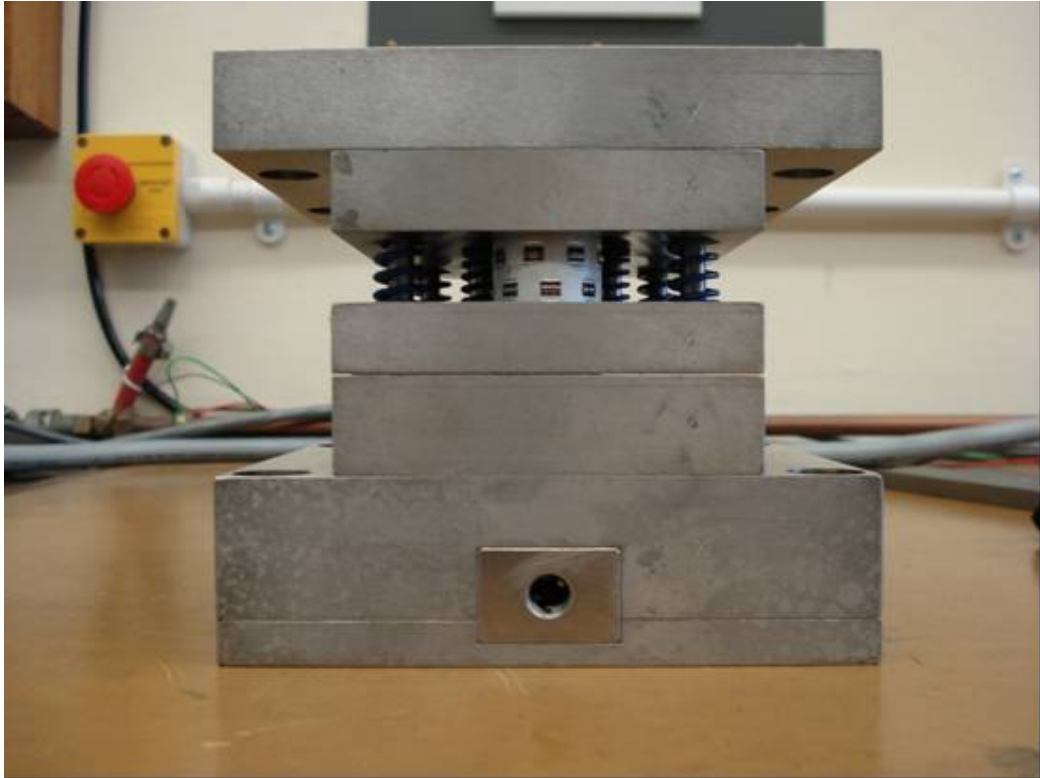The lower half of the micro-stamping tool is connected firmly to the stamping machine.

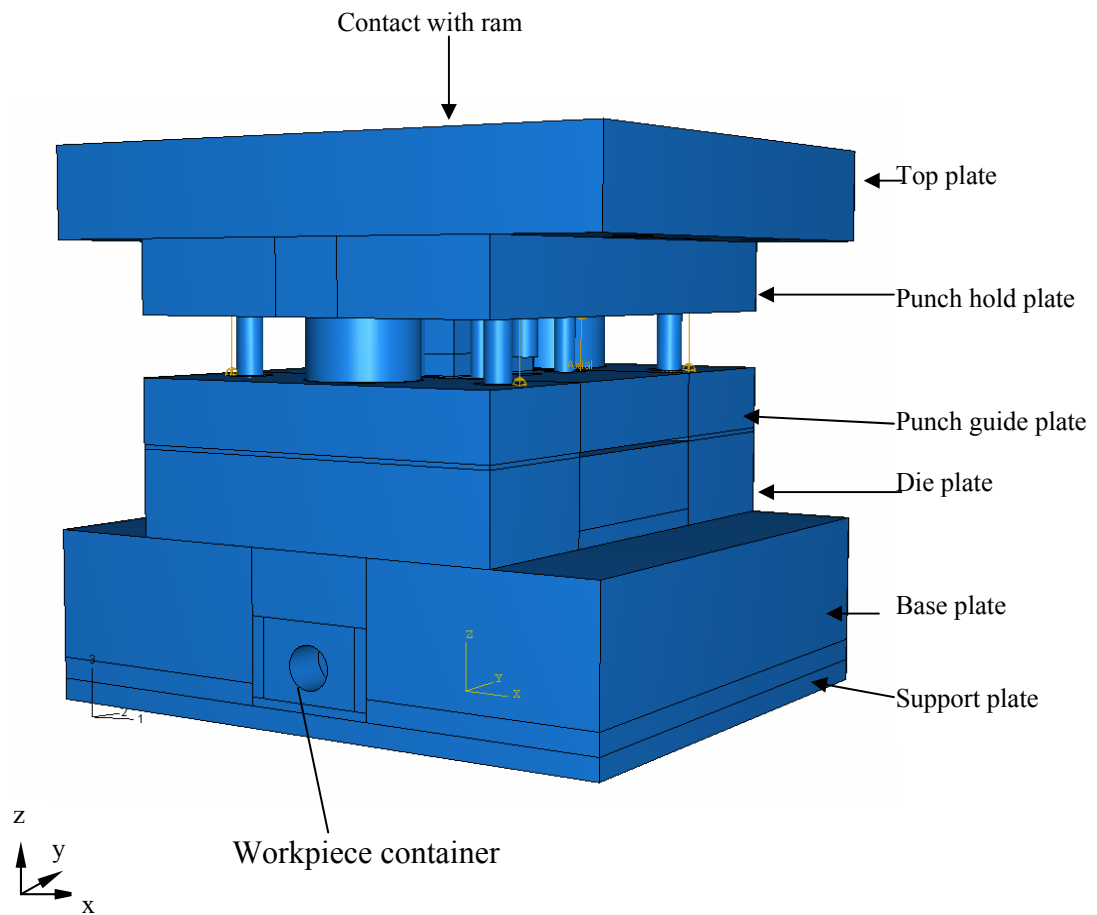**Fig. 7.1 (a)   Photograph of the Micro-stamping tool**

Fig. 7.1 (b)   Geometric model of the Micro-stamping tool
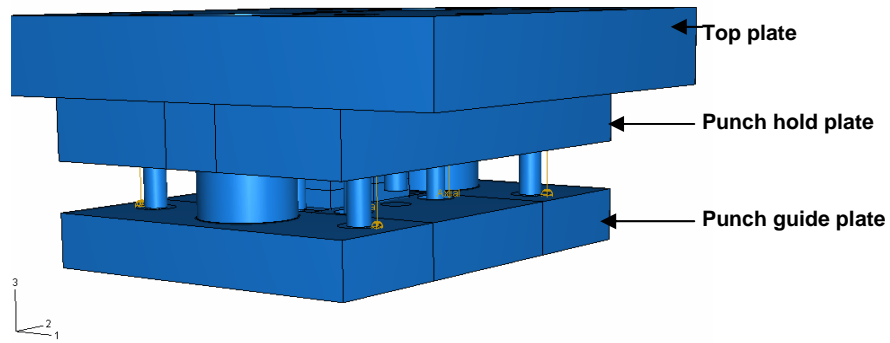
(a) Upper half of micro-stamping tool
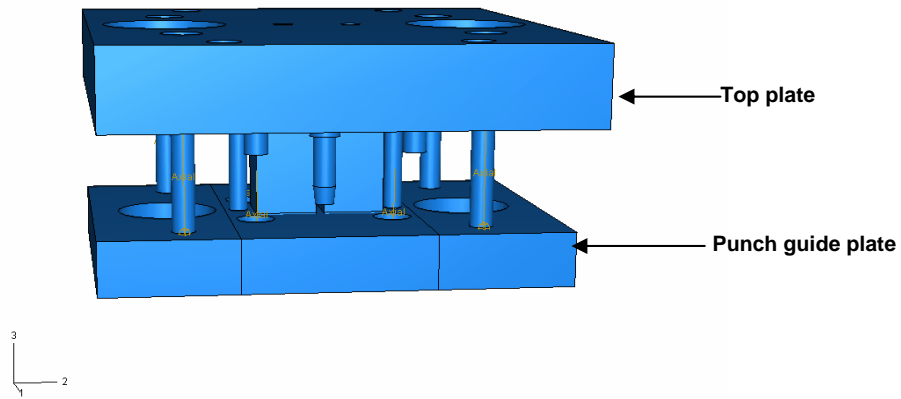
(b) Top plate and punch guide plate
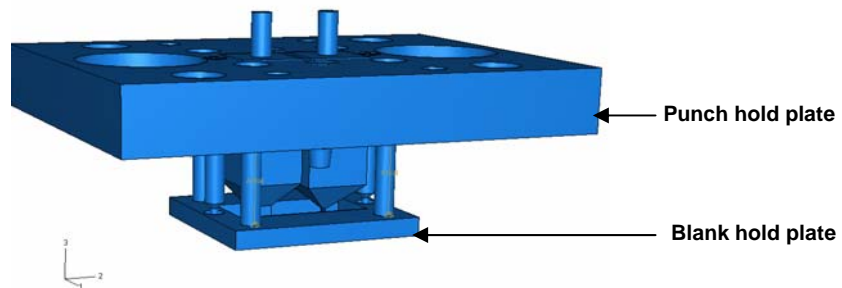
(c) Punch-holder plate and blank-holder plate

Fig. 7.2   Structure of the upper half of the Micro-stamping tool
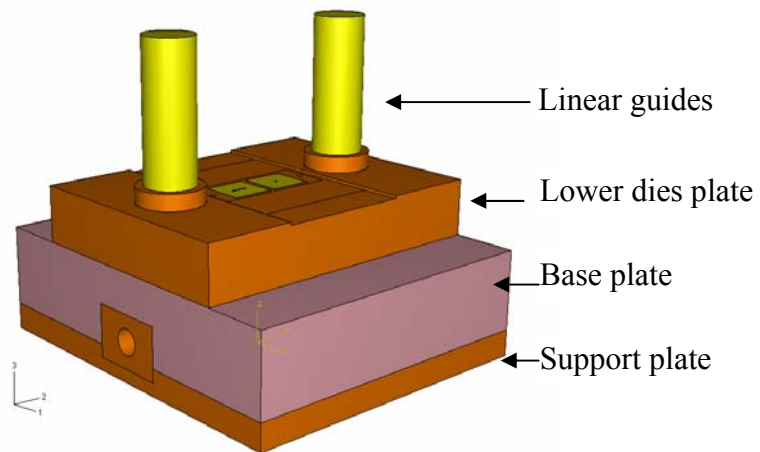
(a) Lower half of micro-stamping tool
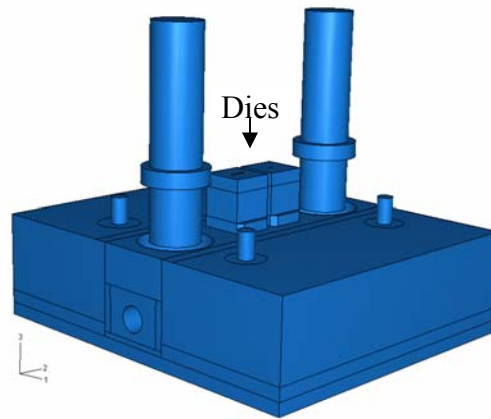
(b) Linear guides and dies
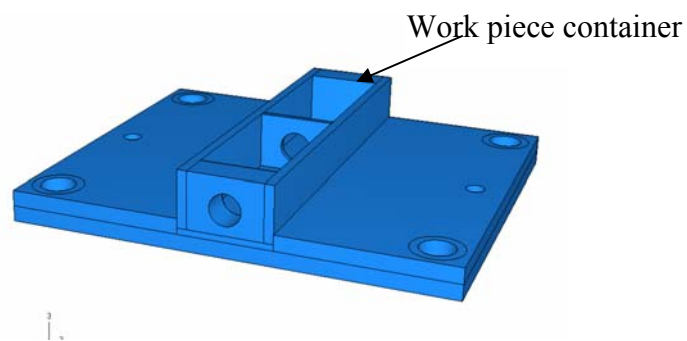
(c) Workpiece container and support plate

Fig. 7.3   Structure of the lower half of the Micro-stamping tool

Top plate

Pushers

Rollers

Stoppers

Linear guides

Springs and bolts

Punches

Blank holder

Dies

Work piece container

Support plate

Fig. 7.4   Inside structure of micro-stamping tool

7.3.2 Functions of the stamping tool

The micro-stamping tool is fixed on the micro-stamping machine bed and driven by a linear motor. It works at high speeds of up to 16Hz. One stamping can produce two workpieces with different shapes. Different metal sheet with different thickness, tens of microns, can be formed. The micro-stamping tool can be connected to a material feeder and a workpiece handing device.

7.4   Dynamic response analysis

The dynamic response analysis focuses on the response of the punches, the moving components such as the blank holder, and the reaction forces from the base.

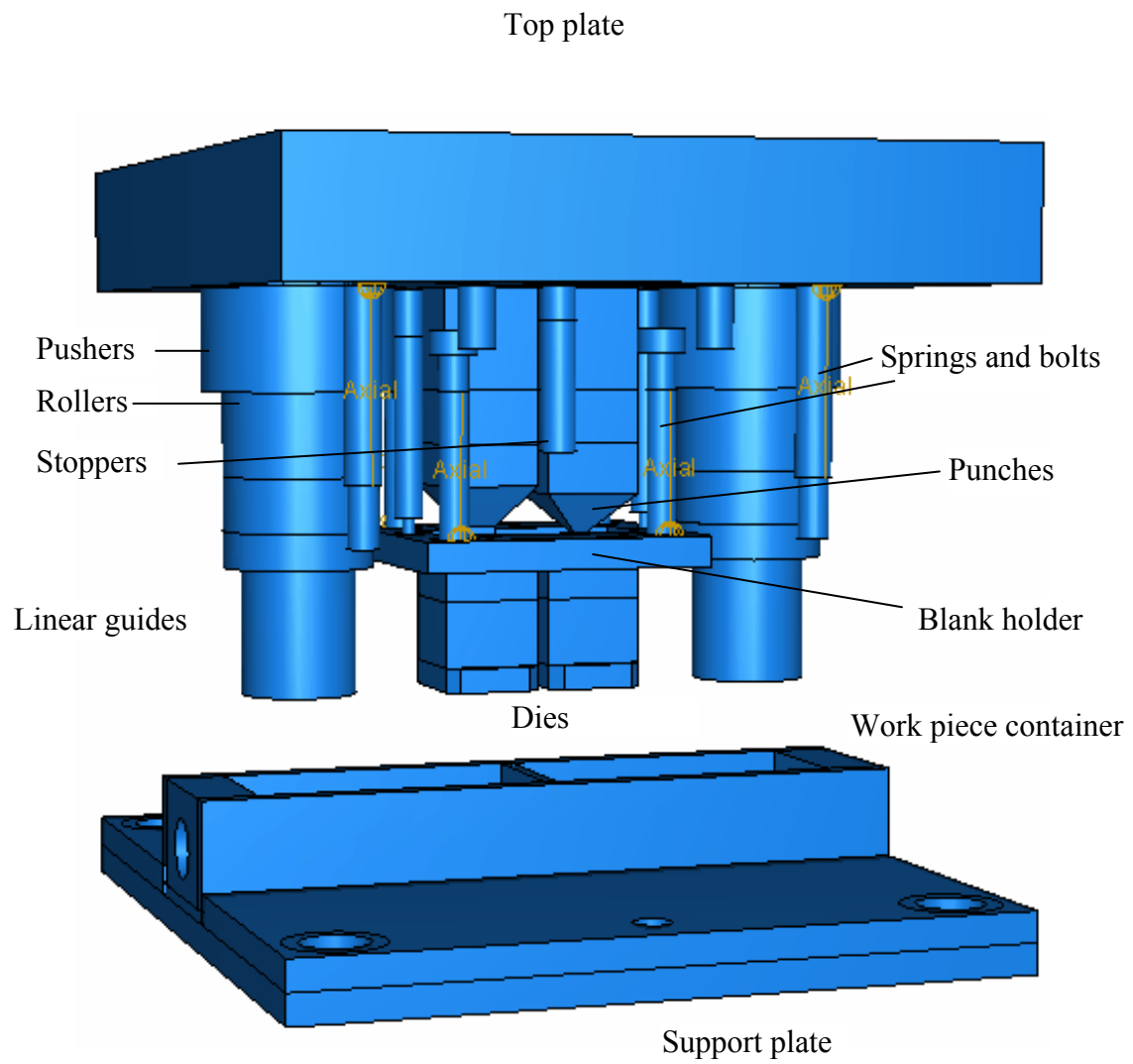ABAQUS/Explicit utilizes an explicit direct integration method to solve the dynamic equation involved. The explicit method is conditionally stable. It needs to use a small time increment (ANAQUS User's Manual; Cook, 1981). The analysis procedure of the dynamic response of the stamping tool is described in the following.

Eight models are built for analysis and the results are compared. The key parameters in the models are listed in Table 7.1. C1 is the friction coefficient of the contact between the tool components, C2 is the friction coefficient of the contact between the blank holder and the sheet metal and C3 is the friction coefficient of the rollers. A0 is the amplitude of ram movement.

Table 7.1   Dynamics analysis models of the micro–stamping tool

Model	Frequency of linear motor (Hz)	Cutting force	Force factor	C1	C2	C3	A0(mm)
1	16	yes	3	0	0	0	1.7565
2	16	no	0	0	0	0	1.7565
3	8	no	0	0	0	0	1.7565
4	16	yes	2	0.05	rough	0	1.7565
[*]5	16	no	0	0	rough	0	1.7565

6	16	no	0	0	rough	0.0011	2.7565
7	16	no	0	0	rough	0.0011	1.4
8	16	no	0	0	rough	0.0015	1.4
*0.02 degrees of inclination of the ram was assumed during the stamping, which could in practice be caused by geometric eccentricity of the machine/tool structures, eccentric loading due to machine-frame deflections, etc.							

7.4.1 Geometry model

All the components are built separately and then assembled. The dynamic "surface-to-surface contact technique" is used to simulate the contact between components. The "axial connector" is used to simulate spring connections.

7.4.2 Material model

Carbon steel C40 and AISI D2 tool steel are used for the tool-parts. Four R204205 springs and four R204104 springs are used.

7.4.3 Mesh model

Owing to the complexity of the structure, three types of element are used (C3D4, C3D6 and C3D8R). Suitable transition of element density is made to achieve high accuracy at an acceptable computational cost.

Two mesh models have been used to analyse the dynamic response of the micro-stamping tool. In the first mesh model, C3D4, C3D6 and C3D8R elements are employed. In the second mesh model, shown in Figs. A7.1 to A7.3, C3D8R elements are used almost entirely through the whole structure. The C3D8R is an 8-node linear brick using reduced integration with hourglass controlled by stiffness. Kinematic split is controlled by average strain. It uses the uniform strain formulation and the hourglass shape vectors in the hourglass control.

The advantage of the reduced integration elements is that the strains and stresses are calculated at the locations that provide optimal accuracy, the so-called Barlow points

(Barlow, 1976). A second advantage is that the reduced number of integration points decreases CPU time and storage requirements. The disadvantage is that the reduced integration procedure can admit deformation modes that cause no straining at the integration points. These zero-energy modes make the element rank-deficient and cause a phenomenon called "hourglassing," where the zero-energy mode starts propagating through the mesh, leading to inaccurate solutions. This problem is particularly severe in first-order quadrilaterals and hexahedra. To prevent these excessive deformations, an additional artificial stiffness is added to the element. In this so-called hourglass control procedure, a small artificial stiffness is associated with the zero-energy deformation modes. This procedure is used in many of the solid and shell elements (ABAQUS Theory Manual).

7.4.4 Contact model

In the surface-to-surface contact, 'hard' contact is assumed for normal behaviour and different friction coefficients are used for tangential behaviour of the contacts. Finite sliding is allowed in the model.

7.4.5 Connect model

In the finite element simulation, the "tie technique" is used to simulate screw and push-fit connections

7.4.6 Boundary conditions

In the test machine, the displacement of the ram takes the form $u = A_0 [1-\cos(\omega t)]$. Four bolts are used to attach the stamping tool to the supporting plate of the machine bed.

7.5   Results of the dynamics analysis

The main dynamic response characteristics of the stamping tool are presented in the following subsections.

7.5.1 Response of the punch

Fig. A7.4 shows the results of the displacements of the punches of the model 1 in the x and y directions (in horizontal plane). Cutting force acts from 0.0235s to 0.0241s. It is seen clearly that during cutting the triangular punch is more unstable than the rectangular punch: it moves away from original balance point in the y direction. This phenomenon also occurs in model 4.

7.5.2 Response of the blank holder

Fig. 7.9 shows the displacement response of the blank holder in the x and y directions. The blank holder is in contact with the strip from 0.0112s to 0.0511s. The nodes 188 and 160 are symmetrical points about the y-axis. Figs. A7.5 (a) and A7.5 (b) show the displacements of node 188 and node 160 in the x and y directions versus the time. Figs. A7.5 (c) and A7.5 (d) are contour plots of the blank holder. The movement of the blank holder is a twisting vibration about the z axis (vertical direction). The blank holder is unstable before and after coming into contact with the strip. The influence of this on the response of the punches can be seen in Fig. A7.4. Similar results are obtained for the other models.

7.5.3 Response of the boundary at the base plate

The reaction forces RFX, RFY and RFZ on the fixed boundary of the supporting plate are shown in Fig. A7.6 for a linear-motor working frequency of 16Hz in model 2. RFX, RFY and RFZ mean the reaction force in the x, y and z directions, respectively. The average frequency of the reaction force is about 30 times that of the linear-motor working frequency. The frictional contact between the components slightly reduces the frequency of the reaction forces.

7.5.4 Response of the punch guide plate

The same phenomena in the response of the punch guide plate have been observed from FE analysis and experimental measurement. The punch guide plate is initially in contact with the upper surface of the die plate. It then moves up during the stamping process. The vertical displacement increases non-linearly with the increase

in the amplitude of ram movement and working frequency. FE simulation results of the vertical response of the punch guide plate for A0=1.4mm and A0=2.76mm are shown in Figs. A7.7 and A7.8, respectively, whilst the results of experimental measurement are shown in Fig. 8.11. and Fig. 8.12 in Chapter 8.

7.5.5 Response of the roller

The results of FE simulation of the response of the roller for different values of the friction coefficient are shown in Fig. A7.9. The amplitude of the movement of the roller is larger when the friction coefficient is larger. This will directly influence the response of the punch guide plate. The response of the punch guide plate should be larger when the amplitude of the movement of the roller is smaller. This has been verified by experimental measurement, shown in Chapter 8 in Fig. 8.16.

7.6   Conclusions

The analysis of the findings obtained from FE simulation and experiment identified the followings to be of particular interest in tool- and machine-design for micro-stamping:

- The dynamic reaction forces acting on the connection between the support plate and the micro-forming machine have a frequency much greater than the working frequency of the linear motor. This frequency will be transmitted to the system during the forming process. The value is very close to the natural frequencies of the lower modes of vibration of the machine in the absence of a rubber base. Therefore the response frequency of the stamping tool should be taken as a crucial parameter in the design of a micro-forming machine system.

- When using spring force to control moving components such as the blank holder, the local vibration generates an excitation for the whole stamping tool and significantly influences the dynamic response of the punches. To improve the design, it is suggested that more control of the dynamic performance should be applied on moving components such as the blank holder.

- The differences in punch geometries result in imbalance of the cutting forces among the punches, which in turn result in different dynamic behaviour of the punches. In the cases studied, the smaller punch tends to move away from its original position, and continual high-speed stamping leads to increasingly greater offset displacement of this punch. This possibly is a main reason why such a punch was always damaged earlier, when the cutting speed was increased. This has to be taken into account when punches are designed for high-speed stamping.

- The punch guide plate moves up during the stamping process. Both the amplitude of ram movement and the working frequency have a significant influence on this movement. An unstable punch guide plate will generate an exciting force on the punches, reducing the precision of the tooling. Because high speed is the target of this micro-stamping tool, the amplitude of ram movement should be made as small as possible in the design of the whole system.

- The different friction coefficients between the roller and the linear guides have a significant influence on the dynamic response: this feature was found in the experimental measurements also.

The findings presented above form a basis for improving the micro-stamping tool and machine/tool connection design.

The findings obtained from the study in this chapter are compared with the results obtained from experimental measurement. The FE model did not include the position sensor and two components which are used for the assembly of the sensor. The details of the sensor and two components are described in Chapter 8. These small components should not have significant influence on the results of the FE analysis.

7.7 References

ABAQUS Theory Manual, 'Element Library Overview,' Section 3.1.1, version 6.4.

Barlow, J. (1976), 'Optimal Stress Locations in Finite Element Models,' International Journal for Numerical Methods in Engineering, Vol.10, pp. 243–251, 1976

Cook, R.D. (1981), 'Concepts and Applications of Finite Element Analysis,' (Second Edition). *John Wiley and Sons.*

Computers & Structure (2006), Available at web site: http://www.csiberkeley.com/support_technical_papers.html

Groche, P. and Schneider, R. (2004), 'Method for the Optimization of Forming Presses for the Manufacturing of Mirco Parts,' *Annals of the CIRP* Vol.53, 281-284.

Newmark, N. M. (1959), 'A method of computation for structural dynamics,' ASCE *J. of Eng. Mech. Division*, Vol.85, No. EM3, 67-94.

Qin, Y. (2004), 'Forming tool design innovation and intelligent tool-structure/system Concepts,' *Proceedings of the International Conference on New Forming Technology*, Harbin, pp351-360.

Qin, Y. (2006), 'Micro-forming and miniature manufacture system-development needs and perspectives,' *Journal of Materials Processing Technology* 177, pp 8-18.

Rolling Bearing Friction (2007), Available at: http://www.roymech.co.uk

Wilson, E. L. (1962), 'Dynamic response by step-by-step matrix analysis,' Proc. Sypo on the Use of Computers in Civil Eng. Lisbon, Portugal. Oct. 1-5

Wilson, E. L. Farhoomand, I. and Bathe, K. J. (1973), 'Nonlinear dynamic analysis of complex structures,' *Earthquake Eng. and Struc. Dynamics*, 1, 241-252

Wilson, E. L. (2002), *Three-Dimensional Static and Dynamic analysis of Structures*, 3rd Ed., Computers and Structures, Inc., Berkeley, California, USA

Hughes, T. (1987), *The Finite Element Method - Linear Static and Dynamic Finite Element Analysis*. Prentice Hall, Inc
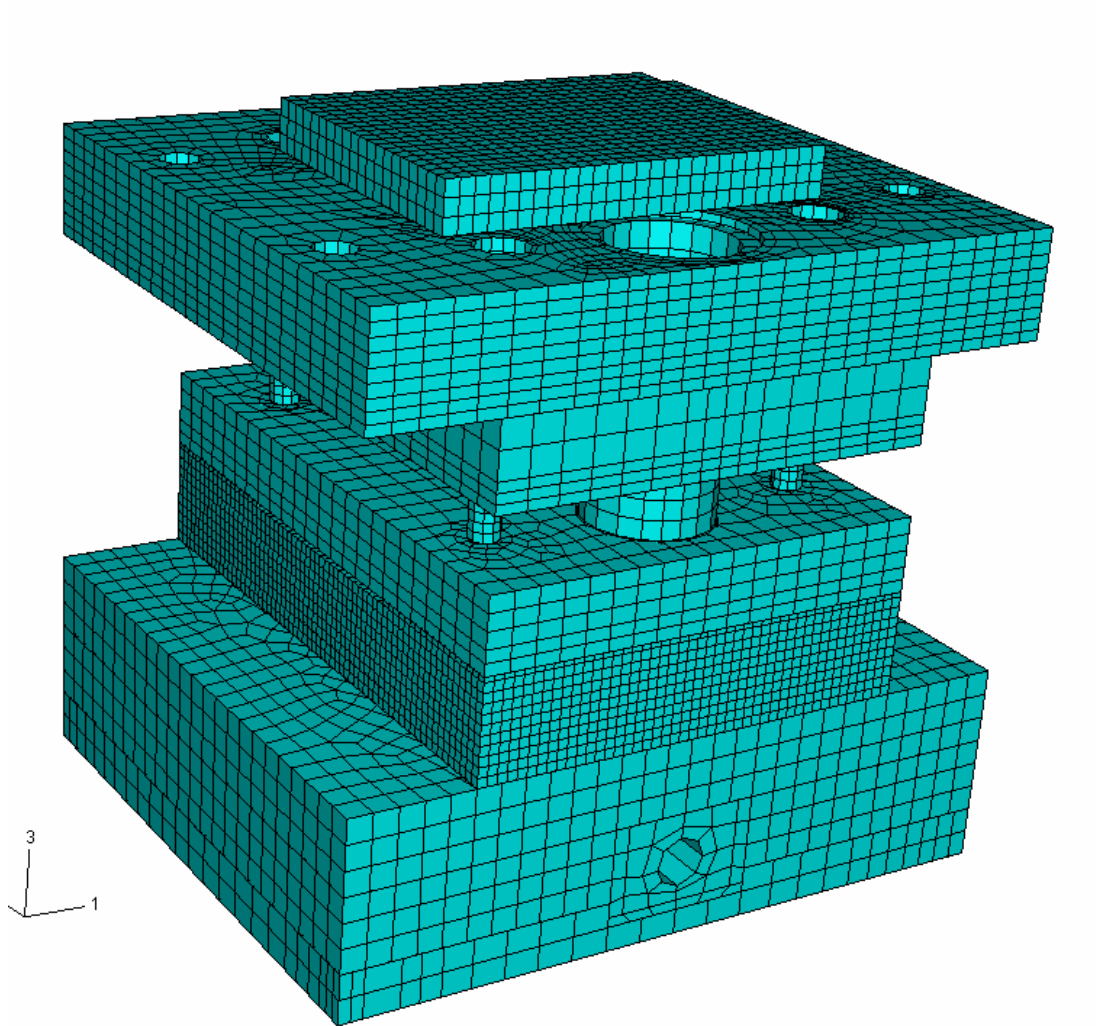
7.8   Appendix A – Figures

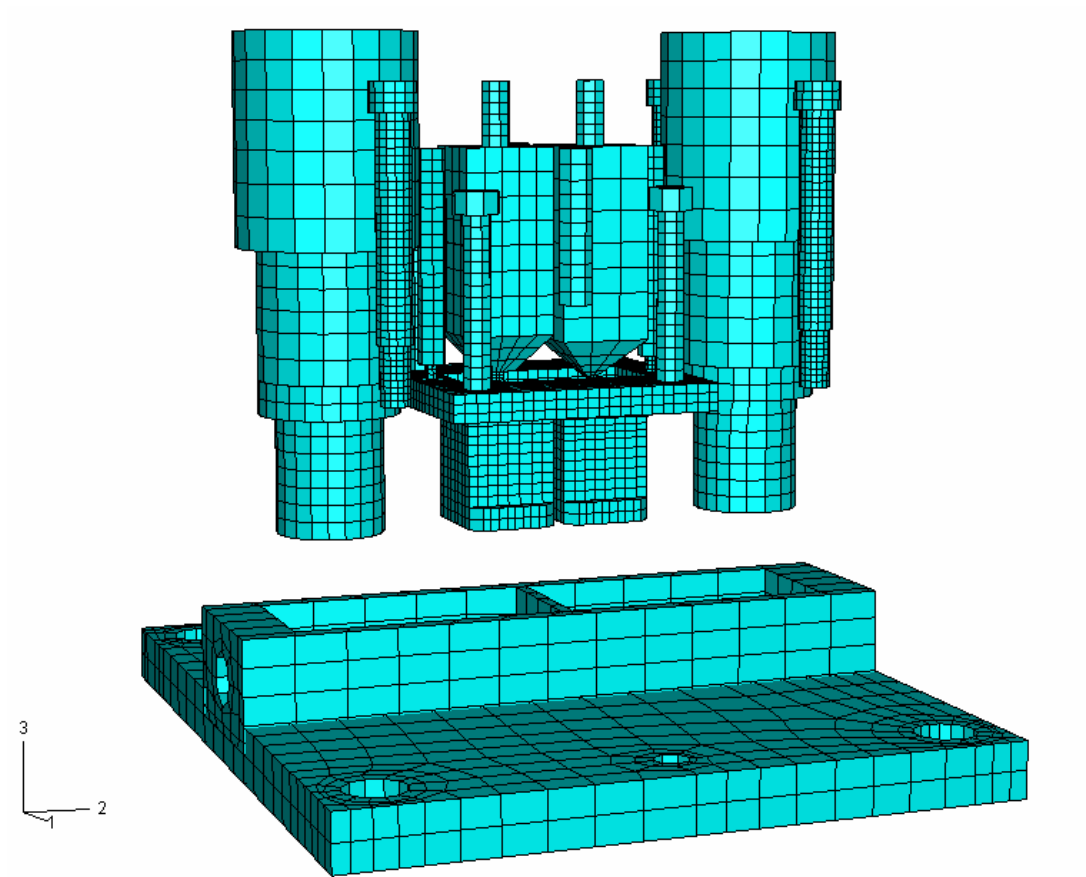**Fig. A7.1   Mesh model of the stamping tool**

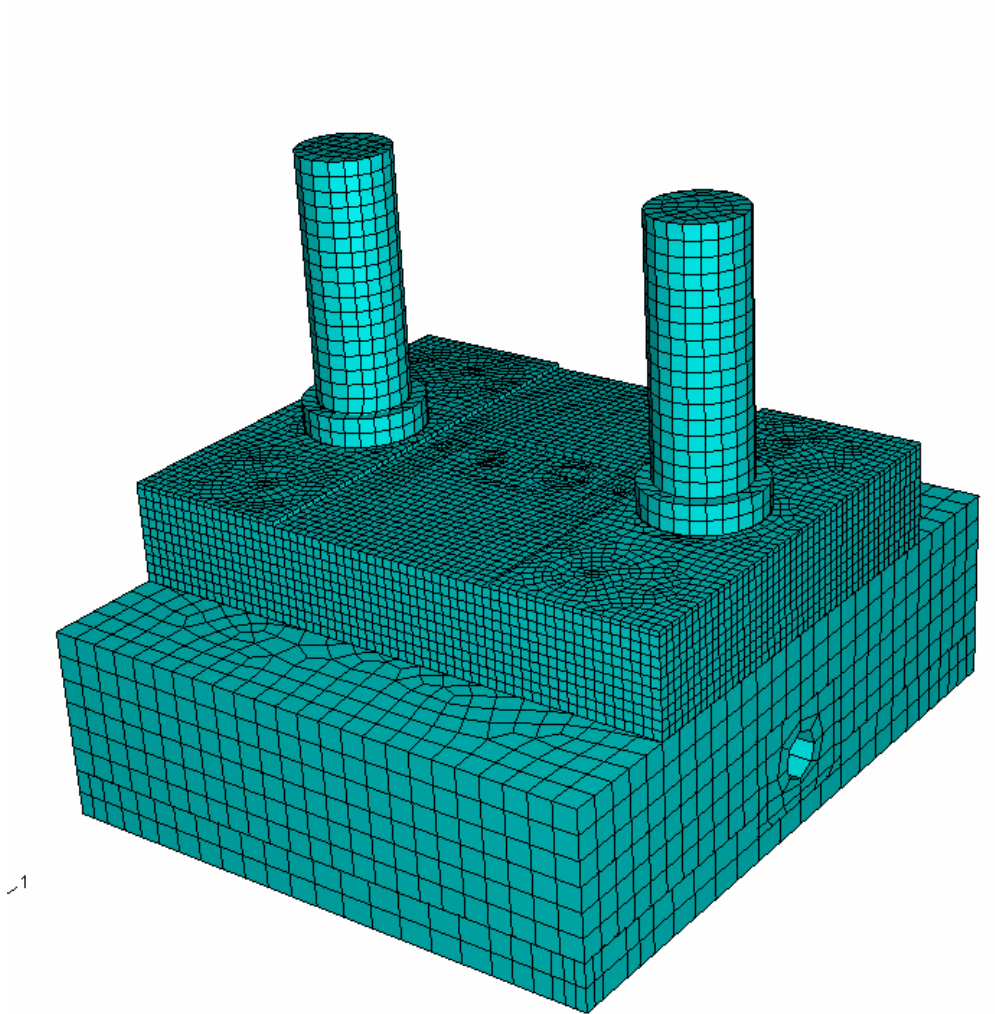**Fig. A7.2   Internal mesh model of the stamping tool**

Fig. A7.3 Lower-half mesh-model of the stamping tool

Rectangular punch   Triangular punch
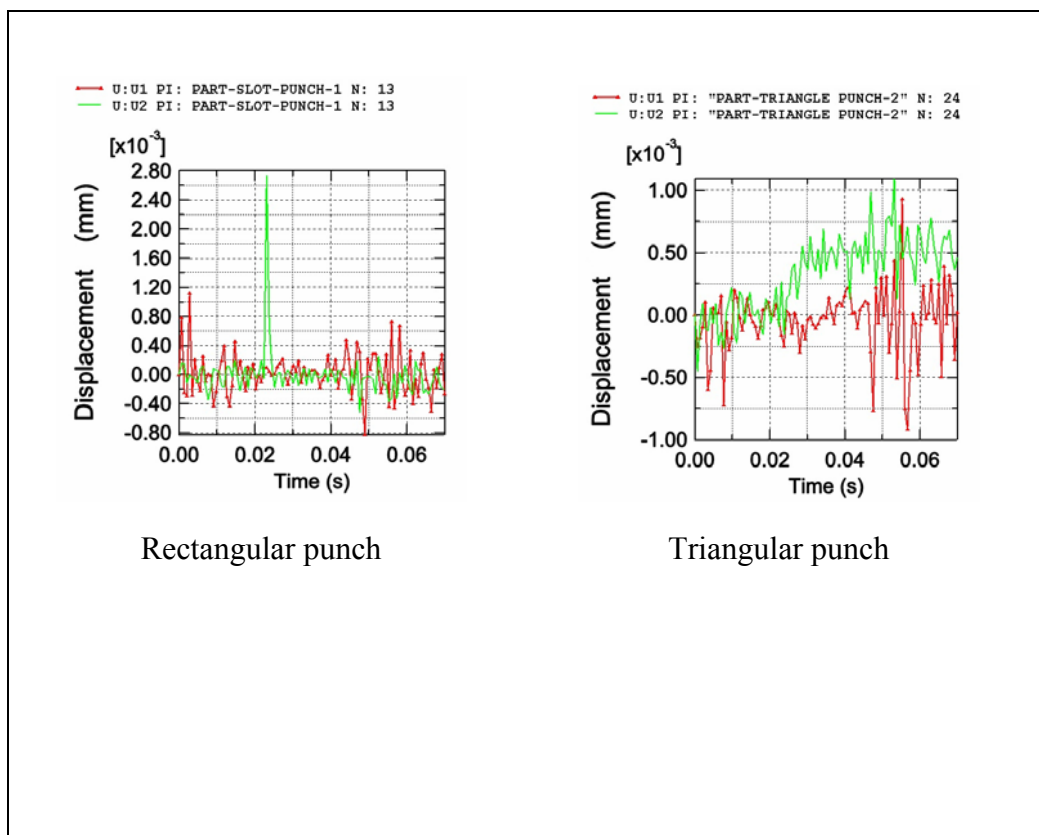
Fig. A7.4   Responses of the punches of model 1

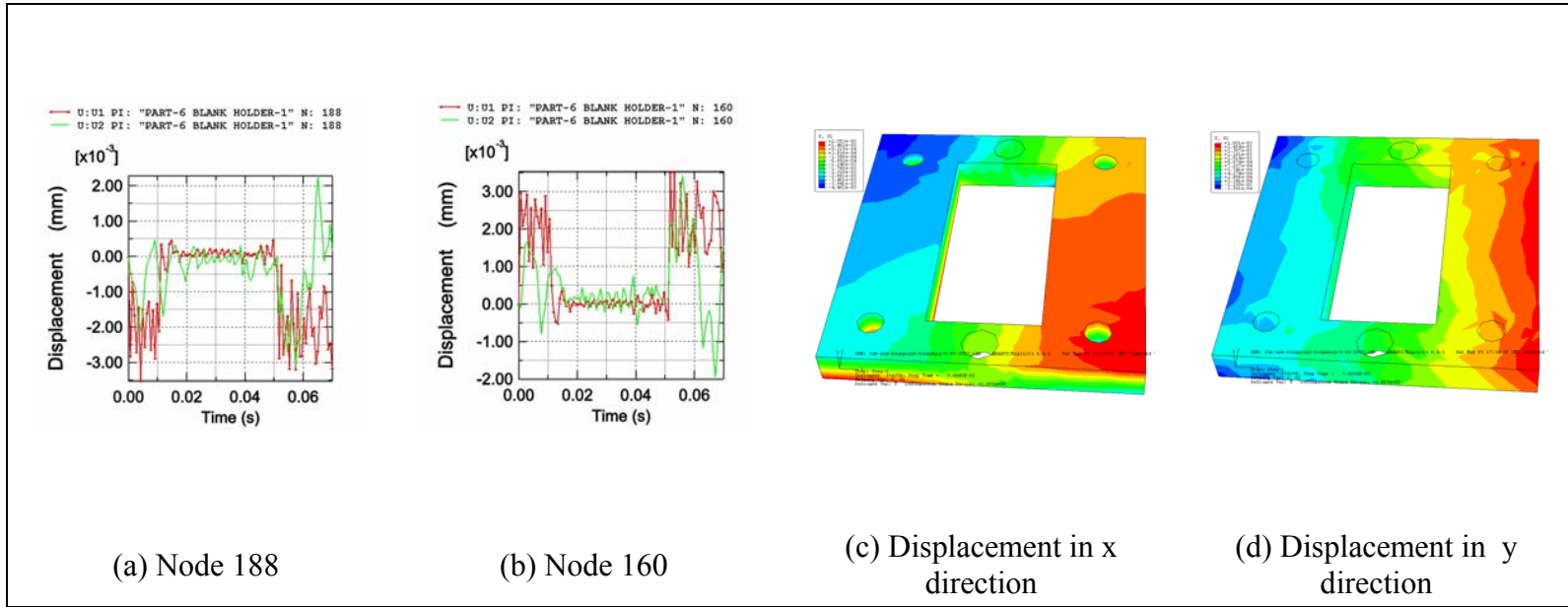|			
(a) Node 188	(b) Node 160	(c) Displacement in x direction	(d) Displacement in y direction

Fig. A7.5   Response of the blank holder

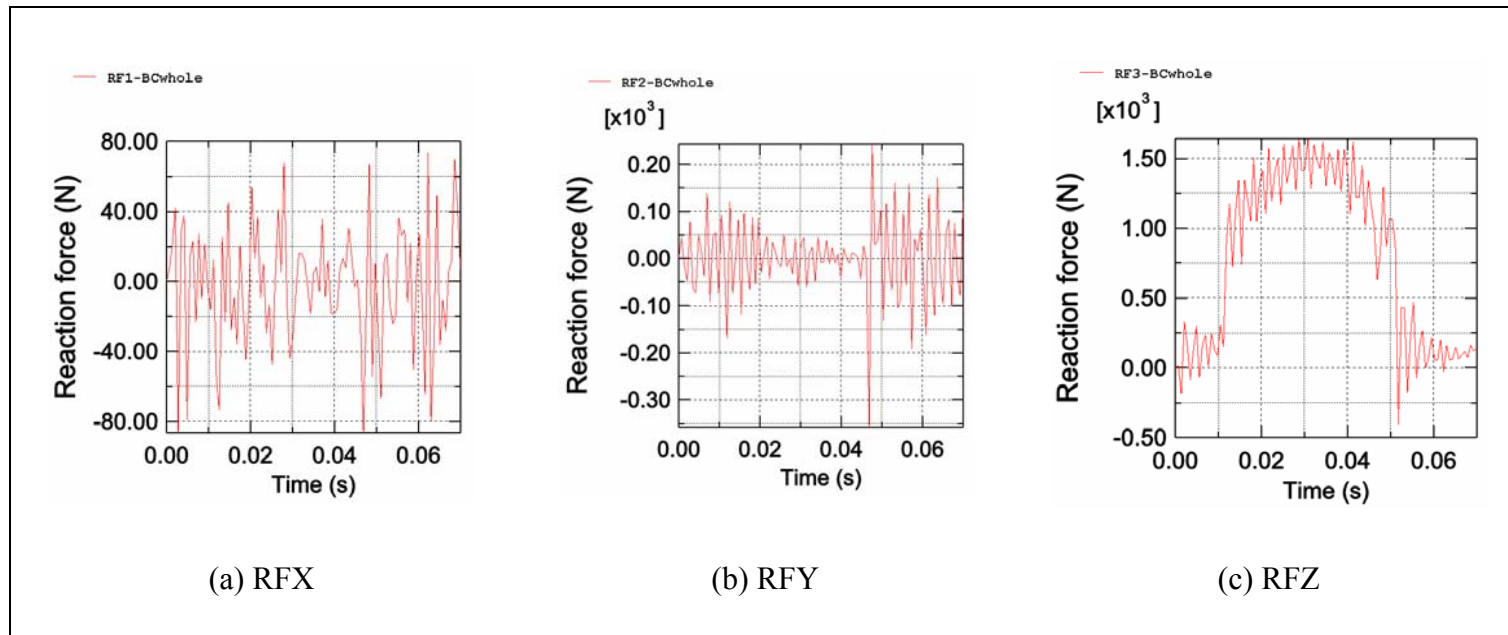**Fig. A7.6   Reaction forces at the fixed boundary**

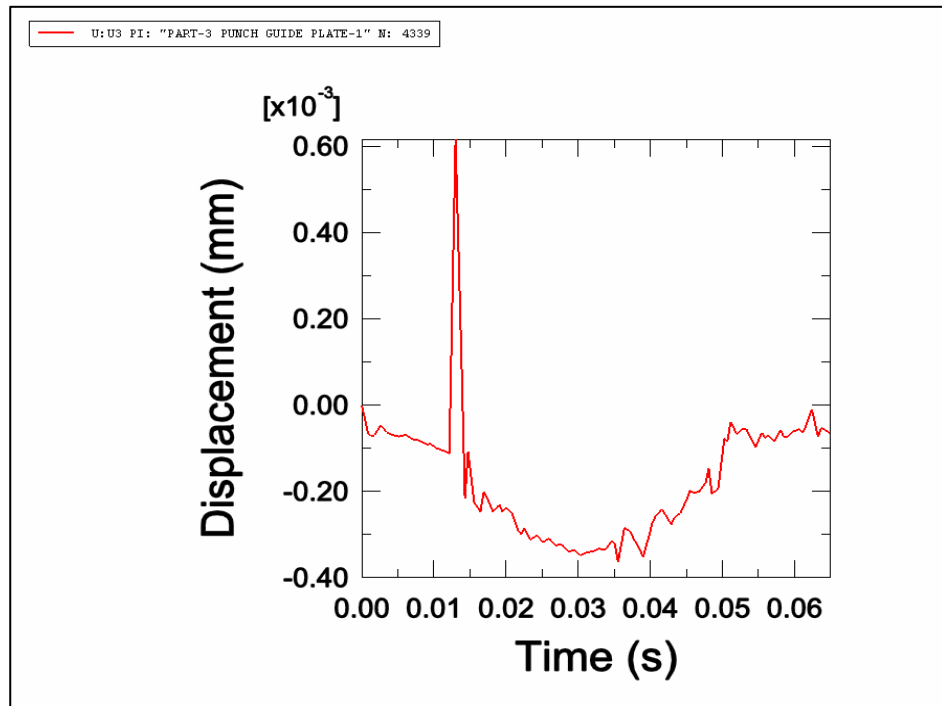**Fig. A7.7   Response of the punch guide plate A0=1.4mm,
linear motor frequency=16Hz**

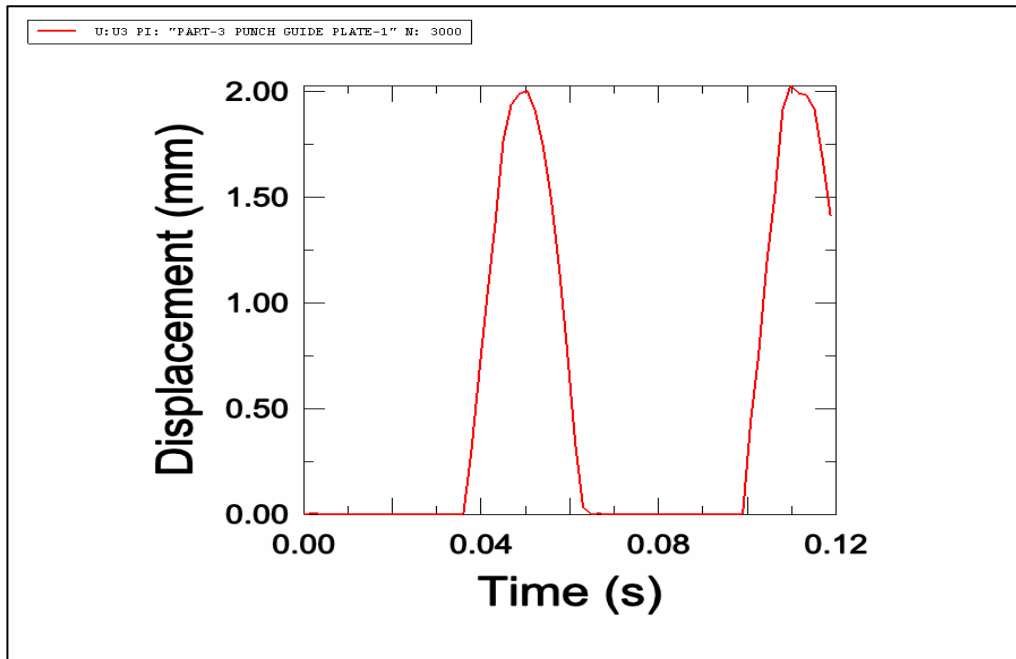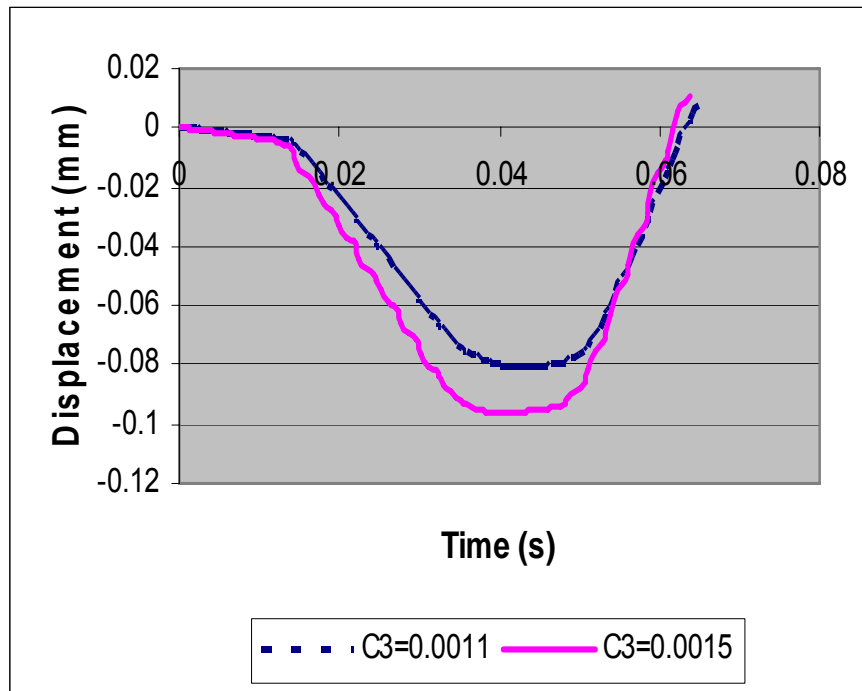**Fig. A7.8   Response of punch guide plate, A0=2.76mm,
linear motor frequency=16Hz**

**Fig. A7.9 Response of roller, A0=1.4mm,
linear motor frequency=16Hz**

Chapter 8 Experimental Validation

8.1   Introduction

The dynamic responses of the components of the stamping tool have been analysed by FE simulation in Chapter 7. In order to further understand and verify the findings from the investigation, the dynamic force and response of the punch guide plate and the top plate of the micro-stamping tool without punches are measured using a piezoelectric load cell and an optical position sensor. The range of working frequency is from 1Hz to 16Hz. Different coefficients of friction of the rollers (http://www.roymech.co.uk) and different amplitudes of the path of the ram are tested. The results are compared between different cases as well as between finite element simulation and experimental measurement.

In order to avoid their being damaged, the two punches are removed when the experiment is carried out.

The problems to be investigated in Chapter 8 are as follows:

- What are the dynamic responses of the top plate of the micro-stamping tool at different working frequencies?
- What are the dynamic responses of the punch guide plate of the micro-stamping tool at different working frequencies?
- What is the relationship between dynamic force applied to the ram and the working frequency of the micro-stamping machine?
- How is the agreement between the results obtained from the FE simulation and the experimental measurement?

The vibration analysis of the micro-stamping machine has been carried out by FE simulation in Chapter 6. This is also validated through the comparison to the vibration test on the machine.

8.2 Equipment

The micro-sheet-forming machine system used for the experiment is shown in Fig. 8.1. The micro-stamping tool is fixed on the machine bed by means of four bolts, as shown in Fig. 8.2. The following equipment is used in the experimental measurement.
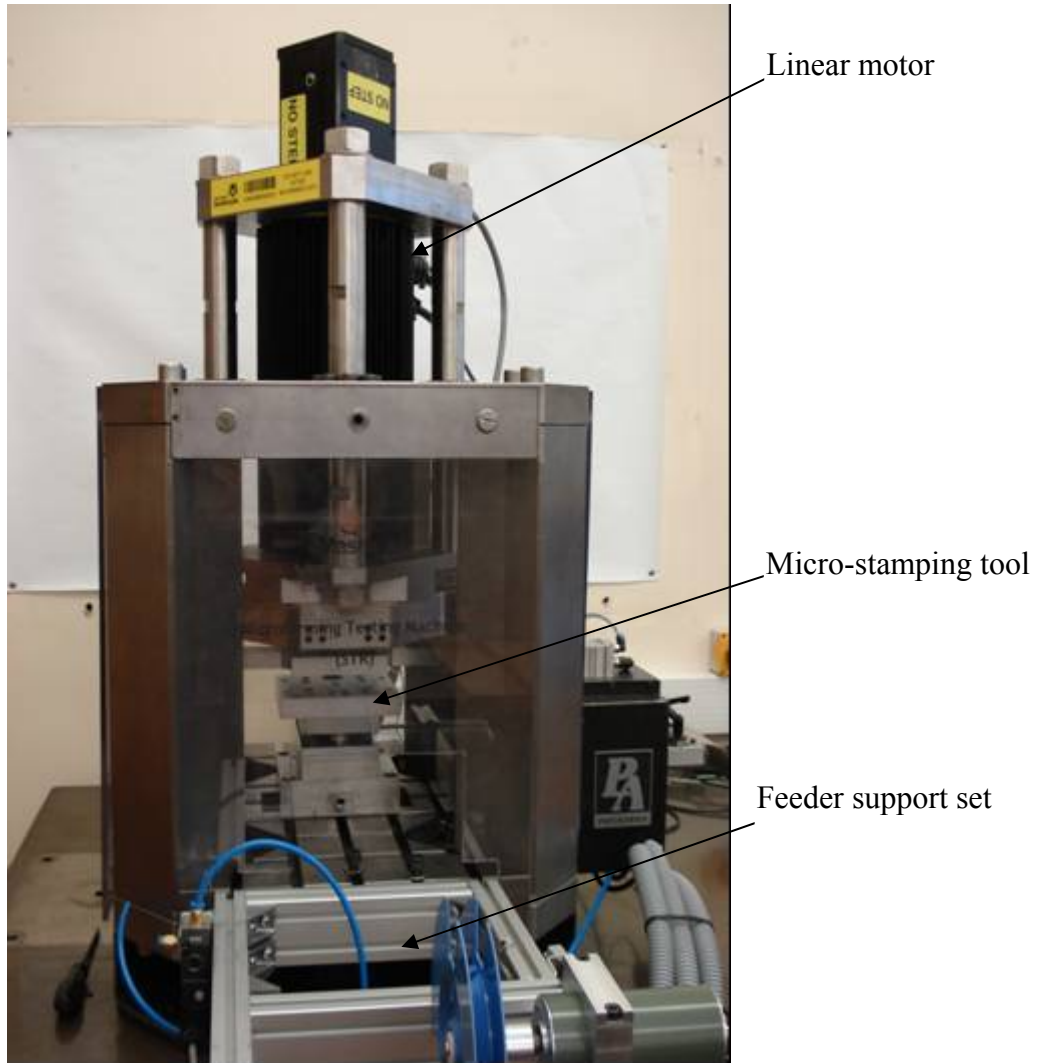

Linear motor

Micro-stamping tool

Feeder support set

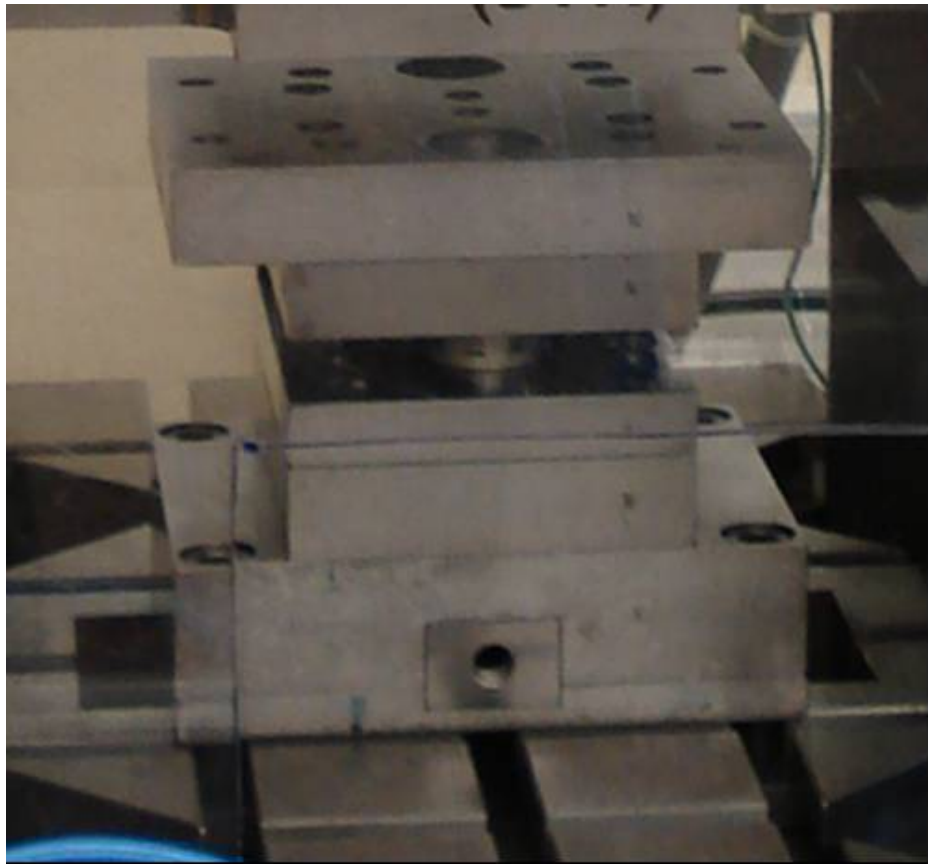**Fig. 8.1 The micro-stamping machine with the micro-stamping tool**

Fig. 8.2 The assembled micro-stamping tool

Load cell:

A piezoelectric force-sensor 9333 from Kistler, shown in Fig. A8.1, is used to measure the dynamic force. It has high sensitivity (from -3.943 to -4.012 pC/N), wide measurement ranges (0-500N, 0-5kN and 0-50kN), compact geometry (30mm in diameter and 34mm in height) and is particularly suitable for dynamic force-measurement (Press force sensor, http://www.intertechnology.com/Kistler).

The assembly of the load cell is shown in Fig. A8.2. The cell is placed between the ram and the shaft of the linear-motor and connected securely to both of them.

Position sensor:

An optical read head RGH24Y from Renishaw, as shown in Fig. A8.3, is used to measure the displacement of the punch guide plate and the top plate in the vertical direction. It has the high resolution of 0.1micron, and it can be used in a non-contact measurement manner. The components that are used for the assembly of the Renishaw read head and scale, are shown in Fig. A8.4 (http://www.trilogysystems.com/pdf/L-9517-0166.pdf). The surface roughness Ra of the components was to be less than 3.2μm. The measurement Ra of the surface of the component was 0.124μm, which is shown in Fig. A8.6.

Data acquisition system:

The data acquisition system contains a computer, a Libview system, a Kister charge meter 5015, and a BNC-2120 connector accessory for the signal transfer of the position sensor and the load cell. They are shown in Figs A8.7 to A8.9.

Control system:

The machine is driven by a linear motor, which can be controlled by a program. The press control cabinet is shown in Fig. A8.10. The difference between the designed path and the actual path of the ram can be reduced by setting control parameters, P_i, P_k and P_d. The details of these parameters are shown in Tables 8.1, 8.2 and 8.3, in which the frequency is the linear-motor working frequency and A0 & AA are the

designed value and the recorded value of the amplitude of the ram movement, respectively.

The details of the linear-motor control parameters are listed in Table 8.1 for the dry-rollers condition, and in Tables 8.2 and 8.3 for the lubricated-rollers conditions. For different frequencies, the range of the control-parameter-change in the dry-rollers condition is greater than that in the lubricated-rollers condition. A comparison between Tables 8.1, 8.2 and 8.3 shows that the system is controlled easily when the rollers are lubricated.

Table 8.1   Control-parameter setting of the linear-motor for non-lubricated rollers

A0=1.5mm

Frequency	AA	Kp	Ki	Kd
1	1.373	50	20	0
2	1.373	120	40	0
3	1.373	120	40	0
4	1.373	180	40	0
5	1.373	260	40	40
6	1.384	340	40	40
7	1.373	380	40	40
8	1.373	400	40	40
9	1.373	420	40	40
10	1.373	460	40	40
11	1.373	480	40	40
12	1.373	500	40	40
13	1.373	520	40	40
14	1.373	540	40	40
15	1.363	540	40	40
16	1.373	800	800	600

Table 8.2 **Control-parameter setting of the linear-motor for lubricated rollers**

A0=1.5mm

Frequency	AA	Kp	Ki	Kd
1	1.35	50	20	0
2	1.35	120	20	0
3	1.35	150	20	0
4	1.35	180	20	0
5	1.35	200	20	0
6	1.35	240	20	0
7	1.35	250	20	0
8	1.35	270	20	0
9	1.35	270	20	0
10	1.35	290	20	0
11	1.35	290	20	0
12	1.35	290	20	0
13	1.35	290	20	0
14	1.35	290	20	0
15	1.35	260	20	0
16	1.35	240	20	0

Table 8.3   Control-parameter setting of the linear-motor for lubricated rollers

A0=3.00mm

Frequency	AA	Kp	Ki	Kd
1	2.883	50	20	0
2	2.883	120	20	0
3	2.883	180	20	0
4	2.883	180	20	0
5	2.883	220	20	0
6	2.883	240	20	0
7	2.883	240	20	0
8	2.883	240	20	0
9	2.883	240	20	0
10	2.883	240	20	0
11	2.883	240	20	0
12	2.883	240	20	0
13	2.883	240	20	0
14	2.883	240	20	0
15	2.883	240	20	0
16	2.883	240	20	0

8.3   Dynamic force measurement

The load cell was assembled by connecting the upper surface with the motor shaft and the lower surface with the ram, as shown in Fig. A8.2. The dynamic force was measured for different frequencies, different frictions of rollers, and different amplitudes of the path of the ram.

8.4 Dynamic displacement measurement

When the dynamic response of the top plate is measured, the read head RGH24Y is fixed onto the top plate and the component, with a RGS20-S scale on, is fixed onto the die plate. When the dynamic response of the punch guide plate is measured, the read head RGH24Y is fixed onto the die plate and the component, with a RGS20-S scale on, is fixed onto the punch guide plate. Fig. A8.5 shows the assembly for dynamic response measurement of the top plate. The surface roughness R_a of the component should be less than 3.2μm. The parallelism of the guide-way (the variation of the height of the read head) must be within 0.05mm. The RGS20-S scale should be straight and level. The measured results of the surface roughness of the guide way are shown in Fig. A8.6. The measured surface roughness Ra is 0.124μm.

8.5 Results of experiment

Experimental measurements have been carried out for working frequencies of from 1Hz to 16Hz. The designed amplitudes of the path of the ram are 1.5mm, 3mm and 6mm. The measured results of force are described in Section 8.5.1 and the measured results of the dynamic response of the top plate and the punch guide plate are given in Sections 8.5.2 and 8.5.3, respectively.

8.5.1 Results of force measurement

The load cell and the assembling are shown in Figs. A8.1 and A8.2. The measured results are shown in Figs. 8.3 to 8.6. The results for different amplitudes of the path of the ram and different conditions of the rollers are listed in Table 8.4. The force decreases with increasing frequency, but when the frequency increases to about 14 Hz the noise increases and the sensor works unstably. The base of test machine is BC-1 described in Chapter 6 and the material used is Nitrile 642. The fundamental frequency of the micro-stamping machine with this machine base obtained from FE analysis is about 16Hz. That means the frequency of the experiment is close to resonance.

The force is greater for a short time at the beginning of the test, as can be seen in Fig. 8.6.

Table 8.4 Results of force measurement

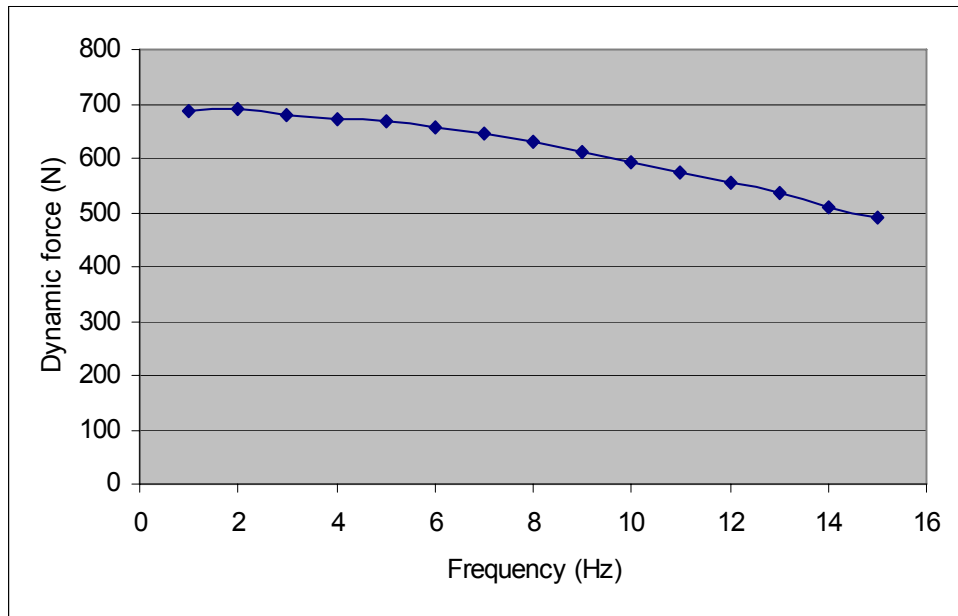| Frequency (Hz)	Force (N)		
	A0=3mm, Lubricated roller	A0=3mm, dry roller	A0=6mm, dry roller
1	688	693	812
2	690	×	783
3	680	661	744
4	670	634	724
5	667	606	701
6	657	576	671
7	645	548	629
8	629	526	580
9	613	492	542
10	593	462	502
11	575	432	465
12	553	400	417
13	535	355	378
14	510		
15	489		

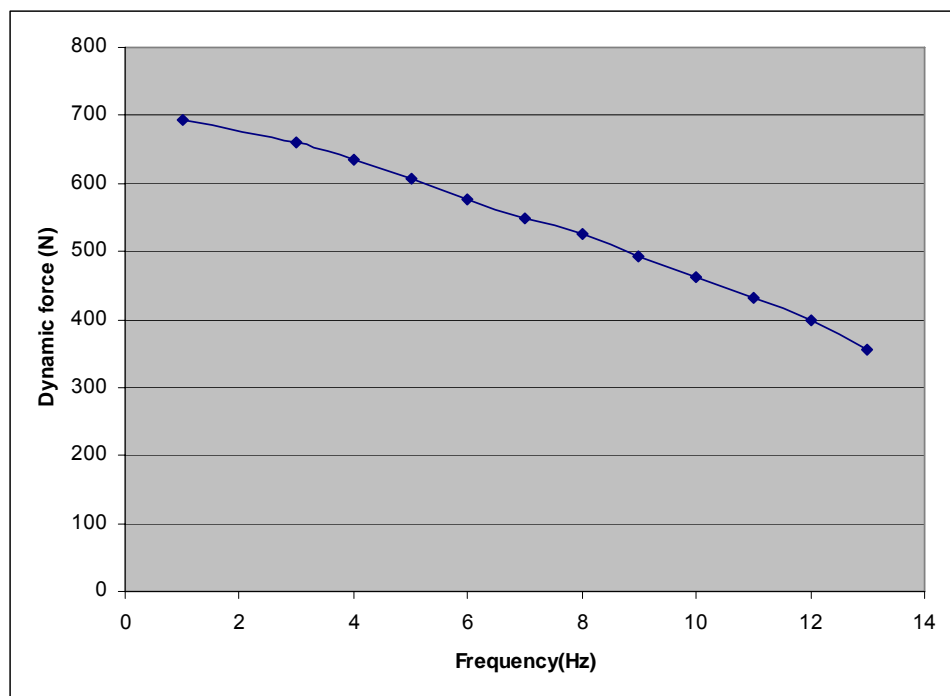**Fig. 8.3 Dynamic force for A0= 3mm and lubricated rollers**

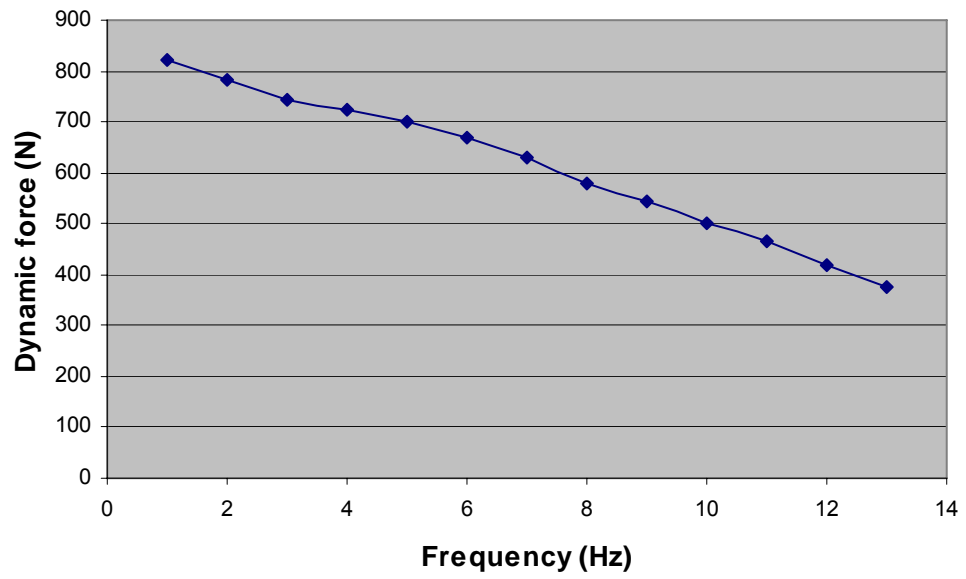**Fig. 8.4 Dynamic force for A0=3mm and dry rollers**

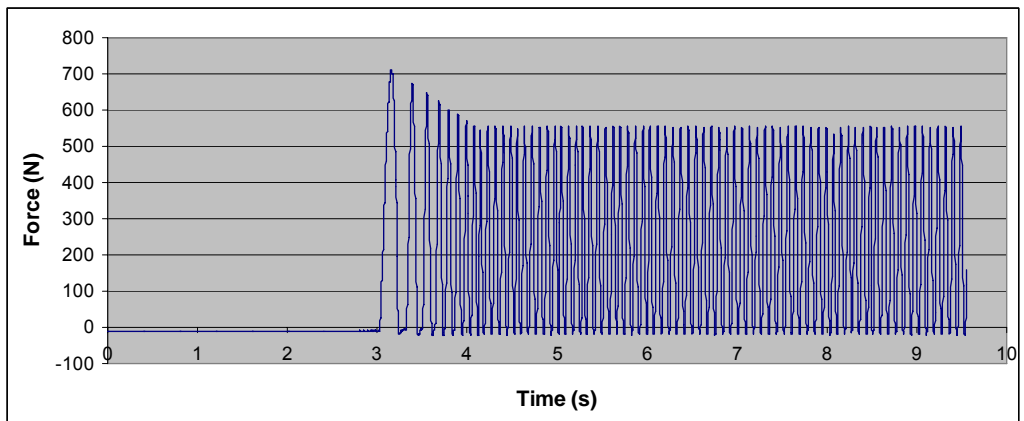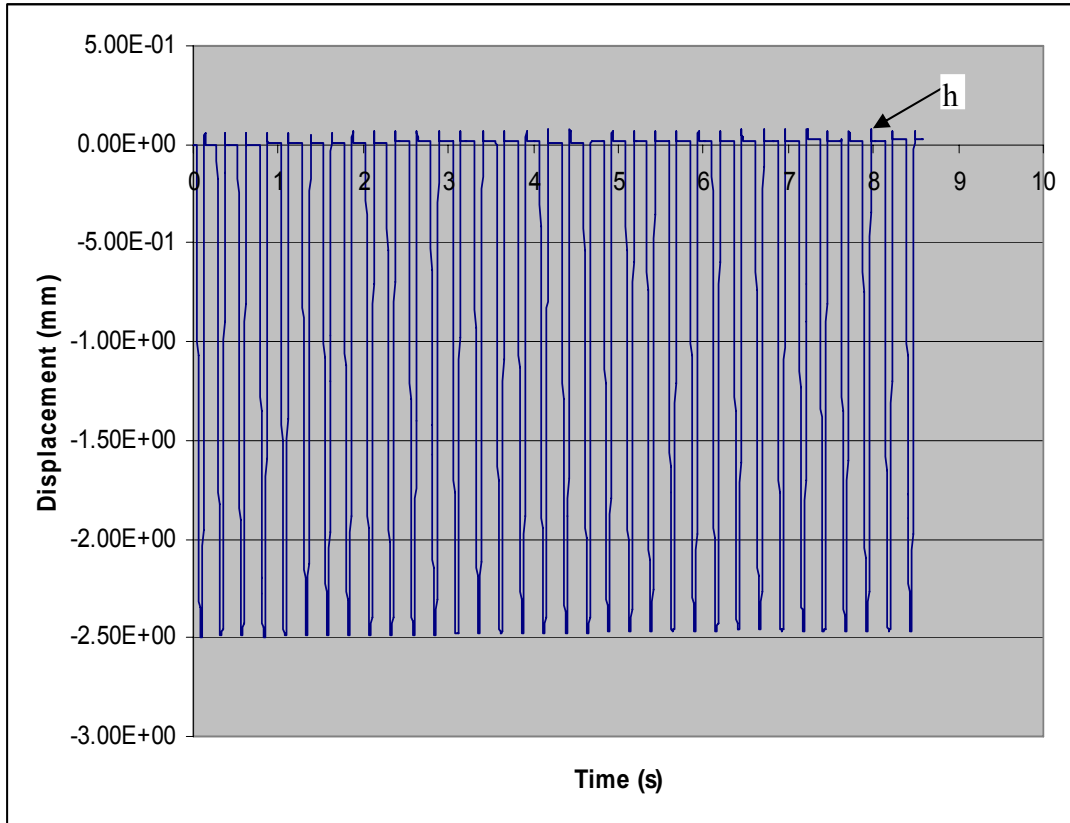**Fig. 8.5 Dynamic force for A0=6mm and dry rollers**

Fig. 8.6 Measurement force versus time

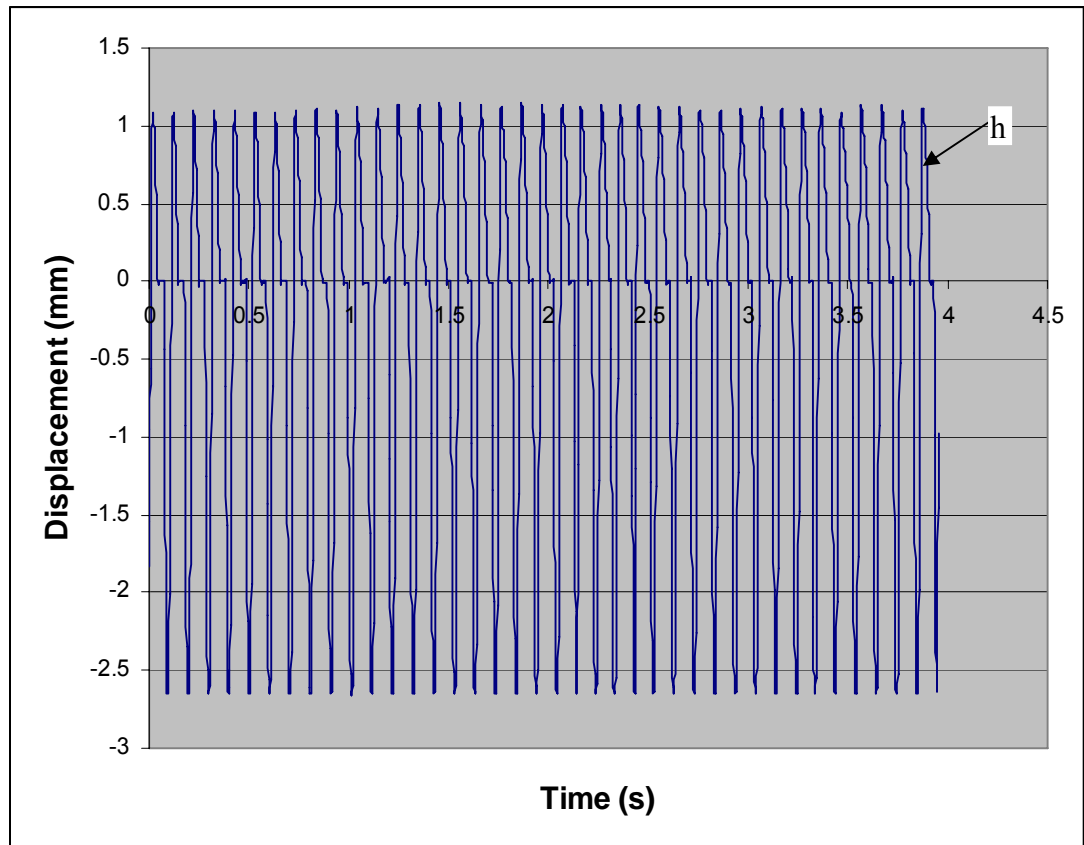### 8.5.2 Results of the dynamic response of the top plate

The results for the dynamic response of the top plate are shown in Figs. 8.7 to 8.9. In Figs. 8.7 and 8.8, h is the value to which the top plate jumps up from its equilibrium position. The value of h increases as the frequency increases. The results of the measurement of h are listed in Table 8.5 and shown in Fig. 8.9. The movement of the top plate makes the contact between the ram and the top plate change in time; that is, the top plate can rebound to above the position of equilibrium (Fig. 8.7 and 8.8). As a consequence, the ram can come into contact with the top plate at any position near to the equilibrium position. This phenomenon has also been observed in the finite element simulation. It may generate some excitation of the system.

Table 8.5 Dynamic response of the top plate

Frequency (Hz)	Jump-up value h (mm) (A0=6mm, dry rollers)
2	0.0013
3	0.003
4	0.07
5	0.126
6	0.388
7	0.53
8	0.74
9	0.882
10	1.146

**Fig. 8.7 Dynamic response of the top plate of the tool
Frequency =4Hz**

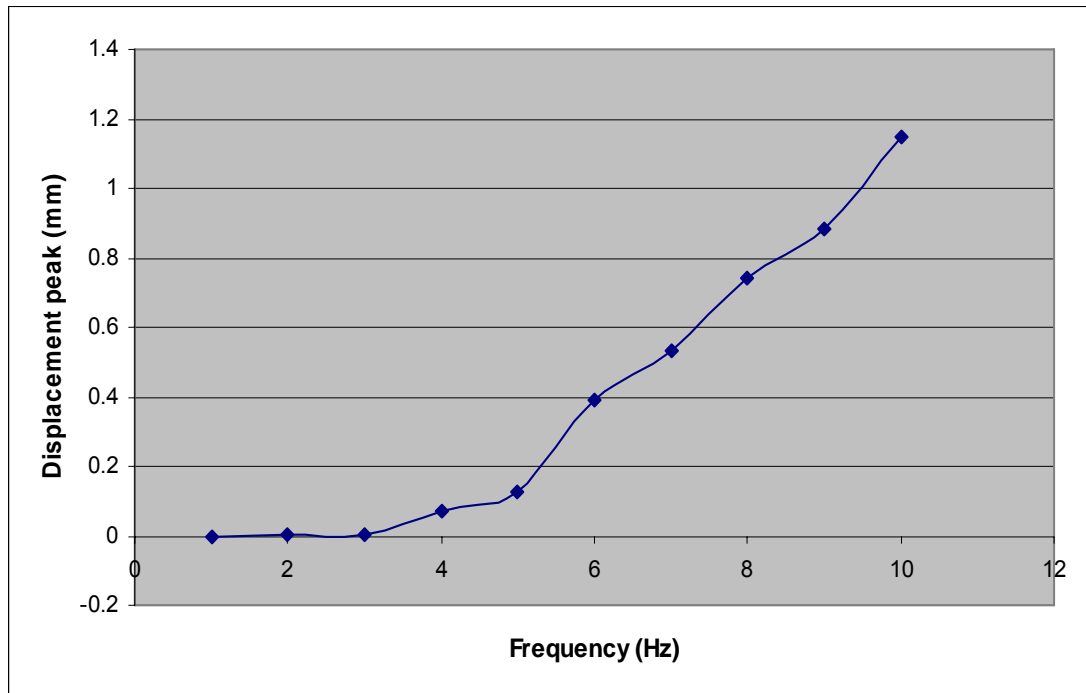**Fig. 8.8 Dynamic response of the top plate of the tool**
Frequency =10Hz

Fig. 8.9 Dynamic response of top plate

8.5.3 Results of the dynamic response of the punch guide plate

The results for the dynamic response of the punch guide plate are listed in Table 8.6: these are also shown in Figs. 8.10 to 8.14. Comparisons between the dry roller and the lubricated roller, as well as for different amplitude of the path of the ram are shown in Fig. 8.15 and Fig. 8.16. After one forming process has been completed, the punch guide plate leaves the lower die and moves up. This phenomenon has been found in both FE analysis and experimentation. The measured results shown in Figs. 8.10 and 8.11 are similar to the results from FE analysis shown in Figs. A7.7 and A7.8. This means that the punch guide plate impacts the lower die in every instance of stamping: this may be another excitation of the system. Especially, the moving-up of the punch guide plate increases non-linearly with increase in the frequency: this is shown in Figs. 8.12 to 8.14. The influence of the lubricant on the dynamic response of the punch guide plate has been measured for the conditions of dry rollers and lubricated rollers. After the rollers are lubricated, the moving-up of the punch guide plate is larger than that for the dry-roller condition. A comparison of the results is shown in Fig. 8.15. The amplitude of the path of ram movement A0 has a significant influence on the dynamic response of the punch guide plate.

A comparison of the results between A0=3mm and A0=6mm is shown in Fig. 8.16. Apparently, when the amplitude A0 is doubled, the corresponding response is more than doubled.

Table 8.6 Dynamic response of the punch guide plate (mm)

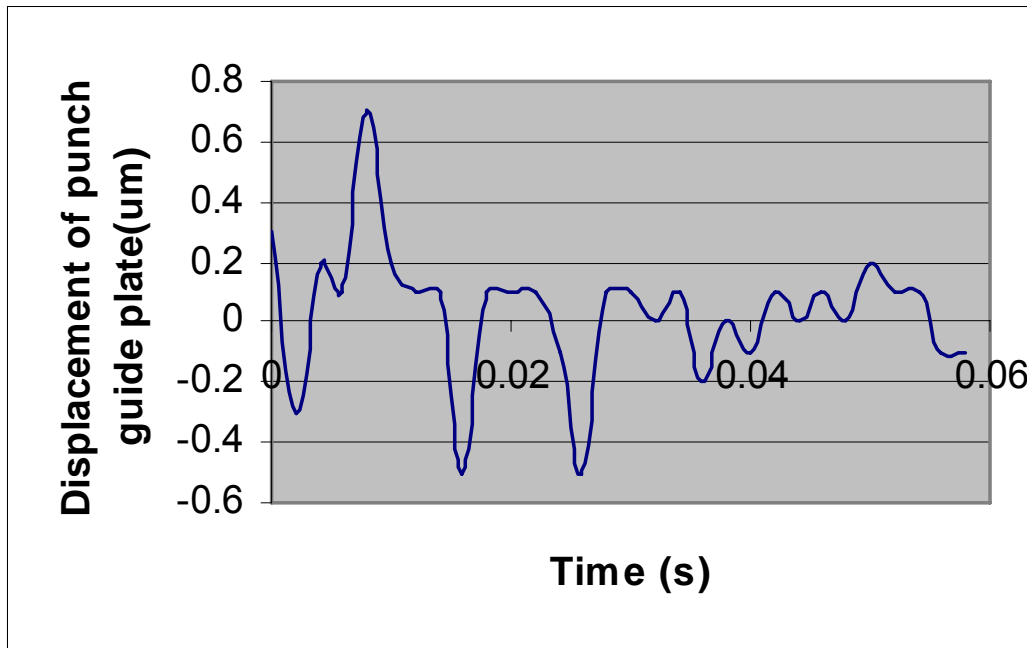| Frequency	Amplitude of the path of the ram		
	3mm (dry rollers)	6mm (dry rollers)	3mm (lubricated rollers)
2	0.025	0.01	0.012
3	0.035	0.12	0.05
4	0.07	0.16	0.073
5	0.11	0.27	0.11
6	0.15	0.44	0.16
7	0.16	0.63	0.21
8	0.23	0.8	0.31
9	0.33	1.09	0.45
10	0.41	1.39	0.6
11	0.56	1.9	0.75
12	0.68	2.16	0.98
13	0.9	2.9	1.1
14	1		1.35
15	1.14		1.547
16	1.29		

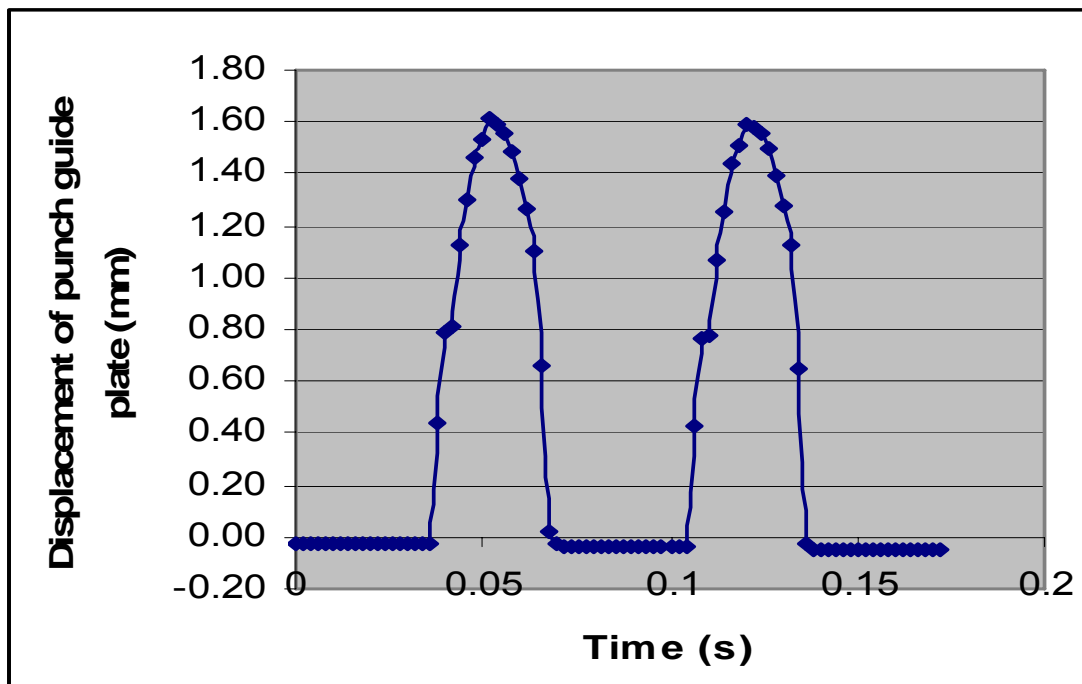**Fig. 8.10 Response of the punch guide plate   AA=1.35mm, 16Hz**

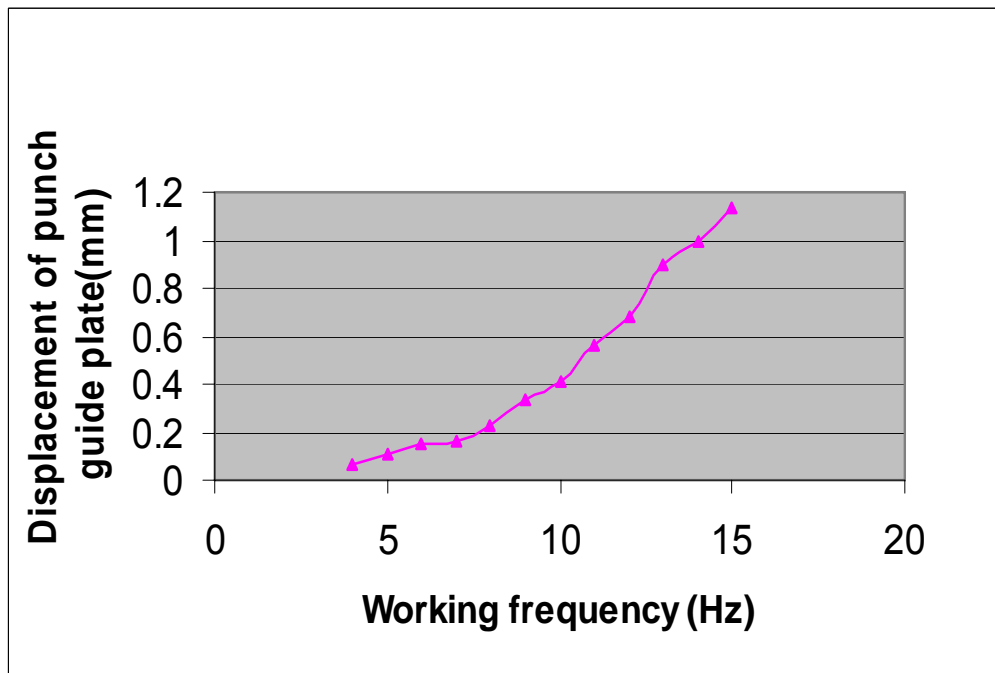**Fig. 8.11 Response of the punch guide plate   AA=2.88mm, 15Hz**

Fig. 8.12 Response of the punch guide plate   A0=3mm, dry rollers

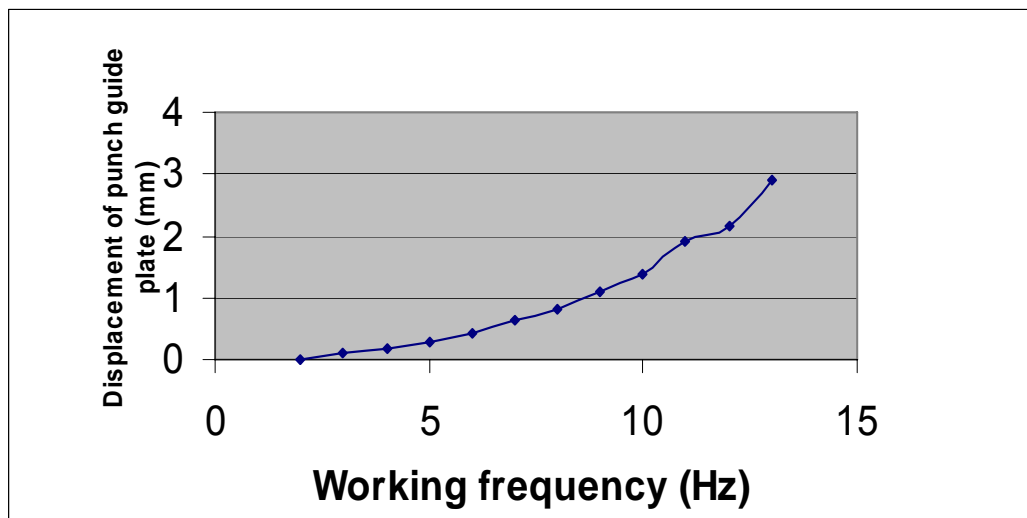**Fig. 8.13 Response of the punch guide plate   A0=6mm, dry rollers**

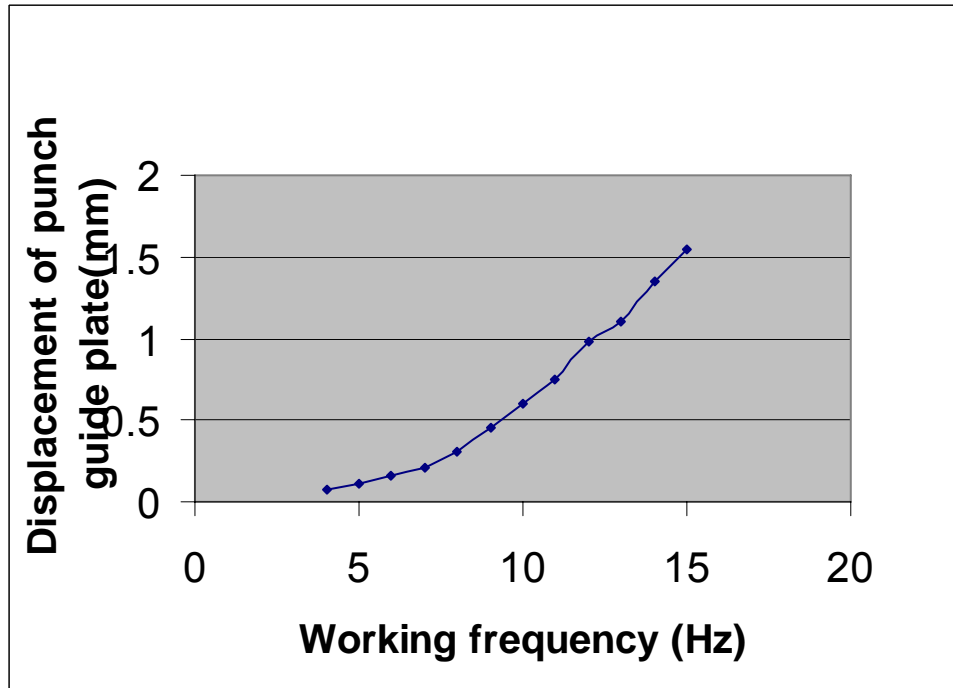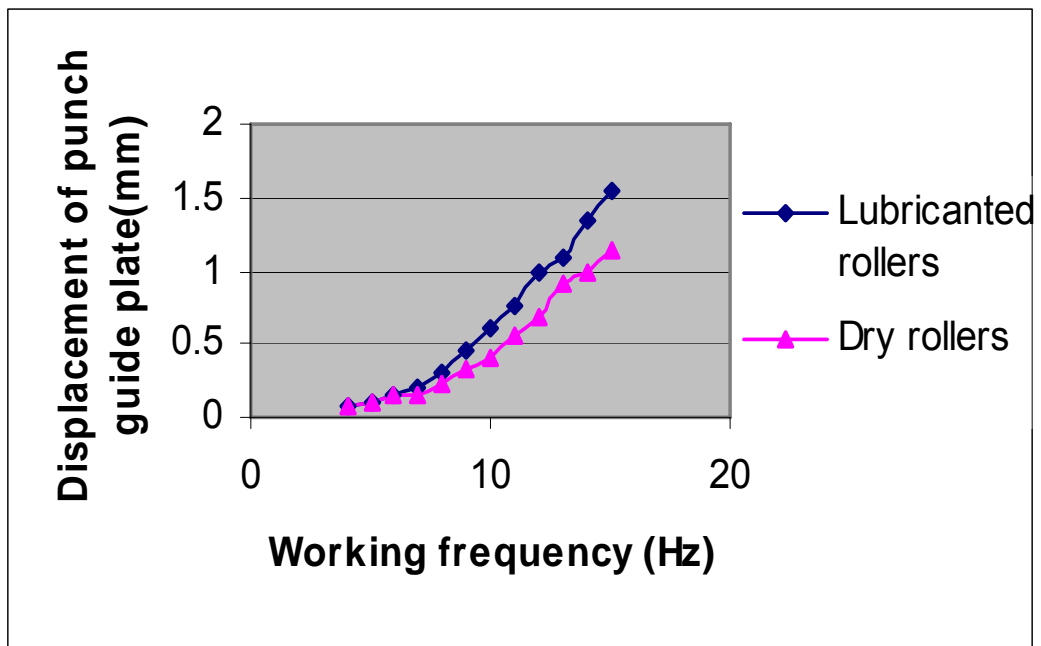**Fig. 8.14 Response of the punch guide plate   A0=3mm, lubricated rollers**

**Fig.8.15 Comparison of the responses of the punch guide plate
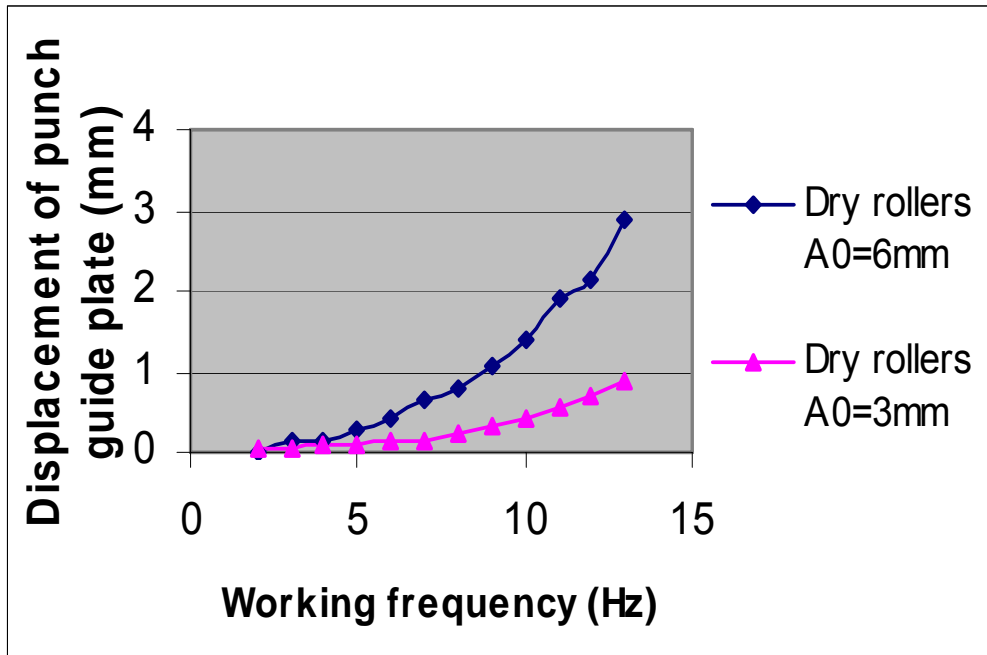between the use of lubricated and dry rollers   A0=3mm**

Fig. 8.16 Comparison of the response of the punch guide plate between A0=3mm and A0=6mm, dry rollers

8.6   Acceleration measurement of the machine

The vibration test of the machine was carried out by other members of the research group. The aim of introducing the vibration test here was to compare the vibration results from FE analysis and from experimental measurement.

The equipment used in the experiment was a Bruel & Kjaer 2635 charge amplifier, Bruel & 4393 Piezo-electric accelerometer and a Hameg 20MHz oscilloscope, as shown in Fig. A8.11.

The procedure of the test was to vary the sinusoidal input frequency generated by the Mayr unit and to record the voltage output from the Hameg 20MHz oscilloscope at various frequencies going from 1Hz to 18Hz.

In the test, the machine became unstable as the frequency approaches 18Hz. The measurement results are shown in Fig. A8.12 for two cases, with and without a sealing ring used to restrain the linear motor from lateral movement. In Fig. A8.12, the measured acceleration (V) tends to be larger at higher frequency and increases non-linearly from 14Hz.

A finding from this test was that the machine entered the resonance region after the frequency approached 18Hz.

This test machine including the machine base had been analysed for vibration in Subsection 6.2.6. The results of FE analysis shown in Table 6.7 were 16 Hz and 20.5 Hz of the first mode and the second mode, respectively. This meant that there was a resonance region around the frequency of 16 Hz or 20.5 Hz. This was in agreement with experiment.

8.7   Comparison between FE analysis and experiment

- Findings on the dynamic response of the punch guide plate: both FE analysis and experiment showed that after one forming process has been completed, the punch guide plate leaves the lower die and moves up. The FE analysis and

experiment were carried out for different frequencies and amplitudes of ram movement. The results for the frequency of 16Hz and 15Hz are listed in Table 8.7, where *A* is the amplitude of the ram movement. *Freq* is the frequency of the micro-stamping machine. *Amp* is the amplitude of the punch guide plate jump. It is seen that punch guide plate jump occurred in both the FE analysis and the experiment. Similar ram movements in FE analysis and experimental measurement resulted in similar jumps. Since the experiment was conducted in the frequency range from 2Hz to 15Hz, the method of least squares was used to fit the results to a second order polynomial, as shown in Fig. A8.13. The fitted jump at a frequency of 16Hz was 1.82mm.

Table 8.7 Comparison of the amplitudes of punch guide plate jump between FE analysis and experiment				
Case	Method	A (mm)	Freq (Hz)	Amp
1	FE analysis	1.4	16	0.62μm
	Experiment	1.35	16	0.70μm
2	FE analysis	2.76	16	2.00mm
	Experiment	2.88	15	1.58mm
	Extension of experiment results	2.88	16	1.82mm

- A finding on the resonance region of the machine: both FE analysis and experimental measurement revealed largely the same resonance region of the micro-stamping machine.

8.8   Conclusions

The analysis of the findings enabled the following to be identified as of particular relevance to tool- and machine-design for micro-stamping:

(1)   The impact between the ram and the top plate due to the jumping-up of the top plate should be controlled to prevent exciting force being generated within the system.

(2)   The punch guide plate moves up during the stamping process. Both the amplitude of ram movement and the working frequency have a significant influence on this movement. An unstable punch guide plate will generate an exciting force on the punches, reducing the precision of the tooling. Because high speed is the target of this micro-stamping tool, the amplitude of ram movement should be made as small as possible in the design of the whole system.

(3)   The guiding rollers should be lubricated during the stamping process. Difference between the design amplitude and the actual amplitude of ram movement is greater in the absence of lubrication. This may cause the punch to be unable to cut material correctly in high-speed stamping. Reducing the friction of the roller can make the whole system easier to control, especially when material forming and material feeding need to be activated at the correct time.

(4)   On the other hand, because the lubrication of the roller reduces the friction between the roller and the punch guide plate, the dynamic response of the punch guide plate has a greater jump-up value; therefore, the punch guide plate should be controlled in some other way in an integrated design.

(5)   The agreement between FE analysis and experimental measurement in the aspects described in Subsection 8.7 can validate the FE model and the experimental method each other. It may be concluded that the findings from FE analysis and experiment are valuable and useful. They can be used for further improvement on the micro-forming machine and micro-stamping tool.

The findings presented above formed a basis for improving the micro-stamping tool and machine/tool connection design for the forming of micro-sheet-components (Zhou, et al., 2008).

The FE analysis model for the vibration analysis of the micro-stamping machine did not include the load cell and micro-stamping tool. The load cell was fixed to the shaft of linear motor and the ram. This does not change the stiffness of the whole structure, and the mass of the load cell is very small compared to the total mass of the micro-

stamping machine structure. Therefore the load cell may have influence on the local mode of the vibration of the structure, but it should not have significant influence on the fundamental frequencies of the vibration of the whole structure. A new model including all of the components may be used in the future.

8.9   References

Press Force Sensor Kistler 9333, available at:

http://www.intertechnology.com/Kistler/Force_Model_9333_9343_9363.htm

Position Sensor RGH24Y, available at:

http://www.trilogysystems.com/pdf/L-9517-0166.pdf

Rolling Bearing Friction (2007), available at:

http://www.roymech.co.uk

Zhou, M., Qin, Y., Harrison, C., Brockett, A. and Ma, Y. (2008), 'Finite-Element and Experimental Analysis of Dynamic Behaviours of a Micro-Stamping Tool System,' *Int. J. of Adv. Manufact. Technol.*, DOI 10.1007/s00170-009-2138-0

8.10   Appendix A – Figures
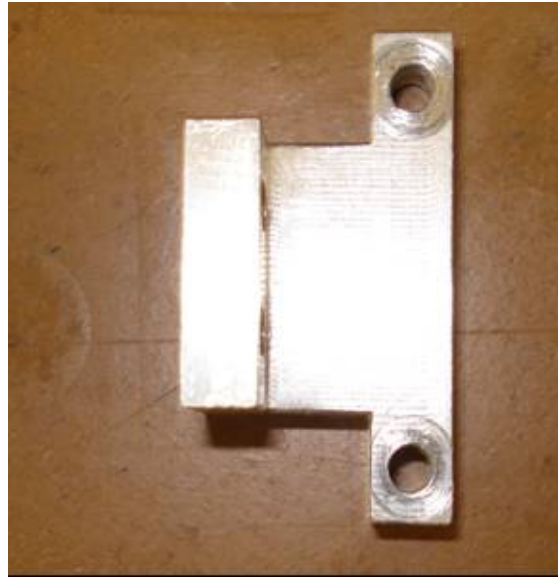

Fig. A8.1 The Kistler force sensor 9333

The force
sensor 9333

Fig. A8.2 The assembly of the force sensor 9333

Fig. A8.3 The Renishaw read head RGH24Y

(a) Guide way for the RGS20-scale (b) Components for the read head

Fig. A8.4 The components of the Renishaw read head RGH24Y assembly

Fig. A8.5 The assembled Renishaw read head RGH24Y

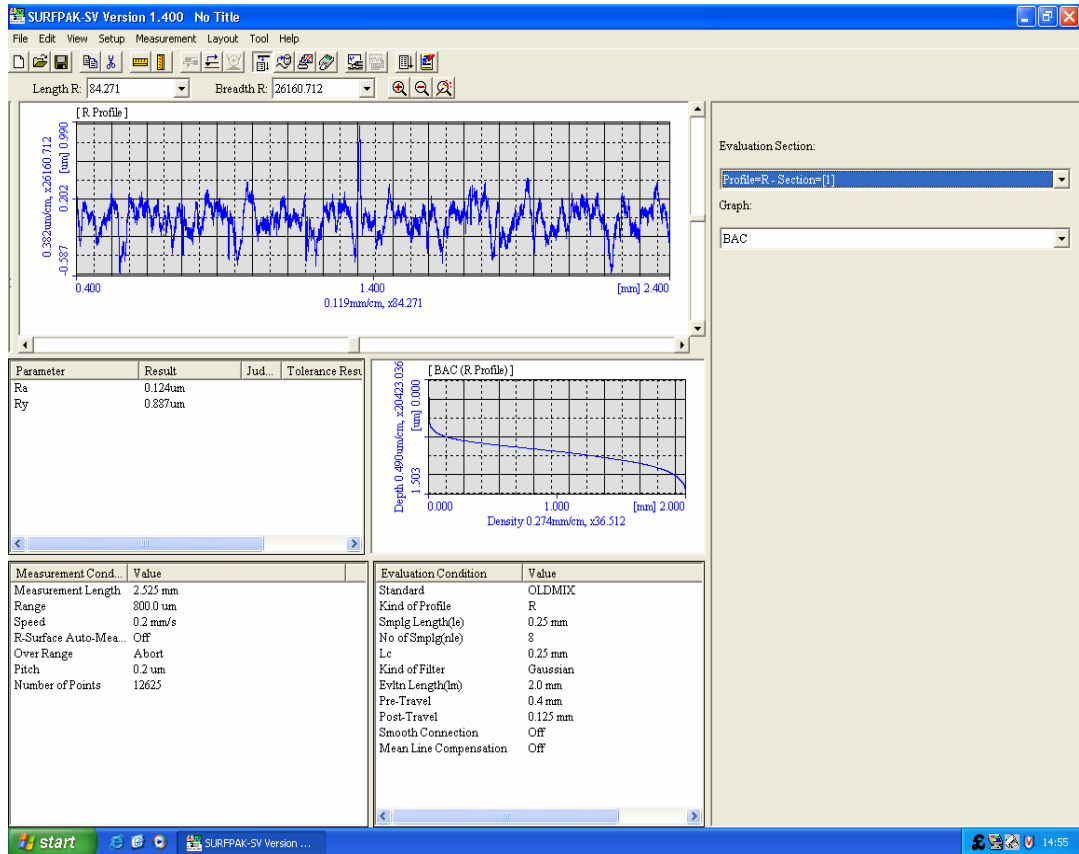**Fig. A8.6 Surface roughness of the assembly components of Renishaw read head RGH24Y**

Data acquisition   Linear motor control

Fig. A8.7 Control system
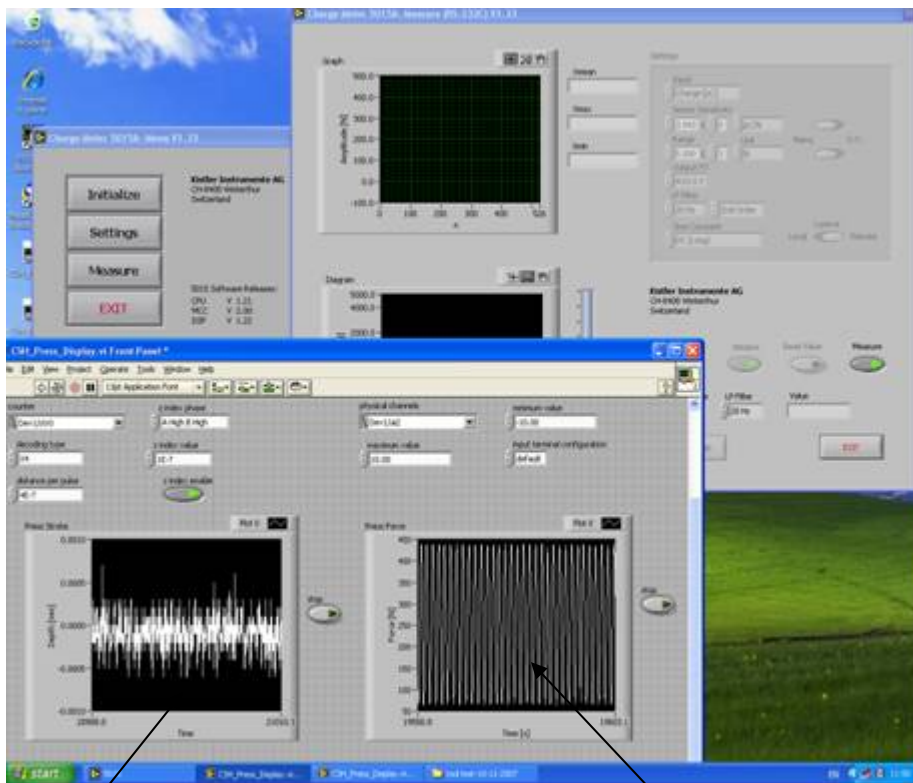
Displacement

Force

Fig. A8.8 Libview data acquisition system

Fig. A8.9 The Kistler charge meter 5015 and the BNC-2120 connector accessory

Fig. A8.10 Press control cabinet

Fig. A8.11 The vibration test set-up

Actual wave form comparison

Fig. A8.12   Results of the vibration test

**Fig. A8.13   Fitting of the responses of the punch guide plate
for lubricated rollers, A0=3mm**
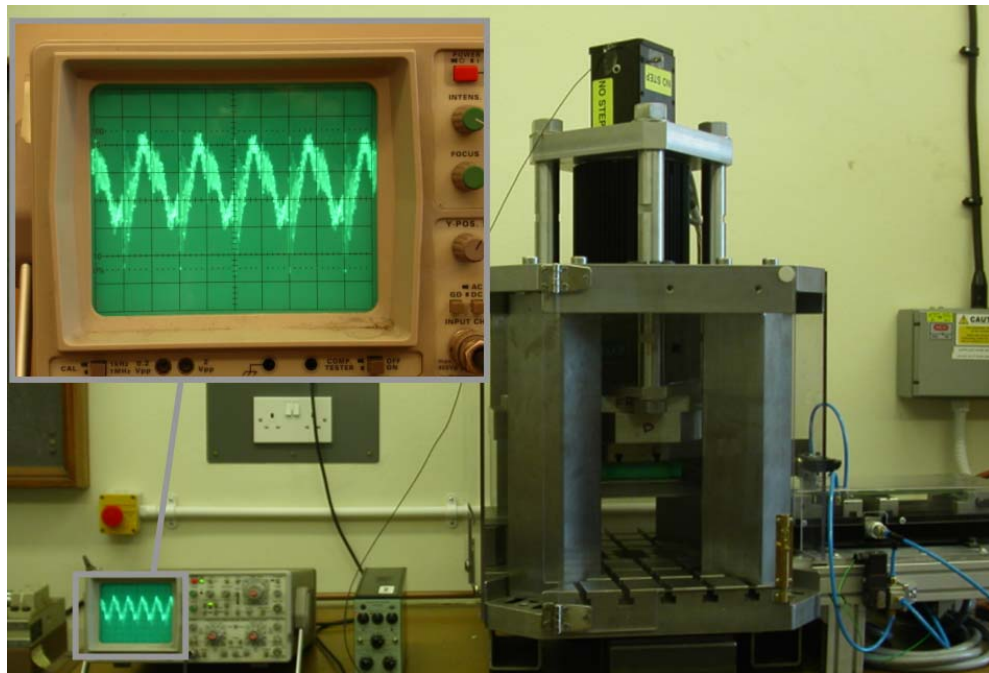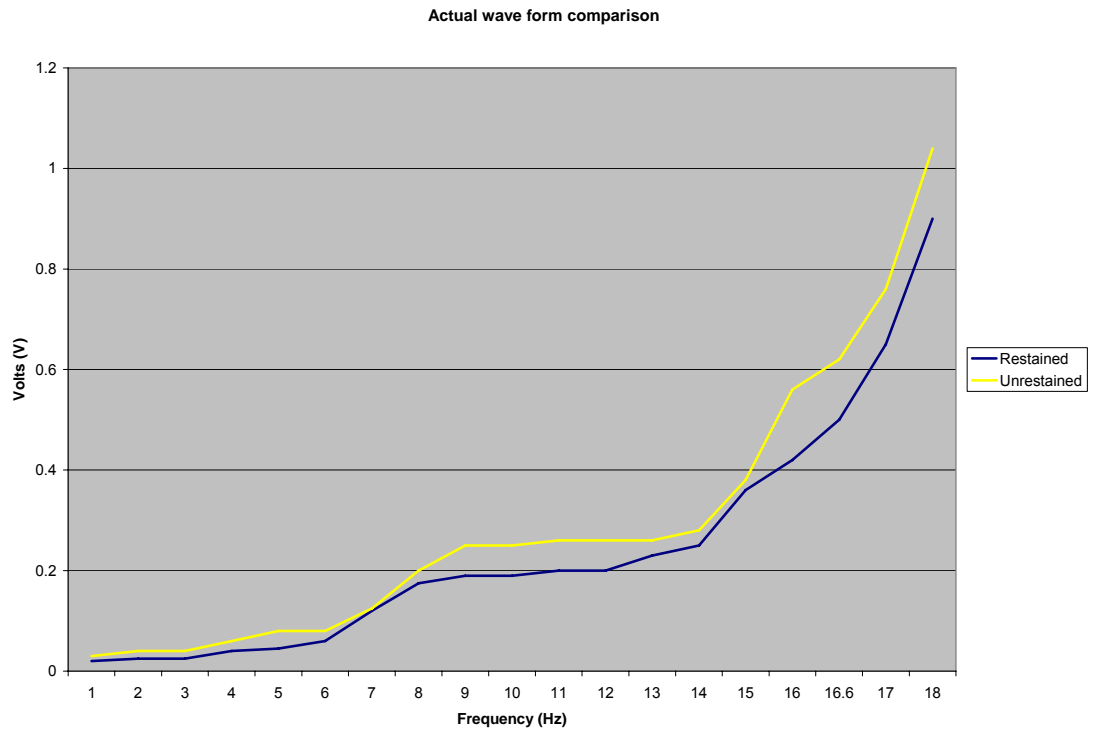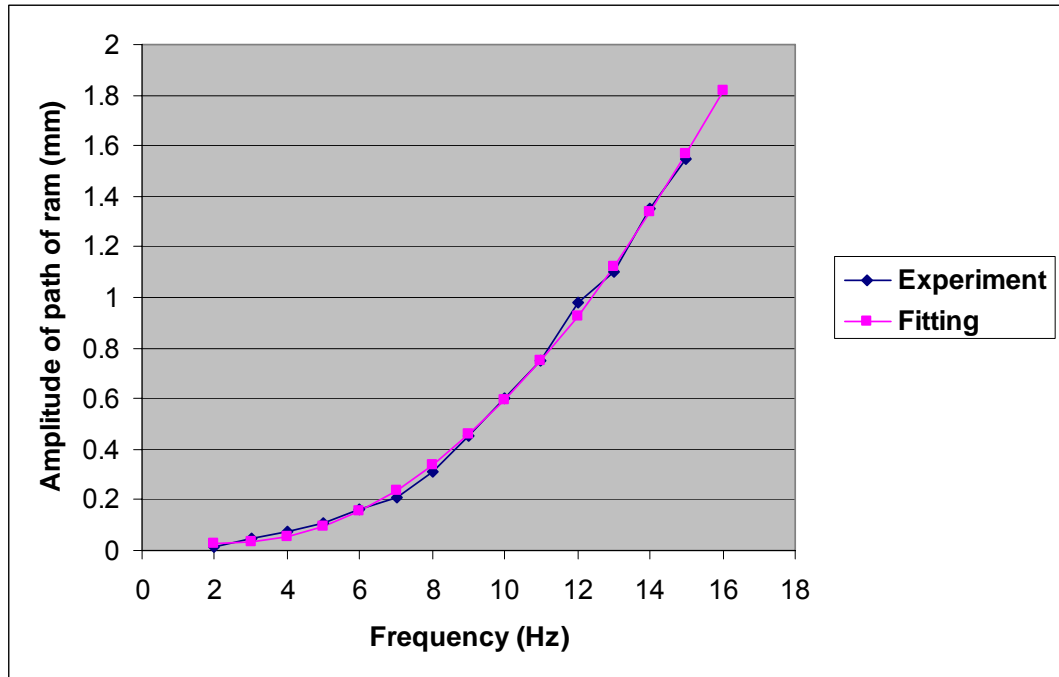
Chapter 9 Conclusions and Recommendations on Future Work

In this chapter, the findings and conclusions in this study are first summarised. Then recommendations for further research work are presented based on the analysis of the findings.

9.1   Summary of findings and conclusions

9.1.1   Effect of surfaces roughness

- The deformation of the peaks of rough contact surfaces contributes directly to: (i) the real contact area; (ii) the thermal conductance of the solid contact surfaces; and (iii) the distribution of the lubricant on the contacting surfaces.

- Not only does the surface roughness have a significant influence on the thermal conductance of the metal surfaces in contact, but also the lubricant affects it. The distribution of the lubricant on the contact surfaces depends on the amount of lubricant used and the deformation of the peaks of the roughness of the contact surfaces. In micro-stamping tool design the lubricant should be used to prevent the rollers and the linear guide from over-heating. Therefore the thermal properties of a lubricant that is used for a micro-stamping tool are important.

- If the flat metal surfaces of two pieces of metal are made progressively smoother, a point will be reached where the resistance to relative movement increases. If their surfaces are very flat and smooth, and all surface contaminants are removed, the surfaces will actually adhere to each other. In the design of the micro-stamping tool, the blank holder and the lower die plate are used to hold the material strip during the stamping process. Therefore, a greater friction force is desirable. In order to obtain a greater friction force, the surface roughness of both the blank holder and the lower die plate should be low and close to that of the surface of the material strip. This can reduce the danger of damage to the workpiece due to the grip on the strip loosing when the punch is leaving the die.

- Depending on the FE analysis of the deformation of the peaks of rough contact surfaces, rough surfaces in contact produce a non-uniform stress

distribution and a non-uniform temperature distribution near to the surfaces. There are local areas of lesser stress below the surface at the position of the valleys. All of these factors may have an influence on the precision of the micro-formed product. The material flow when the peaks are compressed blunt causes the surface at the valley move up relative to the original surface. The surface roughness of the material to be used for micro-forming should be as small as possible and a blunt rough peak is better than a sharp rough peak.

9.1.2   Effect of the structural vibration of the micro-stamping machine

- The contact position between the ram and the linear guide significantly influences the natural frequency of the micro-stamping machine. Therefore, investigating the contact positions and reducing the contact area are both necessary during the design of a micro-stamping machine.

- When a linear motor is used to control the process of stamping for the micro-stamping machine, it is better that the main frame can contribute to supporting the linear-motor assembly. This can make the linear motor more stable, hence helping to achieve a high precision.

- When rubber is used beneath the machine base, there is a group of lower natural frequency modes present, which are close to the working frequency of the micro-stamping machine. This phenomenon has been found in both FE analysis and experiments. All of the parameters of the rubber plates have a significant influence on the results. Therefore, when rubber is used at the base of the micro-stamping machine, special care should be taken in selecting the dimensions of rubber plates and the contact area. Reducing the thickness and increasing the contact area will increase the natural frequency of a micro-stamping machine with a rubber base. Accurate material properties of the rubber used will play an important role during the process of carrying out design calculations for the base of the micro-stamping machine.

- In the design of a micro-stamping machine system, attempt should be made to minimise exiting force in the xy plane generated by the feeder and the workpiece handling device, as the lowest mode of vibration may occur in that plane.

- The dynamic reaction forces acting on the stamping tool at the connection between the support plate and the micro-forming machine have a frequency much greater than the working frequency of the linear motor. This frequency will be transmitted to the system during the forming process. The value is very close to the natural frequencies of the lower modes of vibration of the machine in the absence of a rubber base. Therefore, the response frequency of the stamping tool should be taken into consideration in the design of a micro-forming machine system.

- Natural frequencies of all flexible structure position should be taken into account in the design process.

9.1.3   Factors influencing the micro-stamping tool behaviour

- Differences in punch geometry result in imbalance of the cutting forces among the punches, which in turn result in different dynamic behaviour of the punches. In the cases studied, a smaller punch tends to move away from its original position, and continual high-speed stamping leads to increasingly greater offset displacement of the punch. This could possibly be the reason why a smaller punch is prone to damage, when the cutting speed is increased. This feature has to be taken into account when punches are designed for high speed stamping.

- The punch guide plate moves up during the stamping process. Both the amplitude of ram movement and the working frequency have a marked influence on this movement. This has been found in both FE analysis and experimentation. An unstable punch guide plate will generate an exciting force on the punches, hence reducing the precision of the tooling. Because high speed is the target of this micro-stamping tool, the amplitude of ram movement should be made as small as possible in the design of the whole system

- Different friction coefficients between the roller and the linear guides greatly affects the dynamic response. This has been found in both FE analysis and experimentation. The guiding rollers should be lubricated during the stamping process. The difference between the design amplitude and the actual

amplitude of ram movement is greater in the absence of lubrication. This may cause the punch to be unable to cut material correctly in high-speed stamping. Reducing the friction of the rollers can make the whole system easier to control, especially when material forming and material feeding need to be activated at the correct time.

- When using spring force to control moving components such as the blank holder, the local vibration provides excitation for the whole stamping tool and significantly influences the dynamic response of the punches. To improve the design, it is suggested that more control on the dynamic performance should be given to such moving components as the blank holder.

The findings presented above have helped improving the design of the micro-stamping machine developed at the University of Strathclyde and these are also of generic significance to future micro-stamping machine design (Zhou, et al., 2007; Zhou, et al., 2008; Qin, et al., 2009).

The above conclusions have given the answers to the problems of this study. The finite element method is an effective and efficient method for the analysis of the micro-stamping manufacture system. The objectives of the study have been achieved.

9.2 Recommendations on the integrated design of a micro-stamping machine

9.2.1 Integrated design and FE simulation

As described in the review of the integrated design, a micro-stamping machine system includes a micro-stamping machine, a micro-stamping tool, a micro-stamping machine base, a material feeder, and a workpiece handing device. In order to achieve high precision, apart from requiring the individual high quality of the above-mentioned parts, it is more important to make all of the parts work well as an integrated system. In further studies, both the FE simulation and the experimental investigation should include as many parts in the system as is practical. The investigations should be carried out to find any potential exiting force generated within the system due to moving components. In the dynamic FE analysis model, the

machine base should simulate the actual base as closely as possible. In this study, attempts have been made to identify the cause of unstable behaviour of the stamping machine on the basis of vibration analysis. Following on from this, recommendations have been made as to how to improve the design. Further, dynamic response analysis using the finite element method has been carried out on the micro-stamping tools. In future development, as the improved design becomes increasingly lighter (but the weight of such part as the driving motor may not be able to be reduced proportionately), the working frequency range may not fall far away from the natural frequency of the machine system. This is particularly true when soft base like rubber is employed. As a consequence, dynamic response analysis of the integrated machine system will become necessary. In dynamic FE simulation, it is also of importance to consider non-linear material properties of such components as the rubber base.

9.2.2 Fatigue design

A micro-stamping machine works at high speed and is subjected to cyclic loads. The amplitude of the cyclic force is related to the working frequency, the workpiece material, etc. The stress amplitude is related to the force as well as to the structural geometry. A discontinuity in structural geometry will cause stress concentration. As a result, fatigue may become an issue. The integrated design of a micro-stamping machine system should not only have greater precision, smaller dimensions, and a lighter structure, but also should have a long working life. Therefore, fatigue damage assessment should be involved in the development of the system. Fatigue life should be taken as one of targets of the design. The fatigue-life prediction of steel structures using the hot-spot S–N curve concept has wide application in engineering (Zhou, et al., 2009 and Yu, et al., 2010). The process can be briefly described as follows.
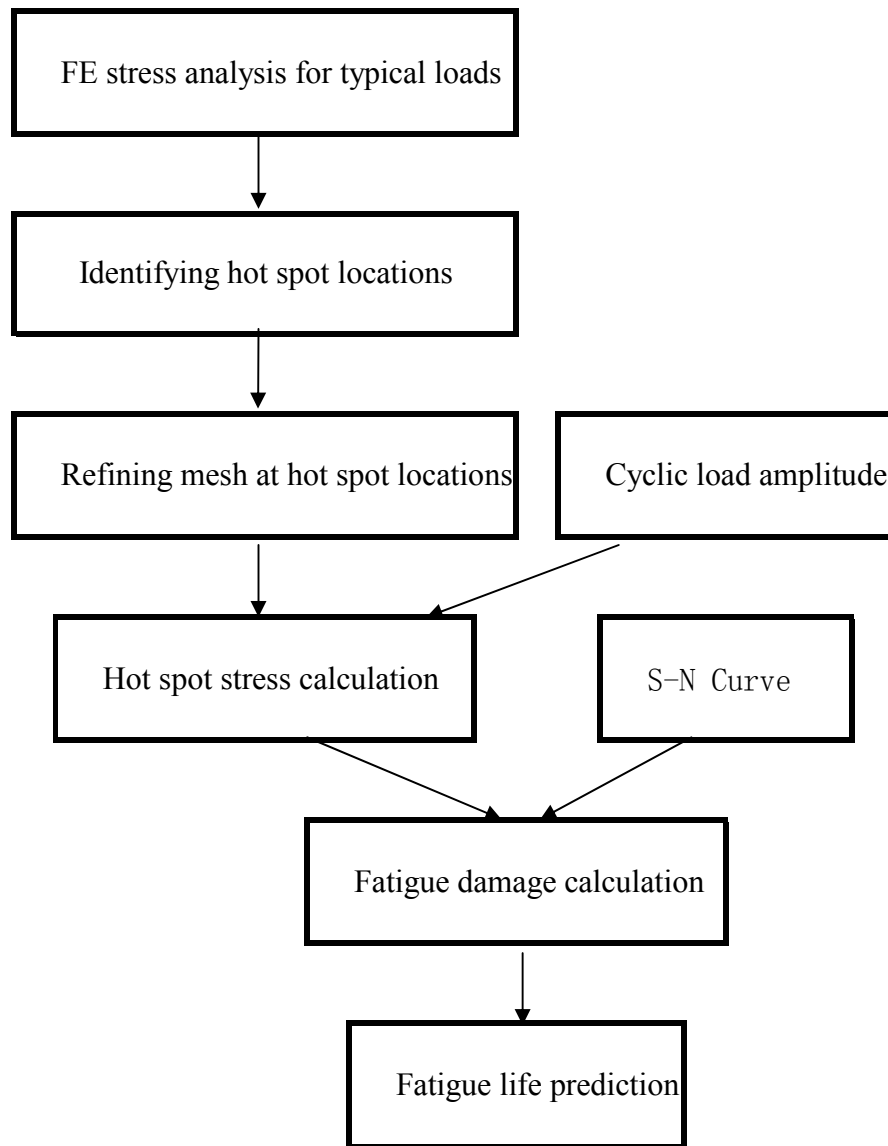
Fig. 9.1 Process of fatigue-life prediction

The S–N curve for steel can normally be defined by a linear equation in a log-axis system:

$$Log(N) = Log(K) - m'Log(S)$$

where:

N is the number of cycles to failure at stress range S.

$Log(K)$ is the intercept of the hot spot S-N curve with the $\log(N)$ axis

S is the stress range

m' is the negative, inverse slope of the S-N curve

In the Palmgren-Miner's Rule linear cumulative damage model, the fatigue damage can be calculated using:

$$D = \sum_{i=1}^{m} \frac{n(S_i)}{N(S_i)}$$

where:

n is the number of cycles of stress range S_i, and

m is the number of stress ranges (levels) experienced.

A micro-stamping machine with high precision, high flexibility, high ability of mass production, and long working life is the goal of the design. To accomplish this goal quickly and economically, advanced numerical simulation can play an important role.

9.3   References

Qin, Y., Ma, Y., Harrison, H., Brockett, A., Zhou, M., Zhao, J., Law, F., Razali, A., Smith, R. and Eguia, J. (2008), 'Development of a new machine system for the forming of micro-sheet-products,' Proceedings of ESAFORM, Springer Paris, ISSN 1960-6214, DOI: 10.1007/s12289-008-0098-9, April, 2008, pp. 1-4.

Yu, L., Zhou, M., Li, T., Tong, J. and Wong, S., (2010), ' Fatigue Reliability of Bulk Carrier – A Case Study,' 5th International SRANet Conference on Integrating Strucutral Analysis, Risk & Reliability, 14 – 16 June 2010, Edinburgh, UK.

Zhou, M., Qin, Y., Ma, Y. and Harrison, C. (2007), 'Investigation of the Dynamic Behaviour of a Micro-Stamping Tool,' Advances in Manufacturing Technology,' 5th International Conference on Manufacturing Research, 2007

Zhou, M., Qin, Y., Harrison, C., Brockett, A. and Ma, Y. (2008), 'Finite-Element and Experimental Analysis of Dynamic Behaviours of a Micro-Stamping Tool System,' *Int. J. of Adv. Manufact. Technol.,* DOI 10.1007/s00170-009-2138-0

Zhou, M., Li, T., Tong, J., Brennan, D., Yu, L., Kumar, R., Wong, S. and Polezhayeva, H. (2009), 'Spectral Fatigue Analysis of a Bulk Carrier –A Case Study,' International conference of Design & Operation of Bulk Carriers, RINA, 26-27 October 2009, Athens, Greece.